INSTITUTE
FOR
AEROSPACE STUDIES

UNIVERSITY OF TORONTO

DYNAMICS OF LARGE FLEXIBLE SOLAR ARRAYS

and

APPLICATION TO SPACECRAFT ATTITUDE CONTROL SYSTEM DESIGN

by

P. C. Hughes and S. C. Garg

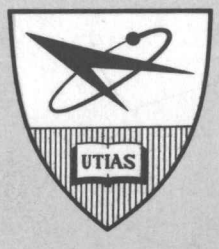

February, 1973.

UTIAS Report No. 179

DYNAMICS OF LARGE FLEXIBLE SOLAR ARRAYS

and

APPLICATION TO SPACECRAFT ATTITUDE CONTROL SYSTEM DESIGN

by

P. C. Hughes and S. C. Garg

Submitted January, 1973.

February, 1973.

UTIAS Report No. 179

Acknowledgement

Certain sections of this analysis (particularly relating to the 'unconstrained' modal representation) were developed while one of the authors (PCH) spent the summer of 1970 at the Communications Research Centre, Ottawa, and the summers of 1971 and 1972 at Spar Aerospace Products Ltd, Toronto, and while the second author (SCG) spent the summer of 1972 at Spar. This report, which incorporates this earlier work in a more extensive and unified treatment, was made possible by the support of the Communications Research Centre under Contract No. 01GR.36100-2-0210.

Summary

Many current three-axis controlled spacecraft have appendages of considerable size and possessing significant structural flexibility. This report examines the resulting interaction between the attitude dynamics and the elastic degrees of freedom. The representation of these additional degrees of freedom in terms of natural modes is discussed and two distinct classes of modes are defined. For both classes, 'constrained' and 'unconstrained', the object of the analysis is to find the natural frequencies of oscillation and the modal gains. The latter indicate the relative influence of each mode on the angular acceleration of the spacecraft. The relationships between these classes of modes, and certain important properties of the modal gains are discussed in general terms. These general considerations are illustrated for a specific satellite configuration which is suggested by the Communications Technology Satellite where the flexibility is provided by a large solar array. The geometrical simplicity of this configuration allows continuum mechanics to be chosen as an appropriate formulation. Numerical results are provided for frequencies and gains (and for both classes of modes) and their dependence on all satellite parameters is exhibited graphically. Both dimensional and dimensionless plots are provided where appropriate. The main contributions of this report include a general discussion of how spacecraft structural flexiblity can be represented from an attitude control viewpoint, of how solar arrays in particular can be successfully treated by traditional techniques, and, even more particularly, of the detailed numerical results when such an analysis is applied to a contemporary spacecraft.

TABLE OF CONTENTS

PRINCIPAL NOTATION

(Notation employed only briefly is defined where used)

Upper Case Roman

A_n	amplitude of array tip rotation with respect to root (n^{th} constrained mode)
B	flexural stiffness ("EI") of support boom
E	see Eq. (4.90)
F_n	for pitch motion, see Eq. (3.68); for roll-yaw motion, see Eq. (4.79)
I	inertia of spacecraft (flexible + rigid)
$\mathcal{I}$	$\mathcal{I}^2/J$
$\mathcal{J}$	$\sqrt{I_{11}I_{33}-I_{13}^2}$
J	$I_{11}\sin^2\gamma + I_{33}\cos^2\gamma + 2I_{13}\sin\gamma\cos\gamma$
K_n	constrained modal gains. For pitch, see Eq. (3.76); for roll-yaw, see Eq. (4.84)
$\underline{M}$	matrix representing linear algebraic equations for mode shape coefficients (roll-yaw)
P	tension in blanket = compressive load in support boom
Q_n	generalized coordinate associated with the n^{th} constrained modal degree of freedom
U_n	constrained mode shape of support boom
V_n	constrained mode shape of blanket

Lower Case Roman

b	distance from satellite centre to root of support boom
d	distance from root of support boom to inner edge of blanket
f_n	for pitch motion, see Eq. (3.39); for roll-yaw motion, see Eq. (4.48)
h	angular momentum
k	in Sect. 5.2, the root stiffness of the support boom
k_n	unconstrained modal gains. For pitch, see Eq. (3.93); for roll-yaw, see Eq. (4.109)
ℓ	length of support boom

m	mass of array tip-piece
q_n	generalized coordinate associated with the n^{th} unconstrained modal degree of freedom
s	Laplace transform variable
t	time
u	deflection of support boom
u_n	unconstrained mode shape of support boom
v	deflection of blanket
v_n	unconstrained mode shape of blanket
w	width of blanket
x	'chordwise' coordinate for blanket
y	'spanwise' coordinate for blanket

Upper Case Greek

Δ	see Eq. (4.90)
Θ	pitch motion if satellite were rigid; see Eq. (3.73)
Ξ_{nm}	scalar product of two constrained modes; for pitch, see Eq. (3.28); for roll-yaw, see Eq. (4.39)
Φ	roll motion if satellite were rigid; see Eq. (4.122)
Ψ	yaw motion if satellite were rigid; see Eq. (4.122)
Ω_n	natural frequency of n^{th} constrained vibration

Lower Case Greek

α	in pitch/twist analysis, the angle of rotation of the array tip with respect to the array root
$\alpha_n(y)$	amplitude of array rotation with respect to root (n^{th} unconstrained mode)
α_n, β_n	in bend/roll-yaw analysis, see Eq. (4.33) for constrained modes and Eq. (4.53) for unconstrained modes
$\beta_n(y)$	in pitch/twist analysis $\beta_n(y) = \theta_n + \alpha_n(y)$
γ	angle between array blanket (nominal) and roll-pitch plane; see Fig.B-1
δ	$\phi\cos\gamma - \psi\sin\gamma$

ϵ	$[(I_{11}\sin\gamma + I_{13}\cos\gamma)\phi + (I_{33}\cos\gamma + I_{13}\sin\gamma)\psi\ ]/\mathcal{J}$
ζ_n	modal damping ratio
η	y/ℓ
θ	pitch angle
κ_n	$\sqrt{\sigma w/P}\ \Omega_n$ (constrained); $\sqrt{\sigma w/P}\ \omega_n$ (unconstrained)
ξ_{nm}	scalar product of two unconstrained modes; for pitch, see Eq. (3.53); for roll-yaw see Eq. (4.61)
ρ	mass per unit length of support boom
σ	mass per unit area of blanket
ϕ	roll angle
ψ	yaw angle
ω_n	natural frequency of n^{th} unconstrained vibration
ω_N	nutation frequency = $h/\mathcal{J}$ (a more precise nomenclature is 'precession' frequency)

Subscripts

1	about roll axis
2	about pitch axis
3	about yaw axis
n, m	mode number
i, j	elements of $\underline{M}$ matrix
b	referring to main spacecraft body (rigid)
A	referring to solar arrays (flexible)
c	control
e	external
f	flexible
r	rigid

Superscripts and Miscellaneous

$(\cdot)^*$	dimensionless variable associated with $(\cdot)$
$(\cdot)'$	$d(\cdot)/dy$

$(\dot{\cdot})$	$d(\cdot)/dt$
$(\bar{\cdot})$	Laplace transform of $(\cdot)$
sh	sinh
ch	cosh
s	sine
c	cosine

1. INTRODUCTION

The stiffness of any real material is finite. This fact has always had important ramifications in many areas of engineering design; for example, structural flexibility is a pervasive element in the ancient technology of bridge-building. The design of architectural structures, and aircraft design, are other notable instances. The underlying cause is readily identified: structures are not mass-effective (and therefore not cost-effective) unless they are flexible.

This argument is now offered in more quantitative terms. Represent the mass/volume (i.e., the volume density) of the material selected by ρ; then those costs which are proportional to weight may be written as

$$\$ \sim \rho A \ell \qquad (1.1)$$

where A is a characteristic cross-section of a typical structural member, and ℓ a characteristic length. In addition to cost, a competing requirement of the design is some degree of structural rigidity. A measure of this rigidity is the (first) frequency of vibration, ω. Dimension analysis indicates that this criterion behaves according to

$$\omega \sim \left(\frac{EA}{\rho \ell} \right)^{1/2} \qquad (1.2)$$

where E is a material stiffness modulus (force/area). Very often the object of the design is to provide the length ℓ, or equivalently an area ℓw where the width w is more or less constrained. In such cases then, ℓ is fixed by specification or perhaps other considerations. The free parameters remaining in Eqs. (1.1) and (1.2) are ρ, E, and A, with the dependence on the first two indicating, not unexpectedly, the necessity for light strong materials. After such a material has been chosen on this basis (and undoubtedly influenced by other considerations as well) the only remaining parameter is A. Equations (1.1) and (1.2) demonstrate that the aims of low \$ and high ω are conflicting. Where the balance is actually struck depends on whether stiffness or cost is more compelling in a particular case.

1.1 Objectives of the Report

This report is concerned with certain aspects of spacecraft structural flexibility, and space vehicles are a dramatic instance in which the balance referred to above must be settled very much in the direction of cost. While in the case of a bridge the weight-related costs are not prohibitive and the stiffness can easily be made as high as required to prevent phenomena like dynamic buckling under high wind conditions, for a spacecraft, on the other hand, the enormous cost per pound placed in orbit, together with the relatively wispy forces the vehicle will encounter in orbit, leads to designs which place understandably greater emphasis on weight than on stiffness.

The authors have had the opportunity to be associated with a specific 'three-axis controlled' spacecraft (see Section 2) for which structural flexibility was significant enough to merit investigation (see Refs. 1 and 2). In a more general context, some further results were given in Ref. 3. The present report is intended to be a unified presentation of the material in those references, and the opportunity is also taken to present additional details which were not appropriate under the space limitations essential to journal publication. In many

cases more details are given here on the derivations which were merely sketched before (Refs. 1,2,3). Alternative approaches to the problems encountered are stressed. More graphical results are also given. Finally, an opportunity will be taken to reflect on the subject through more expansive discussion which it is hoped will prove of interest to other attitude dynamicists.

1.2 Phases of Analysis

The primary motivation for the subsequent discussion is taken to be the attitude control of a spacecraft which cannot readily be assumed 'rigid'. It may be helpful to delineate the requisite tasks which face the analyst who is responsible for 'flexibility effects'. There are essentially three phases.

1.2.1 Natural Motions

For simplicity, the property referred to somewhat vaguely as 'flexibility' will be restricted, for the purposes of this discussion, to linear and nondissipative elasticity. Such deflections as may occur about equilibrium are assumed to be small enough to validate a linear (i.e., a variational) approach to the variables representing these deflections. This latter assumption is not restrictive because large unsteady deflections are likely to be incompatible with current attitude error specifications.

The first step is to find the natural motion of the flexible spacecraft. 'Natural motion' implies that both perturbing torques, and the torques exerted by the control system in response to such perturbations, are identically zero. It is well known that the natural motions of a nondissipative elastic system consist of harmonic oscillations in time.

Classical physics teaches that under the present assumptions a valid model for the natural motion is a superposition of an infinite number of sinusoidal oscillations. Each of these 'modes' of oscillation is specified by its modal 'shape' (i.e., the space dependence of the deflection) and the modal 'frequency' of oscillation. Mathematically this behaviour is characterized by an eigenvalue problem in which the eigenvalues and their associated eigensolutions correspond to the modal frequencies and shapes, respectively.

Of interest is the classical inference that the number of modes is infinite. While this may be a valid result mathematically (under our assumptions), certain further physical considerations must be mentioned which lead to the dismissal of all but the first N (a finite number) of these modes. First of all, the elastic structure will have a finite speed of wave propagation through it and therefore prediction concerning vibrations at comparable frequencies will not be meaningful unless this fact is taken into account. Second, the high frequency motions tend not to be excited by the disturbances the spacecraft actually encounters; they neither have the high frequency nor the spatial variability to have a significant influence on the higher modes. This is reflected in the diminishing values of the higher modal gains (discussed in Section 1.2.2). Finally, even if the very high modes were present, and even if they were excited, they would be of dubious significance since the attitude sensor would filter out these oscillations and they would be "invisible" to the attitude controller; the situation with regard to rate sensors is less clear.

Thus the practical necessity of limiting the number of modes included in the investigation of natural motions is, fortunately, quite consistent with

physical and technical considerations. This step is an enormous simplification since the flexible displacements are now represented by a finite number of degrees of freedom. It is emphasized that this procedure is not a crude "engineering expedient"; it has a rigorous basis both mathematically and physically and can be made, in principle, arbitrarily accurate. Techniques for performing this task are discussed briefly in Section 1.4.

1.2.2 Modal Gains

Having found the 'natural motions' of the spacecraft in the absence of external influences (including control torques), attention is now turned to the 'actual motion' when these heretofore neglected torques are in fact present. If the satellite were rigid, the angular acceleration in response to a given impressed torque is readily calculable. Because the satellite is flexible, however, the actual angular acceleration is different from the rigid result. Speaking somewhat loosely, the modal gains indicate what fraction of this difference is due to each mode.

From the standpoint of attitude control system simulation then, each mode may be thought of as contributing a "correction" term or transfer function to a 'block diagram'. Each such term is characterized by two parameters; the natural frequency, and the modal gain. Recalling the discussion in Section 1.2.1, the natural frequency corresponds to the eigenvalue of a certain eigenproblem. Qualitatively, modal gains are calculated as the integrated effect of a disturbance on that mode shape (eigensolution). These effects (and hence the gains) tend to become increasingly minute for the higher modes.

1.2.3 Flexibility Implications

The preceding two phases (determination of modal frequencies and gains) are distinct from the third phase - assessing the implications of flexibility for the attitude control system. To assume a negligible influence, it is usually sufficient to have the gains $\ll 1$, and the lowest natural frequency $\gg \omega_{BW}$ where ω_{BW} is the bandwidth of the controller. If these conditions are satisfied therefore, inclusion of flexibility effects in a simulation will only reveal an almost imperceptible ripple about the rigid results. If either criterion is not satisfied, a proper simulation of flexibility is indicated.

1.3 Constrained and Unconstrained Modes

Two classes of 'natural motions' are discussed in this report. They are referred to as 'constrained' and 'unconstrained' and the distinction arises in the following way: satellite designs tend to consist of a 'main' or 'core' body from which various appendages are often extended after orbit insertion. In the context of on-orbit attitude control, the main body structure may be regarded as rigid (although in other contexts, during launch for example, it may not be so regarded). The structural flexibility, then, is resident in the appendages. There may be other sources of non-rigidity, such as dampers in the main body, contact friction between moving parts, fuel sloshing, etc., but these may be considered separately and are beyond the scope of the present discussion.

Normally it is the main body whose attitude is to be controlled, and small deflections of the appendages are noteworthy only insofar as they influence the attitude of the main body. Both attitude sensors and control torque actuators are normally located on the main body also. Two choices of natural motions (modes) are then possible.

1.3.1 Constrained Modes

One choice is to consider each appendage separately, regarding the point of attachment to the main body as motionless in both translation and rotation. Motion equations for each appendage are used to deduce the mode shapes and frequencies characteristic of such motion. This approach is dynamically equivalent to finding the mode shapes and frequencies characteristic of the overall spacecraft, subject to the constraint that the main body is motionless.

To study the attitude motions of the spacecraft under the influence of external torques it is necessary to have spacecraft motion equations available. These may be found, for example, by equating the rate of change of the total system angular momentum to the impressed external torque - or by some alternate dynamical formulation. Furthermore, the appendage motion equations must incorporate the fact that the main body is now free to move; in fact the main body motion may be regarded as an 'input' driving the appendages. The appendage motion may be thought of as the sum of two terms - a 'rigid' response, in which the appendage follows exactly the body attitude, and a 'flexible' response which is the additional deflection required to total the actual motion. This latter (flexible) response may be further expanded as a superposition of the natural (constrained) modes.

1.3.2 Unconstrained Modes

An alternative approach is to consider the spacecraft motion equations at the outset. Thus 'spacecraft modes' are found, as distinct from 'appendage modes'. Since there is no longer any constraint on the central body, these may be termed 'unconstrained' modes. All external influences are set to zero during this calculation. The response of the spacecraft to external torques may then be written as the sum of the 'rigid' response together with the 'flexible' response. The latter, in turn, is expanded as a superposition of the natural (unconstrained) modes.

1.4 Techniques for Modal Analysis

Many techniques are available to the analyst which facilitate the extraction of modal information and they all have in common the factors discussed thus far.

1.4.1 Continuum Mechanics

The traditional approach is to formulate motion equations from the principles of continuum mechanics; they lead to differential equations in space variables and time*. Separation of variables is employed to decompose each natural motion into a space-dependent factor (the eigensolution) and a time-dependence (sinusoidal) factor. This decomposition is not unique to the continuum mechanics approach. For simple geometries this method would seem to be the most attractive. In many cases the eigenproblem can be solved in closed form with the attendant insights and economy. Often however, although formulated analytically, the equations will require a computer solution. Even so, the physical assumptions made are usually very explicit and it is relatively easy to assess their impact on the accuracy of the final solution. Furthermore, the number of configurational parameters tends to be quite limited and the presentation and

* For the space variables, an integral equation is sometimes used.

interpretation of data is thereby tractable, especially if dimensionless groupings are employed.

As an example, suppose an appendage consists of a long thin boom whose (mass/length) density and flexural stiffness varies linearly from root to tip; the eigenproblem corresponding to this case is straightforward to formulate. However, it cannot be solved in closed form. Nevertheless a numerical solution found with the aid of a computer is preferable to the abandonment of the continuum approach entirely.

1.4.2 Lumped Parameter Approach

Many appendages are geometrically complex. Thus, although continuum mechanics is still applicable in principle, it becomes unmanageable in practice. When such situations were encountered one or two decades ago, one of two expedients were adopted: lumped parameter or Rayleigh-Ritz. In the former it is assumed that deflections need be known at only a finite number of locations and the distributed parameters of mass and stiffness are taken to be equivalent to lumped masses at these locations with lumped stiffnesses describing the resistance to relative motion. Thus the nature of the approximations made in modelling the structure was physical rather than mathematical. The well-known method of Rayleigh-Ritz consists of prespecifying assumed mode shapes and may be used instead of, or together with, the lumped parameter method depending on where the analytical difficulties arise. In all these methods a finite number of degrees of freedom is used to approximate the infinitude.

1.4.3 Finite Element Approach

The lumped parameter philosophy alluded to above has evolved very far in sophistication, reliability, and range of application. This is reflected in the method of finite elements. Rules have been developed for this discretizing procedure and there is now an extensive catalogue of elements each of which may have several degrees of freedom. This procedure is ideally suited to the capabilities of the digital computer and hundreds (sometimes even thousands) of degrees of freedom are used. Clearly the degree of accuracy in the first few modes is extremely high.

1.5 Summary of Report

The next four Sections (2,3,4,5) deal with the analysis of a specific spacecraft. Section 2 describes the spacecraft and the assumptions made in the analytical model. The geometry is sufficiently simple that a continuum mechanics approach is fruitful. Section 3 discusses the interaction between array twisting and pitch motion of the spacecraft; Section 4 is concerned with the interaction between array bending and the roll-yaw motions of the spacecraft. Section 5 extends the analysis in several respects, and the concluding remarks are made in Section 6.

2. A SPECIFIC APPLICATION

2.1 Introduction

The general principles and considerations discussed in the introduction are applied to a specific satellite in the remainder of this report. An excellent

example is the Communications Technology Satellite (CTS) being jointly sponsored by Canada and the U.S.A. Reference 4 gives an overall description of the CTS. An artist's impression of the satellite appears in Fig. 1, and a conceptual diagram of the subsystems in Fig. 2 (after Ref. 4). The CTS is a high-power communications satellite and is scheduled for launch in 1975. The power needs will be supplied by an array of solar cells which generates about 1.2 kilowatts. It also makes CTS interesting from a dynamics standpoint.

2.2 Flexible Appendages

The solar panels are deployed symmetrically about the central body, forming the major part of the solar array subsystem. The major structural components are shown in Fig. 3, and are as follows:

(a) The support boom which extends out from the satellite and carries a tip piece at the end. It provides bending stiffness and is held in compression by the tip piece, due to the tension acting on the solar panels. The boom itself is of bi -STEM design, that is, it has a hollow thin-walled cross-section consisting of overlapping pieces.

(b) The tip piece, which is attached to the solar panels and serves to hold them in a state of uniform tension. It also carries cables on which the longitudinal edges of the panels are supported. It is connected to the support boom through a bearing which allows the panels to rotate freely without transmitting any appreciable torque to the boom.

(c) The solar cell array, mounted in layers on a flexible substrate. It is kept in tension by the tip piece and is unfolded accordion-fashion from the root, riding on cables attached to the tip piece.

The solar panels are offset from the support booms, to prevent contact with them. This also has the advantage that thermal input to the boom is reduced, alleviating thermal distortions and possibly even more serious dynamic phenomena (thermal flutter - Ref. 5). However, it introduces a static deflection shape which must be taken into account while calculating deflections, as in Section 5.4.

2.3 Basic Motions

The following qualitative considerations apply to the types of motion the satellite may undergo, and will serve to simplify and clarify the subsequent analysis.

(a) Rigid-Body Motions

Considering the spacecraft as a rigid body, it is clear that it has both translational and rotational degrees of freedom. We shall primarily be concerned with the latter. For small-angle motion the pitch dynamics can usually be uncoupled from the roll-yaw dynamics. For the CTS, however, the principal axes are not fixed in the body because part of the spacecraft (the panels) rotates so as to follow the sun. If the axis of rotation is parallel to the pitch axis, the pitch and roll-yaw motions can still be uncoupled. The roll and yaw motions are strongly coupled in any case, due to the presence of a

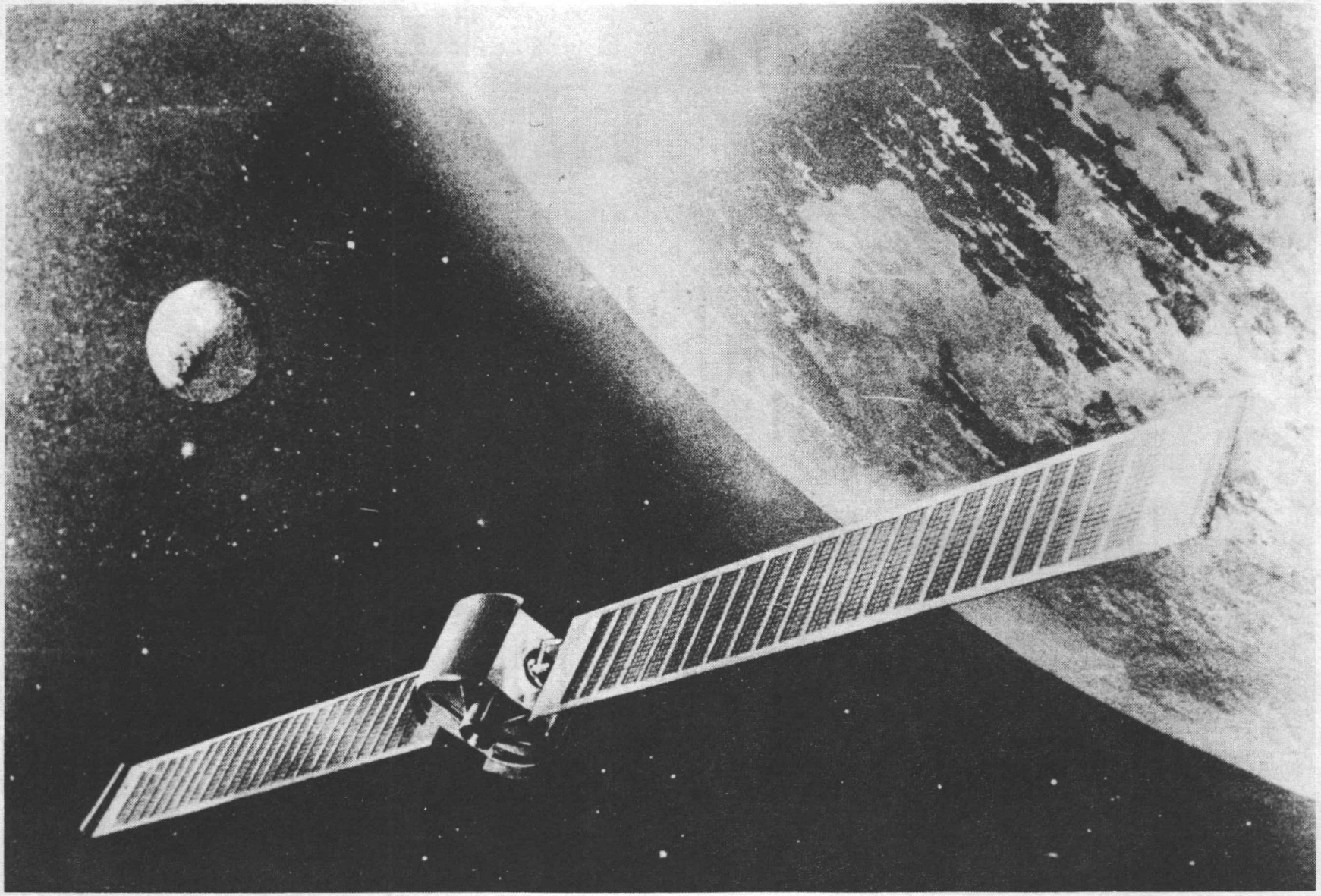

FIG. 1: Artist's Impression of the Communications Technology Satellite (Courtesy Spar Aerospace Products Ltd.)

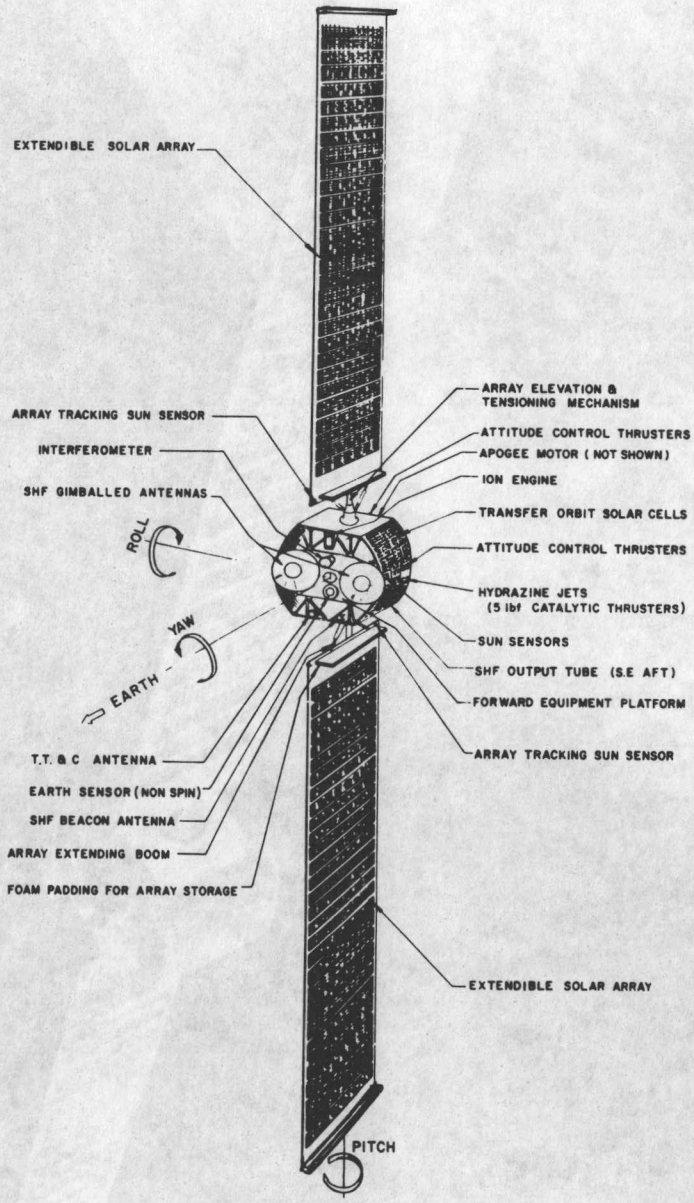

FIG. 2: Communications Technology Satellite as Deployed in Synchronous Orbit (from Ref. 4)

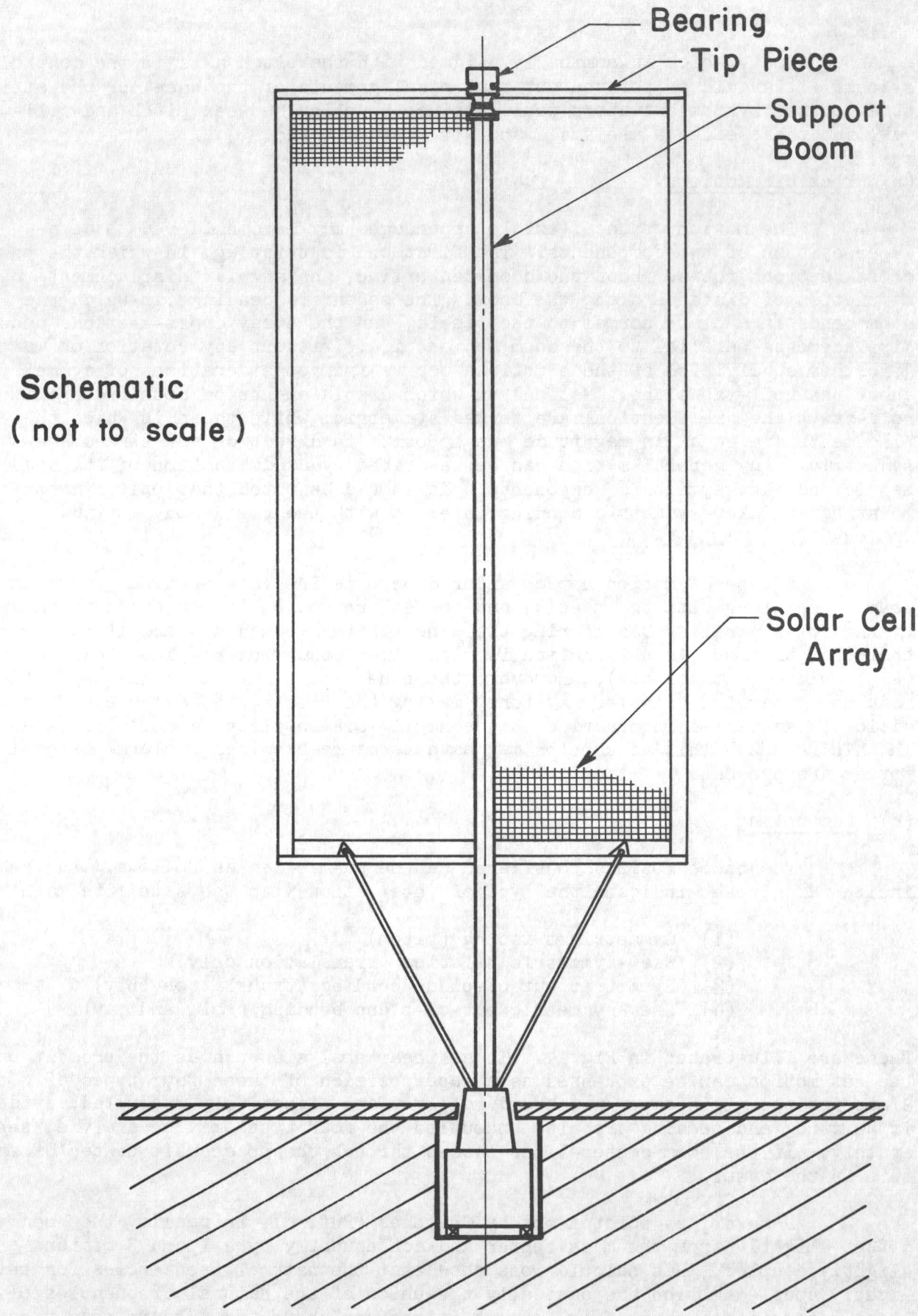

FIG. 3: Schematic Diagram of Solar Cell Array Structure

momentum wheel, which is nominally aligned with the pitch axis in the control system. It should be pointed out that misalignments of the wheel or the attitude control system actuators would produce coupling between pitch and roll-yaw, but these effects are small and will be neglected.

(b) Flexible Motions

The motion of the flexible appendages may be considered to be a superposition of two components. The first one is twisting, in which the panel cross-sections rotate about the boom centerline, the angular displacements being a function of distance along the boom. The second is bending, in which the boom bends in a plane normal to the panels, and the array cross-sections undergo displacements parallel to the boom motion, i.e., without any rotation or warping. A further subdivision of these motions occurs from considerations of symmetry about the roll-yaw plane. Motions on which displacements on both sides of the roll-yaw plane are identical are termed symmetric, while those in which the displacements are equal in magnitude but opposite in direction are termed skew-symmetric. Any general motion can be described by a combination of its symmetric and skew-symmetric components. It should be noted that only symmetric twisting and skew-symmetric bending interact with the rigid-body attitude motions.

A type of motion not considered here is in-plane bending, in which the boom bends along with the panels, but the entire motion is contained in the plane of the solar panels. Considering the panel in tension as a beam, it can be seen that the stiffness in this motion is much larger than out-of-plane bending (since width $\gg$ thickness). However, the panels must have a small compressive modulus, otherwise wrinkles may form, making the problem intractable. This condition is satisfied in practice, hence negligible in-plane motion will be assumed in this report. This assumption may have to be re-examined if large lateral forces are present.

(c) Uncoupling

The basic motions considered can be summarized as follows. The remarks inside parentheses indicate the type of interaction with the satellite main body.

(1) Symmetric twisting (pitch)
(2) Skew-symmetric twisting (translation only)
(3) Symmetric out-of-plane bending (translation only)
(4) Skew-symmetric out-of-plane bending (roll and yaw).

These are illustrated in Fig. 4. In a linear analysis such as the present one, the net motion can be expressed as a superposition of these four types of motions. Since for the rigid case, pitch and roll-yaw are effectively uncoupled, evidently if twisting and bending are also uncoupled the four types may be analyzed separately. If the boom center-lines passes through the spacecraft center of mass, this is the case.

However, as pointed out by Cherchas (Ref. 6), in reality the boom is offset slightly from the mass center and consequently type 1 and 3 motions are slightly coupled. His calculations show that the natural frequencies for this lightly coupled motion are basically the union of the natural frequencies of 1 and 3 considered separately, except in regions where the two are nearly equal. Similar effects may be expected if other small asymmetries exist. Due

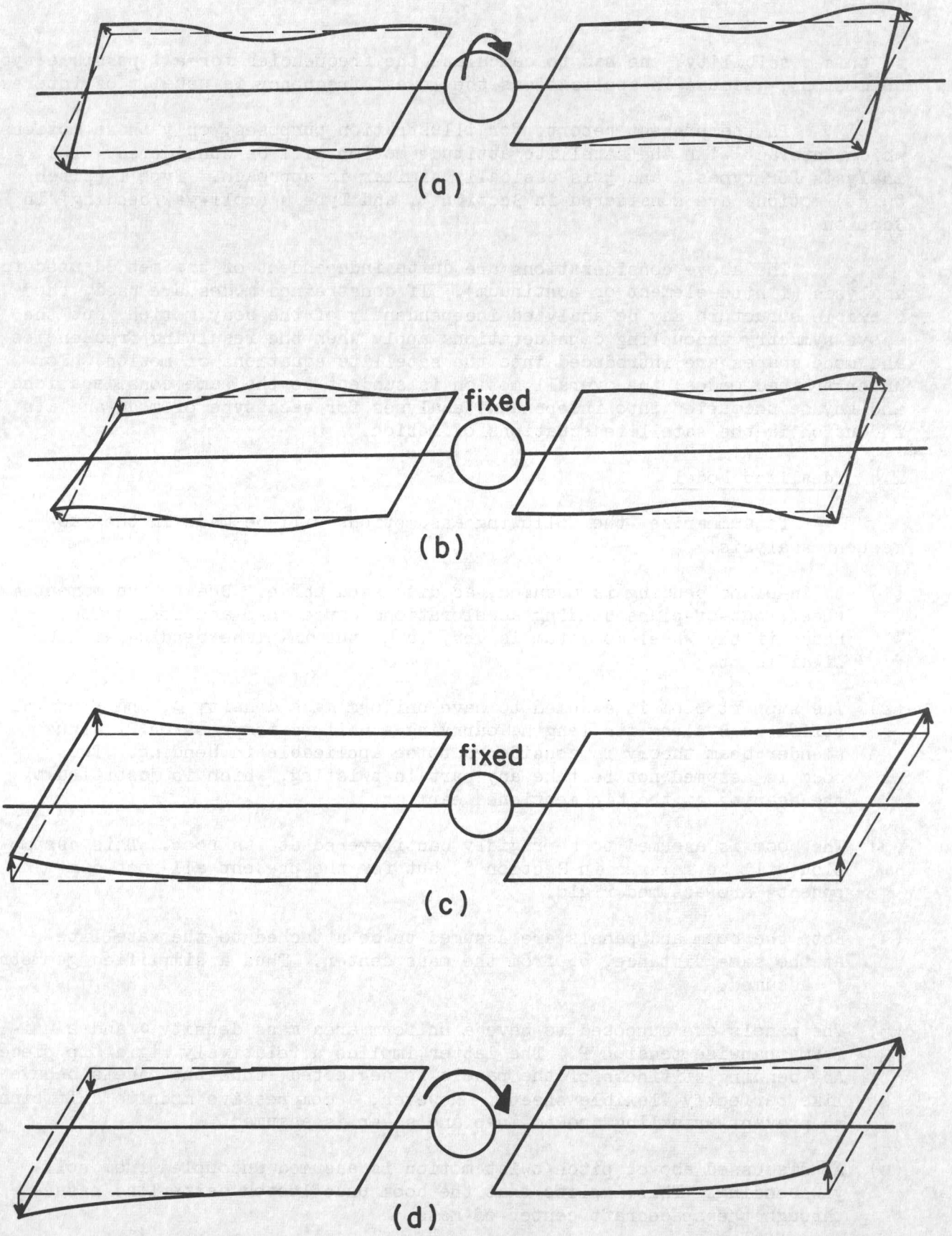

FIG. 4: Basic Types of Motion Considered

to this possibility, one has to calculate the frequencies for all possible types of motions, because in applications the lowest frequency is usually of interest.

In the present report, for illustration purposes, only those motions which interact with the satellite attitude motion will be considered. The analysis for types 2 and 3 is basically similar in approach. Type 1 (pitch/twist) motions are considered in Section 3, and Type 4 (roll-yaw/bending) in Section 4.

The above considerations are quite independent of the method used for analysis (finite-element or continuum). If constrained modes are used, the flexible structure may be analyzed independently of the body motion, but the above symmetry/uncoupling considerations apply when the resulting frequencies and mode shapes are introduced into the satellite equations of motion. For unconstrained modes, the overall motion is subject to the same considerations and may be uncoupled into independent analyses for each type of mode and its inclusion in the satellite equations of motion.

2.4 Idealized Model

To summarize, the following assumptions will be made in the subsequent analysis.

(1) No in-plane bending is assumed, as discussed above. Due to the momentum wheel, out-of-plane bending accelerations cause in-plane forces too. Hence if the wheel momentum is very large the in-plane bending will be significant.

(2) The support boom is assumed to have uniform mass density ρ, and flexural stiffness B along its length, carrying a uniform compression P. Thus slender beam theory is considered to be applicable in bending. The boom is assumed not to take any part in twisting, which is justified by the bearing at the tip mentioned earlier.

(3) The boom is assumed to be rigidly cantilevered at its root. This assumption will be relaxes in Section 5, but for the present all root components are assumed rigid.

(4) Both the boom and panels are assumed to be attached to the satellite at the same distance, b, from the mass center. Thus a simplified geometry is assumed.

(5) The panels are supposed to have a uniform area mass density σ and a uniform spanwise tension P. The latter implies a relatively rigid tip piece. Any bending stiffness of the panels is neglected, thus the panels behave like perfectly flexible sheets. However, a compressive modulus sufficient to prevent wrinkling due to in-plane shear is assumed.

(6) As discussed above, pitch/twist motion is assumed uncoupled from roll-yaw/bending. This implies that the boom undeflected centerline passes through the spacecraft center-of-mass.

(7) The fact that due to panel rotation, the moments of inertia vary with time is considered on a quasi-static basis, since the variation has a period of 24 hours.

(8) Interactions due to thermal distortions concomitant to solar heating are not considered. This effect is minimized due to shielding of the boom from the sun by the panels. Dynamic thermal effects still exist due to eclipse, etc., but these have a very long period and are neglected.

3. ARRAY TWISTING AND PITCH ATTITUDE

The pitch axis of the spacecraft is, by definition, nominally normal to the orbital plane. The axis about which the solar array rotates once per day is also nominally normal to the orbit, and is assumed below to be coincident with the pitch axis, as described in Section 2. Flexible motions of the array about this axis will be termed 'twisting' motions, and these are clearly coupled with pitching motions of the spacecraft as a whole; each excites the other (Ref. 1). For the moment then, bending of the array, and rolling and yawing of the spacecraft are not involved and may be taken to be zero as they are not coupled with twist/pitch; they are considered in Section 4.

This section begins with the differential equations which govern spacecraft pitching and array twisting (motion equations). The geometrical simplicity of the arrays allows a formulation in terms of a continuum mechanical approach. However other alternatives may be used if desired, as discussed in Section 1; this would change certain notational aspects of the relations presented, but the essential features of the development would remain unchanged. The two types of natural motions referred to in general terms in Section 1 ('constrained' and 'unconstrained') are investigated next (Sect. 3.2) and the solutions for natural frequencies and mode shapes are derived. Both families of modes are used as the basis for an expansion of general array twisting motion in Section 3.3, this demonstrates how to incorporate such modal representations into an attitude control system simulation.

3.1 Motion Equations

The coordinate system employed and the principal notation are illustrated in Fig.5. The z-displacement of a point in the array blanket due to pitch is $-x\theta(t)$, where θ is the pitch angle and x has the sense shown in Fig.5 Additional displacements of a twist variety are given the symbol $v(x,y,t)$ and so the total blanket displacement under consideration in this section is

$$\text{displacement} = v(x,y,t) - x\theta(t) \qquad (3.1)$$

3.1.1 Spacecraft Motion Equation

The symbol used for the pitch inertia moment of the centre body is I_{2b}; thus the total angular momentum of the spacecraft motion is

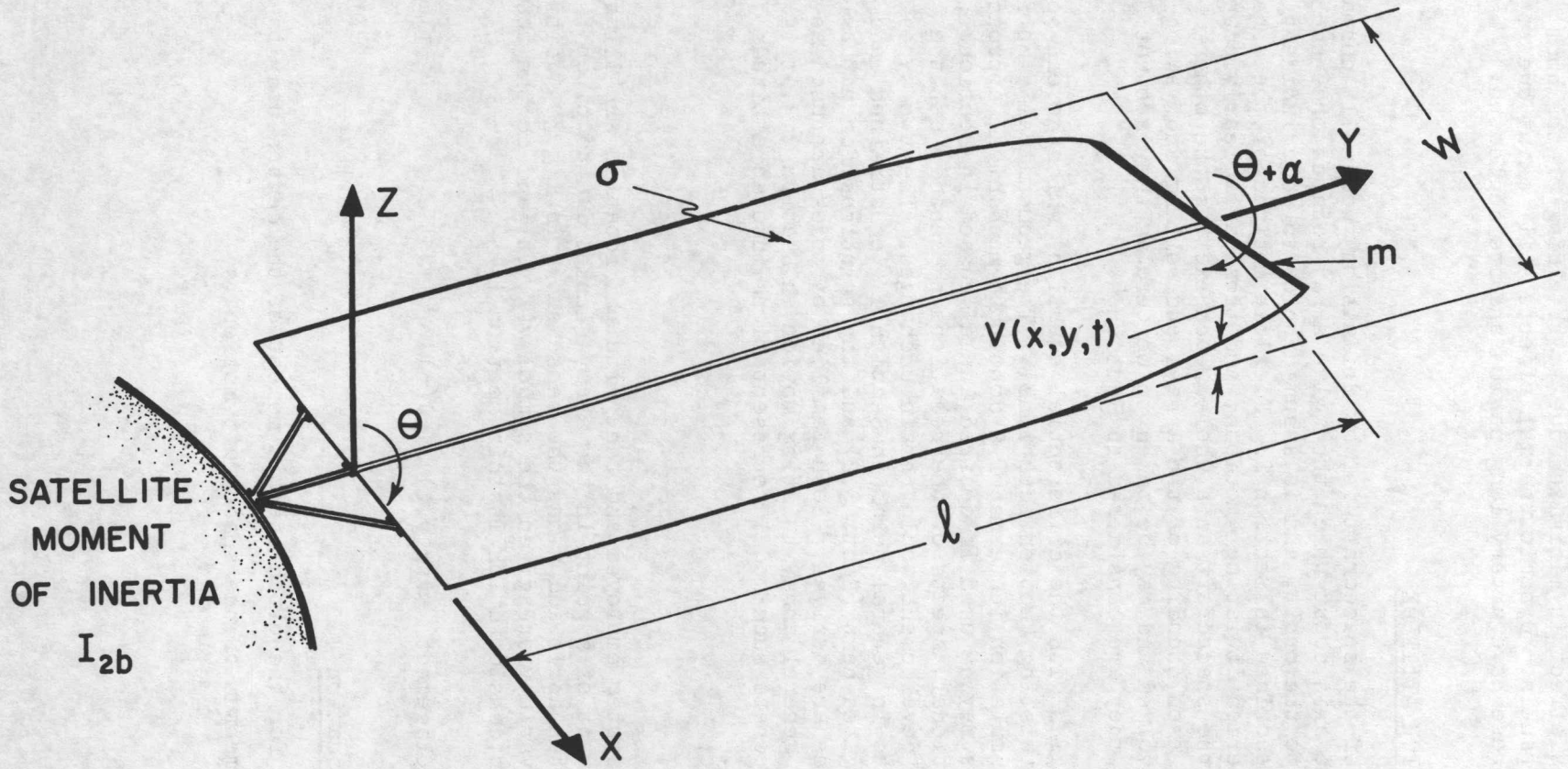

FIG. 5: Coordinate System for Pitch/Twist Motions

$$h = I_{2b}\dot{\theta} - 2\int_0^{\ell}\int_{-w/2}^{w/2}[\dot{v}(x,y,t) - x\dot{\theta}]\sigma\, x\, dxdy$$

$$- 2\int_{-w/2}^{w/2}[\dot{v}(x,\ell,t) - x\dot{\theta}](m/w)\, xdx \qquad (3.2)$$

Here ℓ and w are the array length and width; σ is the mass/area of the blanket; m is the mass of the tip piece (and thus its mass/length is m/w); and the shorthand $(\dot{\cdot})$ is used for time derivatives.

The angular momentum given by Eq. (3.2) will be taken to be relative to an inertial frame. This therefore neglects the once per orbit rotation of the reference axes. Even if a period of vibration was as long as 1 minute, however, this represents 1440 oscillations per orbit (for a synchronous orbit). Evidently the rotation rates associated with orbit true anomaly are negligible in the calculation of natural frequencies for such cases. Gyroscopic torques due to the once-per-orbit rotation of the spacecraft, which for small attitude angles are present only about the roll and yaw axes, may be included as an external torque in the external torque term $\underline{T}_e$ (see below). Similarly, gravity gradient torques, which are the same order of magnitude, are present only about the pitch and roll axes (small angles) and may also be included in $\underline{T}_e$.

The factor of 2 multiplying the two integrals in Eq. (3.2) appears because of the two array 'wings' (Fig. 1). The terms in the integrand which involve $x\dot{\theta}$ may be integrated at once to give

$$h = I_2\dot{\theta} - 2\sigma\int_0^{\ell}\int_{-w/2}^{w/2}\dot{v}(x,y,t)\, x\, dxdy$$

$$- 2(m/w)\int_{-w/2}^{w/2}\dot{v}(x,\ell,t)\, x\, dx \qquad (3.3)$$

where the spacecraft pitch moment of inertia is I_2:

$$I_2 = I_{2b} + 2\left(\frac{1}{12}\sigma w^3\ell + \frac{1}{12}\, m\, w^2\right) \qquad (3.4)$$

Since the angular momentum can only change under the influence of external torques, the equation of motion is found from

$$\dot{h} = T_{2c} + T_{2e} \qquad (3.5)$$

where the subscripts 'c' and 'e' denote control torques and external torques, respectively. More explicitly, combining Eqs. (3.3) and (3.5) yields the spacecraft pitch motion equation:

$$I_2\ddot{\theta} = 2\sigma \int_0^{\ell} \int_{-w/2}^{w/2} \ddot{v}\,(x,y,t)\; x\; dxdy$$

$$+ 2(m/w) \int_{-w/2}^{w/2} \ddot{v}\,(x,\ell,t)\; x\; dx$$

$$+ T_{2c} + T_{2e} \qquad (3.6)$$

When written in this form, the implication is that pitch motions of the spacecraft are excited not only by perturbing and control torques, but by twisting of the array as well.

3.1.2 Blanket Motion Equation

The bending resistance of the blanket to displacements such as $v(x,y,t)$ is assumed negligible, as stated in Section 2. Therefore the twisting 'stiffness' is due entirely to the state of spanwise tension, P. The tension per unit width is (P/w); therefore, using Eq. (3.1) the following differential equation governs the situation:

$$(P/w)\; v''\,(x,y,t) = \sigma[\ddot{v}\,(x,y,t) - x\ddot{\theta}\,] \qquad (3.7)$$

Primes have been used to signify derivatives with respect to y.

Next, two boundary conditions in the y direction are necessary to specify a solution. The first is found from the fact that the blanket is fixed to the satellite at the array root:

$$v(x,0,t) = 0, \qquad (3.8)$$

and the second is found similarly by 'tying' the blanket to the tip piece at the out-board edge. To this end, let $\alpha(t)$ be the angle of rotation of the tip-piece with respect to the spacecraft (about the pitch axis). Then the second boundary condition becomes

$$v(x,\ell,t) = -x\alpha(t) \qquad (3.9)$$

A new unknown, $\alpha(t)$, is thereby introduced, and this requires yet another equation. This extra equation is just the motion equation for the tip piece, which is now derived.

3.1.3 Tip-Piece Motion Equation

The total angle of rotation of the tip piece about the pitch axis is $\theta + \alpha$. The torque on it is due to the component of blanket tension perpendicular to the plane of the array. Again noting that the tension per unit width is P/w, the motion equation for the tip piece must therefore be

$$\frac{1}{12} mw^2 (\ddot{\theta} + \ddot{\alpha}) = (P/w) \int_{-w/2}^{w/2} v'(x,\ell,t)x \, dx \qquad (3.10)$$

which completes the specification of $\alpha(t)$.

3.1.4. Summary of Motion Equations

The equations of motion derived above will be referred to a great deal in the remainder of this section and in parts of Section 5. Therefore a summary of them is convenient.

Spacecraft:

$$I_2\ddot{\theta} = 2\sigma \int_0^{\ell} \int_{-w/2}^{w/2} \ddot{v}(x,y,t)x \, dxdy + 2(m/w)\int_{-w/2}^{w/2} \ddot{v}(x,\ell,t)x \, dx + T_{2c} + T_{2e} \qquad (3.11)$$

Blanket:

$$Pv'' = \sigma w (\ddot{v} - x\ddot{\theta})$$

$$v(x,0,t) = 0 \qquad (3.12)$$

$$v(x,\ell,t) = -x\alpha(t)$$

Tip-piece:

$$\frac{1}{12} mw^3(\ddot{\theta} + \ddot{\alpha}) = P\int_{-w/2}^{w/2} v'(x,\ell,t)x \, dx \qquad (3.13)$$

Particular solutions of these equations may be referred to as 'natural' motions and they are the subject of the next section.

3.2 Natural Motions

The equations of motion, as given by Eqs. (3.11-13) are partial differential equations and, in general, such systems can be difficult to solve. However, if the external disturbances, as represented by T_{2e}, were absent and if the control torques, as represented by T_{2c}, were also absent, then the resulting motion is reasonably called the 'natural' motion. Reflecting on the physical situation - a rigid body with elastic appendages - the natural motions are known from experience to be rigid rotation and harmonic oscillations. These oscillations are now examined in some depth.

3.2.1 Constrained Motions

Natural vibration modes for the array alone are derived first. It is assumed that the centre body has zero pitch and this condition suggests the terminology 'constrained' motion. Furthermore, since by hypothesis

$$\theta(t) \equiv 0 \qquad (3.14)$$

this equation replaces the spacecraft equation of motion, Eq. (3.11), and only Eqs. (3.12) and (3.13) are used. Rewriting these, we now have

$$Pv'' = \sigma w \ddot{v} \tag{3.15}$$

$$v(x,0,t) = 0 \qquad v(x,\ell,t) = -x\alpha(t) \tag{3.16}$$

$$\frac{1}{12} mw^3 \ddot{\alpha} = P \int_{-w/2}^{w/2} v'(x,\ell,t)\, x\, dx \tag{3.17}$$

The time dependence is first removed, in the customary way, by the separation of variables*:

$$\left.\begin{aligned} v(x,y,t) &= -x \sum_{n=1}^{\infty} A_n(y) \cos\Omega_n t \\ \alpha(t) &= \sum_{n=1}^{\infty} A_n(\ell) \cos\Omega_n t \end{aligned}\right\} \tag{3.18}$$

The indicated substitution produces

$$P A_n''(y) + \sigma w \Omega_n^2 A_n(y) = 0 \tag{3.19}$$

as the (ordinary) differential equation for $A_n(y)$, $(n = 1,2,\ldots)$ together with the boundary conditions

$$A_n(0) = 0 \tag{3.20}$$

$$P A_n'(\ell) = m \Omega_n^2 A_n(\ell) \tag{3.21}$$

The second boundary condition in Eq. (3.16) is automatically satisfied by Eq. (3.18). The dependence on x assumed in Eq. (3.18), which has now been validated, is a particularly simple one; it is seen that the chordwise cross-section (to borrow a term from aircraft wing design) of the array, in twist, is a straight line. Other shapes are not present in the steady state.

It is not difficult to satisfy Eqs. (3.19-21):

---

* To assist in the distinction between the constrained modes treated here and the unconstrained modes of the sequel, upper case notation for the former will be used, as distinct from lower case for the latter.

$$A_n(y) \sim \sin(\Omega_n^* y/\ell) \tag{3.22}$$

where the dimensionless natural frequency, Ω_n^*, has been defined as

$$\Omega_n^* = \left(\frac{\sigma w \ell^2}{P} \right)^{1/2} \Omega_n \tag{3.23}$$

To satisfy the condition expressed by Eq. (3.21) the Ω_n^* (n = 1,2,...) must be the countably infinite set of roots of the transcendental equation

$$m^* \Omega^* \sin\Omega^* = \cos\Omega^* \tag{3.24}$$

where

$$m^* = \frac{m}{\sigma w \ell} , \tag{3.25}$$

that is, the ratio of the tip-piece mass to the blanket mass. Equation (3.24) is the characteristic equation for the vibrational frequencies. The sketch shown in Fig. 6 shows that, for all but the first mode or so,

$$\Omega_n^* \tilde{=} (n-1)\ \pi \tag{3.26}$$

The first five values of Ω_n^* are shown plotted vs. I_{2b}^*, the dimensionless body inertia (see Eq.(3.45)) in Fig.6. Of course the Ω_n^* do not depend on I_{2b}^* and so the 'curves' are actually straight horizontal lines. This seemingly pointless plot is made to facilitate comparison with the unconstrained natural frequencies which are plotted in Fig. 7.

An orthogonality condition can be proven for these modes, namely

$$\Xi_{nm} = 0 \tag{3.27}$$

where, for brevity,

$$\Xi_{nm} = \frac{1}{6} \sigma w^3 \int_0^\ell A_n(y) A_m(y) dy + \frac{1}{6} m w^2 A_n(\ell) A_m(\ell) \tag{3.28}$$

This can be demonstrated from Eq. (3.22) but it is ordinarily easier to proceed directly from the differential equation, in this case Eq. (3.19). The steps below do not require detailed comment.

$$P \int_0^\ell A_m(y) A_n''(y) dy + \sigma w\, \Omega_n^2 \int_0^\ell A_m(y) A_n(y) dy = 0$$

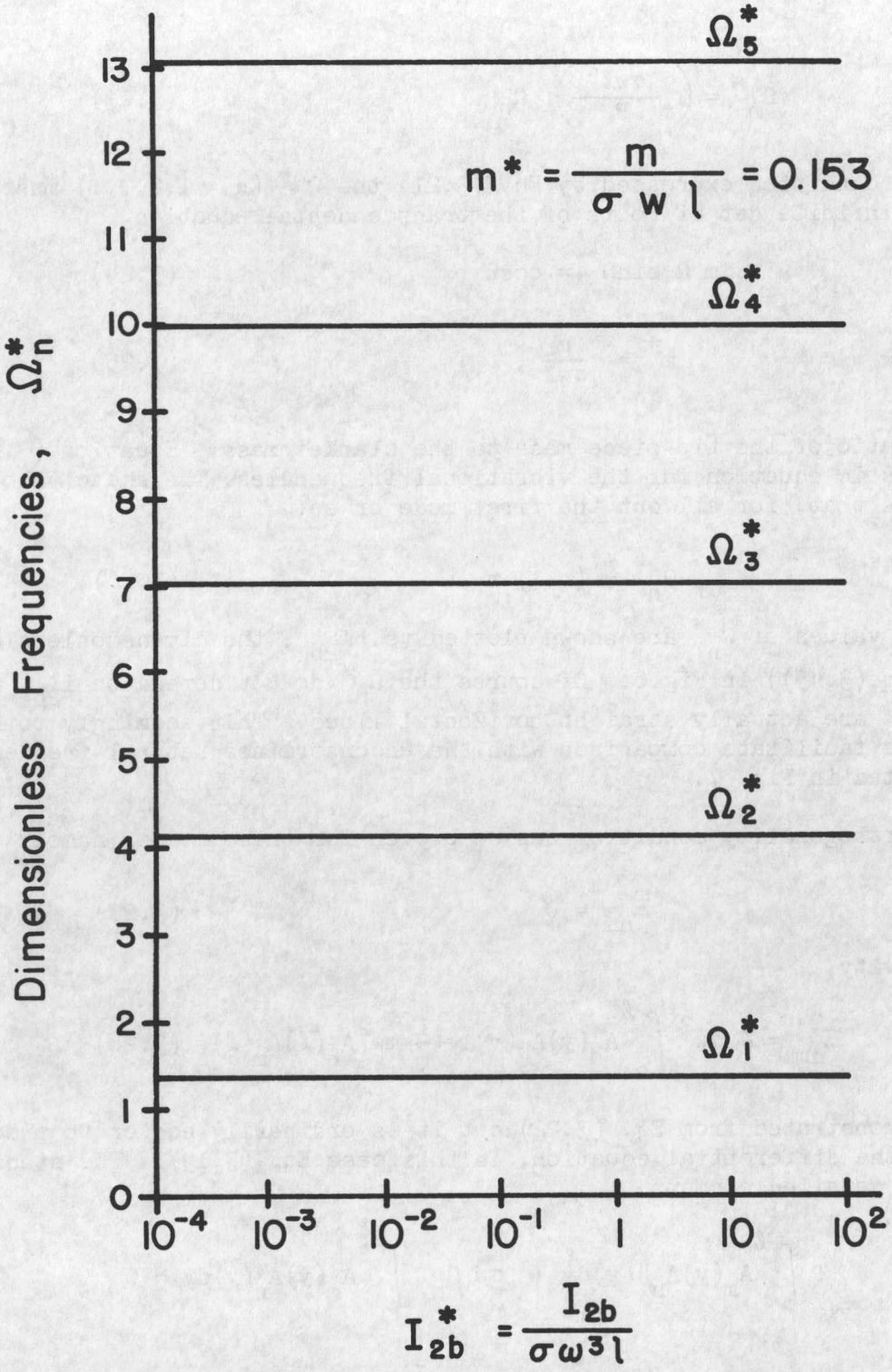

FIG. 6: Dependence of Constrained Frequencies on I_{2b}^*

$$P\, A_m(y)A_n'(y)\Big|_0^{\ell} - P\int A_n'(y)A_m'(y)dy$$

$$+ \sigma_w \Omega_n^{\,2} \int_0^{\ell} A_n(y)A_m(y)dy = 0$$

$$m\,\Omega_n^{\,2} A_m(\ell)A_m(\ell) + \sigma_w \Omega_n^{\,2} \int_0^{\ell} A_n(y)A_m(y)dy$$

$$= P\int_0^{\ell} A_n'(y)\, A_m'(y)\, dy$$

That is

$$\frac{6}{w^2}\,\Omega_n^{\,2}\,\Xi_{nm} = P\int_0^{\ell} A_n'(y)A_m'(y)dy \qquad (3.29)$$

Rewriting Eq. (3.29) with the subscripts n and m interchanged, and noting that $\Xi_{mn} = \Xi_{nm}$,

$$\frac{6}{w^2}\,\Omega_m^{\,2}\,\Xi_{nm} = P\int_0^{\ell} A_n'(y)A_m'(y)dy \qquad (3.30)$$

Subtracting Eq. (3.30) from Eq. (3.29) and realizing from Eq. (3.24) that the frequencies are always distinct ($\Omega_n \neq \Omega_m$ if $n \neq m$) proves the condition of Eq. (3.27).

Finally, the factor of proportionality implied in Eq. (3.22) is specified by a normalization condition:

$$\Xi_{nn} = \sigma\, w^3 \ell \qquad (3.31)$$

When the necessary integration of Eq. (3.28) is done, the mode shape is uniquely specified ($\eta = y/\ell$)

$$A_n(y) = \left[\frac{12}{1 + m^*\sin^2\Omega_n^*}\right]^{1/2} \sin\Omega_n^*\eta \qquad (3.32)$$

This completes the derivation of the constrained modes. The manner in which they may be utilized in a study of general spacecraft motion is discussed in Section 3.2.1.

3.2.2 Unconstrained Motions

Natural vibrations of the spacecraft as a whole are clearly of interest. These are termed 'unconstrained' motions and Eqs. (3.11-13) are used with

$$T_{2c} \equiv 0; \qquad T_{2e} \equiv 0 \qquad (3.33)$$

The time dependence is removed via the substitutions (Ref.1)

$$v(x,y,t) = -x \sum_{n=1}^{\infty} \alpha_n(y)\cos\omega_n t$$

$$\alpha(t) = \sum_{n=1}^{\infty} \alpha_n(\ell)\cos\omega_n t \tag{3.34}$$

$$\theta(t) = \sum_{n=1}^{\infty} \theta_n \cos\omega_n t$$

First, Eq. (3.12) leads to

$$P\,\alpha_n''(y) + \sigma_w\,\omega_n^2\alpha_n(y) = -\sigma_w\;\omega_n^2\theta_n \tag{3.35}$$

as the (ordinary) differential equation for $\alpha_n(y)$, (n = 1,2,...) together with the boundary conditions

$$\alpha_n(0) = 0 \tag{3.36}$$

$$P\,\alpha_n'(\ell) = m\omega_n^2\alpha_n(\ell) + m\omega_n^2\theta_n \tag{3.37}$$

The second boundary condition in Eq. (3.12) is automatically satisfied by Eq. (3.34). To complete the unique specification of the modes, the spacecraft motion equation, Eq. (3.11) is invoked:

$$\omega_n^2\,(I_2\theta_n - f_n) = 0 \tag{3.38}$$

where, for brevity,

$$-f_n = \frac{1}{6}\sigma_w^3\int_0^{\ell}\alpha_n(y)dy + \frac{1}{6}\,mw^2\,\alpha_n(\ell) \tag{3.39}$$

Immediately from Eq. (3.38) the possible roots $\omega = 0,0$ are recognized, corresponding to a constant angular displacement, and angular rate. The mode shape is clearly specified by putting $\omega = 0$ in Eqs. (3.35-37):

$$\alpha_n(y) \equiv 0 \qquad n = 1,2 \tag{3.40}$$

and, from the first of Eq. (3.34),

$$v(x,y,t) \equiv 0 \tag{3.41}$$

showing that, not unexpectedly, there is in fact no twisting at all. These are,

therefore, rigid modes and they are certainly important since they are the primary raison d'etre the attitude control system. However, from the 'flexibility' standpoint they are not really flexible modes, and the designation "n = 1" will now be given to the first 'flexible' mode. This is purely a convenience and an alternative convention proves more suitable in connection with roll-yaw flexibility (Sect. 4).

Having thus dealt with the factor $\omega^2 = 0$, Eq. (3.38) becomes

$$I_2\theta_n = f_n \tag{3.42}$$

and this equation, together with Eqs. (3.35-37) specify the natural 'unconstrained' modes. It is not difficult to satisfy Eqs. (3.35-37):

$$\alpha_n(\eta) = \theta_n[\cos\omega_n^*\eta - 6\, I_{2b}^*\, \omega_n^*\, \sin\omega_n^*\eta - 1] \tag{3.43}$$

where $\eta = y/\ell$ and the dimensionless natural frequency, ω_n^*, has been defined as

$$\omega_n^* = \left(\frac{\sigma_w \ell^2}{P} \right)^{1/2} \omega_n \tag{3.44}$$

and the dimensionless body pitch inertia is

$$I_{2b}^* = \frac{I_{2b}}{\sigma_w^3 \ell} \tag{3.45}$$

To satisfy Eq. (3.42), the ω_n^* (n = 1,2,...) must be the countably infinite set of roots of the transcendental equation

$$(6m^*\, I_{2b}^*\omega^{*2} - 1)\, \sin\omega^* = (6\, I_{2b}^* + m^*)\, \omega^*\, \cos\omega^* \tag{3.46}$$

It is physically plausible that the frequencies of the unconstrained modes should approach those of the constrained modes as $I_{2b} \to \infty$. That is

$$\lim_{I_{2b}^* \to \infty} \left\{\text{unconstrained modes}\right\} = \left\{\text{constrained modes}\right\} \tag{3.47}$$

In particular, if the limit $I_{2b}^* \to \infty$ is taken in Eq. (3.46) the characteristic equation reduces to

$$m^*\, \omega^*\, \sin\omega^* = \cos\omega^* \tag{3.48}$$

which is precisely Eq. (3.24) - the characteristic equation for the constrained modes.

Moreover, the Eq. (3.46) is symmetrical with respect to the parameters m^* and $6I_{2b}^*$; although the case where the tip mass becomes infinite is not of practical importance (at least for the CTS design) some thought will verify that such a symmetry should exist.

The first few values of ω_n^* are shown plotted vs. I_{2b}^* in Fig. 7. It is particularly interesting to compare this figure with Fig. 6. Not only do the Ω_n^* form the asymptotes for ω_n^* as $I_{2b}^* \to \infty$, as indicated by Eq. (3.47), they also bound the ω_n^* for all I_{2b}^*. That is

$$\Omega_1^* < \omega_1^* < \Omega_2^* < \omega_2^* < \text{----} \tag{3.49}$$

Just as the lower limits for ω_n^* (as $I_{2b}^* \to \infty$) are Ω_n^*, so the upper limits ($I_{2b}^* \to 0$) are the roots of

$$\tan\omega^* = -m^*\omega^* \tag{3.50}$$

which are denoted λ_n^* ($n = 1,2,\ldots$). Thus Inequality (3.49) is sharpened to become

$$\Omega_1^* < \omega_1^* < \lambda_1^* < \Omega_2^* < \omega_2^* < \lambda_2^* < \text{----} \tag{3.51}$$

An orthogonality condition can be proven for the unconstrained modes, namely,

$$\xi_{nm} = I_2\theta_n\theta_m \tag{3.52}$$

where, for brevity,

$$\xi_{nm} = \frac{1}{6}\sigma w^3\int_o^\ell \alpha_n(y)\alpha_m(y)dy + \frac{1}{6}mw^2\,\alpha_n(\ell)\alpha_m(\ell) \tag{3.53}$$

This can be demonstrated from Eq. (3.43) but it is more easily proved directly from the differential equation, in this case Eq. (3.35). The steps are as follows:

$$P\int_o^\ell \alpha_m(y)\alpha_n''(y)dy + \sigma w\ \omega_n^2\int_o^\ell \alpha_m(y)\alpha_n(y)dy$$

$$= -\sigma w\,\omega_n^2\,\theta_n\int_o^\ell \alpha_m(y)dy$$

$$P\,\alpha_m(y)\alpha_n'(y)\Big|_o^\ell - P\int_o^\ell \alpha_n'(y)\alpha_m'(y)dy$$

$$+ \sigma w\,\omega_n^2\int_o^\ell \alpha_n(y)\alpha_m(y)dy = -\sigma w\,\omega_n^2\theta_n\int_o^\ell \alpha_m(y)dy$$

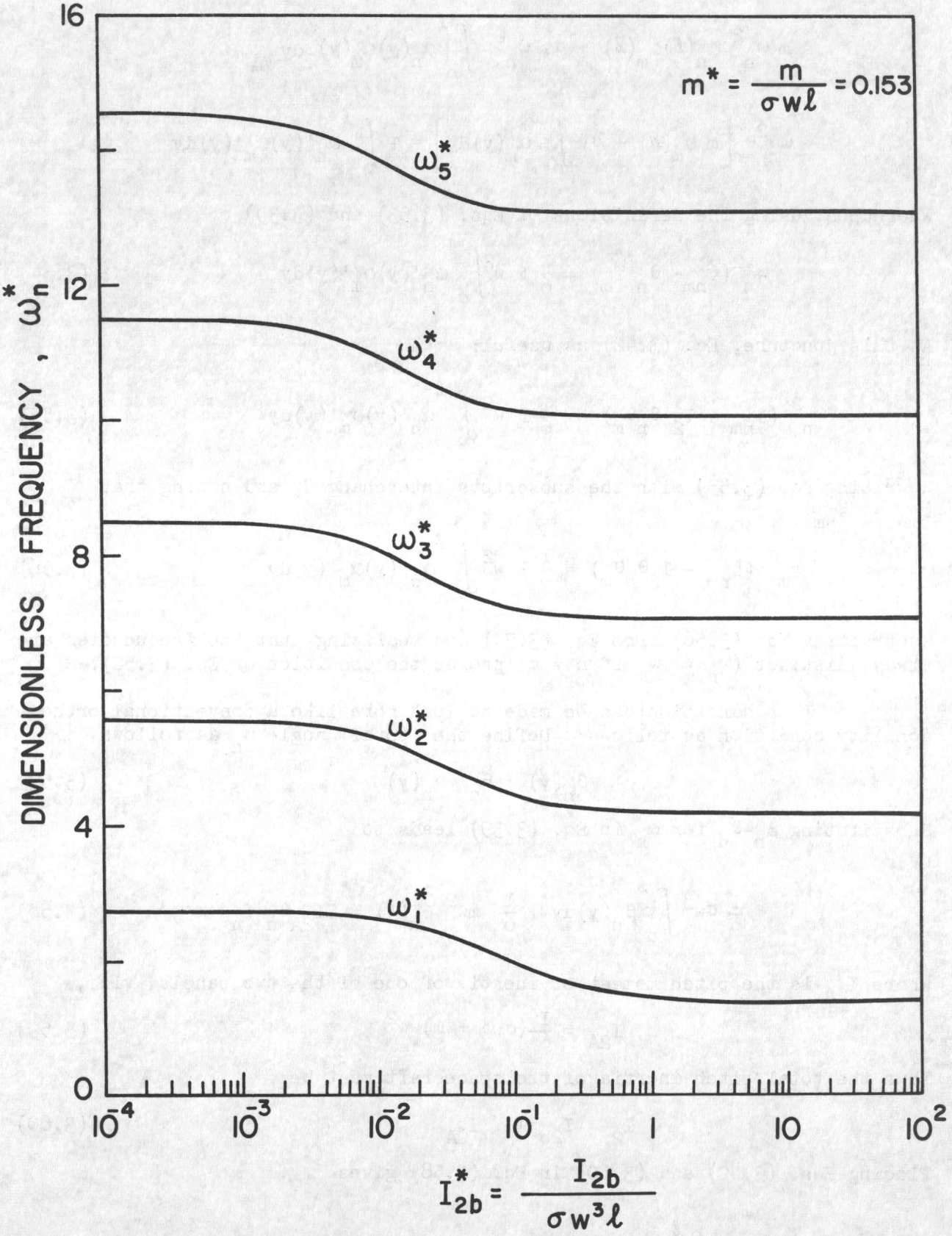

FIG. 7: Dependence of Unconstrained Frequencies on I_{2b}^*

$$m\omega_n^2\alpha_n(\ell)\alpha_m(\ell) + \sigma_w\omega_n^2\int_o^\ell \alpha_n(y)\alpha_m(y)\,dy$$

$$+\omega_n^2\theta_n\left[m\alpha_m(\ell) + \sigma_w\int_o^\ell \alpha_m(y)dy\right] = P\int_o^\ell \alpha_n'(y)\alpha_m'(y)dy$$

Whereupon, using the definitions of Eqs. (3.53) and (3.39)

$$\omega_n^2(\xi_{nm} - \theta_n f_m) = \frac{1}{6} P w^2\int_o^\ell \alpha_n'(y)\alpha_m'(y)dy \tag{3.54}$$

At this juncture, Eq. (3.42) as useful:

$$\omega_n^2(\xi_{nm} - I_2\theta_n\theta_m) = \frac{1}{6} P w^2\int_o^\ell \alpha_n'(y)\alpha_m'(y)dy \tag{3.55}$$

Rewriting Eq. (3.55) with the subscripts interchanged, and noting that $\xi_{mn} = \xi_{nm}$,

$$\omega_m^2(\xi_{nm} - I_2\theta_n\theta_m) = \frac{1}{6} P w^2\int_o^\ell \alpha_n'(y)\alpha_m'(y)dy \tag{3.56}$$

Subtracting Eq. (3.56) from Eq. (3.55) and realizing that the frequencies are always distinct ($\omega_n \neq \omega_m$ if $n \neq m$) proves the condition of Eq. (3.52).

This condition can be made to look more like a conventional orthogonality condition as follows: Define the 'total' angle β_n as follows

$$\beta_n(y) = \theta_n + \alpha_n(y) \tag{3.57}$$

Substituting $\beta_n - \theta_n$ for α_n in Eq. (3.39) leads to

$$\frac{1}{6}\sigma_w^3\int_o^\ell \beta_n(y)dy + \frac{1}{6} mw^2\beta_n(\ell) = 2I_{2A}\theta_n - f_n \tag{3.58}$$

where I_{2A} is the pitch moment of inertia of one of the two panels, viz.,

$$I_{2A} = \frac{1}{6}(\sigma_w\ell + m)w^2 \tag{3.59}$$

Thus the total pitch inertia of the spacecraft must be

$$I_2 = I_{2b} + 2I_{2A} \tag{3.60}$$

Placing Eqs. (3.42) and (3.60) in Eq. (3.58) gives

$$\frac{1}{6}\sigma_w^3\int_o^\ell \beta_n(y)dy + \frac{1}{6} mw^2\beta_n(\ell) = -I_{2b}\theta_n \tag{3.61}$$

Next, substituting $\beta_n - \theta_n$ for α_n in Eq. (3.52) leads to

$$\frac{1}{6}\,\rho w^3 \int_0^{\ell} \beta_n(y)\beta_m(y)dy + \frac{1}{6}\,mw^2\beta_n(\ell)\,\beta_m(\ell) + I_{2b}\,\theta_n\theta_m = 0 \tag{3.62}$$

where the prepared relation (3.61) has been inserted. In this form (Eq. (3.62)) the condition looks more like an orthogonality condition, wherein a generalized inner product is found to be zero.

Finally, the value of θ_n is specified by a normalization condition:

$$\xi_{nn} = \sigma w^3 \ell \tag{3.63}$$

More explicitly, Eq. (3.43) is substituted in Eq. (3.53) to give

$$\theta_n = \left[\frac{6}{\int_0^1 \left\{\frac{\alpha_n(\eta)}{\theta_n}\right\}^2 d\eta + m^*\left\{\frac{\alpha_n(1)}{\theta_n}\right\}^2}\right]^{1/2} \tag{3.63a}$$

where $\alpha_n(\eta)/\theta_n$ is implied by Eq. (3.43).

This completes the derivation of the unconstrained modes. The manner in which they may be utilized in a study of general spacecraft motion is discussed next. Further remarks on the comparison of the constrained and unconstrained modes will be postponed until after this next stage has been investigated.

3.3 General Motion

Following the general outline of Section 1.2, the next step is to expand the general flexible motion of array twisting in terms of the natural mode shapes. Since two classes of natural motion have been derived, each will be considered in turn.

3.3.1 Expansion in Terms of Constrained Modes

The equations which must be satisfied are Eqs. (3.11-13). The modal representation is accomplished by expansions in terms of generalized coordinates Q_n.

$$\left.\begin{aligned} v(x,y,t) &= -x\sum_{n=1}^{\infty} A_n(y)Q_n(t) \\ \alpha(t) &= \sum_{n=1}^{\infty} A_n(\ell)Q_n(t) \end{aligned}\right\} \tag{3.64}$$

When these are inserted in Eq. (3.12) there results:

$$\sum_{n=1}^{\infty} (\ddot{Q}_n + \Omega_n^2 Q_n)\, A_n(y) + \ddot{\theta} = 0 \tag{3.65}$$

Similarly, when inserted in Eq. (3.13), one obtains

$$\sum_{n=1}^{\infty} (\ddot{Q}_n + \Omega_n^2 Q_n) A_n(\ell) + \ddot{\theta} = 0 \tag{3.66}$$

Finally, when inserted in the spacecraft motion equation, Eq. (3.11), one finds

$$I_2 \ddot{\theta} = \sum_{n=1}^{\infty} F_n \ddot{Q}_n + T_{2c} + T_{2e} \tag{3.67}$$

where (compare with Eq. (3.39))

$$-F_n = \frac{1}{6}\, \sigma w^3 \int_0^{\ell} A_n(y)\, dy + \frac{1}{6}\, m w^2 A_n(\ell) \tag{3.68}$$

The integration, using Eq. (3.32), gives for F_n:

$$F_n = -\frac{1}{6\Omega_n^*} \left[\frac{12}{1 + m^* \sin^2 \Omega_n^*} \right]^{1/2} \sigma w^3 \ell \tag{3.69}$$

The equations for the modal coordinates may be uncoupled as follows. In view of the orthogonality and normality conditions, Eq. (3.27) and (3.31), form the following combination:

$$\frac{1}{6}\, \sigma w^3 \int_0^{\ell} [\text{Eq.}(3.65)] A_m(y)\, dy + \frac{1}{6}\, m w^2 [\text{Eq.}(3.66)]\, A_m(\ell) = 0 \tag{3.70}$$

that is,

$$\sum_{n=1}^{\infty} \Xi_{nm} (\ddot{Q}_n + \Omega_n^2 Q_n) = F_m \ddot{\theta} \tag{3.71}$$

Then the conditions ($\Xi_{nm} = 0$, $n \neq m$) and ($\Xi_{nm} = \sigma w^3 \ell$) may be invoked to complete the uncoupling

$$\ddot{Q}_m + \Omega_m^2 Q_m = \left(\frac{F_m}{\sigma w^3 \ell} \right) \ddot{\theta} \quad (m = 1,2,\ldots) \tag{3.72}$$

This set of equations, along with Eq. (3.67), completely specify the system.

In order to arrive at transfer functions for the conventional block diagram, Laplace-transformed variables will be denoted by an overbar. Thus, defining

$$s^2\ \bar{\Theta} = (\bar{T}_{2c} + \bar{T}_{2e})/I_2 \tag{3.73}$$

(the Laplace transform of the rigid response), the system equations are combined to give

$$\bar{\theta} = \bar{\Theta} + \left(\sum_{n=1}^{\infty} \frac{s^2 K_n}{s^2 + \Omega_n^2} \right) \bar{\theta} \tag{3.74}$$

where the dimensionless constants K_n (n = 1,2,...) are referred to as 'modal gains' and are calculated from

$$K_n = \frac{F_n^2}{\sigma_w^3 \ell\ I_2} \tag{3.75}$$

From Eq. (3.69) then, the result given in Ref. 3 is obtained:

$$K_n = \frac{1}{3I_2^* \Omega_n^{*2}(1 + m^* \sin^2 \Omega_n^*)} \tag{3.76}$$

Here I_2^* is the expected notation for

$$I_2^* = \frac{I_2}{\sigma_w^3 \ell} = I_{2b}^* + \frac{1}{6}(1 + m^*) \tag{3.77}$$

Note that these gains are always positive.

In some respects it is more illuminating to define dimensional gains K_n' by

$$K_n' = K_n\ I_2 \tag{3.78}$$

The expansion then takes the form

$$I_2\ s^2\ \bar{\theta} = \bar{T}_{2c} + \bar{T}_{2e} + \left(\sum_{n=1}^{\infty} \frac{s^2 K_n'}{s^2 + \Omega_n^2} \right)\ s^2 \bar{\theta} \tag{3.79}$$

where K_n' now depends only on array parameters.

The gains K_n are independent of the tension P; they depend only on I_{2b}^* and m^*.

The expansion corresponding to Eq. (3.74) is shown in Fig. 8 and the first few gains, as given by Eq. (3.76) are plotted in Fig. 9. Small damping terms can be included in the customary somewhat arbitrary fashion.(see also Fig.30).

In the limit as $I_{2b}^* \to \infty$, $K_n \to 0$ (from Eqs. (3.76) and (3.77)), while

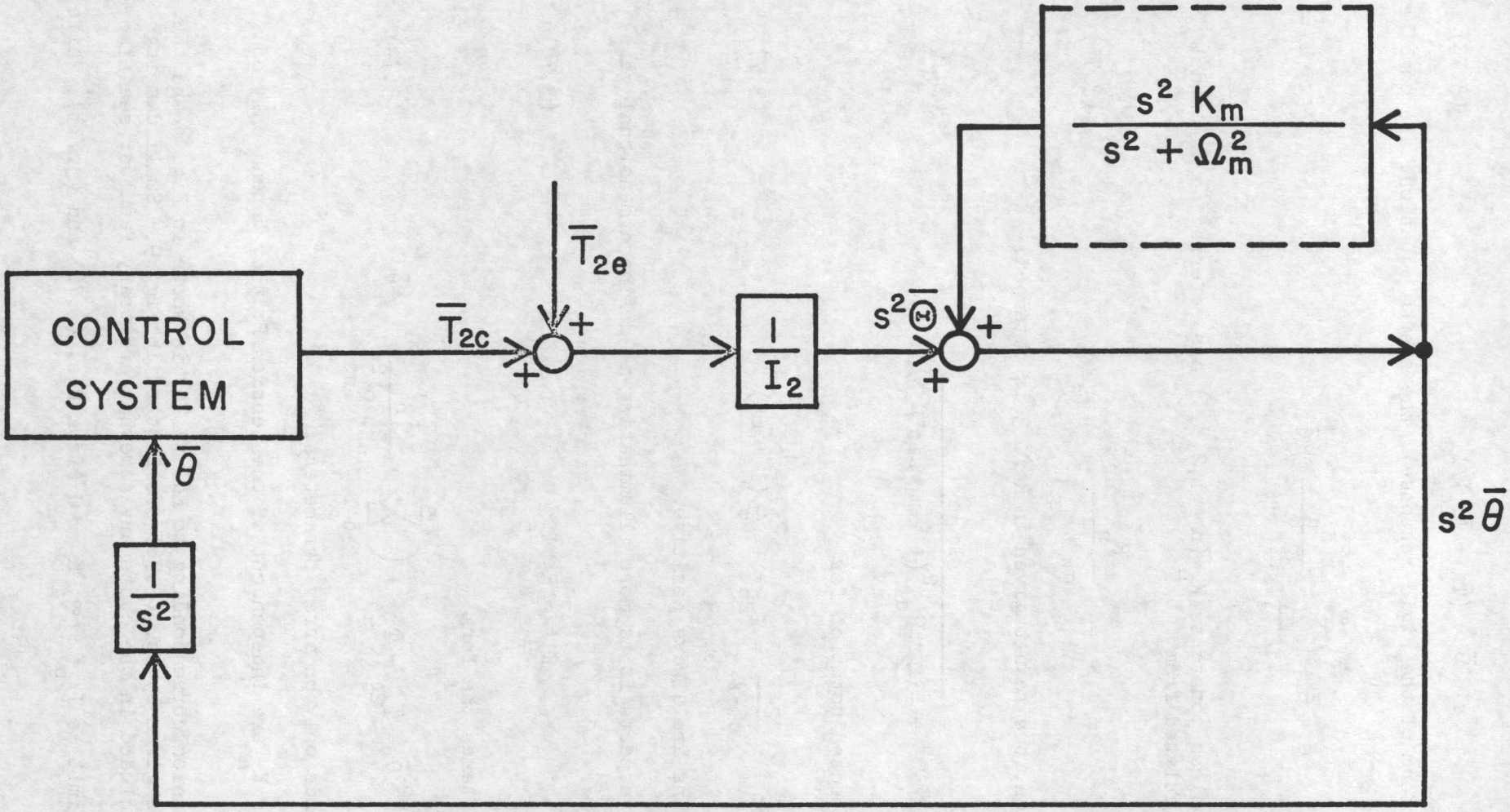

FIG. 8: Pitch Attitude Control Block Diagram Incorporating Constrained Twisting Modes

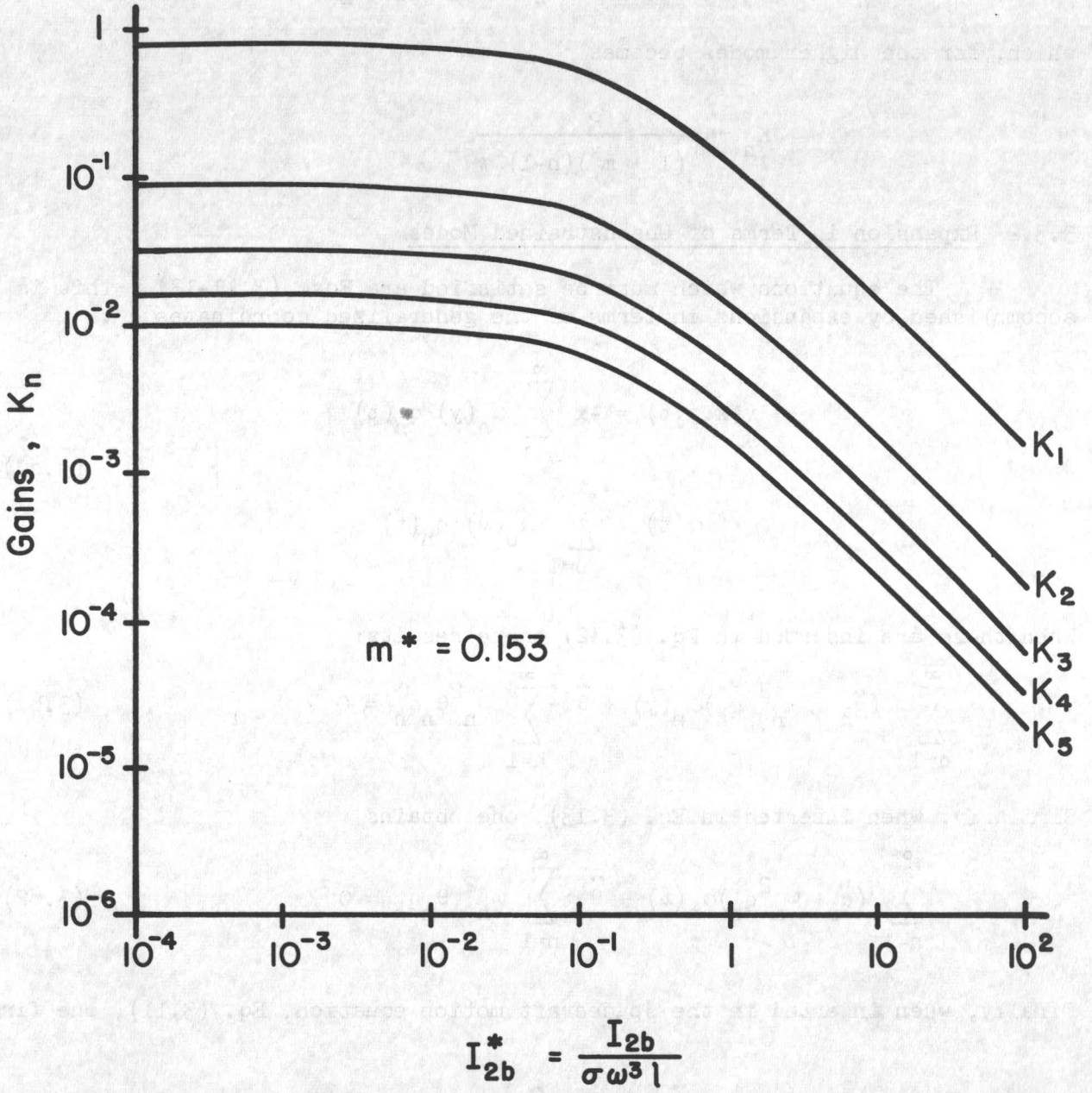

FIG. 9: Dependence of Constrained Gains on I_{2b}*

for $I_{2b}^* \to 0$, K_n approaches the values

$$K_n \to \frac{2}{(1 + m^*)\,\Omega_n^{*2}(1 + m^* \sin^2 \Omega_n^*)}$$

which, for the higher modes becomes

$$K_n \to \frac{2}{(1 + m^*)(n-1)^2 \pi^2}$$

3.3.2 Expansion in Terms of Unconstrained Modes

The equations which must be satisfied are Eqs. (3.11-13). This is accomplished by expansions in terms of the generalized coordinates q_n.

$$\left.\begin{aligned} v(x,y,t) &= -x \sum_{n=1}^{\infty} \alpha_n(y)\, q_n(t) \\ \alpha(t) &= \sum_{n=1}^{\infty} \alpha_n(\ell)\, q_n(t) \end{aligned}\right\} \qquad (3.80)$$

When these are inserted in Eq. (3.12) there results:

$$\sum_{n=1}^{\infty} (\ddot{q}_n + w_n^2 q_n)\alpha_n(y) + \ddot{\theta} + \sum_{n=1}^{\infty} \omega_n^2 \theta_n q_n = 0 \qquad (3.81)$$

Similarly, when inserted in Eq. (3.13), one obtains

$$\sum_{n=1}^{\infty} (\ddot{q}_n + \omega_n^2 q_n)\alpha_n(\ell) + \ddot{\theta} + \sum_{n=1}^{\infty} \omega_n^2\, \theta_n q_n = 0 \qquad (3.82)$$

Finally, when inserted in the spacecraft motion equation, Eq. (3.11), one finds

$$I_2 \ddot{\theta} = \sum_{n=1}^{\infty} f_n \ddot{q}_n + T_{2c} + T_{2e} \qquad (3.83)$$

where, recall, f_n is given by Eq. (3.39).

To assist in uncoupling the equations for modal coordinates, q_n, define

$$\theta(t) = \sum_{n=1}^{\infty} \theta_n\, q_n(t) + \Theta(t) \qquad (3.84)$$

where, for the moment, this may be regarded as a definition of Θ. However, when Eq. (3.84) is used in conjunction with Eq. (3.83), noting also that $f_n = I_2 \theta_n$, it is seen that

$$\ddot{\Theta} = (T_{2c} + T_{2e})/I_2 \tag{3.85}$$

that is, it is just the 'rigid body' response and is identical with the Θ of Sect. 3.3.1 as given by Eq.(3.73). Next, use Eq. (3.84) in Eqs. (3.81) and (3.82) to obtain

$$\sum_{n=1}^{\infty} (\ddot{q}_n + \omega_n^2 q_n)\{\alpha_n(y) + \theta_n\} + \ddot{\Theta} = 0 \tag{3.86}$$

$$\sum_{n=1}^{\infty} (\ddot{q}_n + \omega_n^2 q_n)\{\alpha_n(\ell) + \theta_n\} + \ddot{\Theta} = 0 \tag{3.87}$$

In view of the orthogonality and normality conditions, Eqs. (3.52) and (3.63), form the following combination:

$$\frac{1}{6}\sigma w^3 \int_0^{\ell} \Big[\text{Eq.(3.86)}\Big]\,\alpha_m(y)\,dy + \frac{1}{6} m w^2 \Big[\text{Eq.(3.87)}\Big]\,\alpha_m(\ell) = 0 \tag{3.88}$$

that is,

$$\sum_{n=1}^{\infty} (\xi_{nm} - f_m \theta_n)(\ddot{q}_n + \omega_n^2 q_n) = f_m \ddot{\Theta} \tag{3.89}$$

Then the conditions ($\xi_{nm} = I_2 \theta_n \theta_m$, $n \neq m$) and ($\xi_{nn} = \sigma w^3 \ell$) may be invoked to complete the uncoupling (recall, again, that $f_m = I_2 \theta_m$)

$$\ddot{q}_m + \omega_m^2 q_m = \left(\frac{f_m}{\sigma w^3 \ell - f_m \theta_m}\right)\ddot{\Theta} \quad (m = 1,2,\ldots) \tag{3.90}$$

This set of equations, along with Eqs. (3.85) and (3.84) completely specify the system.

In order to arrive at transfer functions for the conventional block diagram, Laplace-transformed variables will be denoted by an overbar. Thus, from Eq. (3.85),

$$s^2 \bar{\Theta} = (\bar{T}_{2c} + \bar{T}_{2e})/I_2 \tag{3.91}$$

and the other equations are combined to give

$$\bar{\theta} = \bar{\Theta} + \left(\sum_{n=1}^{\infty} \frac{s^2 k_n}{s^2 + \omega_n^2} \right) \bar{\Theta} \tag{3.92}$$

where the dimensionless constants k_n (n = 1,2,---) are referred to as 'modal gains' and are calculated from

$$k_n = \frac{I_2 \theta_n^2}{\sigma w^3 \ell - I_2 \theta_n^2} \tag{3.93}$$

An explicit form for k_n may be achieved by the substitution of Eq. (3.63a) into Eq. (3.93) bu the resulting expression is rather lengthy (although still in closed form)and therefore will not be reproduced. In terms of dimensionless quantities, Eq. (3.93) is written

$$k_n = \frac{I_2^* \theta_n^2}{1 - I_2^* \theta_n^2} \tag{3.94}$$

in agreement with Ref. 1.

At first sight, it is not evident that these gains are always positive. However they are shown to be so with the aid of the following inequality:

$$\frac{1}{6} \sigma w^3 \int_0^{\ell} \left\{ \alpha_n(y) + \theta_n \right\}^2 dy + \frac{1}{6} m w^2 \left\{ \alpha_n(\ell) + \theta_n \right\}^2 \geq 0 \tag{3.95}$$

Expanding,

$$\xi_{nn} - 2 f_n \theta_n + I_{2A} \theta_n \geq 0 \tag{3.96}$$

But $\xi_{nn} = \sigma w^3 \ell$, $f_n = I_2 \theta_n$, and $2I_{2a} - I_{2A} = I_{2b}$, so inequality becomes

$$\sigma w^3 \ell - I_2 \theta_n^2 \geq I_{2b} \theta_n^2 > 0 \tag{3.97}$$

which proves the positiveness of the denominator in Eq. (3.93).

The expansion corresponding to Eq. (3.92) is shown in Fig. 10 and the first few gains, as given by Eq. (3.94) are plotted in Fig. 11. Small damping terms can be included in the customary somewhat arbitrary fashion. (see also Fig. 30).

In the limit as $I_{2b} \to \infty$, $\theta_n \to 0$ in such a way that $f_n = I_2 \theta_n$ is finite. At the other extreme, as $I_{2b} \to 0$

$$\frac{6}{\theta_n^2} \to \frac{3}{2} + m^*(1 + 2\cos\omega_n^* + \tfrac{1}{2} \cos^2 \omega_n^*) \tag{3.98}$$

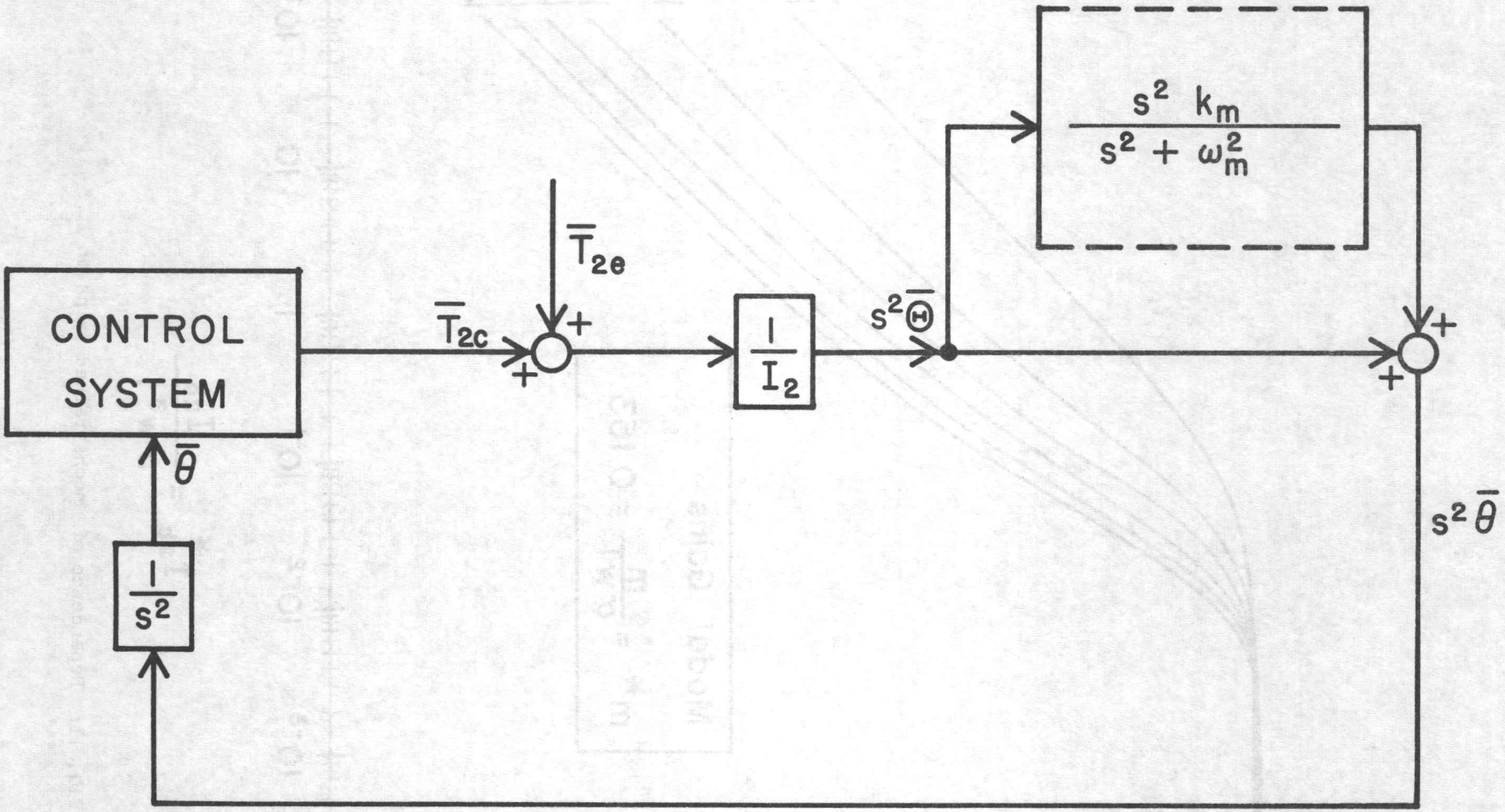

FIG. 10: Pitch Attitude Control Block Diagram Incorporating Unconstrained Twisting Modes

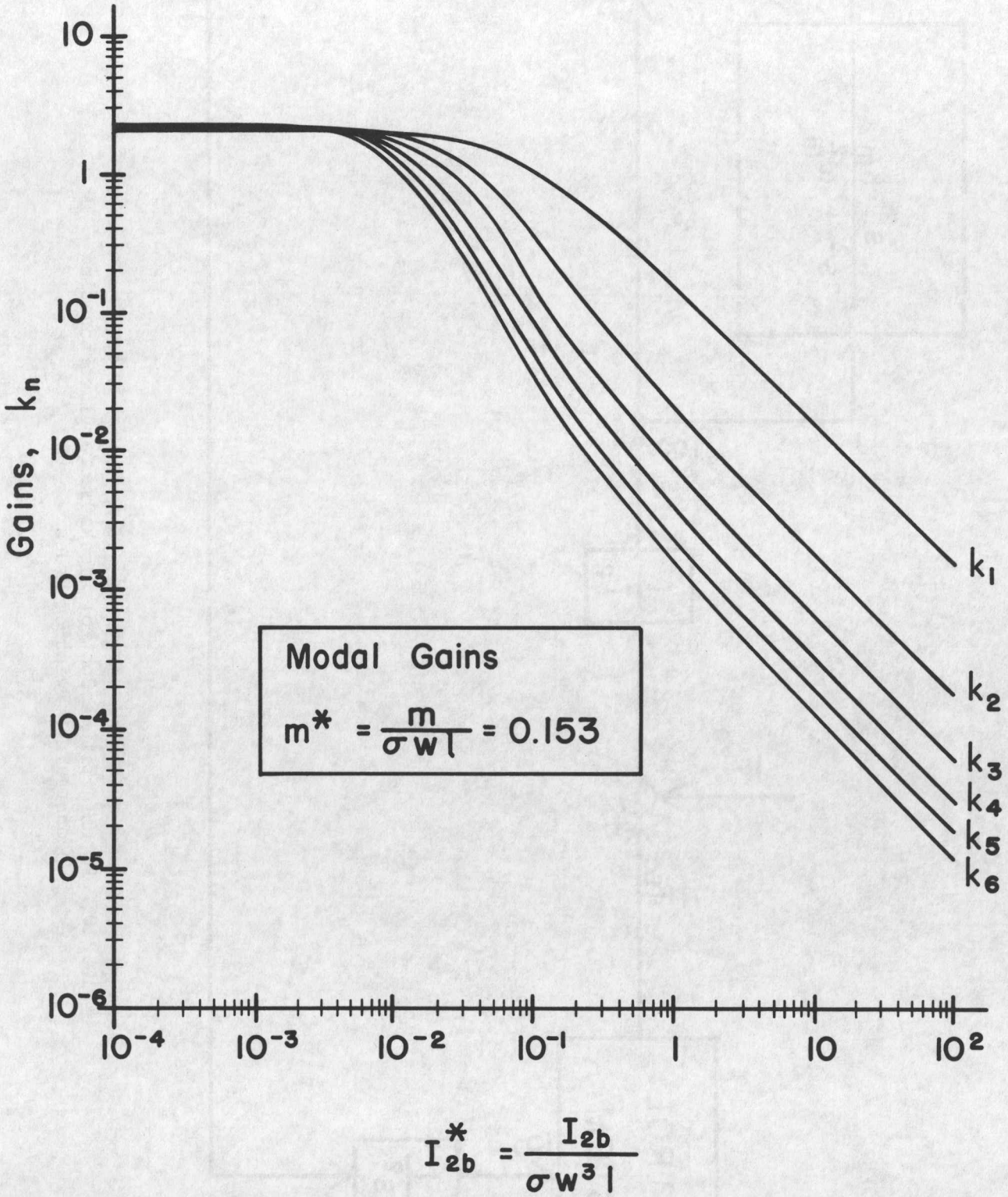

FIG. 11: Dependence of Unconstrained Gains on I_{2b}^*

whence, as $I_{2b}^* \to 0$

$$k_n \to \frac{2(1 + m^*)}{1 + m^*(4\cos\omega_n^* + \cos^2\omega_n^*)} \tag{3.99}$$

since the frequencies must satisfy Eq. (3.50), $\cos\omega_n^* \simeq 0$ for the higher modes. Therefore, for these higher modes

$$k_n \to 2(1 + m^*) \tag{3.100}$$

4. ARRAY BENDING AND ROLL-YAW ATTITUDE

Following the description of the pitch motion, this section discusses the analysis of array bending and its interaction with the spacecraft attitude control. Under the assumptions of section 2, it was shown that bending interacts only with the roll and yaw attitude, so that the pitch motion is uncoupled and may be effectively taken to be zero. The roll and yaw motions are, however, strongly coupled due to the momentum wheel along the pitch axis. It will be seen that this gyroscopic coupling adds both complexity and interest to the analysis of the natural as well as forced motion. The continuum mechanics approach remains tractable in this situation because the geometrical simplicity of the arrays is not affected. Here again as in Section 3, other formulations may be used for the flexibility analysis without changing the underlying ideas of the development.

The organization of this section is intentionally similar to Section 3 so that both the similarities and the differences may be more readily appreciated. The differential equations for the motion are derived first (Section 4.1). The natural motion in the absence of external torques is discussed in Section 4.2. Both the constrained and unconstrained varieties of natural modes are analyzed. Finally, the general array motion and its effect on the satellite attitude motion are considered in section 4.3. Alternative developments are presented in which the general motion is expanded in terms of the two types of modes, showing the method by which these modes may be incorporated into an attitude control system simulation.

4.1 Motion Equations

The coordinate system used is shown in Fig. 12., together with some basic notation. The spacecraft attitude angles are roll (ϕ) and yaw (ψ) respectively. These must be considered simultaneously due to the coupling induced by the momentum wheel. The angular momentum vector of the wheel has magnitude h and is nominally pointing along the negative y-direction. The boom centerline deflection u now enters explicitly in the flexible appendage dynamics, unlike the pitch case where the tension provided the only means of stiffness. In the absence of twisting, the deflections of the panel are independent of the chordwise coordinate, and all points at the same spanwise location y have the same deflection, v. Thus

$$v(x,y,t) = v(y,t) \tag{4.1}$$

Note that both u and v are taken relative to the undeflected boom centerline. Thus if the entire spacecraft underwent rotation as a rigid body, u and v would be zero.

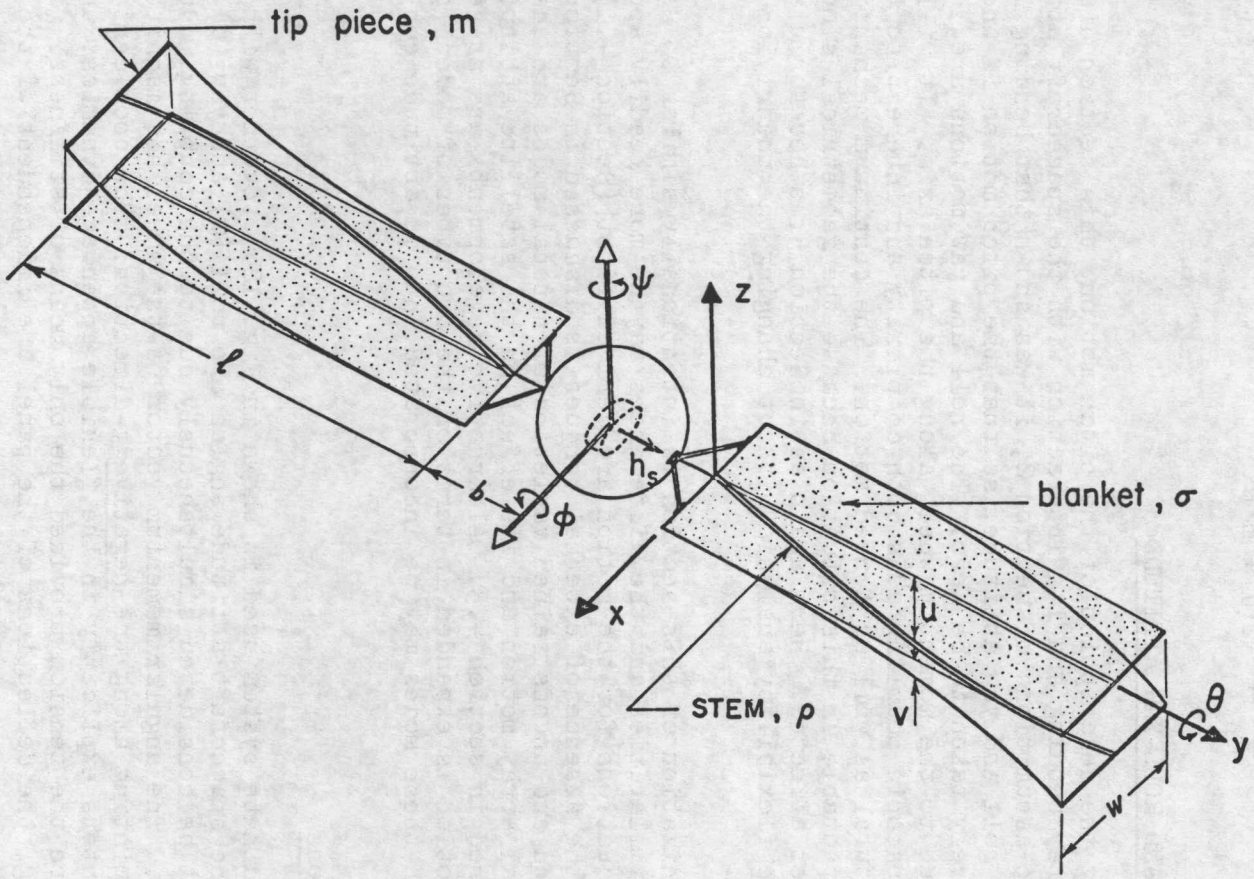

FIG. 12: Coordinate System for Roll-Yaw/Bending Motions

4.1.1 Spacecraft Motion Equations

The roll and yaw motion of the spacecraft involves angular momentum about all three coordinate axes, unlike the pitch case where only one axis need be considered. The wheel angular momentum about the pitch axis comes into the picture because, for example, even a small roll offset of the body causes a gyroscopic reaction torque, due to the wheel, about the yaw axis and vice versa. Another major difference from section 3 is that the moments of inertia are no longer constant. This is because one part of the spacecraft (the array) rotates relative to another, and unless the rotating part is axisymmetric, this causes the moments of inertia about the roll and yaw axes - fixed in the non-rotating main body - to change with time. The principal moments of inertia and the principal axes themselves are also functions of time. Expressions for the moments of inertia are derived in Appendix B. Here we note only that a roll-yaw product of inertia exists due to the panel rotation.

Further simplification of the motion equations is made below by neglecting terms arising due to the orbital motion of the spacecraft center of mass, so that the coordinate system of Fig. 12 is taken to be fixed relative to inertial space. This is justified because the natural frequencies of interest are known to be much higher than the orbital rate. In the actual simulation of the spacecraft motion, the terms omitted may be included as "external" i.e., forcing torques. This also applies to gravity-gradient torques and other gravitational and environmental perturbations. Change in angular momentum due solely to time variation of the moments of inertia is also ignored. It is of the same order of magnitude as the gravity-gradient torques, if the array rotation is continuous. For the case of array stepping considered in section 5, rates of change of the inertia moments can be much greater than the continuous case, for brief periods. The effect of this may again be included as an external torque if significant for a particular satellite. All the terms omitted here can be included in the analysis if need be, but in the discussion of this report, these merely serve to complicate the details and perhaps to obscure significant aspects of the motion.

Let $\underline{\Omega}_s$ be the spacecraft angular velocity vector; then for small roll and yaw angles (taking pitch to be zero for convenience), the angular momentum $\underline{H}_R$ of the spacecraft considered as a rigid body is

$$\underline{H}_R = \begin{bmatrix} I_{11} & 0 & I_{13} \\ 0 & I_2 & 0 \\ I_{13} & 0 & I_{33} \end{bmatrix} \begin{pmatrix} \dot{\varphi} \\ 0 \\ \dot{\psi} \end{pmatrix} + \begin{pmatrix} 0 \\ -h \\ 0 \end{pmatrix} \qquad (4.2)$$

where we have used the fact that for small angles,

$$\underline{\Omega}_s = (\dot{\varphi},\ 0,\ \dot{\psi})^T \qquad (4.3)$$

In addition to $\underline{H}_R$, there is an angular momentum due to the flexible deflections of the panels and boom, denoted $\underline{H}_F$. For small deflections it can be simply added to $\underline{H}_R$. Now $\underline{H}_F$ only consists of components along an axis lying in the plane of the solar panels (no in-plane bending). If γ be the angle between the panel plane and the roll-pitch plane, we have

$$\underline{H}_F = \begin{pmatrix} H_F \cos\gamma \\ 0 \\ -H_F \sin\gamma \end{pmatrix}$$

where

$$H_F = 2\int_0^{\ell} (b+y)\ (\rho\dot{u} + \sigma w\ \dot{v})dy + 2m\ (b+\ell)\ \dot{u}(\ell) \qquad (4.4)$$

The factor of 2 results from the fact that two flexible appendages are involved, one on each side of the main body. Here b is the distance from the spacecraft center of mass to the boom root. Note also that the net flexible angular moment would be zero in the case of symmetric bending.

The spacecraft motion equation is now

$$\dot{\underline{H}} + \underline{\Omega}_s \times \underline{H} = \underline{T} \qquad (4.5)$$

where

$$\underline{H} = \underline{H}_R + \underline{H}_F = \begin{pmatrix} I_{11}\dot{\Phi} + 0 + I_{13}\dot{\psi} + H_F\cos\gamma \\ I_{33}\dot{\psi} + I_{13}\dot{\Phi} - H_F\sin\gamma \end{pmatrix}$$

Here T denotes the external torques acting on the spacecraft. In expanding (4.5), the usual small-angle approximations are used, neglecting products of small quantities. The roll and yaw component of the motion equations are then

$$\begin{aligned} I_{11}\ddot{\Phi} + I_{13}\ddot{\psi} + h\dot{\psi} + f\cos\gamma &= T_{c1} + T_{e1} \quad (+\omega_o h\Phi)^* \\ I_{33}\ddot{\psi} + I_{13}\ddot{\Phi} - h\dot{\Phi} - f\sin\gamma &= T_{c3} + T_{e3} \quad (+\omega_o h\psi)^* \end{aligned} \qquad (4.6)$$

where T_{c1} and T_{c3} are control torques and T_{e1} and T_{e3} are external disturbance torques, and

$$f = \dot{H}_F = 2\int_0^{\ell} (b+y)\ (\rho\ddot{u} + \sigma w\ \ddot{v})dy + 2m(b+\ell)\ \ddot{u}(\ell) \qquad (4.7)$$

The pitch component of (4.5) simply gives h = constant because zero pitch torques, are assumed in keeping with the assumption of pitch - roll/yaw uncoupling. As mentioned above, small terms omitted in (4.6) may be modelled as part of the external torques.

Equation (4.6) can be put into a particularly elegant form, which is useful in the ensuing discussion, as follows. We multiply the first of (4.6) by $\sin\gamma$ and the second by $\cos\gamma$, and add to obtain

$$(I_{11}\sin\gamma + I_{13}\cos\gamma)\ \ddot{\Phi} + (I_{33}\cos\gamma + I_{13}\sin\gamma)\ \ddot{\psi} - h(\dot{\Phi}\cos\gamma - \dot{\psi}\sin\gamma)$$

$$= T_1 \sin\gamma + T_3 \cos\gamma \qquad (4.8)$$

Now, multiply the first of (4.6) by $(I_{33}\cos\gamma + I_{13}\sin\gamma)$ and subtract from it $(I_{11}\sin\gamma + I_{13}\cos\gamma)$ times the second equation, to get after some algebraic manipulations,

---

* These coupling terms, due to the orbital rate ω_o, are also present (though not considered in the simple derivation here). They are important from an attitude control standpoint but do not affect the present modal analysis (see Ref. 2).

$$(I_{11}I_{33}-I_{13}^2)(\ddot{\varphi}\cos\gamma-\ddot{\psi}\sin\gamma)+ h[(I_{11}\sin\gamma + I_{13}\cos\gamma)\dot{\varphi} + (I_{33}\cos\gamma + I_{13}\sin\gamma)\dot{\psi}]$$

$$+ f(I_{33}\cos^2\gamma + I_{11}\sin^2\gamma + 2I_{13}\sin\gamma\cos\gamma)=(I_{33}\cos\gamma + I_{13}\sin\gamma)T_1-(I_{11}\sin\gamma + I_{13}\cos\gamma)T_3$$

Now we define the following quantities:

$$\delta = \varphi\cos\gamma - \psi\sin\gamma$$

$$\epsilon = [(I_{11}\sin\gamma + I_{13}\cos\gamma)\varphi + (I_{33}\cos\gamma + I_{13}\sin\gamma)\psi]/\sqrt{I_{11}I_{33}-I_{13}^2}$$

$$\beta_1 = \frac{(I_{33}\cos\gamma + I_{13}\sin\gamma)T_1-(I_{11}\sin\gamma + I_{13}\cos\gamma)\,T_3}{I_{11}I_{33} - I_{13}^2}$$

$$\beta_3 = \frac{T_1\sin\gamma + T_3\cos\gamma}{I_{11}I_{33}-I_{13}^2}$$

$$I = \frac{I_{11}I_{33} - I_{13}^2}{I_{33}\cos^2\gamma + I_{11}\sin^2\gamma + 2I_{13}\sin\gamma\cos\gamma} \qquad (4.9)$$

$$\omega_N = h/\sqrt{I_{11}I_{33}-I_{13}^2}$$

The motion equations then become simply

$$\begin{aligned} \ddot{\delta} + \omega_N\,\dot{\epsilon} + \frac{f}{I} &= \beta_1 \\ \ddot{\epsilon} - \omega_N\,\dot{\delta} &= \beta_3 \end{aligned} \qquad (4.10)$$

The physical significance of the definitions (4.9) should be noted at this stage. The angle δ is the attitude angle of the spacecraft about the axis generated by the intersection of the roll-yaw plane and the plane of the arrays. The angle ϵ, for a symmetrical satellite, ($I_1 = I_3$, $I_{13} = 0$) is the attitude angle about an axis normal to the δ -axis; in the general case it still has the dimensions of an angle. The rigid nutation frequency ω_N is the frequency of the rigid-body natural coming motion. More will be said about this in section 4.2. Finally, β_1 and β_3 are the angular accelerations about the δ and ϵ axes respectively, due to external (control as well as disturbance) torques. Again, for a symmetrical satellite these axes have physically identifiable, being mutually orthoganl orientations, - in, and normal to, the plane of the arrays respectively. Note that flexibility directly affects only the δ equation because only out-of-plane bending is considered significant.

4.1.2 Flexible Appendage Motion Equations

Consider first the solar array blanket. The acceleration of a point on the blanket can be written as

$$a = (b + y)\,\ddot{\delta} + \ddot{v} \qquad (4.11)$$

where v is the deflection normal to the plane of the blanket. Since stiffness is provided only by the uniform spanwise tension, the blanket behaves essentially as a string, and the motion equation can then be written as:

$$Pv'' = \sigma_w[\ddot{v} + (b+y)\ddot{\delta}] \tag{4.12}$$

In the above, attention is drawn to the fact that $v = v(y,t)$ as given in equation (4.1).

The boom equation of motion is considered next. The acceleration of a point on the boom is given by (4.11) with v replaced by u, the boom deflection. The bending moment at a section of the boom is

$$M = Bu'' + Pu \tag{4.13}$$

where slender-beam theory is used, and B is the uniform flexural stiffness of the boom. Now the "inertial force" corresponding to (4.11) is normal to the boom axis, so that it is equal to the second derivative of the moment given by (4.13). This gives

$$Bu'''' + Pu'' = -\rho\,[\ddot{u} + (b+y)\ddot{\delta}] \tag{4.14}$$

The appropriate boundary conditions for equations (4.12) and (4.14) are now considered, six are needed to completely specify the problem. Since the boom is rigidly cantilevered at the root, and the blanket is also assumed to be attached to the satellite at the same point, we have

$$u(0,t) = 0 \quad u'(0,t) = 0 \quad v(0,t) = 0 \tag{4.15}$$

Further, at the tip of the boom, there is no net bending moment, and the blanket and boom deflections must be equal for continuity, hence

$$u''(\ell,t) = 0 \qquad u(\ell,t) = v(\ell,t) \tag{4.16}$$

One more boundary condition is needed, which follows from the notion equation for the tip piece, to which the blanket and the boom are attached. We also note that the spacecraft equations must be simultaneously satisfied; this places a condition on the term δ appearing in equations 4.12 and 4.14.

4.1.3 Tip Piece Motion Equation

The tip piece in array bending does not undergo any rotation, but only a translation normal to the array plane, of its center of mass. The forces acting on the tip piece arise from the boom shear and the normal components of the blanket tension and the boom compression. The equation governing this translatory motion is then

$$(Bu''' + Pu' - Pv')\Big|_{y=\ell} = m\left[\ddot{u}\Big|_{y=\ell} + (b+\ell)\ddot{\delta}\right] \tag{4.17}$$

where all the derivatives are evaluated at $y = \ell$, that is, the physical location of the tip piece. Equation (4.17) essentially provides a boundary condition for the flexible appendage equations.

4.1.4 Summary of Motion Equations

The motion equations derived above will be referred to a great deal in the sequel, therefore they are summarized below.

Spacecraft:
$$\ddot{\delta} + \omega_N \dot{\epsilon} + \frac{f}{I} = \beta_1 \tag{4.18}$$
$$\ddot{\epsilon} - \omega_N \dot{\delta} = \beta_3 \tag{4.19}$$
$$f = 2\int_0^{\ell} (b+y)(\rho\ddot{u} + \sigma_w \ddot{v})\,dy + 2m(b+\ell)\,\ddot{u}(\ell) \tag{4.20}$$

Here the transformations given by Eq. (4.9) are used so as to simplify the notation.

Blanket:
$$Pv'' = \sigma_w[\ddot{v} + (b+y)\ddot{\delta}] \tag{4.21}$$

Boom:
$$Bu'''' = Pu'' = -\rho[\ddot{u} + (b+y)\ddot{\delta}] \tag{4.22}$$

Tip Piece:
$$(Bu''' + Pu' - Pv')\Big|_{y=\ell} = m[\ddot{u}\,|_{y=\ell} + (b+\ell)\ddot{\delta}] \tag{4.23}$$

Boundary Conditions:
$$u(0) = v(0) = u'(0) = 0$$
$$u(\ell) - v(\ell) = 0,\ u''(\ell) = 0 \tag{4.24}$$

Although for simulation purposes the spacecraft equations are better dealt with in the original form (4.6), for completeness the inverse transformation to (4.9), relating roll and yaw angles to δ and ϵ, is also given below.

$$\phi = \frac{I_{33}\cos\gamma + I_{13}\sin\gamma}{J}\,\delta + \frac{\mathcal{J}\sin\gamma}{J}\,\epsilon$$
$$\psi = -\frac{I_{11}\sin\gamma + I_{13}\cos\gamma}{J}\,\delta + \frac{\mathcal{J}\cos\gamma}{J}\,\epsilon \tag{4.25}$$

with
$$\mathcal{J} = \sqrt{I_{11}I_{33} - I_{13}^2}$$
$$J = I_{33}\cos^2\gamma + I_{11}\sin^2\gamma + 2I_{13}\sin\gamma\cos\gamma$$

Having derived the motion equations, we shall first look for and determine the natural modes of vibration, and then show how to use them in spacecraft attitude control simulation.

4.2 Natural Motions

The equations (4.18-4.24) define the spacecraft motion in roll-yaw/bending . These are more complicated than in the pitch/twist case, but can fortunately still be solved in closed form, although the solution still depends on the numerical solution of a transcendental equation, and the algebra is more complicated. We first investigate the natural motions, defined as those existing in the absence of any external torques, that is, $\beta_1 = \beta_3 = 0$ in equations (4.18-

4.19). The "constrained" and "unconstrained" cases are treated separately.

It is instructive first to consider the natural rigid-body motion, i.e., that which exists with no flexibility and no external torques. Then $u \equiv v \equiv 0$ and we have

$$\begin{aligned} \ddot{\delta} + \omega_N \dot{\epsilon} &= 0 \\ \ddot{\epsilon} - \omega_N \dot{\delta} &= 0 \end{aligned} \tag{4.26}$$

The solution to these equations is of the form

$$\delta = A\sin(\omega_N t + \bar{\varphi})$$

$$\epsilon = A\cos(\omega_N t + \bar{\varphi})$$

where the constants A and $\bar{\varphi}$ depend on the initial conditions. Thus both δ and ϵ are periodic functions of time, but out of phase by $\pi/2$ radians. This is the rigid coning motion which exists due to the momentum wheel. It is in contrast to the rigid rotation which was the rigid natural motion in the pitch case, corresponding to the double zero root. In this motion the panels and the main body are by definition assumed to move together as a single rigid body. When flexibility is introduced, this simple motion no longer describes the real situation, as will be seen in section 4.2.2 on unconstrained modes.

4.2.1 Constrained Motions

We consider here the natural motions of the flexible appendages themselves, when there are no external torques and the main body is constrained not to move, that is,

$$\delta(t) = \epsilon(t) \equiv 0 \tag{4.27}$$

Equation (4.27) now replaces the spacecraft equations of motion, and we are left with the following:

$$\begin{aligned} Pv'' &= \sigma_w \ddot{v} \\ Bu'''' + Pu'' &= -\rho\ddot{u} \end{aligned} \tag{4.28}$$

The applicable boundary conditions are

$$\begin{aligned} u(0) = u'(0) = v(0) &= 0 \\ u(\ell) - v(\ell) = u''(\ell) &= 0 \\ Bu'''(\ell) + Pu'(\ell) - Pv'(\ell) &= m\ddot{u}(\ell) \end{aligned} \tag{4.29}$$

These define the solution for the panel and boom deflections completely. We note that we have a system of linear constant-coefficient partial differential equations which may be solved by separation of variables. Furthermore, the boundary conditions are homogeneous, i.e., unforced, so that the solution exists only for certain special cases, which are called the natural modes. It is known from the physical situation that the solution consists of harmonic oscillations with a discrete set of frequencies called the natural frequencies. This can also be shown more formally; however, we shall use the physical argument to seek solutions of the following form:

$$u(y,t) = \sum_{n=1}^{\infty} U_n(y) \cos\Omega_n t$$

$$v(y,t) = \sum_{n=1}^{\infty} V_n(y) \cos\Omega_n t \qquad (4.30)$$

Substituting (4.30) into equations (4.28) and (4.29) leads to the time-dependent factor being divided out. We have as a result the following equations for $U_n(y)$ and $V_n(y)$, involving the natural frequencies Ω_n defined implicitly by equation (4.30). These equations describe motion in the n^{th} natural mode:

$$P V_n'' + \sigma_w \Omega_n^2 V_n = 0$$

$$BU_n'''' + P U_n'' - \rho \Omega_n^2 U_n = 0 \qquad (4.31)$$

with

$$U_n(0) = U_n'(0) = V_n(0) = 0$$

and

$$(BU_n''' + PU_n' - PV_n' + m \Omega_n^2 U_n)\Big|_{y=\ell} = 0$$

$$U_n(\ell) - V_n(\ell) = 0 \qquad (4.32)$$

$$U_n''(\ell) = 0$$

Equation (4.31) are now linear constant-coefficient ordinary differential equations. Using the standard techniques for such equations, it is straightforward to show that the solution can be expressed as:

$$U_n = a_1 \cosh \alpha_n y + a_2 \sinh \alpha_n y + b_1 \cos\beta_n y + b_2 \sin\beta_n y$$

$$V_n = a_3 \sin\kappa_n y + a_4 \cos\kappa_n y$$

where

$$\alpha_n = \left(\left(\sqrt{P^2 + 4\rho B \Omega_n^2} - P\right)/2B\right)^{1/2}$$

$$\beta_n = \left(\left(\sqrt{P^2 + 4\rho B \Omega_n^2} + P\right)/2B\right)^{1/2} \qquad (4.33)$$

$$\kappa_n = \sqrt{\sigma_w/P}\ \Omega_n$$

and a_1, b_1 etc are coefficients to be determined. The boundary conditions at y=0 are simple enough to be directly satisfied, leading to the elimination of three unknown constants. We then have the following form, which obviously satisfies the conditions at the root:

$$U_n = a_1(\cosh\alpha_n y - \cos\beta_n y) + a_2\left(\sinh\alpha_n y - \frac{\alpha_n}{\beta_n}\sin\beta_n y\right)$$

$$V_n = a_3 \sin\kappa_n y \qquad (4.34)$$

The remaining coefficients are found by application of the three boundary conditions at $y = \ell$, equations 4.32. The resulting simultaneous linear algebraic equations are most conveniently expressed in matrix form:

$$\underline{M}\,\underline{c} = 0 \qquad (4.35)$$

where

$$\underline{c} = (a_1, a_2, a_3)^T$$

The elements of $\underline{M}$ are easily shown to be as given below. The rows of $\underline{M}$ are arranged in the order implied by (4.32), and the columns in accordance with the definition of $\underline{c}$. Other arrangements of the matrix are possible, but of course this will not affect the solution. In writing the elements of $\underline{M}$, the subscripts n will be omitted for the sake of compactness. Also, the symbols $s \equiv \sin$, $c \equiv \cos$, $sh \equiv \sinh$, $ch \equiv \cosh$ are used.

$$m_{11} = B(\alpha^2 sh\alpha\ell - \beta^3 s\beta\ell) + P(\alpha sh\alpha\ell + \beta s\beta\ell) + m\Omega^2(ch\alpha\ell - c\beta\ell)$$

$$m_{12} = B(\alpha^3 ch\alpha\ell + \beta^3 c\beta\ell) + P(\alpha ch\alpha\ell + \alpha c\beta\ell) + m\Omega^2(sh\alpha\ell - \alpha/\beta\, s\beta\ell)$$

$$m_{13} = -P\kappa\, c\kappa\ell$$

$$m_{21} = ch\alpha\ell - c\beta\ell$$

$$m_{22} = sh\alpha\ell - \alpha/\beta\, s\beta\ell \qquad (4.36)$$

$$m_{23} = -s\kappa\ell$$

$$m_{31} = \alpha^2 ch\alpha\ell + \beta^2 c\beta\ell$$

$$m_{32} = \alpha^2 sh\alpha\ell + \alpha\beta s\beta\ell$$

$$m_{33} = 0$$

In order for a solution of the assumed form to exist, the matrix $\underline{M}$ must be singular:

$$\det \underline{M} = 0 \qquad (4.37)$$

This is a transcendental equation for Ω in terms of the sheet and boom parameters. An infinite number of solutions exist, corresponding to a countably infinite set of natural frequencies Ω_n, for n = 1,2, etc. The infinitude exists because of the periodicity of the sinusoidal terms. When $\underline{M}$ is singular, equation 4.35 may be solved for the coefficients a_1, a_2 and a_3 which are then sufficient to give the shape functions $U_n(y)$ and $V_n(y)$ via (4.34). Due to the homogeneity of (4.35), the solution is only determined to within an arbitrary constant multiplier. The "eigenfunctions" or natural mode shapes are thus nonunique unless normalized by imposing a subsidiary constraint. This will be

done below. A unique solution of course exists when external torques of given magnitude are present; this will be shown in section 4.3.1.

An orthogonality condition for the natural modes is now derived. This involves, as expected, the blanket and boom mode shapes and the tip mass deflection and is expressed as

$$\Xi_{mn} = 0, \quad m \neq n \tag{4.38}$$

where

$$\Xi_{mn} = 2\rho \int_0^{\ell} U_m U_n dy + 2\sigma_w \int_0^{\ell} V_m V_n dy + 2m\, U_m(\ell) U_n(\ell) \tag{4.39}$$

The proof can be demonstrated from the expressions for U and V in Eqs. 4.34, but it is easier to prove it from the differential equations and boundary conditions directly. From (4.31) we obtain

$$B\int_0^{\ell} (U_m U_n'''' - U_n U_m'''')dy + P\int_0^{\ell} (U_m U_n'' - U_n U_m'')dy$$
$$= \rho \int_0^{\ell} (\Omega_n^2 U_m U_n - \Omega_m^2 U_n U_m)dy$$
$$= \rho\,(\Omega_n^2 - \Omega_m^2) \int_0^{\ell} U_m U_n dy \tag{4.40a}$$

Handling the equation for V similarly, we get

$$-P\int_0^{\ell} (V_m V_n'' - V_n V_m'')dy = \sigma_w(\Omega_n^2 - \Omega_m^2) \int_0^{\ell} V_m V_n dy \tag{4.40b}$$

From the first of equations 4.32,

$$\left\{-B(U_m U_n''' - U_n U_m''') - P(U_m U_n' - U_n U_m') + P(V_m V_n' - V_n V_m')\right\}\Big|_{y=\ell}$$
$$= m(\Omega_n^2 - \Omega_m^2)\, U_m U_n \Big|_{y=\ell} \tag{4.40c}$$

The left hand side of (4.40a) is reduced as follows, using integration by parts, and the other boundary conditions:

$$B\int_0^{\ell} U_m U_n'''' - U_n U_m'''')dy + P\int_0^{\ell} (U_m U_n'' - U_n U_m'')dy$$
$$= B[(U_m U_n''' - U_n U_m''')\Big|_0^{\ell} - \int_0^{\ell} (U_m' U_n''' - U_n' U_m''')dy]$$
$$+ P\,[(U_m U_n' - U_n U_m')\Big|_0^{\ell} - \int_0^{\ell} (U_m' U_n' - U_n' U_m')dy]$$

$$= \left\{ B(U_m U_n''' - U_n U_m''') + P(U_m U_n' - U_n U_m') \right\} \Big|_{y=\ell}$$

$$-B[U_m' U_n'' - U_n' U_m'') \Big|_0^{\ell} - \int_0^{\ell} (U_m'' U_n'' - U_n'' U_m'')dy]$$

$$\therefore \left\{B(U_m U_n''' - U_n U_m''') + P(U_m U_n' - U_n U_m')\right\} \Big|_{y=\ell} = \rho(\Omega_n^2 - \Omega_m^2)\int_0^{\ell} U_m U_n dy \qquad (4.40d)$$

Similarly, equation (4.40b) reduces as follows:

$$-P[V_m V_n' - V_n V_m') \Big|_0^{\ell} - \int_0^{\ell} (V_m' V_n' - V_n' V_m')dy \ ] = \sigma w(\Omega_n^2 - \Omega_m^2) \int_0^{\ell} V_m V_n dy$$

$$\therefore \quad -P\ (V_m V_n' - V_n V_m') \Big|_{y=\ell} = \sigma w(\Omega_n^2 - \Omega_m^2)\int_0^{\ell} V_m V_n dy \qquad (4.40e)$$

Adding equations (4.40c,d,e) and using (4.39) gives

$$0 = \tfrac{1}{2}\ (\Omega_n^2 - \Omega_m^2)\ \Xi_{mn}$$

From which the orthogonality condition (4.38) follows.

The natural modes are now normalized using the following normalization condition:

$$\Xi_{nn} = \sigma w \ell^3 \qquad (4.41)$$

Note that the normalizing factor chosen here has the same dimensions but is different from that in pitch, Eq. (3.31). This is purely a matter of convenience and can be chosen at will. Now the mode shapes are rendered unique, because Eq. (4.41) is in effect a subsidiary condition to be satisfied by the coefficients a_1, a_2, a_3 occurring in the shape functions.

Numerical Results

Having completed the specification of the constrained frequencies and mode shapes, we consider some numerical calculations of the former. In order to reduce the number of variables involved, dimension analysis is useful. From the equations of motion and the boundary conditions, we expect a functional dependence of the following form:

$$\Omega_n = \Omega_n\ (\rho, \sigma w, \ell, P, B, m) \qquad (4.42)$$

The dimensionless groups formed by combinations of dimensional variables in (4.42) are then related as

$$\Omega_n^* = \Omega_n^*\ (\rho^*,\ m^*,\ B^*) \qquad (4.43)$$

where

$$\Omega_n^* = \Omega_n \sqrt{\sigma_w \ell^2 / P}$$

$$\rho^* = \rho / \sigma_w$$

$$m^* = m / \sigma_w \ell$$

$$B^* = P\ell^2 / B$$

Asterisks are used to denote dimensionless quantities. The dependence (4.43) can also be deduced directly from the motion equations and boundary conditions by writing them in nondimensional terms. Using the groups defined above, the dependence of the frequencies on relevant parameters will be presented. The nominal values used are $m^* = \rho^* = 0.2$ and $B^* = 1.0$, unless specified otherwise.

Figure 13 shows the first few frequencies Ω_n^* as a function of ρ^*, where only ρ^* is varied, in the range $(0 < \rho^* \leq 3.5)$. Similarly, the dependence on m^* is shown in Fig.14, for $(0 \leq m^* \leq 1.4)$. In both these cases the frequencies decrease, as expected, when a "mass" parameter is increased, for constant "stiffness" parameters.

The dependence of frequencies on B^* is somewhat more complex, due to the fact that, for a given compressive load P, the support boom buckles at certain values of the flexural stiffness. Alternatively, a boom of given stiffness buckles at certain values of the compressive load, the Euler critical load. The analysis of the boom and sheet separately is given in Appendix C, wherein it is shown that this condition exists when

$$\sqrt{B^*} = n\pi, \quad n = 1,2,\ldots \tag{4.44}$$

At these values, the lowest natural frequency is zero. Figure 15 shows the variation of Ω_n^* with $\sqrt{B^*}$, for $(0 < \sqrt{B^*} \leq 7.0)$, a range which includes the first two buckling points. Note that the first and second natural frequencies respectively go to zero at these points.

In interpreting this plot, it is instructive to compare it with the natural frequencies of the sheet and the boom separately, i.e., in the absence of one of the flexible elements. These expressions are derived in Appendix C, and are plotted in Fig. 16. The sheet frequencies are independent of $\sqrt{B^*}$, while the boom frequencies show the buckling behaviour. Note that the boom frequencies are nondimensionalized by the same factor as the sheet frequencies, which is different from the more customary factor $\sqrt{\rho\ell^4/B}$ which depends only on the boom properties. The remarkable similarity of Figs. 15 and 16 is intuitively plausible when one considers that the sheet and boom are two vibrating systems, each with its unique characteristics which are only attached at one point. Hence, qualitatively speaking, the combined system will have characteristics of both the components. Physically, regions where the natural frequency curves are "flat" correspond to a string-like behaviour, with the (dimensional) frequency varying directly as the square root of the tension. This is the dominant behaviour, which changes only in regions where the boom and sheet frequencies are close together. For the numbers chosen, the sheet is much more massive than the boom ($\rho^* = 0.2$), and it may be expected that the situation would be different for $\rho^* \gg 1$.

The completes the development of the constrained motions. More

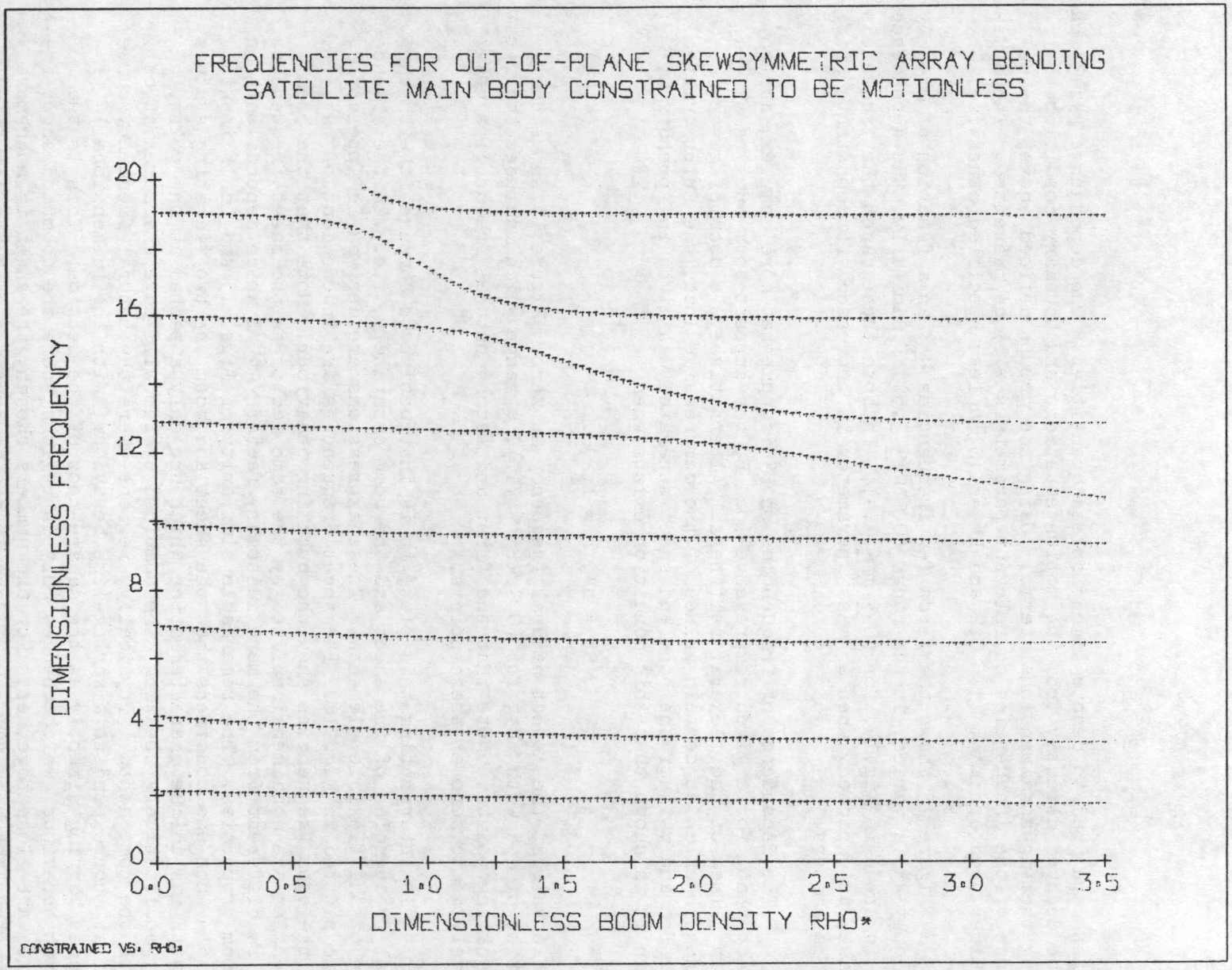

FIG. 13: Dependence of Constrained Frequencies on ρ^*

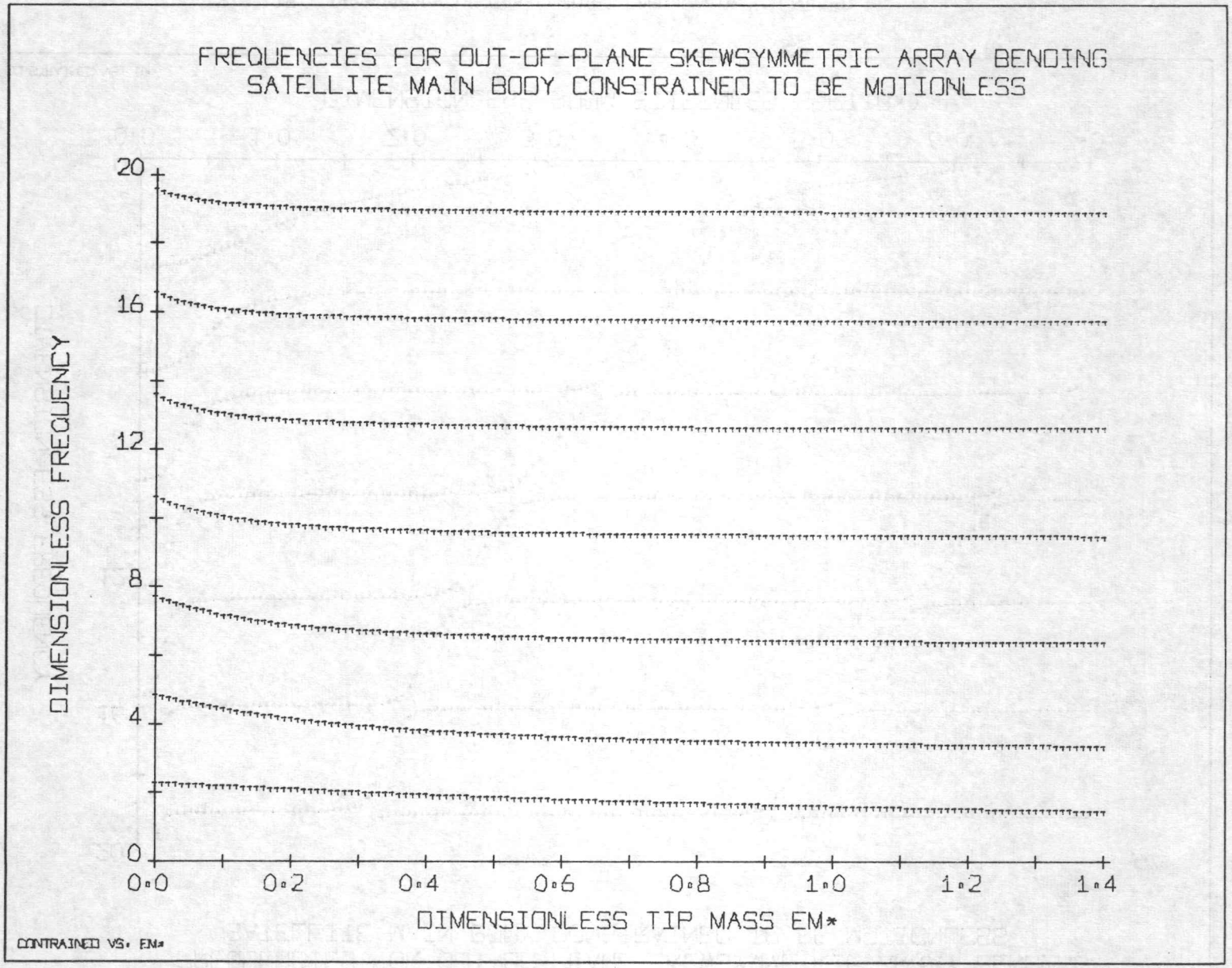

FIG. 14: Dependence of Constrained Frequencies on m*

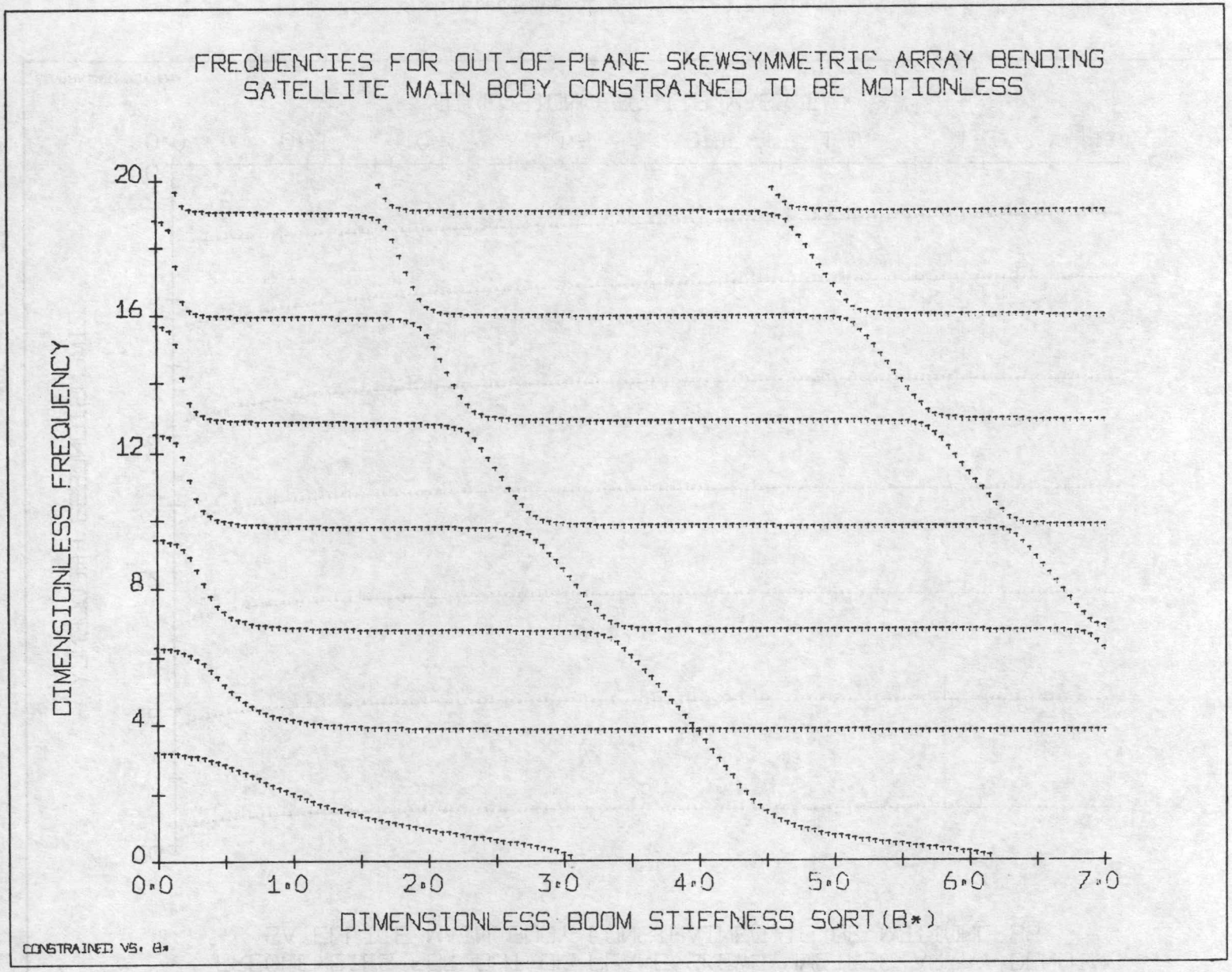

FIG. 15: Dependence of Constrained Frequencies on $\sqrt{B^*}$

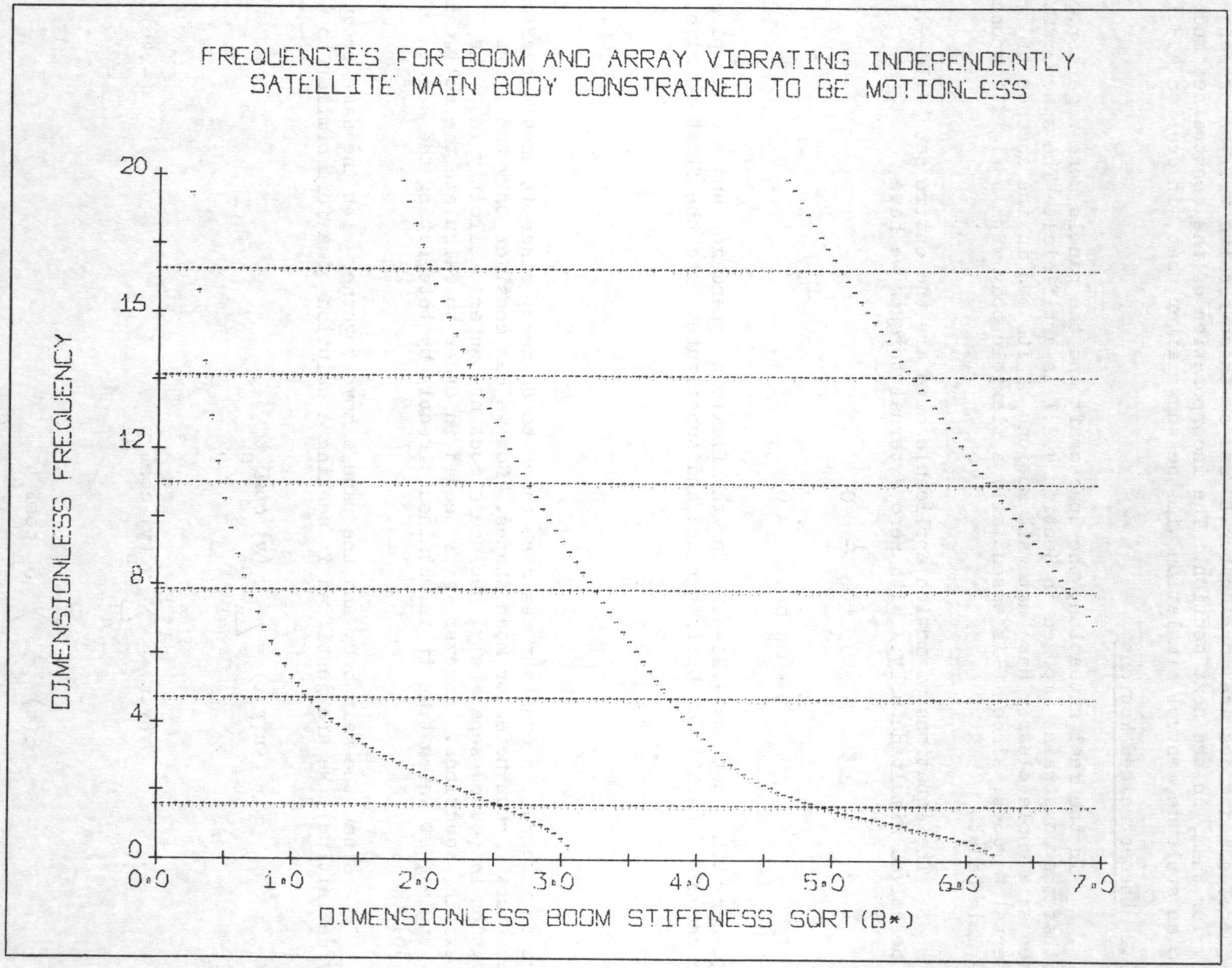

FIG. 16: "Constrained" Frequencies for Boom and Array Vibrating Independently; Dependence on $\sqrt{B^*}$

extensive numerical results could be included, for example mode shapes, and the frequencies in dimensional terms. However for design purposes the unconstrained frequencies and modes are more "natural" and so these results will be presented only for them, in the next section. The incorporation of the constrained modes into an attitude control simulation will be shown after that, in section 4.3.1.

4.2.2 Unconstrained Motions

In the real situation, the spacecraft and the panels more together, so that the constraint imposed in Section 4.2.1 is artificial. The spacecraft taken as a whole clearly has "natural" motions of its own in the absence of external torques, since it is essentially a flexible body with a rigid component, the main body.

The equations of motion applicable here are the entire set (4.18-4.24), to be solved simultaneously. With zero external torques we have

$$\begin{aligned} \ddot{\delta} + \omega_N \dot{\epsilon} + \frac{f}{I} &= 0 \\ \ddot{\epsilon} - \omega_N \dot{\delta} &= 0 \end{aligned} \tag{4.45}$$

together with equations 4.21-4.24 for the flexible appendages and the tip piece. The second of (4.45) can be integrated and substituted into the first to give

$$\begin{aligned} \ddot{\delta} + \omega_N^2 \delta + \frac{f}{I} &= 0 \\ \dot{\epsilon} &= \omega_N \delta \end{aligned} \tag{4.46}$$

Here an integration constant has been taken to be zero, since it does not affect the natural frequencies or mode shapes. Now we can consider only the first equation in (4.46) separately, because ϵ does not enter explicitly into the "flexible" equations. However, ϵ is needed in order to calculate the roll and yaw angles, at which time it is obtained directly by integrating the second of (4.46).

Since the main body and the panels move together with the same frequency (by definition), we are justified in seeking a solution of a form similar to (4.30):

$$\begin{aligned} u(y,t) &= \sum_{n=1}^{\infty} \bar{u}_n(y) \cos\omega_n t \\ v(y,t) &= \sum_{n=1}^{\infty} \bar{v}_n(y) \cos\omega_n t \\ \delta(t) &= \sum_{n=1}^{\infty} \delta_n \cos\omega_n t \end{aligned} \tag{4.46}$$

Substituting these into Eq. (4.46) gives, for motion in the n^{th} natural mode:

$$f_n = I\,\delta_n(1-\omega_N^2/\omega_n^2) \tag{4.47}$$

where

$$f_n = -2\int_0^{\ell}(b+y)(\rho u_n + \sigma w v_n)dy - 2m(b+\ell)\,u_n(\ell) \tag{4.48}$$

Similarly, substituting (4.46) into the flexible appendage equations and boundary conditions, (4.21-4.24) leads to cancelling out of the time-dependent factors, yielding the following set of equations for the shape functions $u_n(y)$ and $v_n(y)$, and the natural frequencies ω_n.

$$Pv_n'' + \sigma w\ \omega_n^2[v_n + (b+y)\delta_n] = 0 \tag{4.49}$$

$$BU_n'''' + P\,u_n'' - \rho\omega_n^2\,[u_n + (b+y)\delta_n] = 0 \tag{4.50}$$

with

$$u_n(0) = u_n'(0) = v_n(0) = 0 \tag{4.51}$$

and

$$Bu_n''' + Pu_n' - Pv_n' + m\omega_n^2[(b+\ell)\delta_n + u_n]\Big|_{y=\ell} = 0$$

$$u_n(\ell) - v_n(\ell) = 0$$

$$u_n''(\ell) = 0 \tag{4.52}$$

One method of simultaneously solving (4.47-4.52) is to regard δ_n as a known forcing term in (4.49-4.51) and solve for the mode shapes, and then use the boundary conditions (4.52) and the spacecraft motion equation (4.47) together to solve for the natural frequencies ω_n and δ_n. Thus the spacecraft motion equation may be thought of as an extra "boundary condition" giving δ_n, when solving the partial differential equations of the appendage motion. We have already taken this approach earlier, when the tip piece motion equation was used similarly.

Using standard techniques for constant coefficient linear ordinary differential equations, it is straightforward to show that the solution to (4.49-4.50) is of the form given below. Note that the terms involving δ_n are treated as forcing terms leading to a particular integral.

$$u_n(y) = a_1\cosh\alpha_n y + a_2\sinh\alpha_n y + b_1\cos\beta_n y + b_2\sin\beta_n y - (b+y)\delta_n$$

$$v_n(y) = a_3\sin\kappa_n y + \beta_4\cos\kappa_n y - (b+y)\,\delta_n$$

where

$$\alpha_n = ((\sqrt{P^2 + 4\rho B\omega_n^2} - P)/2B)^{1/2}$$

$$\beta_n = ((\sqrt{P^2 + 4\rho B\omega_n^2} + P)/2B)^{1/2} \qquad (4.53)$$

$$\kappa_n = \omega_n \sqrt{\sigma w/P}$$

and a_1, b_1 etc. are constants to be determined. Applying the condition $v(0) = 0$ to the function v_n gives

$$a_4 - b\,\delta_n = 0$$

so

$$v_n(y) = a_3 \sin\kappa_n y + \delta_n(b\cos\kappa_n y - b - y) \qquad (4.54)$$

Similarly the conditions $u(0) = 0$, $u'(0) = 0$ give

$$a_1 + b_1 - b\delta_n = 0$$

$$\alpha_n a_2 + \beta_n b_2 - \delta_n = 0$$

Hence

$$b_1 = -(a_1 - b\delta_n), \quad b_2 = -\frac{\alpha_n}{\beta_n}\left(a_2 - \frac{\delta_n}{\alpha_n}\right)$$

Substituting these into the expression and rearranging gives

$$u_n(y) = (a_1 - b\delta_n)(\cosh\alpha_n y - \cos\beta_n y) + \left(a_2 - \frac{\delta_n}{\alpha_n}\right)\left(\sinh\alpha_n y - \frac{\alpha_n}{\beta_n}\sin\beta_n y\right)$$

$$+ \delta_n(b\cosh\alpha_n y - \alpha_n^{-1}\sinh\alpha_n y - b - y)$$

Since as yet a_1, a_2 are entirely arbitrary constants, the above equation can equally well be written in the form

$$u_n(y) = a_1(\cosh\alpha_n y - \cos\beta_n y) + a_2\left(\sinh\alpha_n y - \frac{\alpha_n}{\beta_n}\sin\beta_n y\right)$$

$$+ \delta_n(b\cosh\alpha_n y - \alpha_n^{-1}\sinh\alpha_n y - b - y) \qquad (4.55)$$

It is readily verified that this expression satisfies the boundary conditions at the root. The remaining three boundary conditions (4.25) and the spacecraft equation (4.47) together yield four linear algebraic equations to determine the four remaining coefficients δ_n, a_1, a_2 and a_3. This simultaneous equations are most conveniently written in matrix form

$$\underline{M}\,\underline{c} = 0$$

where

$$\underline{c} = (\delta_n, a_1, a_2, a_3)^T$$

the elements of $\underline{M}$ are found by carrying out the operations (integration, differentiation etc.) involved in the remaining boundary conditions and grouping terms multiplying δ_n, a_1, a_2, and a_3 separately, in that order. The expressions (4.54) and (4.55) for u_n and v_n are to be substituted in the equations below, obtained from (4.47) and (4.52) but repeated for convenience:

$$I\left(1 - \frac{\omega_N^2}{\omega_n^2}\right)\delta_n + 2\int_0^{\ell} (b+y)(\rho u_n + \sigma w v_n)dy + 2m(b+\ell)\, u_n(\ell) = 0$$

$$Bu_n'''(\ell) + Pu_n'(\ell) - Pv_n'(\ell) + m\omega_n^2[(b+\ell)\delta_n + u_n(\ell)] = 0$$

$$u_n(\ell) - v_n(\ell) = 0$$

$$u_n''(\ell) = 0$$

The elements of $\underline{M}$, arranged by rows in the order implied by the above equations, and by columns in the order dictated by the definition of $\underline{c}$, are found to be as given below. Again for compactness, the subscript 'n' will be omitted and the abbreviations used in Eq. 4.36 are adopted.

$$m_{11} = I(1-\omega_N^2/\omega^2) - 2m(b+\ell)^2 + 2mb(b+\ell)ch\alpha\ell + 2m(b+\ell)\frac{sh\,\alpha\ell}{\alpha}$$
$$+ 2\sigma w\left[\frac{b^2}{\kappa}s\kappa\ell + \frac{b}{\kappa^2}(c\kappa\ell + \kappa\ell\, s\kappa\ell - 1) - (b^2\ell + b\ell^2 + \frac{1}{3}\ell^3)\right]$$
$$+ 2\rho\left[b^2\frac{sh\alpha\ell}{\alpha} + b\ell\frac{sh\alpha\ell}{\alpha} + \frac{\alpha\ell ch\alpha\ell - sh\alpha\ell}{\alpha^3} - (b^2\ell + b\ell^2 + \frac{1}{3}\ell^3)\right]$$

$$m_{12} = 2m(b+\ell)(ch\alpha\ell - c\beta\ell) + 2\rho b\left(\frac{sh\,\alpha\ell}{\alpha} - \frac{s\beta\ell}{\beta}\right)$$
$$+ 2\rho\left[\frac{\alpha\ell\, sh\alpha\ell - ch\alpha\ell + 1}{\alpha^2} - \frac{c\beta\ell + \beta\ell\, s\beta\ell - 1}{\beta^2}\right]$$

$$m_{13} = 2m(b+\ell)(sh\alpha\ell - \frac{\alpha}{\beta}s\beta\ell) + 2\rho b\left[\frac{ch\alpha\ell - 1}{\alpha} - \frac{\alpha(1-c\beta\ell)}{\beta^2}\right]$$
$$+ 2\rho\left[\frac{\alpha\ell ch\alpha\ell - sh\alpha\ell}{\alpha^2} - \frac{\alpha}{\beta^3}(s\beta\ell - \beta\ell c\beta\ell)\right]$$

$$m_{14} = 2\sigma wb\left(\frac{1-c\kappa\ell}{\kappa}\right) + 2\sigma w\left(\frac{s\kappa\ell - \kappa\ell c\kappa\ell}{\kappa^2}\right)$$

$$m_{21} = B(\alpha^2 bsh\alpha\ell + \alpha^2 ch\alpha\ell) + P(\alpha bsh\alpha\ell + ch\alpha\ell + \kappa bs\kappa\ell)$$
$$+ m\omega^2(bch\alpha\ell + \frac{1}{\alpha}sh\alpha\ell)$$

$$m_{22} = B(\alpha^3 sh\alpha\ell - \beta^3 s\beta\ell) + P(\alpha sh\alpha\ell + \beta s\beta\ell) + m\omega^2(ch\alpha\ell - c\beta\ell)$$

$$m_{23} = B(\alpha^3 ch\alpha\ell + \alpha\beta^2 c\beta\ell) + P(\alpha ch\alpha\ell - \alpha c\beta\ell) + m\omega^2(sh\alpha\ell - \frac{\alpha}{\beta} s\beta\ell)$$

$$m_{24} = -P\kappa\ c\kappa\ell$$

$$m_{31} = bch\alpha\ell + \frac{1}{\alpha} sh\alpha\ell - bc\kappa\ell$$

$$m_{32} = ch\alpha\ell - c\beta\ell$$

$$m_{33} = sh\alpha\ell - \frac{\alpha}{\beta}\ s\beta\ \ell \qquad (4.56)$$

$$m_{34} = -s\kappa\ell$$

$$m_{41} = \alpha^2 b\ ch\alpha\ell + \alpha\ sh\alpha\ell$$

$$m_{42} = \alpha^2 ch\alpha\ell + \beta^2\ c\beta\ell$$

$$m_{43} = \alpha^2\ sh\alpha\ell + \alpha\beta\ s\beta\ell$$

$$m_{44} = 0$$

In order for a solution of the assumed form to exist, the matrix $\underline{M}$ must be singular:

$$\det \underline{M} = 0 \qquad (4.57)$$

This gives a transcendental equation for ω in terms of the sheet, boom and spacecraft parameters. An infinite number of solutions exist, corresponding to a countably infinite set of natural frequencies ω_n, n = 1,2, etc. The infinitude arises from the periodicity of the sinusoidal terms. When M is singular, Eq. (4.56) may be solved for δ_n, a_1, a_2, a_3 and then the solution for the mode shapes $u_n(y)$ and $v_n(y)$is given by Eqs. (4.55 and 4.54) respectively. Due to the homogeneity of (4.56), the solution is arbitrary to the extent of a constant multiplier. Thus the "eigenfunctions" or natural mode shapes are nonunique unless normalized by a subsidiary constraint; this will be done below. A unique solution of course exists in the presence of external torques of given magnitude; this is done in Section 4.3.2.

It is physically expected that the unconstrained frequencies should tend to the constrained ones as the body inertia moments I_{1b} and $I_{3b} \to \infty$. This will now be demonstrated. Let C_{ij} denote the cofactor of m_{ij} in the determinantal equation (4.57), which may then be written as

$$m_{11}C_{11} + m_{12}C_{12} + m_{13}C_{13} + m_{14}C_{14} = 0$$

Inspection of the matrix elements in (4.56) shows that this may be written as

$$I(1-\omega_N^2/\omega_n^2)C_{11} + (\text{Terms independent of } I_{1b} \ \&\ I_{3b}) = 0$$

Now if the body inertias are increased while keeping other parameters constant, $I \to \infty$. Rewriting the above equation and taking limits:

$$C_{11} + \lim_{I_{b1}, I_{b3} \to \infty} \frac{\text{Terms independent of } I_{1b},\ I_{3b}}{I(1-\omega_N^2/\omega_n^2)} = 0,$$

We are left only with $C_{11} = 0$ as the characteristic equation. Now, comparing the expressions for the constrained (Eq. 4.36) and the unconstrained (Eq. 4.56) matrix elements, we find that C_{11} is identical with the constrained determinants, since the corresponding elements are equal.

$$(m_{ij})_{\text{constrained}} = (m_{i+1,j+1})_{\text{unconstrained}}, \quad i,j = 1,2,3 \tag{4.59}$$

Hence the equivalence of frequencies as $I_{1b}, I_{3b} \to \infty$ follows. The mode shapes (and gains to be defined later) will also be identical inasmuch as $\delta_n \to 0$ as the body inertia becomes infinite.

An orthogonality condition is now proved for the unconstrained mode shapes. The form of the condition is complicated, as in the pitch case, by having extra terms due to the spacecraft motion. In the present case it is further complicated by the presence of the wheel momentum. The condition may be expressed as

$$\xi_{mn} = I\,\delta_m\delta_n\,[1-\omega_N^2/\omega_m^2 - \omega_N^2/\omega_n^2], \quad m \neq n \tag{4.60}$$

where, as before,

$$\xi_{mn} \equiv 2\rho\int_0^\ell u_m u_n dy + 2\sigma w\int_0^\ell v_m v_n dy + 2m\,u_m(\ell)\,u_n(\ell) \tag{4.61}$$

Equation (4.60) should be compared with the corresponding condition (4.38) for the constrained modes, where the right hand side was zero.

The proof of (4.60) is similar to that of (4.38). From equation (4.50) we obtain

$$B\int_0^\ell (u_m u_n'''' - u_n u_m'''')dy + P\int_0^\ell (u_m u_n'' - u_n u_m'')dy = \rho(\omega_n^2-\omega_m^2)\int_0^\ell u_m u_n dy$$

$$+ \rho[\omega_n^2\delta_n\int_0^\ell (b+y)u_m dy - \omega_m^2\,\delta_m\int_0^\ell (b+y)u_n dy\,] \tag{4.62a}$$

Similarly, equation (4.49) gives

$$-P\int_0^\ell (v_m v_n'' - v_n v_m'')dy = \sigma w(\omega_n^2-\omega_m^2)\int_0^\ell v_m v_n dy$$

$$+ \sigma w\,[\omega_n^2\delta_n\int_0^\ell (b+y)v_m dy - \omega_m^2\,\delta_m\int_0^\ell (b+y)v_n dy\,] \tag{4.62b}$$

From the first of equations (4.52) we get

$$\left\{-B(u_m u_n'''' - u_n u_m'''') - P(u_m u_n' - u_n u_m') + P(v_m v_n' - v_n v_m')\right\}\Big|_{y=\ell}$$

$$= m(\omega_n^2 - \omega_m^2)\, u_m u_n + m(b+\ell)[\omega_n^2 \delta_n u_m - \omega_m^2 \delta_m u_n]\Big|_{y=\ell} \qquad (4.62c)$$

The left-hand sides of the above equations can be reduced exactly as in the constrained case, since the same boundary conditions still apply. Adding the resulting equations, and recalling the definition of f_n, Eq. (4.48), yields

$$0 = (\omega_n^2 - \omega_m^2)\, \xi_{mn} - \tfrac{1}{2}\,[\omega_n^2 \delta_n f_m - \omega_m^2 \delta_m f_n] \qquad (4.62d)$$

Now using Eq. (4.47) for f_m and f_n and rearranging,

$$(\omega_n^2 - \omega_m^2)\, \xi_{mn} = I\, \delta_m \delta_n [\omega_n^2 (1 - \omega_N^2/\omega_m^2) - \omega_m^2 (1 - \omega_N^2/\omega_n^2) \qquad (4.62e)$$

The term inside the square brackets on the right hand side of (4.62e) is reduced as follows:

$$[\cdot] = (\omega_n^2 - \omega_m^2) - \omega_N^2 \left(\frac{\omega_n^2}{\omega_m^2} - \frac{\omega_m^2}{\omega_n^2}\right)$$

$$= (\omega_n^2 - \omega_m^2)\left[1 - \omega_N^2 \left(\frac{\omega_n^2 + \omega_m^2}{\omega_m^2\, \omega_n^2}\right)\right.$$

Hence (4.62e) finally becomes

$$(\omega_n^2 - \omega_m^2)\, \xi_{mn} = I\, \delta_m \delta_n (\omega_n^2 - \omega_m^2)\left[1 - \frac{\omega_N^2}{\omega_m^2} - \frac{\omega_N^2}{\omega_n^2}\right] \qquad (4.63)$$

When $n \neq m$, the "orthogonality condition" (4.60) follows. Note that the term orthogonality is somewhat of an misnomer since usually orthogonality is associated with an inner product being zero. The transformation of (4.63) to an inner product type of expression is possible, like in the pitch case, as follows.

Let
$$\hat{u}_n \equiv u_n + (b+y)\, \delta_n$$
$$\hat{v}_n \equiv v_n + (b+y)\, \delta_n \qquad (4.64)$$

and
$$\hat{\xi}_{mn} \equiv 2\rho \int_o^\ell \hat{u}_m \hat{u}_n\, dy + 2\sigma w \int_o^\ell \hat{v}_m \hat{v}_n\, dy + 2m\, \hat{u}_m(\ell)\hat{u}_n(\ell)$$

Now, for example,

$$2\rho\int_o^\ell \hat{u}_m\hat{u}_n dy = 2\rho\int_o^\ell u_m u_n dy + 2\rho\delta_m\delta_n\int_o^\ell (b+y)^2 dy$$
$$+ 2\rho\,\delta_n\int_o^\ell (b+y)u_m dy + 2\rho\,\delta_m\int_o^\ell (b+y)u_n dy \qquad (4.65a)$$

Similarly,

$$2\sigma w\int_o^\ell \hat{v}_m\hat{v}_n dy = 2\sigma w\left[\int_o^\ell v_m v_n dy + \delta_n\int_o^\ell (b+y)v_m dy + \right.$$
$$\left. \delta_m\int_o^\ell (b+y)v_n dy + \delta_m\delta_n\int_o^\ell (b+y)^2 dy\right] \qquad (4.65b)$$

$$2m\,\hat{u}_m(\ell)\hat{u}_n(\ell) = 2m\,[u_m(\ell)u_n(\ell) + \delta_n(b+\ell)u_m(\ell) + \delta_m(b+\ell)u_n(\ell) + \delta_m\delta_n(b+\ell)^2] \qquad (4.65c)$$

Adding the previous three equations, using the definitions of f_m and f_n, and defining

$$I_A \equiv 2\int_o^\ell (\rho + \sigma w)(b+y)^2\, dy + 2m\,(b+\ell)^2 \qquad (4.66)$$

we get the relation

$$\hat{\xi}_{mn} = \xi_{mn} - \delta_n f_m - \delta_m f_n + I_A\delta_m\delta_n$$
$$= \xi_{mn} - I\,\delta_m\delta_n\left[\left(1 - \frac{\omega_N^2}{\omega_m^2}\right) + \left(1 - \frac{\omega_N^2}{\omega_n^2}\right) - \frac{I_A}{I}\right]$$
$$= \xi_{mn} - I\,\delta_m\delta_n[(1-\omega_N^2/\omega_m^2 - \omega_N^2/\omega_n^2) + (1-I_A/I)]$$

Rearranging this, finally we obtain

$$\xi_{mn} - I\,\delta_m\delta_n(1-\omega_N^2/\omega_m^2 - \omega_N^2/\omega_n^2) = \hat{\xi}_{mn} + (I-I_A)\,\delta_m\delta_n \qquad (4.67)$$

Hence the orthogonality condition (4.63) can be written finally as a generalized inner product:

$$\hat{\xi}_{mn} + (I-I_A)\,\delta_m\delta_n = 0, \quad m \neq n \qquad (4.68)$$

Thus, in one sense, the mode shapes which are orthogonal correspond to the total boom and sheet "deflections" $\hat{u}_m$ and $\hat{v}_m$. Note the similarity of (4.68) to the corresponding equation for pitch/twist, (3.62).

A normalization condition for the modes can now be given. One

possibility is to take the expression (4.68) for m = n and set it equal to some positive inertia-like quantity. However, it is desirable to keep the normalization the same for constrained and unconstrained modes, to facilitate their use in analysis. Hence we choose

$$\xi_{nn} = 2\rho\int_0^{\ell} u_n^2 dy + 2\sigma w\int_0^{\ell} v_n^2 dy + 2m\, u_n^2(\ell) = \sigma w \ell^3 \qquad (4.69)$$

By making all modes satisfy this condition, they are rendered unique. This fact is useful when the general motion in response to external torques is considered.

The analysis of the unconstrained natural motions is now complete. The actual motion will consist of a natural mode only for special initial conditions, for instance, if the deflection at t = 0 is a natural mode shape, with no initial velocity. In general, an infinite series representation similar to the assumed form (4.46) exists for a natural, i.e., unforced, motion. A unique solution can only be determined for given initial conditions. Similarly, a unique solution exists for given initial conditions and external torques. This will be developed in section 4.3.2. Before concluding the present section we present some numerical results.

Numerical Examples

Some illustrative numerical examples are now given. Dimension analysis is again found useful in order to reduce the number of variables to be considered. From the equations of motion and boundary conditions, we may expect a functional dependence of the form

$$\omega_n = \omega_n(\rho, \sigma w, \ell, b, P, m, I_\infty, \omega_N) \qquad (4.70)$$

Here we have used the fact that σ and w occur only as the product σw. The inertia parameter I depends, for given boom and sheet properties on the body inertias I_{1b} and I_{3b} and the angle γ (see Eq. 4.9 and Appendix B). The rigid nutation frequency ω_N is also specified by these three parameters, plus the angular momentum h. Since I_{1b}, I_{3b}, γ are inherently independent of the boom and sheet parameters, it is better to write (4.70) as

$$\omega_n = \omega_n(\rho, \sigma w, \ell, b, P, B, m, I_{1b}, I_{3b}, \gamma, \omega_N) \qquad (4.71)$$

By forming appropriate dimensionless groups, a simplified functional dependence is obtained:

$$\omega_n^* = \omega_n^*(\rho^*, m^*, b^*, B^*, I_{1b}^*, I_{3b}^*, \omega_N^*, \gamma) \qquad (4.72)$$

where

$$\omega_n^* = \omega_n \sqrt{\sigma w \ell^2 / P}$$

$$\rho^* = \rho/\sigma w$$

$$B^* = P\ell^2/B$$

$$b^* = b/\ell$$

$$I_{1b}^* = I_{1b} / \sigma w \ell^3$$

$$I_{3b}^* = I_{3b} / \sigma w \ell^3$$

$$\omega_N^* = \omega_N \sqrt{\sigma w \ell^2 / P}$$

These definitions are the same as for the constrained case, where applicable. The following nominal values are chosen for the independent variables in (4.72) and should be understood unless otherwise specified.

$$\rho^* = 0.2 \qquad m^* = 0.2 \qquad B^* = 1.0$$

$$I_{1b}^* = 1.0 \quad I_{3b}^* = 1.0 \qquad \gamma = \omega_N^* = 0.0 \tag{4.73}$$

The variation of ω_n^* when ρ^* varies in the range $(0 < \rho^* \leq 3.5)$ is shown in Fig. 17, for the first few modes, similarly, Fig. 18 shows ω_n^* when m^* varies in the range $(0 \leq m^* \leq 1.4)$. In both cases the frequencies decrease slowly as these "mass" properties are increased. A similar effect exists when the body moment of inertia is increased. Figure 19 shows the variation of ω_n^* for $(0 < I_{1b}^* \leq 7.0)$, with I_{3b}^* held constant at 1.0, and $\gamma = 0^o$. Here the frequencies level off to a value corresponding to the constrained modes quite rapidly, as I_{1b}, and therefore I, is increased. A comparison of Figs. 19 and 15 (for $B^* = 1.0$) shows this limiting behaviour clearly.

The effect on ω_n^* of increasing $\sqrt{B}^*$ is more complicated due to the possibility of buckling of the support boom, just as in the constrained case. Since buckling is essentially a static condition ($\omega = 0$), the critical load is unaffected by allowing the main body to move, and we still have

$$\sqrt{B}^* = n\pi, \quad n = 1,2,\ldots \tag{4.74}$$

The frequencies ω_n^* are shown, for $(0 < \sqrt{B}^* \leq 7.0)$, in Fig. 20. This range includes the first two buckling points. Notice that the first two natural frequencies go to zero respectively at these points. For a physical design, of course, $\sqrt{B}^*$ would be below the first buckling load.

The angular momentum stored in the wheel introduces a unique parameter, reflected in ω_N^*, which is directly proportional to h if other quantities are fixed. The variation of ω_n^* with this parameter is shown in Fig. 21, in the range $(0 \leq \omega_N^* \leq 7.0)$. For small ω_N^*, the lowest natural frequency is very close to, and asymptotes to, the rigid nutation frequency, but the two are equal only when $h = 0$. However, as h is increased, one of the higher natural frequencies may be equal to ω_N^*. When this happens, a unique situation exists in that both the flexible elements deflect, but the mode shapes are such that the spacecraft motion is the same as it would be without flexibility, i.e., the flexible motion does not exert any net torque on the main body. The frequencies ω_n^* are for the most part insensitive to ω_N^*, except in a region that appears to lie on an almost-straight curve passing through the origin, where an increase in ω_n^* takes place. The increase is expected as the gyroscopic "stiffness" is

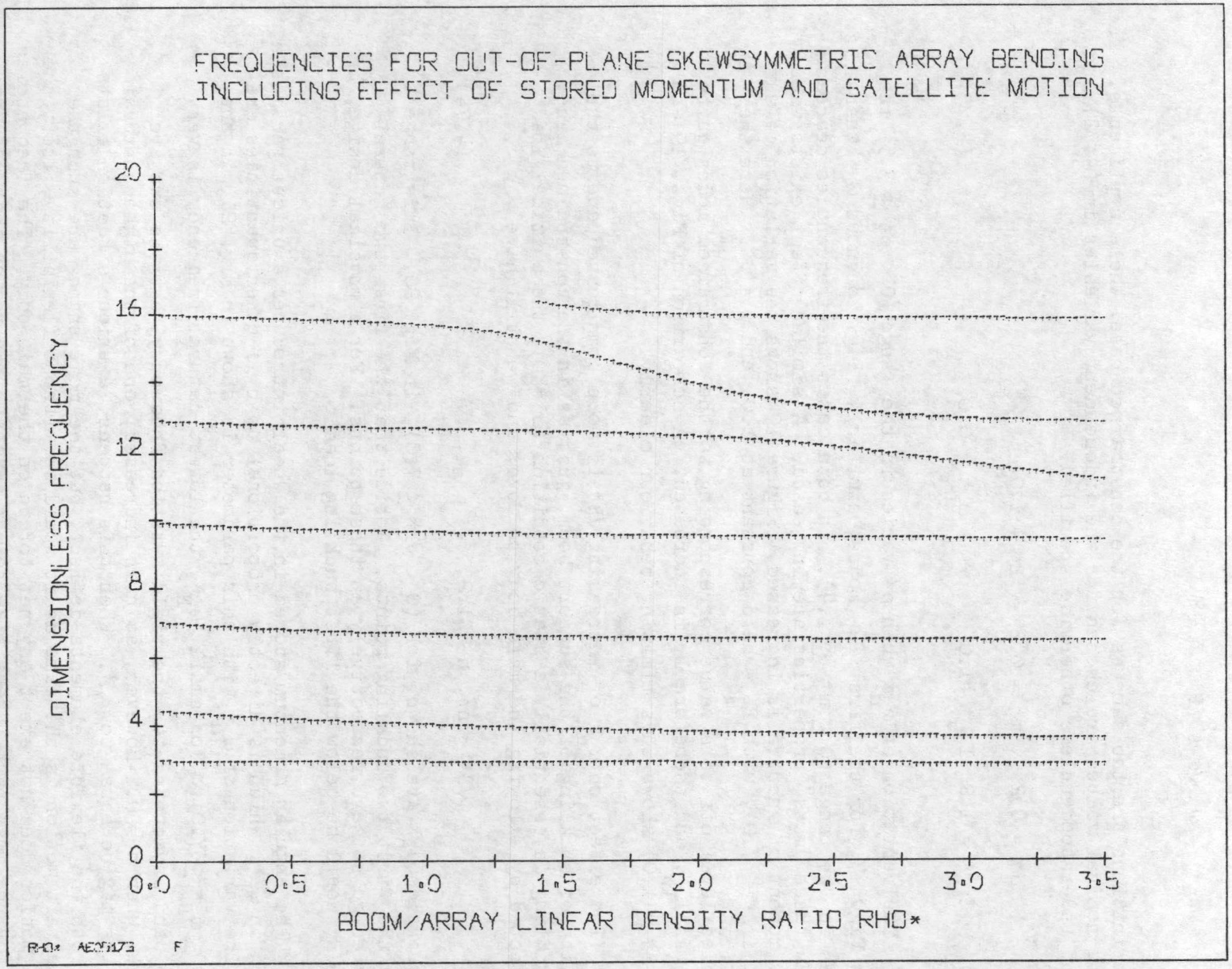

FIG. 17: Dependence of Unconstrained Frequencies on ρ*

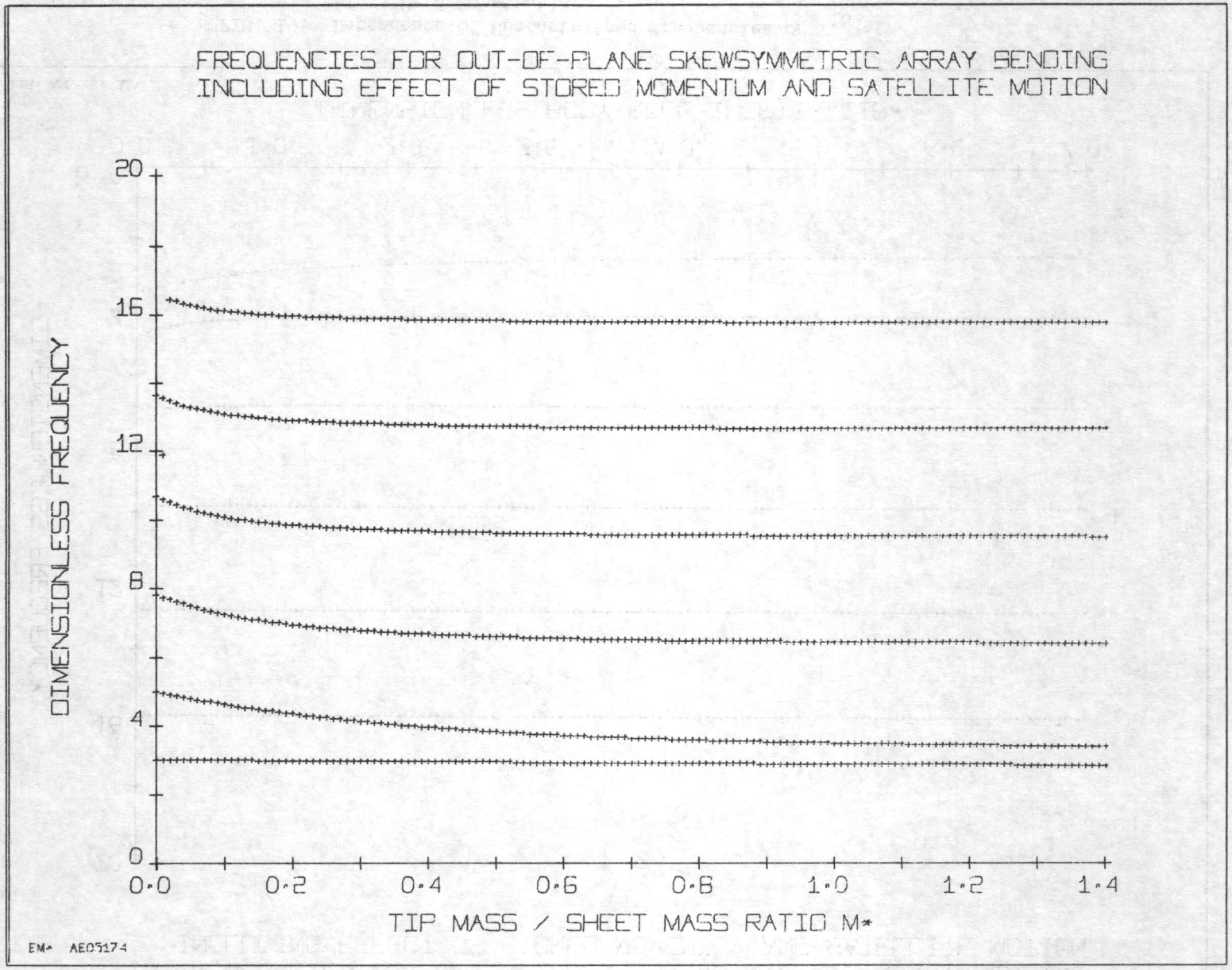

FIG. 18: Dependence of Unconstrained Frequencies on m*

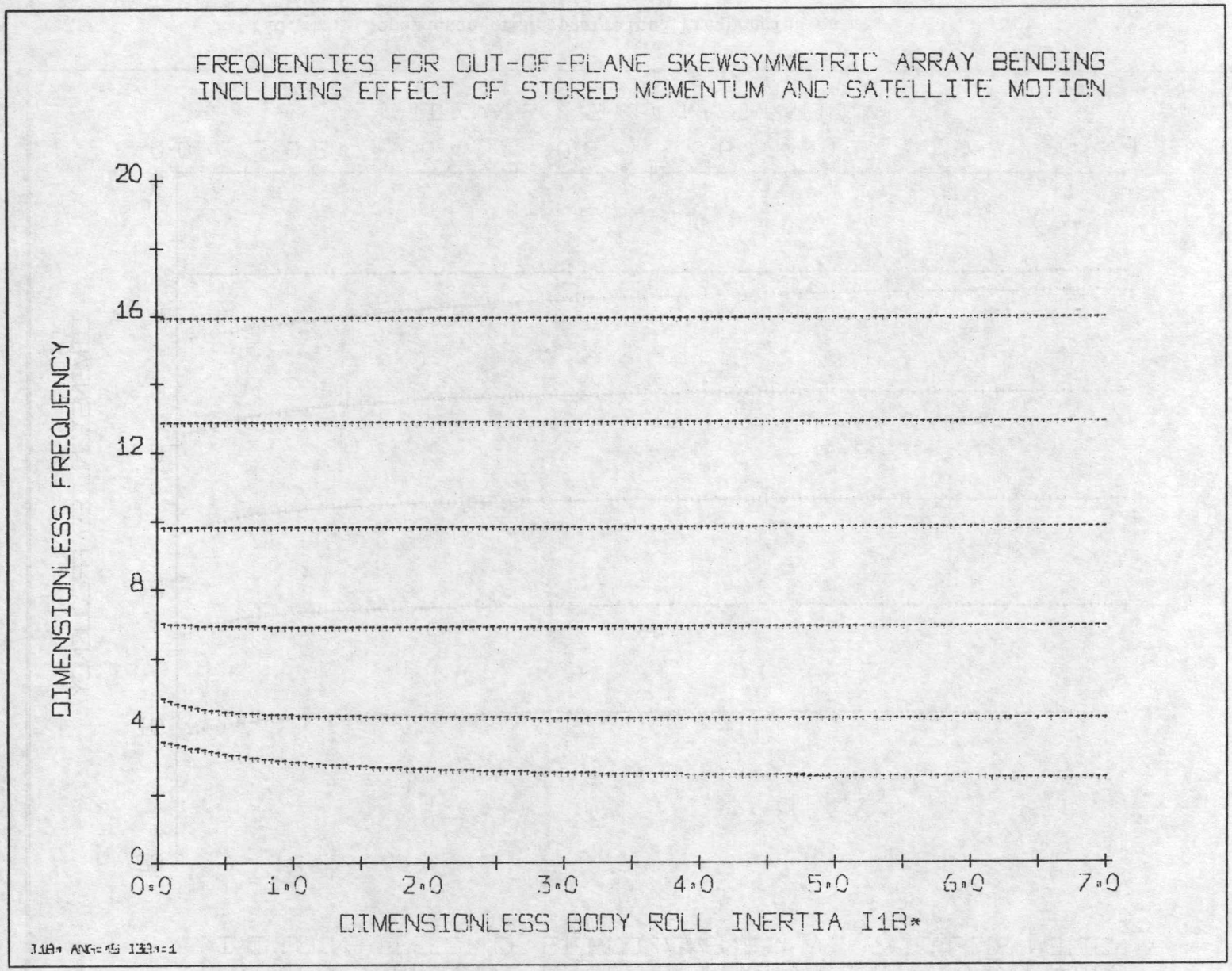

FIG. 19: Dependence of Unconstrained Frequencies on I_{1b}^* (I_{3b}^* Held Constant)

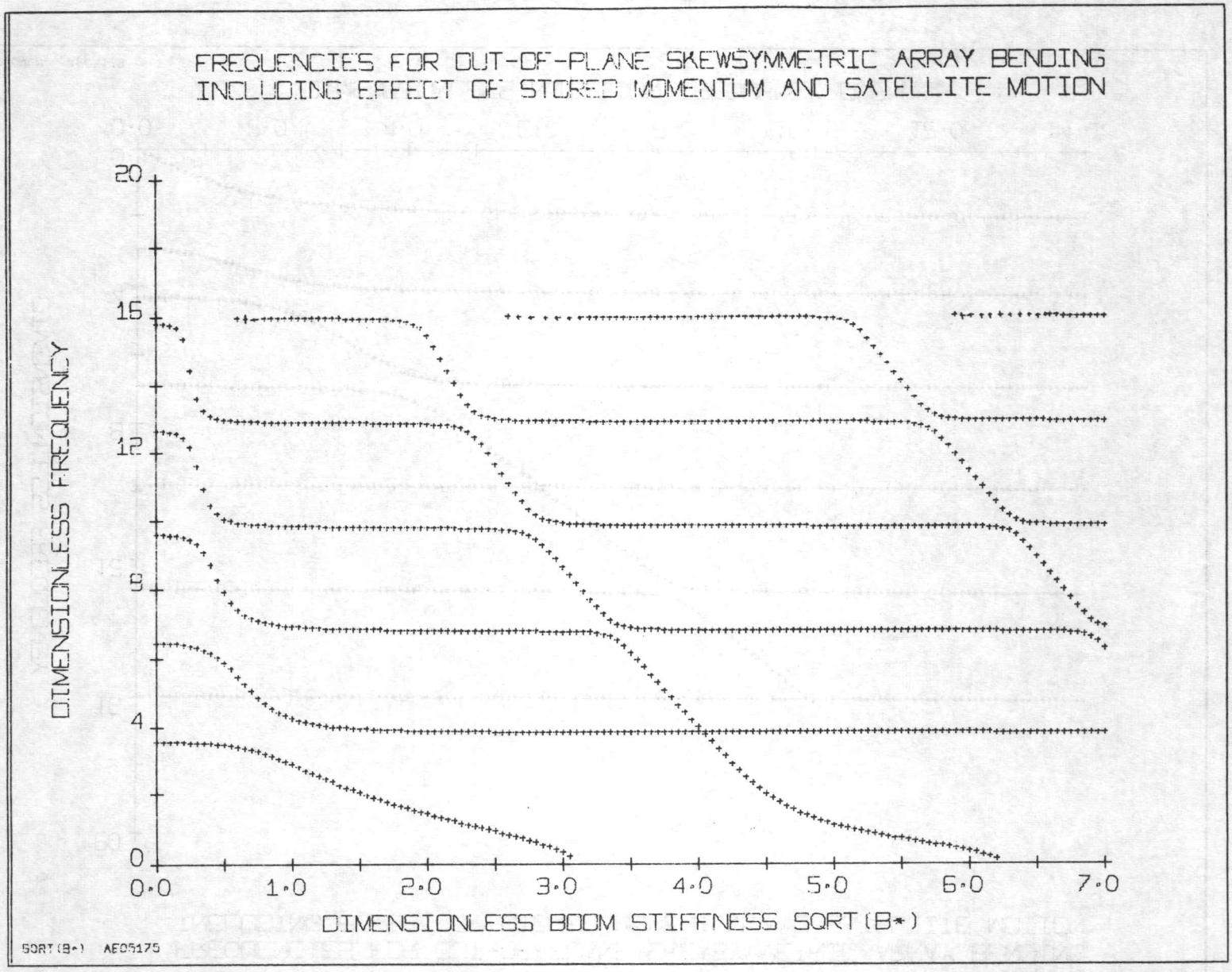

FIG. 20: Dependence of Unconstrained Frequencies on $\sqrt{B^*}$

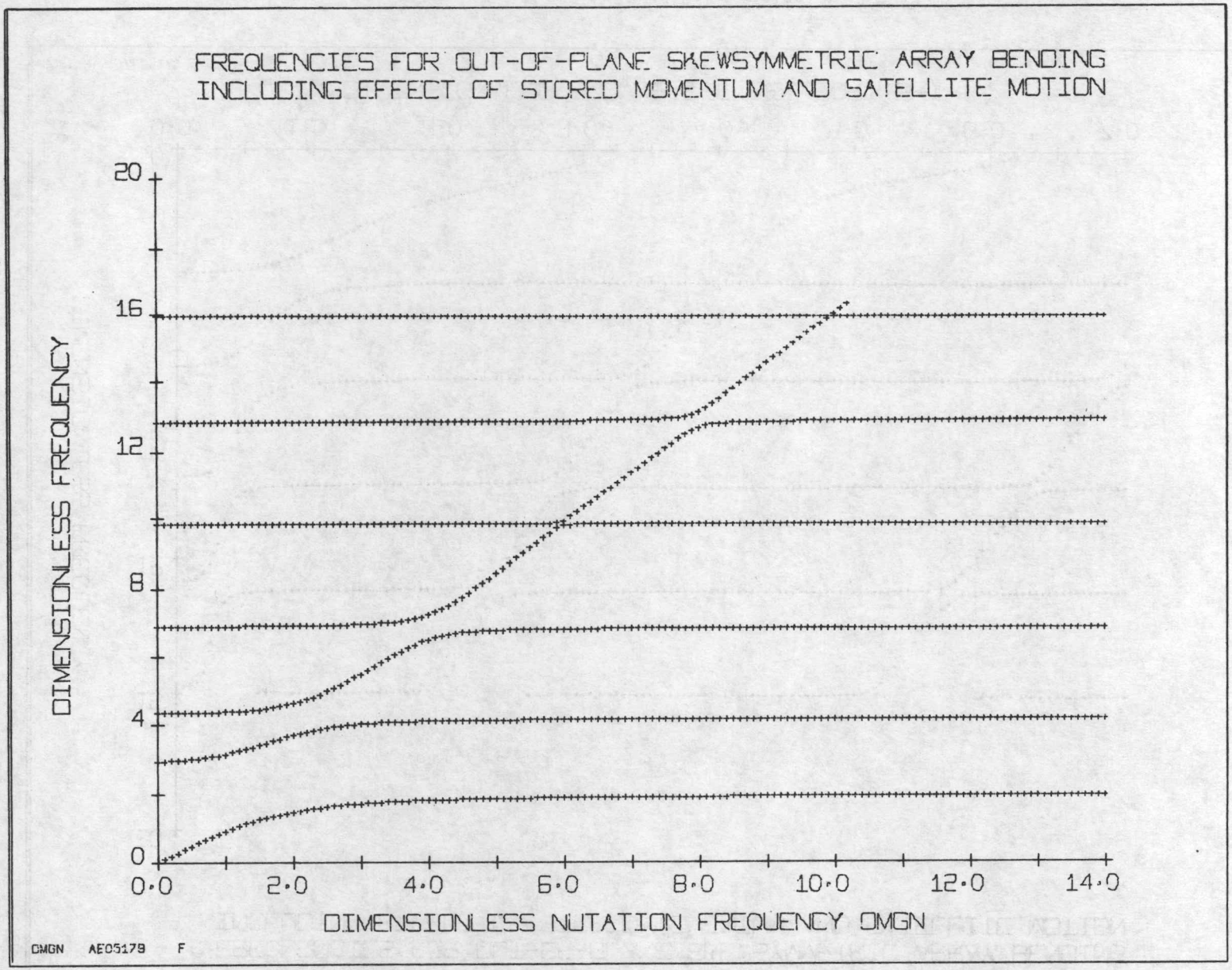

FIG. 21: Dependence of Unconstrained Frequencies on ω_N^*

increased, although why it occurs only in a particular region and not more gradually is not entirely clear. It may be verified that the frequencies in the limit $\omega_N^* \to \infty$ and $I_b^* \to \infty$ are the same, and are equal to the constrained frequencies. The case $\omega_N^* \to \infty$ is not physically realistic since it would cause strong in-plane forces due to gyroscopic coupling, thus invalidating a major assumption.

The variation of ω_n^* with γ is periodic with a period in γ of π radians, since I is periodic with this period, as may be readily verified. The amplitude of this variation is imperceptible when $I_{1b} \simeq I_{3b}$. Hence, in Fig. 22 are plotted ω_n^* as a function of γ, for $I_{1b}^* = 1$, $I_{3b}^* = 10$, i.e., a highly non-symmetrical main body. Even in this case only the first frequency is significantly affected. However, this is not true for the modal gains - which are a measure of the torque on the main body due to the flexible deflections - as will be seen later in section 4.3.2.

For design purposes it is necessary to know the natural frequencies in dimensional terms. To provide an appreciation of these, we consider some examples in which some physical parameters, rather than dimensionless groups, are varied. For this purpose, we choose

$$\begin{aligned} \ell &= 20.0 \text{ ft.} \\ \sigma &= .005 \text{ slugs/ft}^2 \\ P &= 15 \text{ lb}_f \end{aligned} \tag{4.75}$$

The values for ρ, m, B, I_{1b}, I_{3b}, h and γ are chosen in accordance with the nominal dimensionless quantities (4.73) chosen earlier. Note that in the plots to follow, (4.73) is satisfied only for these nominal values, not at all points on the plots.

Figure 23 shows ω_n as a function of σ, for $(0 < \sigma \leq .07 \text{ slugs/ft}^2)$. The other dimensional quantities are kept constant at their nominal values as defined above. From the nondimensional variables it is seen that in regions where ω_n^* is constant, $\omega_n \sim \sigma^{-1/2}$. This behaviour is evident in Fig. 23, where the frequencies decrease with increasing σ.

The variation of ω_n with ℓ is shown in Fig. 24, for $(0 < \ell \leq 70 \text{ ft})$. Here, if ω_n^* were constant, we would expect a dependence $\omega_n \sim \ell^{-1}$. This is seen for the shorter lengths in Fig. 24. We also see the first natural frequency going to zero at $\ell \simeq 62$ ft. This is a consequence of the buckling condition $B^* = \pi^2$, which becomes a condition on ℓ for fixed P and B.

Figure 25 shows the variation of ω_n as the tension is varied in the range $(0 < P \leq 168.0 \text{ lbf})$. Again, for constant ω_n^*, we expect a dependence $\omega_n \sim \sqrt{P}$ as the tension is varied. This is evident for low tensions and for the higher frequencies. However, quite soon the first natural frequency reaches a maximum and then gradually decreases until the first buckling load, near 146 lbf. The three examples considered here are complementary to the dimensionless plots where none of these parameters were varied. Other dimensional plots can easily

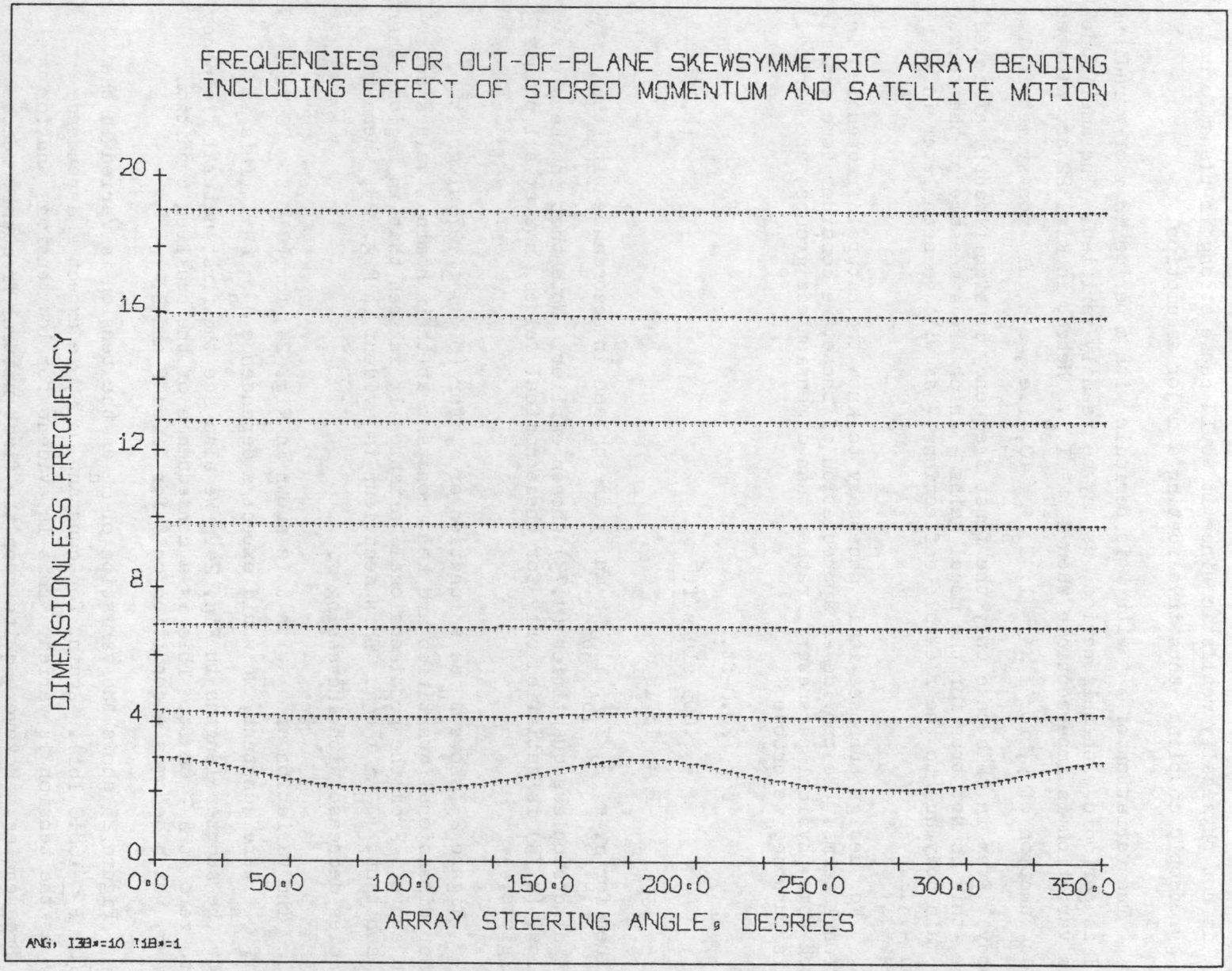

FIG. 22: Dependence of Unconstrained Frequencies on γ
(Unsymmetrical Configuration)

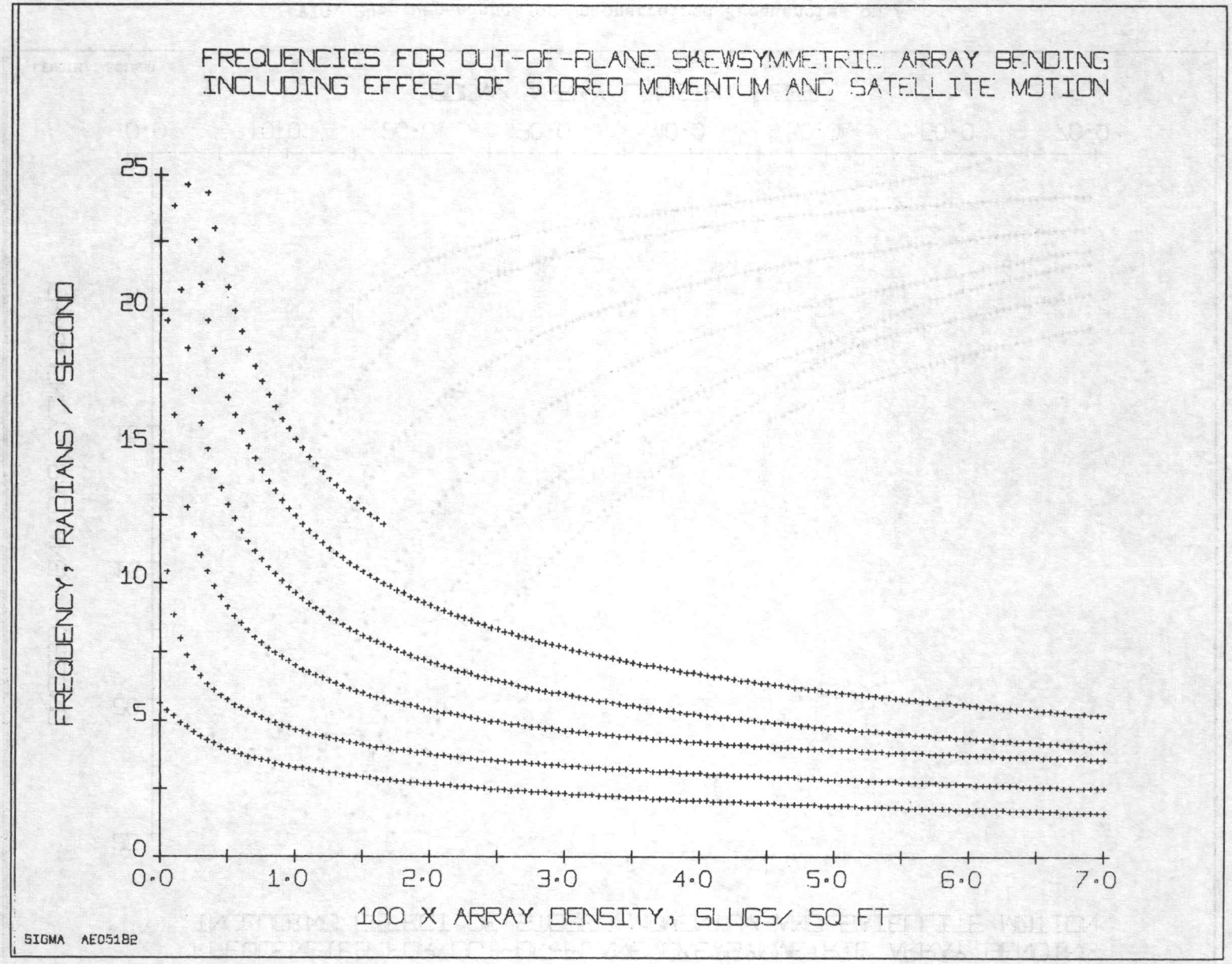

FIG. 23: Dependence of Unconstrained Frequencies on σ

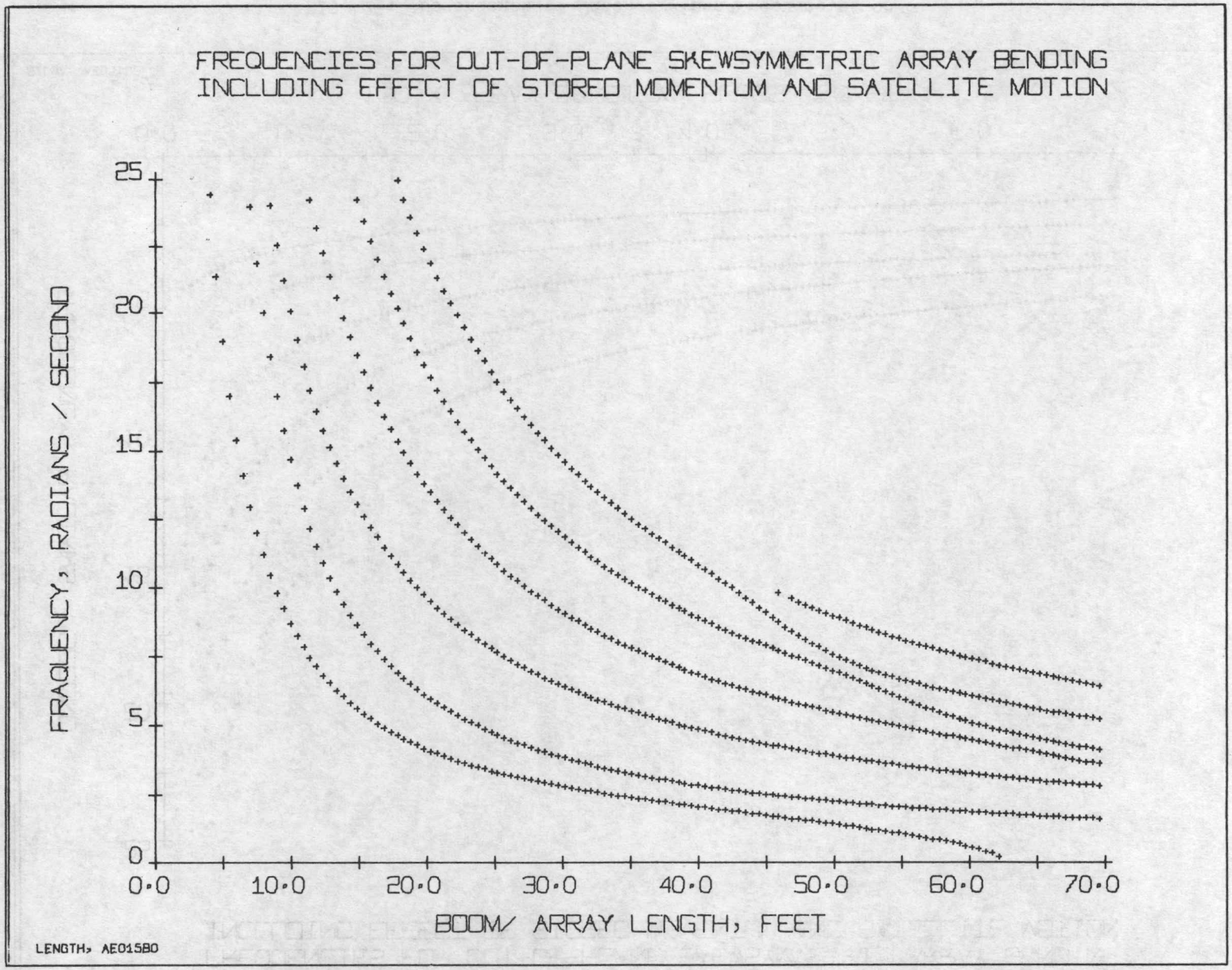

FIG. 24: Dependence of Unconstrained Frequencies on ℓ

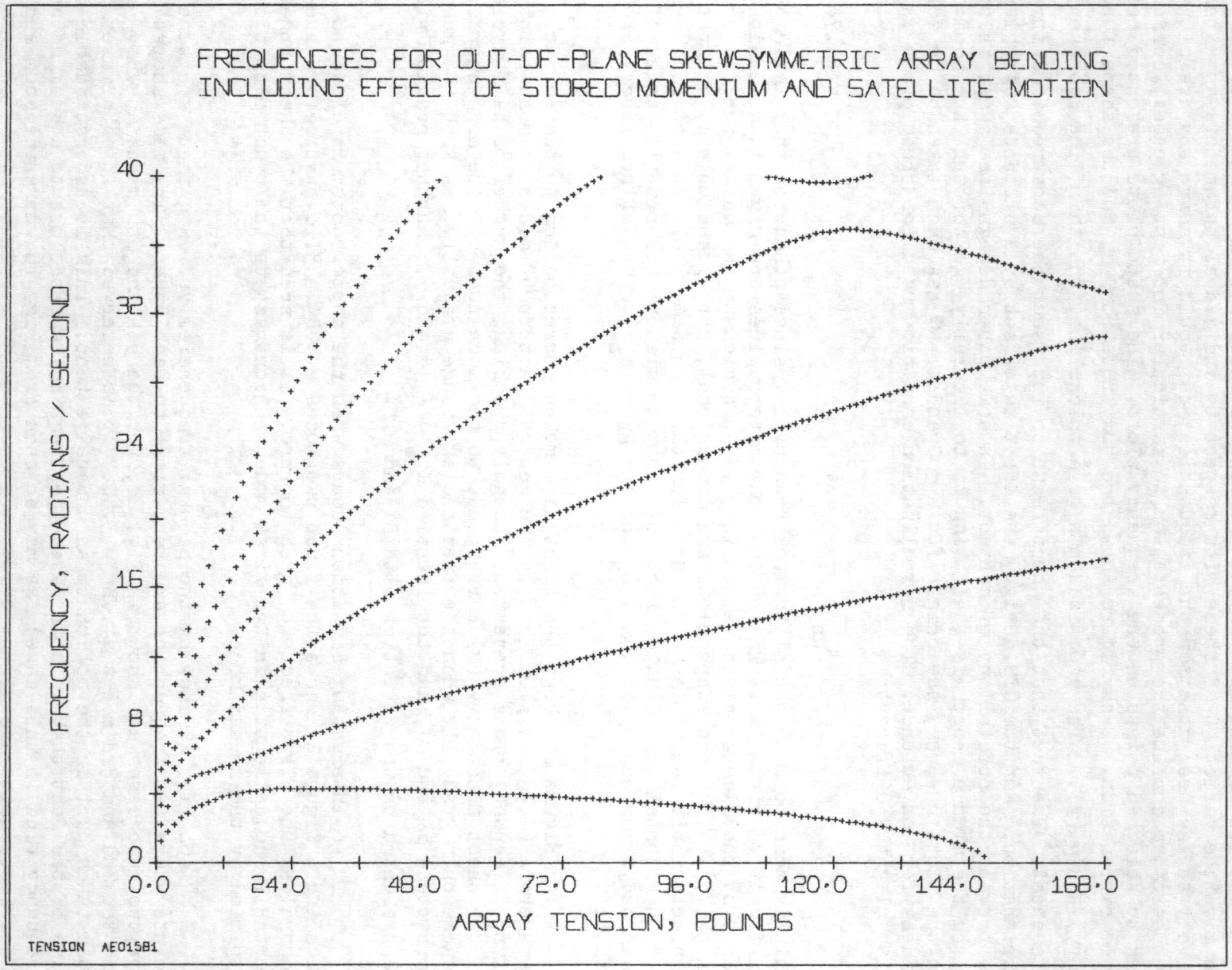

FIG. 25: Dependence of Unconstrained Frequencies on P

be obtained, but will only reflect the dimensionless behaviour in greater detail.

The natural mode shapes are also of interest. It is not possible here to give the variation of these with respect to individual parameters as extensively as has been done for the frequencies, nor would it serve any useful purpose. We therefore confine the presentation to particular interesting cases, corresponding to selected points on the frequency plots. The shape plots presented need some explanation. Each figure shows the body rotation δ_n and the shape functions $u_n(y)$ and $v_n(y)$. The boom is shown as a thick line, the thin line representing the sheet. The fact that the sheet seems to intersect the boom requires further explanation. For the CTS design, the sheet is offset by a distance sufficient to prevent the possibility of contact. In some other designs the sheet is split along the middle lengthwise, allowing it to literally "go through" the boom. On the plots however, the origin for u = 0 and v = 0 has been taken to be coincident for convenience. The normalization condition used for these plots is also slightly different:

$$\xi_{nn} = \frac{1}{16} \sigma w \ell^3 \qquad (4.76)$$

This is done to make the plots look reasonable, since otherwise they would be difficult to visualize. The nominal parameter values are given in dimensional terms by the dimensionless values in (4.73), scaled to the values for ℓ, σ and P in (4.75). Thus the shape plots are dimensional, not dimensionless, and the characteristic length is ℓ, the boom length. The same scale is used for "vertical" and "horizontal" coordinate axes, so as not to distort the rotation angle of the main body. On each plot, ω_n, δ_n and the gains k_n (to be defined later) are printed.

Figure 26 shows the first five modes corresponding to the nominal parameters (4.73, 4.75). This is the general pattern of modes on most points of the frequency plots presented. Roughly speaking, the number of half cycles of the sheet function $v_n(y)$ corresponds to the mode number. The mode shapes change only gradually when the frequencies change gradually, as with the mass parameters ρ^* and m^*, and the inertias I_{1b}^*, I_{3b}^* and γ. Further results will be presented on the variation with B^* and ω_N^*.

An interesting situation occurs when the support boom is close to buckling. Figure 27 shows the first two modes at $\sqrt{B^*} = 3.1$, just before buckling occurs and the first frequency goes to zero. It is seen that the sheet undergoes virtually no deflection in the first mode, in contrast to the usual situation typified by the second mode.

On Fig. 20 showing the natural frequencies vs. $\sqrt{B^*}$, there are some points where two frequencies are very close to each other. The mode shapes for two such cases are shown in Fig. 28, for the 5th and 6th modes at $\sqrt{B^*} = 2.35$ and the 2nd and 3rd modes at $\sqrt{B^*} = 3.40$. It is observed that in both cases the boom takes part in the motion to an unusual extent. This is understandable in view of the fact that in both cases the frequencies are close to a boom natural frequency (2nd in this case), as may be seen from Fig. 16 where the boom and sheet frequencies are given.

Two natural frequencies are also observed to be very close together on the plot of ω_n^* vs. ω_N^*, Fig. 21. It is interesting to see what happens here

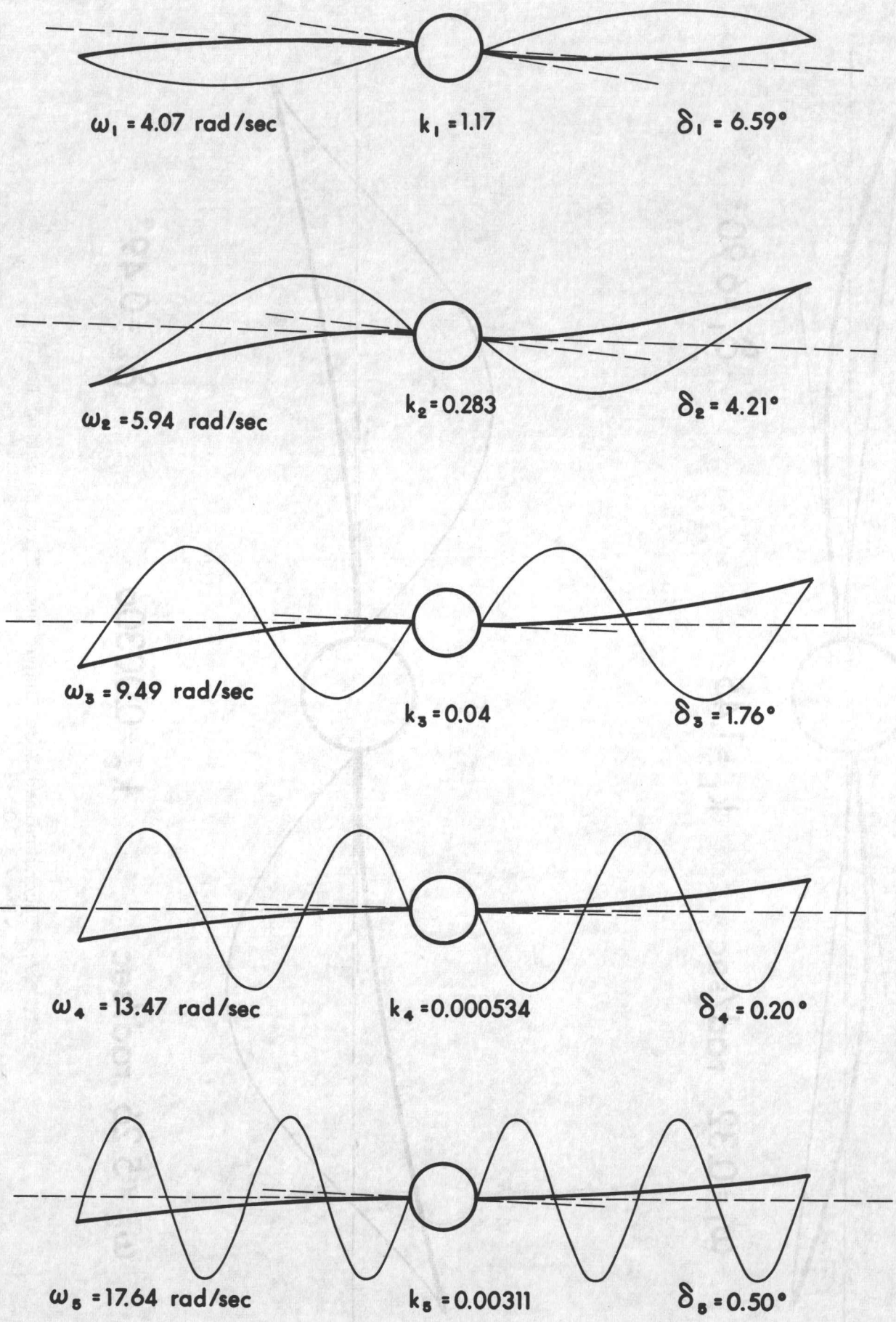

FIG. 26: Unconstrained Mode Shapes, Nominal Parameter Values

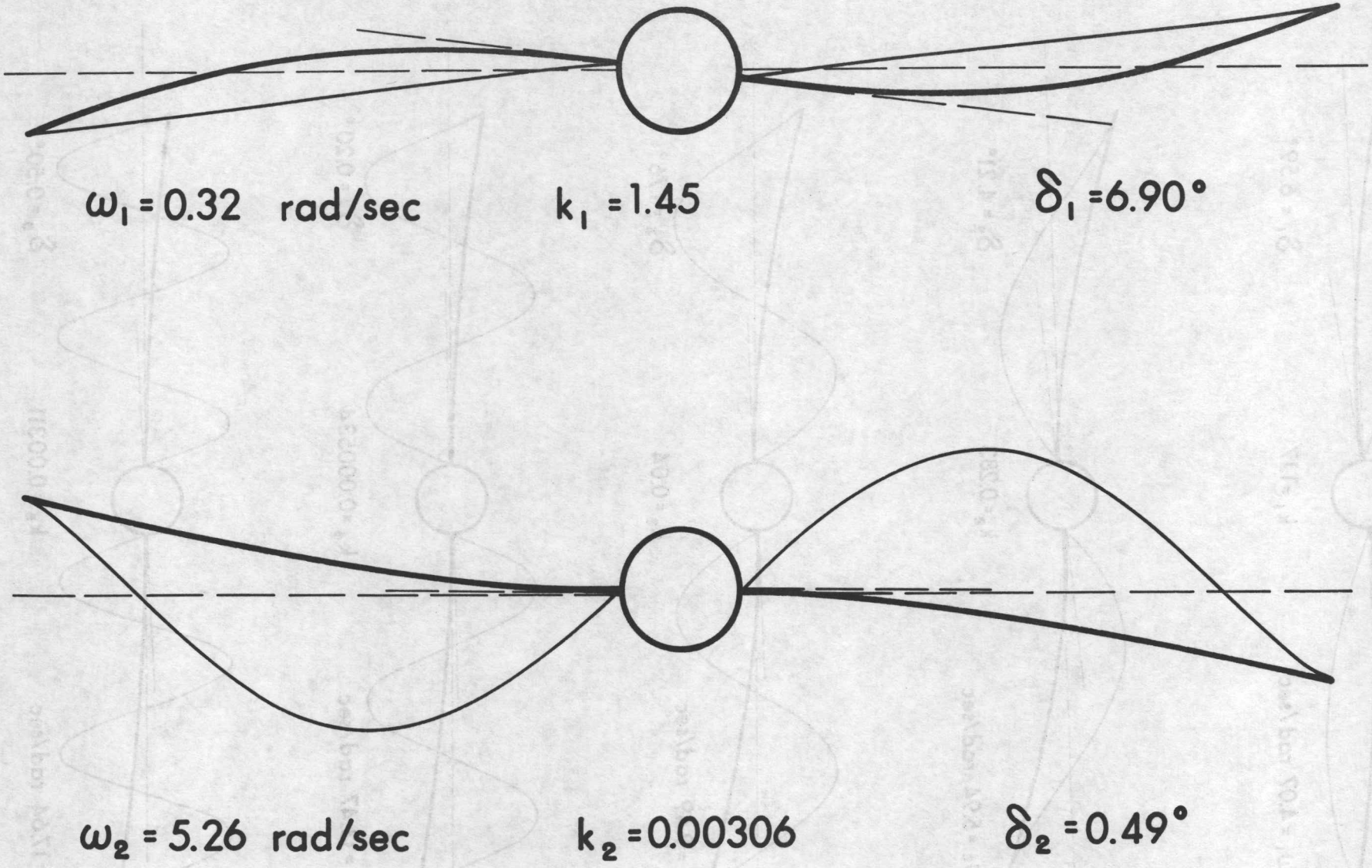

FIG. 27: Unconstrained Mode Shapes Near First Buckling Load, $\sqrt{B^*} = 3.10$

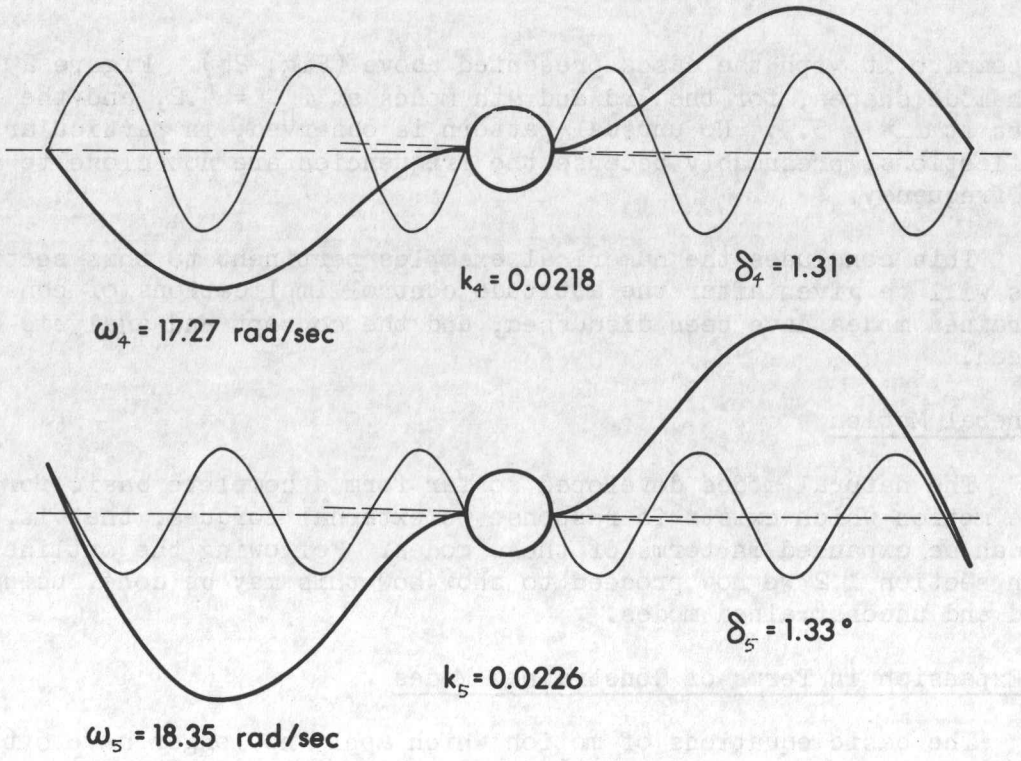

FIG. 28a: Unconstrained Mode Shapes at $\sqrt{B}^* = 2.35$, where $\omega_4 \simeq \omega_5$

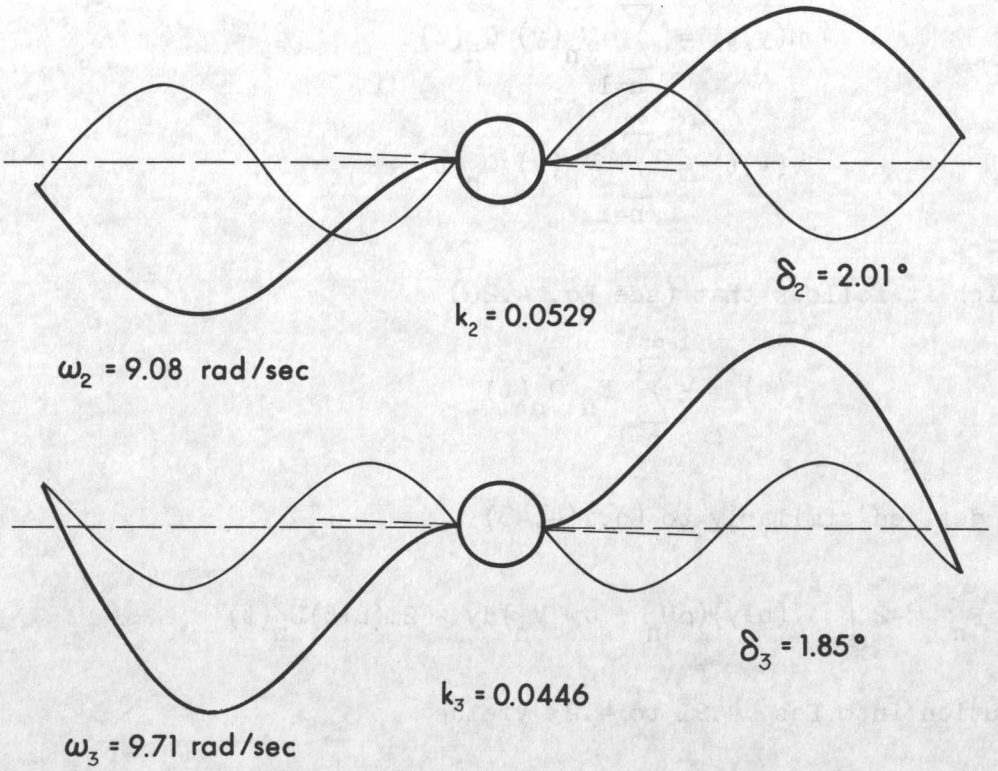

FIG. 28b: Unconstrained Mode Shapes at $\sqrt{B}^* = 3.40$, where $\omega_2 \simeq \omega_3$

and to compare it with the cases presented above (Fig. 28). Figure 29 presents two such mode shapes, for the 3rd and 4th modes at $\omega_N^* = 4.2$, and the 4th and 5th modes at $\omega_N^* = 5.9$. No unusual pattern is observed, in particular no large boom deflections, presumably because the frequencies are not close to a boom natural frequency.

This concludes the numerical examples pertinent to this section. Further examples will be given after the attitude control implications of constrained and unconstrained modes have been discussed, and the concept and analysis of 'gains' introduced.

4.3 General Motion

The natural modes developed so far form a complete basis for the general attitude motion which exists in response to external torques, that is, the general motion can be expanded in terms of these modes. Following the outline of analysis given in section 1.2 we now proceed to show how this may be done, using both constrained and unconstrained modes.

4.3.1 Expansion in Terms of Constrained Modes

The basic equations of motion which apply no longer have $\delta(t) \equiv 0$, and it is in fact desired to solve for the spacecraft attitude motion. Thus the full set of equations and boundary conditions (4.18-4.24) apply. It is noted that flexibility affects only one of the spacecraft equations, the"δ-equation" 4.18. We seek to expand the boom and sheet deflections in terms of $U_n(y)$, $V_n(y)$ and the generalized "modal coordinates" $Q_n(t)$, to be determined below:

$$u(y,t) = \sum_{n=1}^{\infty} U_n(y)\, Q_n(t)$$
$$v(y,t) = \sum_{n=1}^{\infty} V_n(y)\, Q_n(t) \qquad (4.77)$$

from which it follows that (see Eq. 4.20)

$$f(t) = -\sum_{n=1}^{\infty} F_n \ddot{Q}_n(t) \qquad (4.78)$$

with F_n defined similarly to Eq. (4.48):

$$F_n = -2\int_o^{\ell} (b+y)(\rho U_n + \sigma w\, V_n)dy - 2m(b+\ell)U_n(\ell) \qquad (4.79)$$

Substitution into Eqs. 4.21 to 4.23 yields

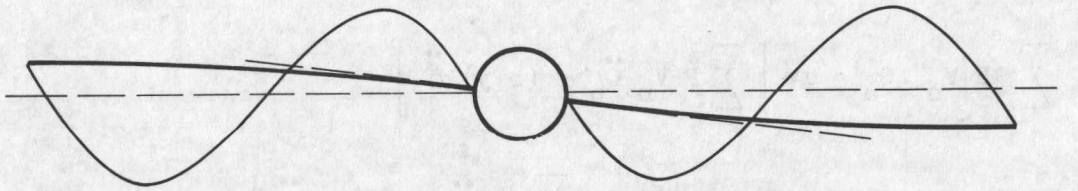

$\omega_2 = 9.10$ rad/sec $\quad k_2 = 0.255 \quad \delta_2 = 7.06°$

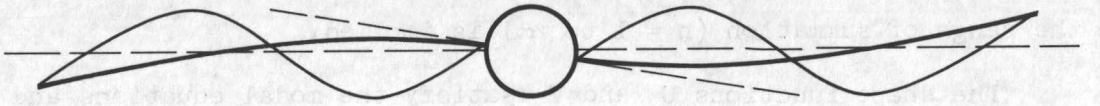

$\omega_3 = 10.18$ rad/sec $\quad k_3 = 0.803 \quad \delta_3 = 9.25°$

FIG. 29a: Unconstrained Mode Shapes for $\omega_N^* = 4.20$, where $\omega_2 \simeq \omega_3$

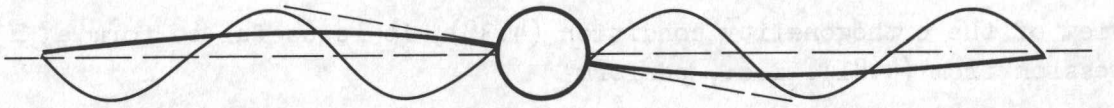

$\omega_4 = 13.29$ rad/sec $\quad k_4 = 0.767 \quad \delta_4 = 10.15°$

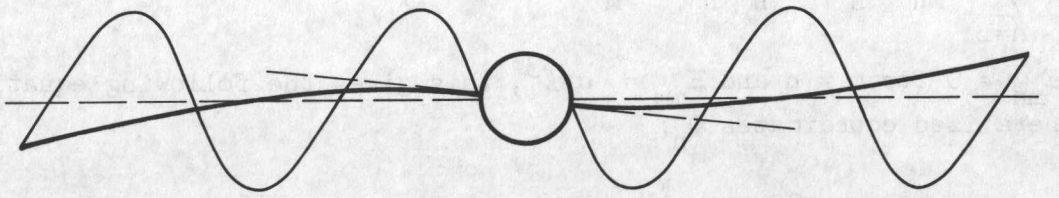

$\omega_5 = 13.52$ rad/sec $\quad k_5 = 0.213 \quad \delta_5 = 6.01°$

FIG. 29b: Unconstrained Mode Shapes for $\omega_N^* = 5.90$, where $\omega_4 \simeq \omega_5$

$$\sum P V_n'' Q_n = \sigma w \left[\sum P V_n \ddot{Q}_n + (b+y) \ddot{\delta} \right]$$

$$\sum (B U_n'''' + P U_n'') Q_n = - \rho \left[\sum U_n \ddot{Q}_n + (b+y) \ddot{\delta} \right] \qquad (4.80)$$

$$\sum (B U_n''' + P U_n' - P V_n') Q_n \Big|_{y=\ell} = m \left[\sum U_m \ddot{Q}_n \Big|_{y=\ell} + (b+\ell) \ddot{\delta} \right]$$

Here the range of summation (n = 1 to ∞) is implied.

The shape functions U_n and V_n satisfy the modal equations and boundary conditions(4.31 and 4.32). Forming the sum of these for n = 1 to ∞ and subtracting from (4.80) leads to the following equations:

$$\sum_{n=1}^{\infty} U_n(y) (\ddot{Q}_n + \Omega_n^2 Q_n) + (b+y) \ddot{\delta} = 0 \qquad (4.81a)$$

$$\sum_{n=1}^{\infty} V_n(y) (\ddot{Q}_n + \Omega_n^2 Q_n) + (b+y) \ddot{\delta} = 0 \qquad (4.81b)$$

$$\sum_{n=1}^{\infty} U_n(\ell) (\ddot{Q}_n + \Omega_n^2 Q_n) + (b+\ell) \ddot{\delta} = 0 \qquad (4.81c)$$

In view of the orthogonality condition (4.38), it is useful to form a Ξ_{mn}-type expression from (4.81), i.e., perform

$$2\rho \int_0^{\ell} U_m (4.81a)\,dy + 2\sigma w \int_0^{\ell} V_m (4.81b)\,dy + 2m\, U_m(\ell)(4.81c) = 0$$

using the definition of Ξ_{mn}(4.39), this gives

$$\sum_{n=1}^{\infty} \Xi_{mn} (\ddot{Q}_n + \Omega_n^2 Q_n) - F_m \ddot{\delta} = 0$$

since $\Xi_{mn} = 0$ for $m \neq n$ and $\Xi_{mm} = \sigma w \ell^3$, this gives the following equations for the generalized coordinates Q_n:

$$\ddot{Q}_m + \Omega_m^2 Q_m = \frac{F_m}{\sigma w \ell^3} \ddot{\delta}, \quad m = 1,2,\ldots\infty \qquad (4.82)$$

The flexibility implications for the spacecraft main body motion are contained in f(t), which is now completely specified.

For simulation purposes it is convenient to introduce Laplace transformed quantities (denoted by an overbar) and arrange the motion equations in block-diagram form. This yields, from Eqs. 4.18 and 4.19,

$$s^2 \bar{\delta} + \omega_N s \bar{\epsilon} - \sum_{n=1}^{\infty} \frac{\mathbb{K}_n s^4}{s^2 + \Omega_n^2} \bar{\delta} = \bar{\beta}_1 \qquad (4.83)$$

$$s^2 \bar{\epsilon} - \omega_N s \bar{\delta} = \bar{\beta}_3$$

Where s is the Laplace transform variable, and the "modal gains" $\mathbb{K}_n$ are dimensionless quantities defined as

$$K_n = \frac{F_n^2}{I \sigma w \ell^3}$$

or,

$$K_n = F_n^{*2}/I^* \qquad (4.84)$$

where $F_n^{**} = F_n/\sigma w \ell^3$ is the dimensionless value of F_n.

A bound on the gains will now be demonstrated. From equations 4.81, we form a F_n-type expression, i.e. perform

$$2 \int_o^{\ell} (b+y)[\rho(4.81a) + \sigma w(4.81b)]\, dy + 2m(b+\ell)(4.81c) = 0$$

This leads to

$$-\sum_{n=1}^{\infty} F_n (\ddot{Q}_n + \Omega_n^2 Q_n) + I_A \ddot{\delta} = 0$$

where I_A is the array moment of inertia defined as

$$I_A = 2(\rho + \sigma w) \int_o^{\ell} (b+y)^2\, dy + 2m(b+\ell)^2 \qquad (4.85)$$

Now, using (4.82) and the definition of $\mathbb{K}_m$ (4.86) can be re-written as

$$(-I \sum_{n=1}^{\infty} K_n + I_A) \ddot{\delta} = 0$$

Since $\ddot{\delta}$ is not zero in forced motion, we get

$$\sum_{n=1}^{\infty} K_n = I_A/I \qquad (4.85b)$$

This relation is useful in checking the values of the gains obtained. Note that, since the gains as defined by (4.85) are always positive, we have an upper bound on the K_n from this condition.

Sometimes it is more convenient to define new gains K_n' as

$$K_n' = I\, K_n = F_n^{\,2}/\sigma w \ell^3$$

The advantage of this is that K_n' depend only on the appendage properties, being independent of satellite size. Of course the K_n' are no longer dimensionless.

A block diagram representation of the Laplace transformed equations (4.83) is shown in Fig. 31. A special notation is used to indicate the infinite block corresponding to the sum in (4.83), this is explained in Fig. 30. It is possible to include a damping ratio ζ which is approximate and is usually small enough for the modal representation to be valid. The block labelled "control system" is assumed to produce correction torques β_1 and β_2 corresponding to attitude errors in terms of δ and ϵ. Thus the transformations from (δ,ϵ) to the roll-yaw angles, Eq. (4.25), and from the control torques (T_1, T_3) to the accelerations β_1 and β_3, Eq. (4.9), are assumed to be an intrinsic part of the control-system block. The solution for $\bar\delta$ and $\bar\epsilon$ may be explicitly stated from Eq. (4.84) as

$$\bar\delta = \left(s^2 + \omega_N^{\,2} - \sum_{n=1}^{\infty} \frac{s^4 K_n}{s^2 + \Omega_n^{\,2}}\right)^{-1} \left(\bar\beta_1 - \frac{\omega_N}{s}\,\bar\beta_3\right)$$

$$\bar\epsilon = \frac{1}{s^2}\,\bar\beta_3 + \frac{\omega_N}{s}\,\bar\delta \qquad (4.86)$$

The angles δ,ϵ were introduced mainly to simplify the motion equations for the satellite center body. In a computer simulation of the attitude control system such as the one given above, however, it may be more convenient to solve for ϕ and ψ directly, using the original motion equations (4.6). In the Laplace transformed form these can be written as

$$s^2 I_{11}\bar\phi + s^2 I_{13}\bar\psi + h\,s\bar\psi - \sum_{n=1}^{\infty} \frac{K_n s^2}{s^2 + \Omega_n^{\,2}} (\bar\phi\, c\gamma - \bar\psi s\gamma)\, c\gamma = \bar T_1$$

$$s^2 I_{33}\bar\psi + s^2 I_{13}\bar\phi - h\,s\bar\phi + \sum_{n=1}^{\infty} \frac{K_n s^2}{s^2 + \Omega_n^{\,2}} (\bar\phi c\gamma - \bar\psi s\gamma) s\gamma = \bar T_3 \qquad (4.87)$$

The block-diagram representation of (4.87) is shown in Fig. 32. It is more complicated than Fig. 13, but is more realistic since an actual control system would operate directly in terms of the roll and yaw angles.

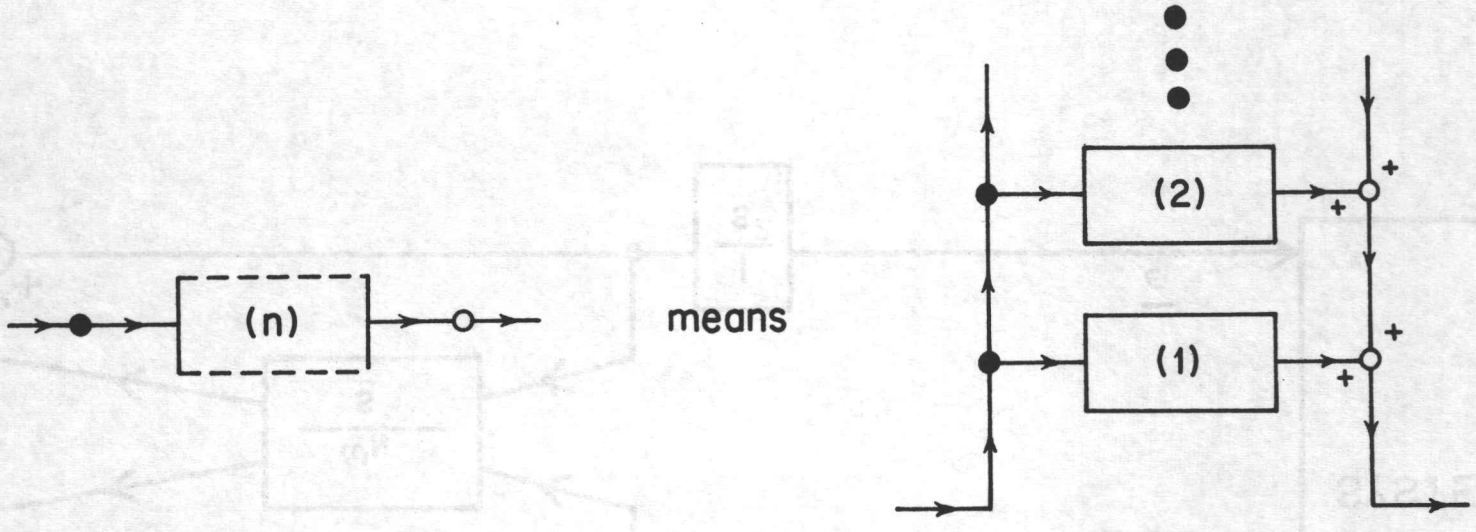

NOTATION

FIG. 30: Notation Used for Representation of Infinite Modal Transfer Functions

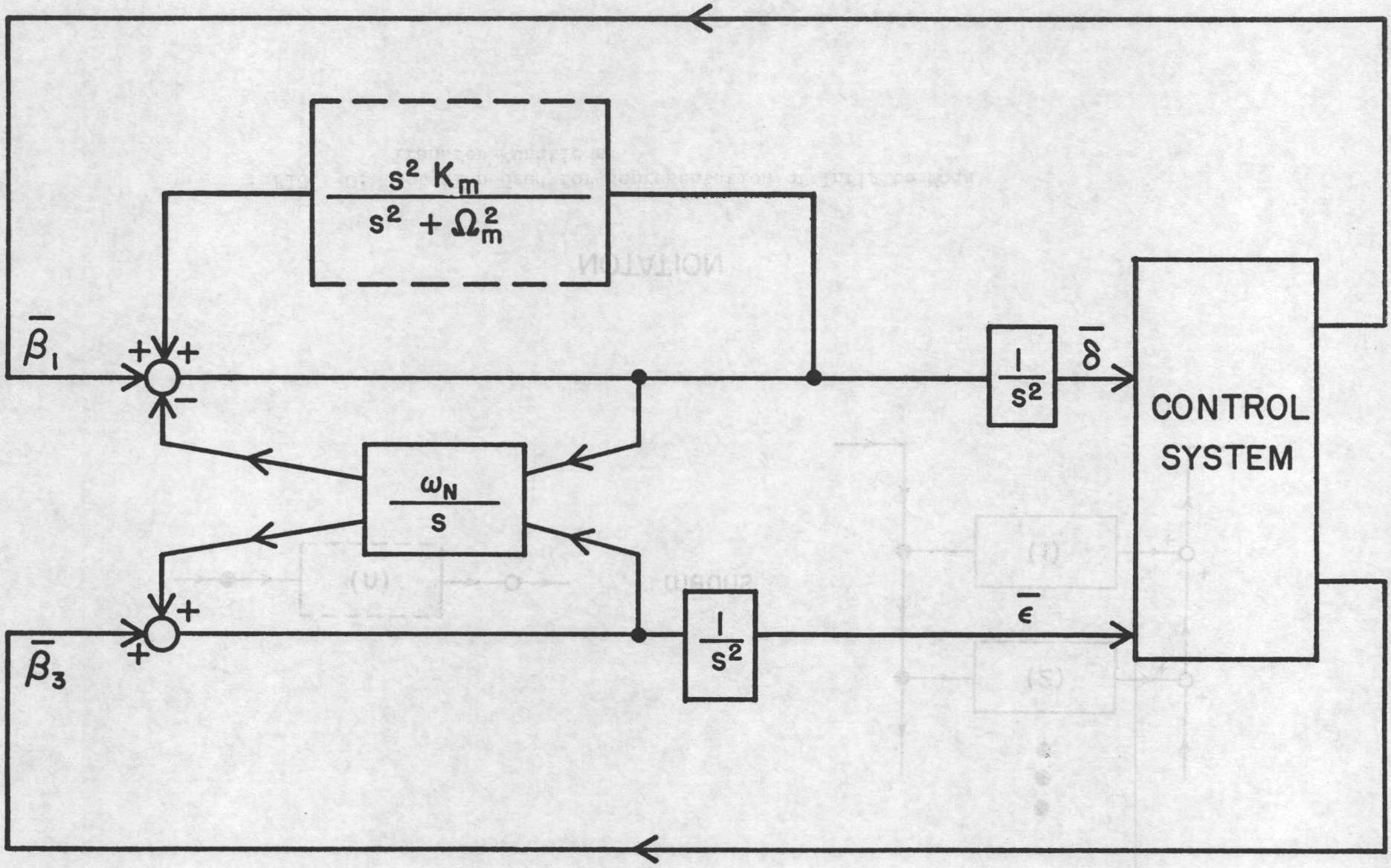

FIG. 31: δ-ϵ Attitude Control Block Diagram Incorporating Constrained Bending Modes

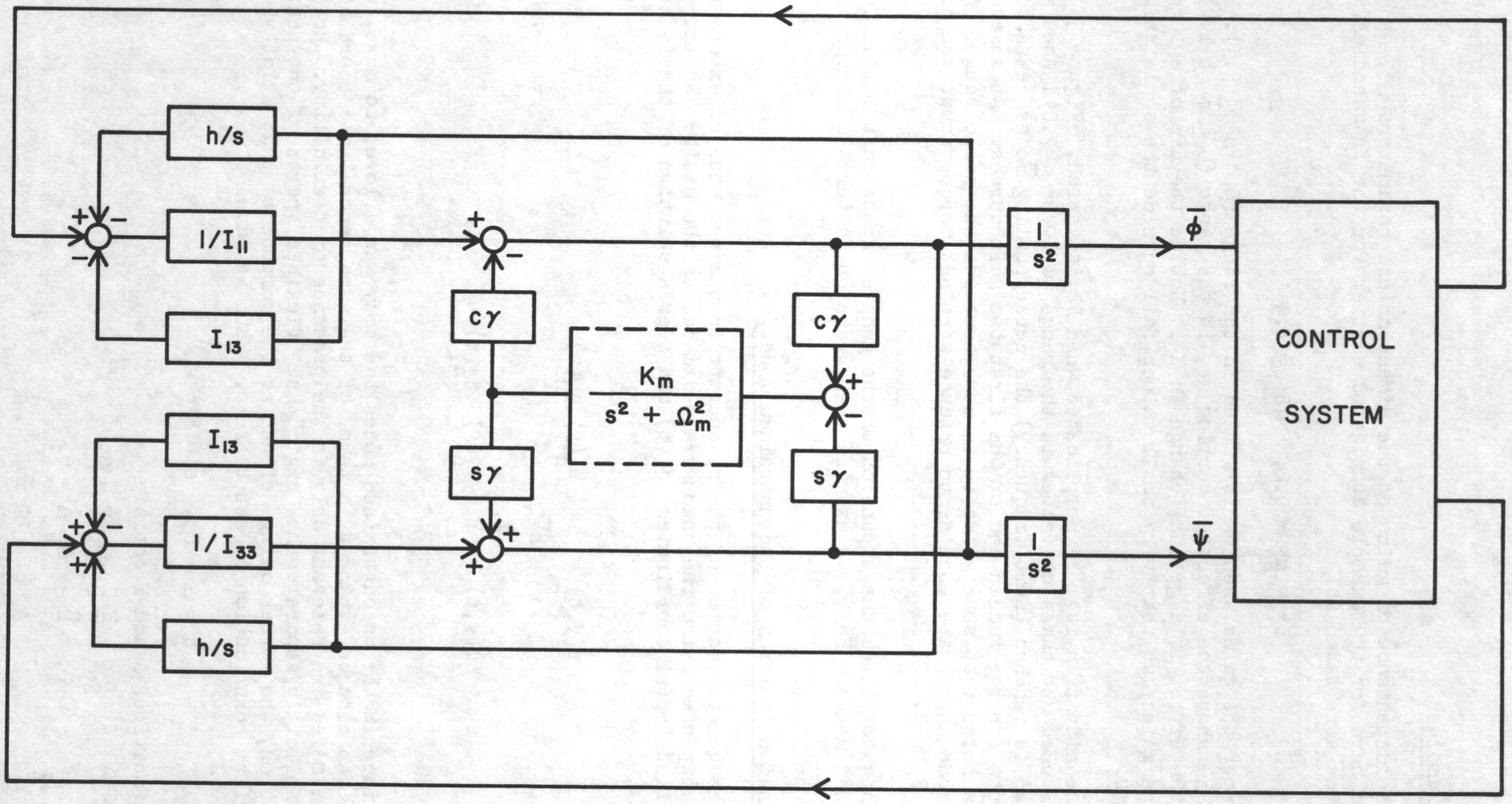

FIG. 32: Roll-Yaw Attitude Control Block Diagram Incorporating Constrained Bending Modes

Numerical Examples

The dependence of gains on the dimensionless parameters ρ^*, m^* and B^* is presented here for the example considered earlier for the frequencies. The nominal values were taken as

$$\rho^* = m^* = 0.2, \quad \sqrt{B^*} = 1.0$$

Figure 33 shows the gains when ρ^* is varied in the range $(0 < \rho^* \leq 3.5)$. Similarly, Fig. 34 shows the effect of varying m^*, in the range $(0 \leq m^* \leq 1.4)$. In both cases the effect is a gradual change in K_m. Notice the use of a logarithmic scale for the gains, so that very small values fall outside the scale range and are not shown.

The situation is more complicated when B^* is varied. Figure 35 shows what happens when $\sqrt{B^*}$ takes on values in the range $(0 < \sqrt{B^*} \leq 7.0)$. When a buckling load is reached (zero frequency) the corresponding modes cease to exist, which accounts for the sudden end of the first two gain curves. At some other points it is noted that some gains to to zero, outside the scale range. At these points the mode shapes are such as to produce zero net torque about the center of mass, i.e., $F_m = 0$.

This completes the expansion of the general spacecraft motion in terms of constrained modes. Next, we examine the expansion in terms of unconstrained modes.

4.3.2 Expansion in Terms of Unconstrained Modes

The general motion of the spacecraft in the presence of external torques can also be expanded using the unconstrained modes as the basis. We introduce the generalized "modal coordinates" $q_n(t)$ and seek a solution of the form

$$u(y,t) = \sum_{n=1}^{\infty} u_n(y)\, q_n(t)$$
$$v(y,t) = \sum_{n=1}^{\infty} v_n(y)\, q_n(t) \qquad (4.88)$$

Since in the unconstrained modes the body was allowed to move, the body motion can also be expanded in terms of the same generalized coordinates. However, the modes are relevant only in the presence of flexibility. Hence it is useful to explicitly separate the "rigid" and "flexible" parts of the net attitude motion, the former being defined as the components that exist when the flexibility contribution is set to zero. Thus we have

$$\delta = \Delta + \delta_f, \quad \epsilon = E + \epsilon_f \qquad (4.89)$$

where by definition, Δ and E satisfy

$$\ddot{\Delta} + \omega_N \dot{E} = \beta_1$$
$$\ddot{E} - \omega_N \dot{\Delta} = \beta_3 \qquad (4.90)$$

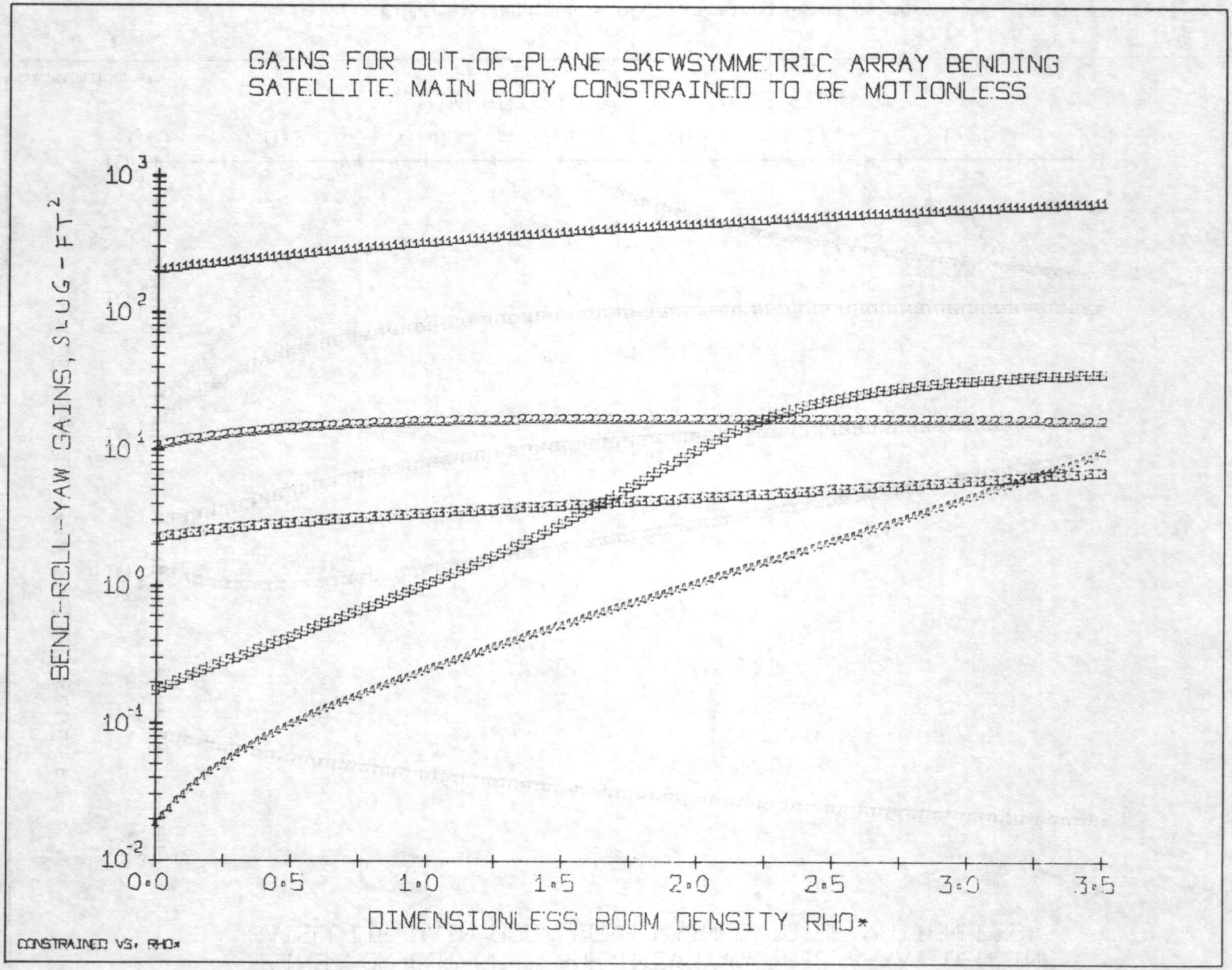

FIG. 33: Dependence of Constrained Gains on ρ*

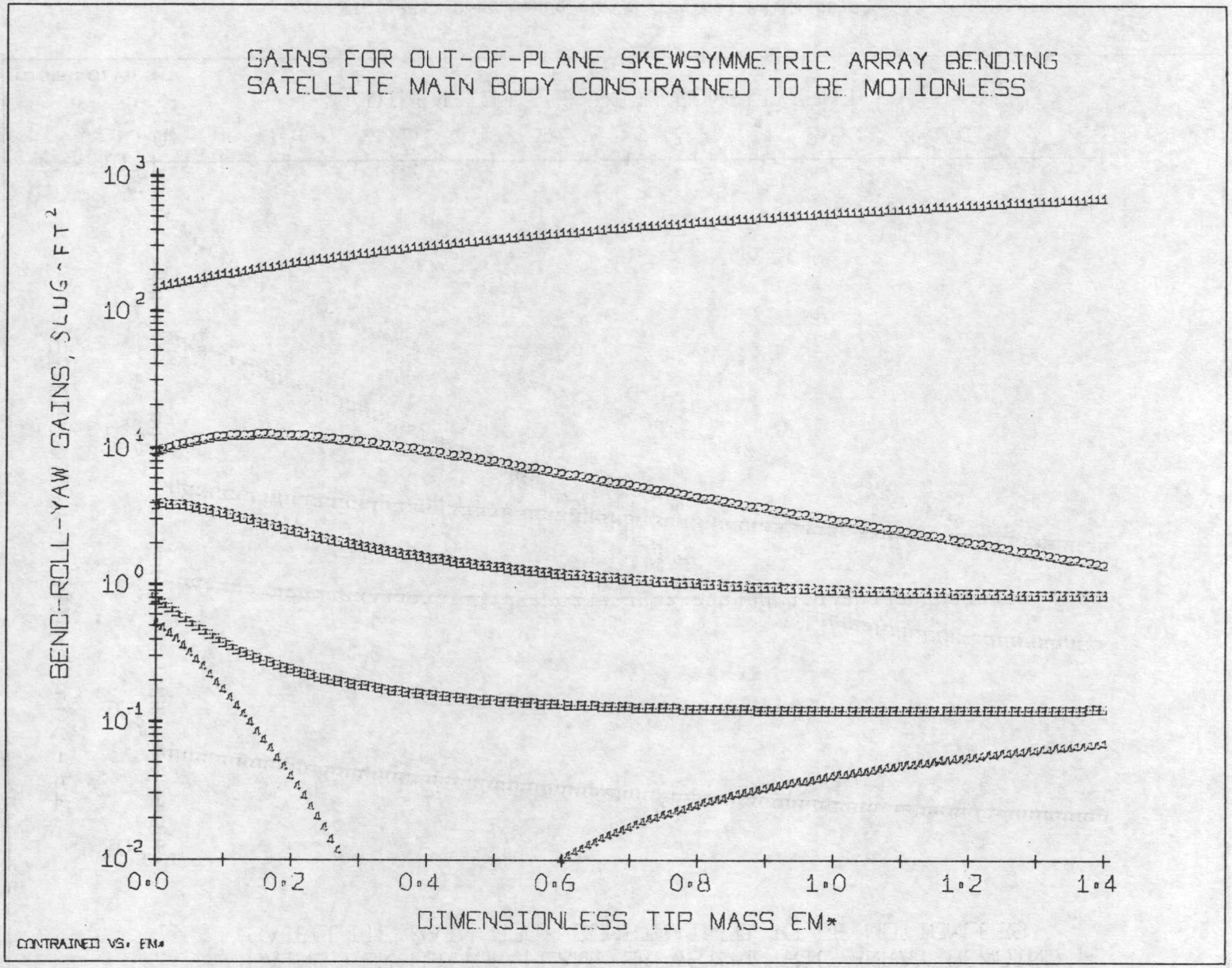

FIG. 34: Dependence of Constrained Gains on m*

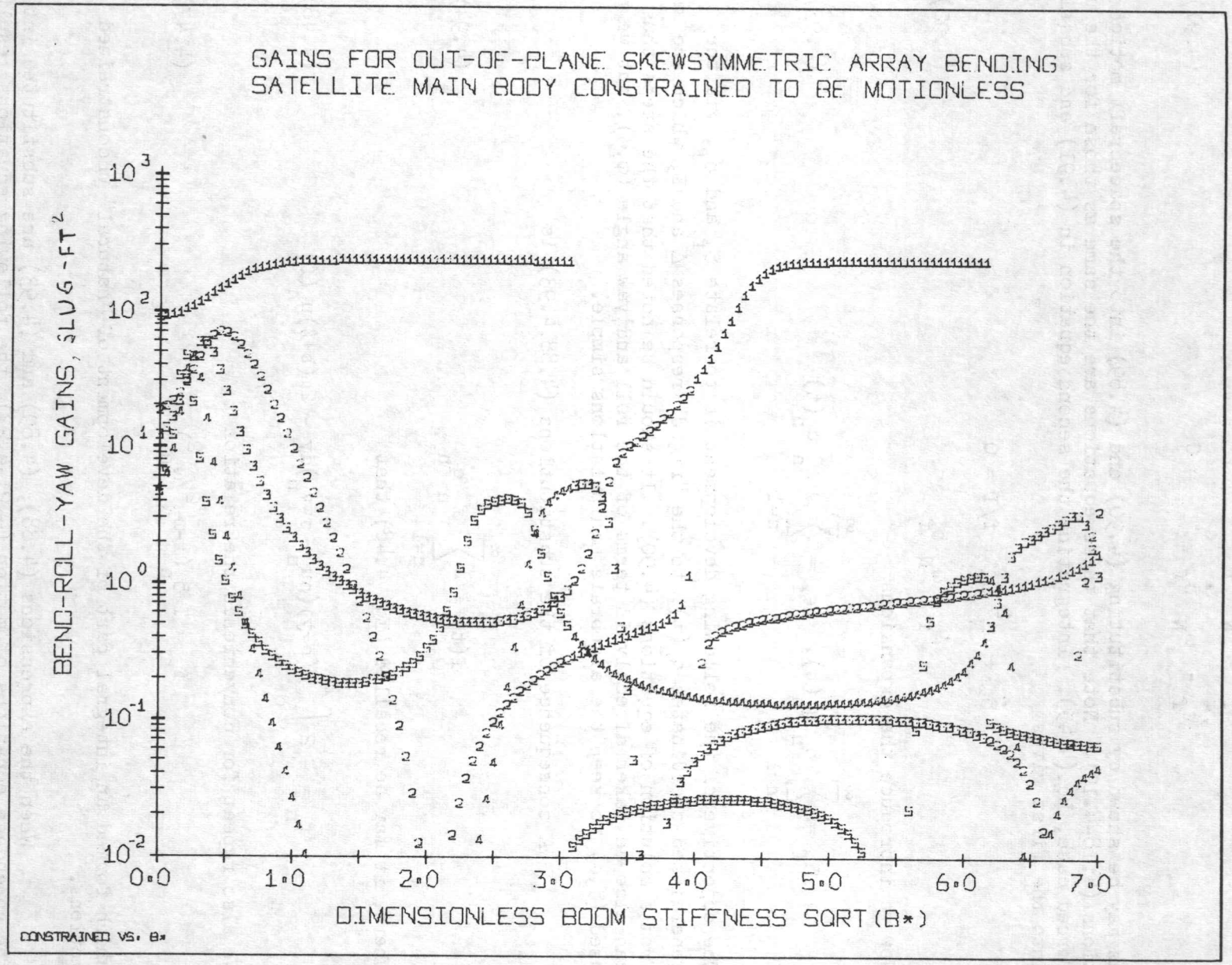

FIG. 35: Dependence of Constrained Gains on $\sqrt{B^*}$

The subscript "f" denotes the "flexible" part, which satisfies the equations:

$$\begin{aligned} \ddot{\delta}_f + \omega_N \dot{\epsilon}_f + f/I &= 0 \\ \dot{\epsilon}_f - \omega_N \dot{\delta}_f &= 0 \end{aligned} \tag{4.91}$$

as may be shown by substituting (4.90) and (4.89) into the spacecraft motion equations (4.18-4.19). Note that these equations are the same as those for the unforced case, Eq.(4.45). Integrating the second equation in (4.91) and substituting into the first gives

$$\begin{aligned} \ddot{\delta}_f + \omega_N^2 \delta_f + f/I &= 0 \\ \dot{\epsilon}_f &= \omega_N \delta_f \end{aligned} \tag{4.92}$$

Now we introduce the expansions

$$\delta_f = \sum_{n=1}^{\infty} \delta_n q_n(t), \quad \epsilon_f = \sum_{n=1}^{\infty} \epsilon_n q_n(t) \tag{4.93}$$

The objective of the following development is to relate δ_f and ϵ_f, via the generalized coordinates $q_n(t)$, to the "rigid" responses Δ and E, which are known from a solution of equations (4.90). It should be noted that the steps thus far can also be taken directly in terms of the roll and yaw angle (φ,ψ), but we have used (δ,ϵ) to keep the algebraic manipulations simple.

A consequence of the substitutions (4.88,4.93) is

$$f(t) = -\sum_{n=1}^{\infty} f_n \ddot{q}_n \tag{4.94}$$

where, it may be recalled (Eq. 4.48) that

$$f_n = -2\int_o^{\ell} (b+y)(\rho u_n + \sigma w v_n)dy - 2m(b+\ell)u_n(\ell) \tag{4.48}$$

We also repeat for convenience the relation

$$f_n = I\,\delta_n(1-\omega_N^2/\omega_n^2) \tag{4.47}$$

which formed an integral part of the development of "natural" unconstrained motions.

When the expressions (4.88), (4.89) and (4.93) are substituted into the appendage equations of motion (4.21-4.23), the following equations result:

$$\sum_{n=1}^{\infty} P\, v_n'' q_n = \sigma w \left[\sum_{n=1}^{\infty} (v_n + (b+y)\delta_n)\, \ddot{q}_n + (b+y)\ddot{\Delta} \right]$$

$$\sum_{n=1}^{\infty} (Bu_n'''' + Pu_n'')q_n = \rho \left[\sum_{n=1}^{\infty} (u_n + (b+y)\delta_n)\, \ddot{q}_n + (b+y)\, \ddot{\Delta} \right] \qquad (4.95)$$

$$\sum_{n=1}^{\infty} \left\{ (Bu_n''' + Pu_n' - Pv_n') \Big|_{y=\ell} \right\} q_n = m \left[\sum_{n=1}^{\infty} (u_n(\ell) + (b+\ell)\delta_n)\ddot{q}_n + (b+\ell)\ddot{\Delta} \right]$$

The mode shape functions $u_n(y)$ and $v_n(y)$ satisfy the differential equations and boundary conditions (4.49-4.52) derived earlier. Taking Eqs. (4.49), (4.50) and the first of (4.52) respectively, summing for n = 1 to ∞, and subtracting the result from equations (4.95) in the same order, yields

$$\sum_{n=1}^{\infty} [v_n(y) + (b+y)\delta_n](\ddot{q}_n + \omega_n^2 q_n) + (b+y)\, \ddot{\Delta} = 0 \qquad (4.96a)$$

$$\sum_{n=1}^{\infty} [u_n(y) + (b+y)\delta_n](\ddot{q}_n + \omega_n^2 q_n) + (b+y)\, \ddot{\Delta} = 0 \qquad (4.96b)$$

$$\sum_{n=1}^{\infty} [u_n(\ell) + (b+\ell)\delta_n](\ddot{q}_n + \omega_n^2 q_n) + (b+\ell)\ddot{\Delta} = 0 \qquad (4.96c)$$

In view of the orthonality condition (4.63) derived earlier, we form a Ξ_{mn} - type expression from (4.96), i.e., perform the operation

$$2\sigma w \int_0^{\ell} (4.96a)\; v_m(y)dy + 2\rho \int_0^{\ell} (4.96b) u_m(y)dy + 2m(4.96c)u_m(\ell) = 0$$

Using the definitions of Ξ_{mn}, (4.61) and f_m, (4.48), the resulting expression can be compactly written as

$$\sum_{n=1}^{\infty} (\Xi_{mn} - f_m \delta_n)(\ddot{q}_n + \omega_n^2 q_n) = f_m\, \ddot{\Delta} \qquad (4.97)$$

We now wish to uncouple this infinite system of equations into separate equations governing the generalized coordinates. Using the orthogonality condition (4.63) and the relation (4.47) between f_m and δ_m, we get

$$\xi_{mm} - f_m \delta_m = \sigma w \ell^3 - I \delta_m^2 (1-\omega_N^2/\omega_m^2) \tag{4.98}$$

$$\xi_{mn} - f_m \delta_n = I\delta_m\delta_n\left(1 - \frac{\omega_N^2}{\omega_m^2} - \frac{\omega_N^2}{\omega_n^2}\right) - I\delta_m\delta_n(1-\omega_N^2/\omega_m^2)$$

$$= -I \delta_m\delta_n (\omega_N^2/ \omega_n^2), \quad m \neq n$$

The normalization $\xi_{mm} = \sigma w \ell^3$ has also been used here. Hence Eq. (4.97) may be written

$$[\sigma w \ell^3 - I\delta_m^2(1-\omega_N^2/ \omega_m^2)] (\ddot{q}_m + \omega_m^2 q_m)$$
$$- I \omega_N^2 \delta_m \sum_{\substack{n=1 \\ n\neq m}}^{\infty} (\delta_n/\omega_n^2)(\ddot{q}_n + \omega_n^2 q_n) = \ddot{\Delta}\, I\, \delta_m(1-\omega_N^2/\omega_m^2) \tag{4.99}$$

In order to uncouple the equations still further, we must get rid of the infinite sum in (4.99). This can be accomplished as follows. We substitute the expansions (4.93) and (4.94) into the first of the "flexible" equations (4.92), to get

$$\sum_{n=1}^{\infty} (\delta_n - f_n/I)\, \ddot{q}_n + \omega_N^2 \sum_{n=1}^{\infty} \delta_n q_n = 0 \tag{4.100}$$

When the relation (4.47) is inserted in (4.100), it gives

$$\omega_N^2 \sum_{n=1}^{\infty} (\delta_n/\omega_n^2)(\ddot{q}_n + \omega_n^2 q_n) = 0 \tag{4.101}$$

Thus the infinite sum in (4.99) becomes simply

$$I \omega_N^2 \delta_m \sum_{\substack{n=1 \\ n\neq m}}^{\infty} (\delta_n/\omega_n^2)(\ddot{q}_n + \omega_n^2 q_n) = -I \omega_N^2 (\delta_m^2/\omega_m^2)(\ddot{q}_m + \omega_m^2 q_m)$$

Using this relation finally leads to an uncoupled form for (4.99):

$$\ddot{q}_m + \omega_m^2 q_m = r_m \ddot{\Delta}, \quad m = 1,2,\ldots \infty \tag{4.102}$$

where

$$r_m = \frac{I \delta_m (1 - \omega_N^2/\omega_m^2)}{\sigma w \ell^3 - I \delta_m^2 (1-2\omega_N^2/ \omega_m^2)} \tag{4.103}$$

The complete solution for δ and ϵ is obtained when Eqs. (4.90) and (4.102) are solved simultaneously for Δ, E and the generalized coordinates $q_n(t)$. It is convenient to express this solution in Laplace transformed form. From Eq.(4.102)

$$\bar{q}_n = \frac{s^2 r_n}{s^2 + \omega_n^2} \bar{\Delta} \tag{4.104}$$

To obtain $\bar{\delta}_f$, we have two alternate formulations:

(i) One is directly obtained from (4.93):

$$\bar{\delta}_f = \sum_{n=1}^{\infty} \frac{s^2 k_n'}{s^2 + \omega_n^2} \bar{\Delta} \tag{4.105}$$

where

$$k_n' \equiv r_n \delta_n = \frac{I \delta_n^2 (1 - \omega_N^2/\omega_n^2)}{\sigma w \ell^3 - I \delta_n^2 (1 - 2\omega_N^2/\omega_n^2)} \tag{4.106}$$

(ii) Another approach is to use the "flexible" motion equation (4.92), with the expansion (4.94) for f(t). From equation (4.92) we have

$$\bar{\delta}_f = - \left(\frac{1}{s^2 + \omega_N^2} \right) \bar{f}/I \tag{4.107}$$

Now from (4.94) and (4.47) we have

$$\bar{f} = - \sum_{n=1}^{\infty} [\, I \delta_n (1 - \omega_N^2/\omega_n^2) \,] \, s^2 \bar{q}_n$$

combining this relation with (4.107) we obtain

$$\bar{\delta}_f = \left(\frac{s^2}{s^2 + \omega_N^2} \right) \sum_{n=1}^{\infty} \delta_n (1 - \omega_N^2/\omega_n^2) \bar{q}_n$$

Now we insert equation (4.104) for $\bar{q}_n$ to give

$$\bar{\delta}_f = \left(\frac{s^2}{s^2 + \omega_N^2} \right) \sum_{n=1}^{\infty} \frac{s^2 k_n}{s^2 + \omega_n^2} \bar{\Delta} \tag{4.108}$$

where

$$k_n = \frac{I \delta_n^2 (1 - \omega_N^2/\omega_n^2)^2}{\sigma w \ell^3 - I \delta_n^2 (1 - 2\omega_N^2/\omega_n^2)} \tag{4.109}$$

Once $\bar{\delta}_f$ is known by either of the above formulations, $\bar{\epsilon}_f$ is directly available from (4.92):

$$\bar{\epsilon}_f = \frac{\omega_N}{s} \bar{\delta}_f \tag{4.110}$$

The roll and yaw angles φ and ψ can be obtained as before by transforming δ and ϵ, via Eq. (4.25).

With an appropriate definition for the gains, the expressions (4.108) and (4.105) only differ in the presence of the factor $(s^2/(s^2+\omega_N^2))$ in the former. While formulation (i) is thus simpler to simulate, formulation (ii) has the property that all the gains are positive. This may be proved as follows. We start with the inequality

$$2\sigma w \int_0^\ell [v_n + (b+y)\,\delta_n]^2 dy + 2\rho \int_0^\ell [u_n + (b+y)\,\delta_n]^2\, dy$$

$$+ 2m\,[u_n(\ell) + (b+\ell)\delta_n]^2 \geq 0$$

Expanding the terms in the brackets and recognizing the familiar terms Ξ_{nn} and f_n, we obtain

$$\Xi_{nn} - 2 f_n \delta_n + I_A \delta_n^2 \geq 0 \tag{4.111}$$

where I_A is the array moment of inertia, as previously defined:

$$I_A = 2(\rho + \sigma w) \int_0^\ell (b+y)^2\, dy + 2m(b+\ell)^2 \tag{4.85}$$

Now, $I_A \delta_n^2$ is transposed to the other side of (4.111), and the term $I\,\delta_n^2$ added to both sides. Inserting then the relation (4.47) between f_n and δ_n yields

$$\sigma w \ell^3 - I\,\delta_n^2\,(1-2\omega_N^2/\omega_n^2) \geq (I-I_A)\,\delta_n^2 \tag{4.112}$$

Since $I > I_A$ for any finite center body, the denominator of the gain expression (4.109) is always positive. The numerator is a square, hence it follows that $k_n \geq 0$ always. From (4.112) we also obtain an upper bound on k_n, so that

$$0 < k_n \leq \frac{I(1-\omega_N^2/\omega_n^2)^2}{(I-I_A)} \tag{4.113}$$

A property of the unconstrained gains of the first kind, k_n', will now be proved, corresponding to the sum of the "constrained" gains K_n in Eq.(4.88). To do this we go back to the equations (4.96) and form from them a f_n-type expression, i.e., perform the operation

$$2\int_0^{\ell}(b+y)[\sigma w(4.96a)+\rho(4.96b)]dy + 2m(b+\ell)\ (4.96c) = 0$$

This leads to

$$\sum_{n=1}^{\infty}(-f_n + I_A\delta_n)(\ddot{q}_n + \omega_n^2 q_n) + I_A\ddot{\Delta} = 0 \qquad (4.114)$$

where again I_A is the array moment of inertia. Substituting for f_n in terms of I and δ_n and rearranging, we obtain

$$\sum_{n=1}^{\infty}\delta_n(-I + I_A)(\ddot{q}_n + \omega_n^2 q_n) + I\,\omega_N^2\sum_{n=1}^{\infty}(\delta_n/\omega_n^2)(\ddot{q}_n + \omega_n^2 q_n) = -I_A\ddot{\Delta} \qquad (4.115)$$

The second term vanishes by virtue of (4.101). Using the modal equations (4.102) and the definition of k_n' in (4.106) reduces (4.115) to

$$\sum_{n=1}^{\infty}k_n'(I_A-I)\ddot{\Delta} = -I_A\ddot{\Delta}$$

Since $\ddot{\Delta} \neq 0$ in general, we must have

$$\sum_{n=1}^{\infty}k_n' = \frac{I_A}{I-I_A} \qquad (4.116)$$

Thus although the k_n' may be both positive and negative, they form a convergent sequence. Another identity concerning the k_n' follows from (4.101). First we combine Eqs. (4.104) and (4.106) to give

$$(\ddot{q}_n + \omega_n^2 q_n)\,\delta_n = k_n'\ddot{\Delta}$$

substituting this relation into (4.101) and recognizing that $\ddot{\Delta} \neq 0$ in general, we obtain

$$\sum_{n=1}^{\infty}\frac{k_n'}{\omega_n^2} = 0 \qquad (4.117)$$

All k_n' are not positive, but we note that, since the denominator of (4.106) is always positive,

$$\text{sign}(k_n') = \text{sign}(1-\omega_N^2/\omega_n^2)$$

Thus $k_n' < 0$ only if the corresponding natural frequency is less than the rigid

body nutation frequency. For CTS, this is true only of the first frequency. The remaining k_n' are in fact almost identical to k_n, in view of the fact that, from (4.106) and (4.109),

$$k_n = (1-\omega_N^2/\omega_n^2)k_n'$$

and $\omega_N \ll \omega_2$ for CTS.

A simulation block diagram in terms of δ and ϵ is drawn in Fig. 36, corresponding to gains of the second kind. The block diagram corresponding to the first kind k_n' will be identical, except that the $(s^2/s^2 + \omega_N^2)$ block will be absent. As in the constrained case, the control system block is assumed to contain the transformations necessary from (δ,ϵ) to (φ,ψ) and from the control and environmental torques (T_1,T_3) to the accelerations (β_1,β_3), in the interests of simplicity. Figure 36 should be compared with the corresponding diagram for the constrained case, Fig. 31. The damping ratio ζ may be heuristically inserted as before. The solution for $\bar{\delta}$ and $\bar{\epsilon}$ can be explicitly written as

$$\bar{\delta} = \frac{1}{s^2+\omega_N^2}\left[1 + \left(\frac{s^2}{s^2+\omega_N^2}\right)\sum_{n=1}^{\infty}\frac{s^2 k_n}{s^2+\omega_n^2}\right](\bar{\beta}_1 - \frac{\omega_N}{s}\bar{\beta}_3)$$

$$\bar{\epsilon} = \frac{1}{s^2}\bar{\beta}_3 + \frac{\omega_N}{s}\bar{\delta} \qquad (4.118)$$

These expressions correspond to Eq. (4.86) for the constrained case. When $\omega_N = 0$ (no stored momentum), there is no coupling between δ and ϵ. Under these circumstances, equations (4.86) and (4.118) yield respectively

$$s^2\,\bar{\delta} = \left(1 - \sum_{n=1}^{\infty}\frac{s^2 k_n}{s^2+\Omega_n^2}\right)^{-1}\bar{\beta}_1$$

$$s^2\,\bar{\delta} = \left(1 + \sum_{n=1}^{\infty}\frac{s^2 k_n}{s^2+\omega_n^2}\right)\bar{\beta}_1 \qquad (4.119)$$

Note also that in this case the distinction between k_n' and k_n disappears. Thus when $\omega_N = 0$, the following relation between the constrained and unconstrained frequencies and gains exists:

$$\left(1 - \sum_{n=1}^{\infty}\frac{s^2 k_n}{s^2+\Omega_n^2}\right)\left(1 + \sum_{n=1}^{\infty}\frac{s^2 k_n}{s^2+\omega_n^2}\right) = 1 \qquad (4.120)$$

We now present a more useful but entirely equivalent block diagram representation, explicitly in terms of the roll and yaw angles ϕ and ψ respectively. For this purpose the following relations are defined, analogous to the (δ,ϵ) case

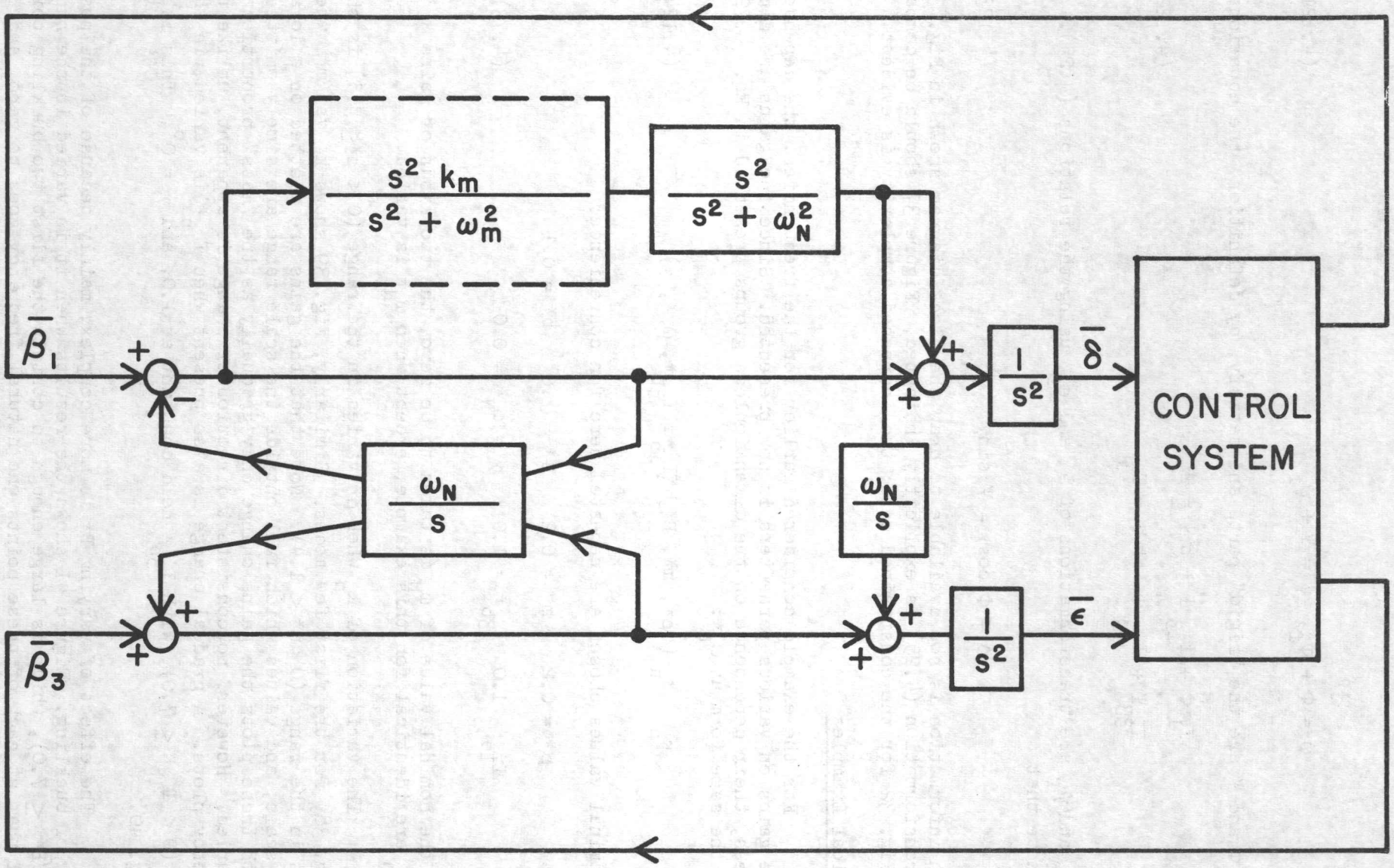

FIG. 36: δ-ϵ Attitude Control Block Diagram Incorporating Unconstrained Bending Modes

$$\phi = \Phi + \varphi_f, \quad \psi = \Psi + \psi_f \tag{4.121}$$

where Φ and Ψ are the "rigid" parts and satisfy, by definition, the equations

$$\begin{aligned} I_{11}\ddot{\Phi} + I_{13}\ddot{\Psi} + h\dot{\Psi} &= T_1 \\ I_{33}\ddot{\Psi} + I_{13}\ddot{\Phi} - h\dot{\Phi} &= T_3 \end{aligned} \tag{4.122}$$

and ϕ_f and ψ_f are transformations of δ_f and ϵ_f, using the relations (4.25). We also note that

$$\Delta \equiv \Phi \cos\gamma - \Psi \sin\gamma \tag{4.123}$$

Enough information is now available to draw the block diagram shown in Fig. 37. The transformation (4.25) is explicitly indicated. Figure 37 should be compared with Fig. 32 for the constrained case; the increased complexity is evident.

Numerical Examples

For the example considered earlier for the frequencies, the dependence of the gains on various parameters is now presented. Since the gains are dimensionless, their dependence on the dimensionless groups presented in Eq. (4.72) is of the same form as ω_n^*:

$$k_n = k_n (\rho^*, m^*, B^*, b^*, I_{1b}^*, I_{3b}^*, \omega_N^*, \gamma) \tag{4.124}$$

The nominal values chosen are repeated here for convenience:

$$\begin{aligned} &\rho^* = 0.2 \quad m^* = 0.2 \quad B^* = 1.0 \quad b^* = 0.1 \\ &I_{1b}^* = 1.0 \quad I_{3b}^* = 1.0 \quad \gamma = \omega_N^* = 0.0 \end{aligned} \tag{4.73}$$

Since the nominal value of ω_N is taken to be zero, the two kinds of gains k_n' and k_n are identical for this example, except when ω_N^* is varied.

The variation of k_n when ρ^* varies in the range $(0 < \rho^* \leq 3.5)$ is shown in Fig. 38, for the first few modes. Similarly, Fig. 39 shows k_n vs. m^*, when m^* varies in the range $(0 < m^* \leq 1.4)$. Note that the gains are plotted on a logarithmic scale, and values which fall outside the scale range are simply omitted. In both these plots the gains change only gradually as the "mass" properties are varied. However, no consistent direction of change is apparent, unlike the frequency plots. A gradual change is also present when I_{1b}^* is varied, in the range $(0 < I_{1b}^* \leq 7.0)$, with I_{3b}^* held constant at 1.0, and $\gamma = 0^\circ$. This is shown in Fig. 40.

The effect of varying B^* is more complex, mainly because of the possibility of buckling. Figure 41 shows the results when it is varied in the range $(0 < \sqrt{B^*} \leq 7.0)$, which is large enough to contain the first two buckling points. Recall that at each of these points one natural frequency goes to zero, and

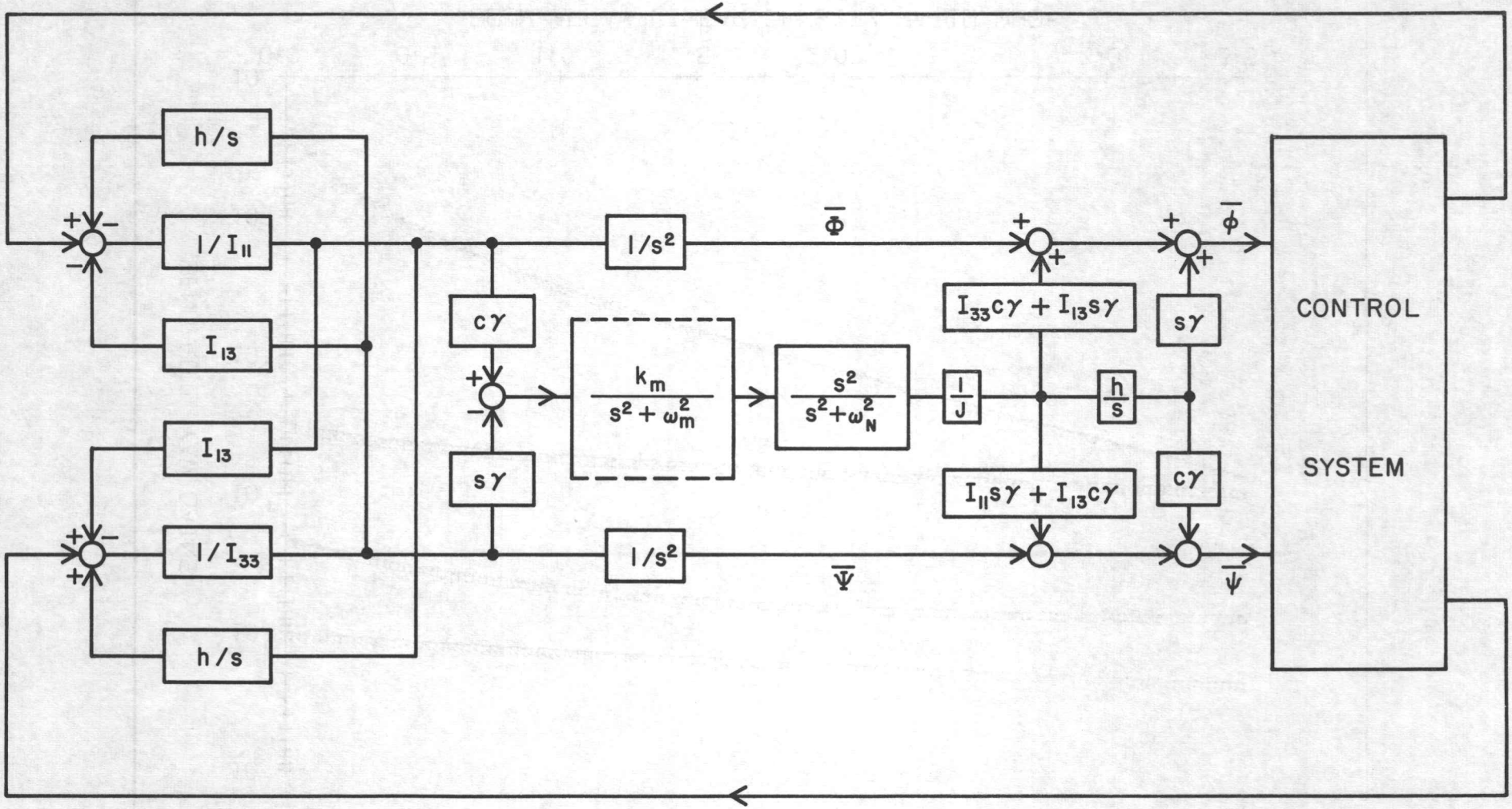

FIG. 37: Roll-Yaw Attitude Control Block Diagram Incorporating Unconstrained Bending Modes

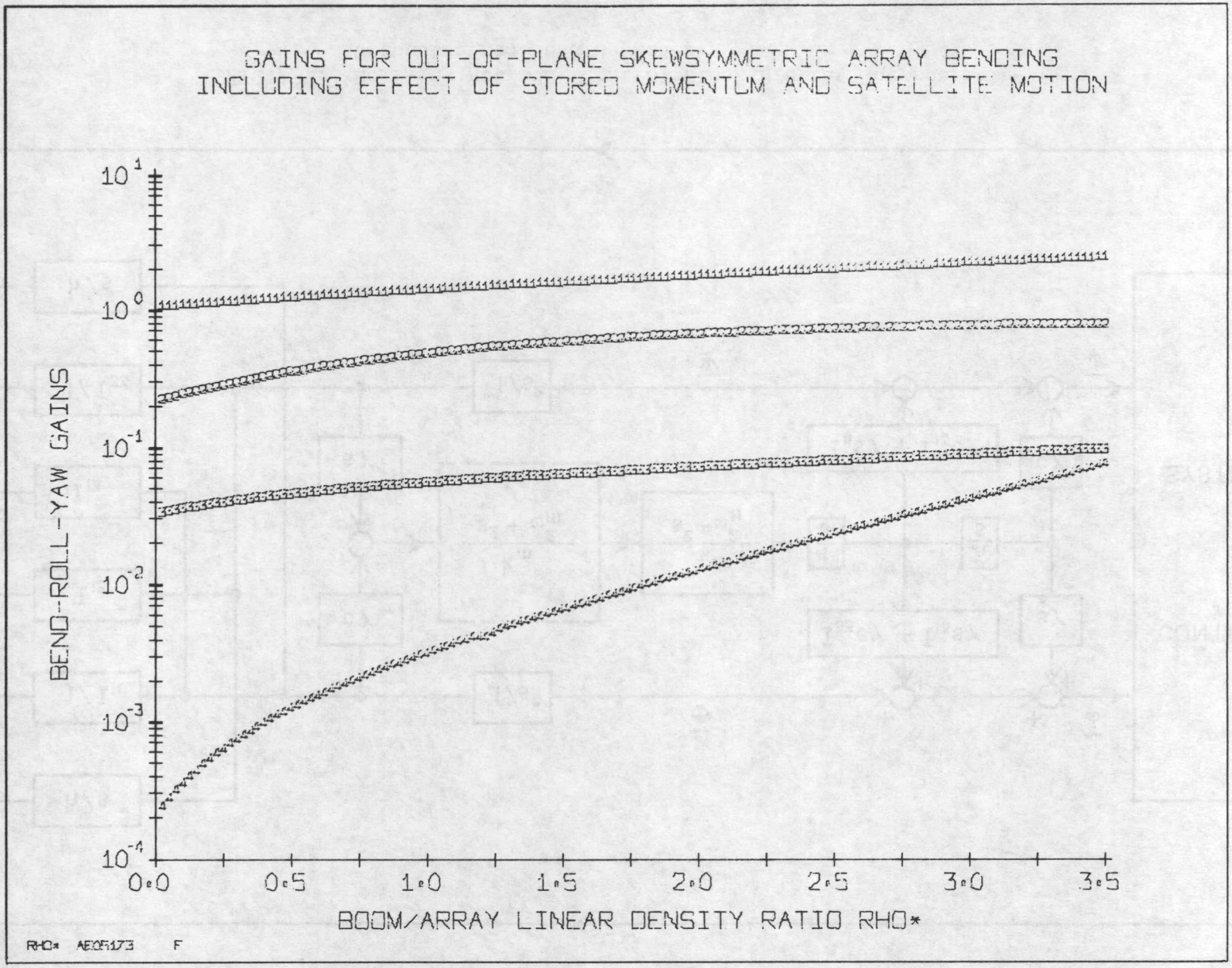

FIG. 38: Dependence of Unconstrained Gains on ρ*

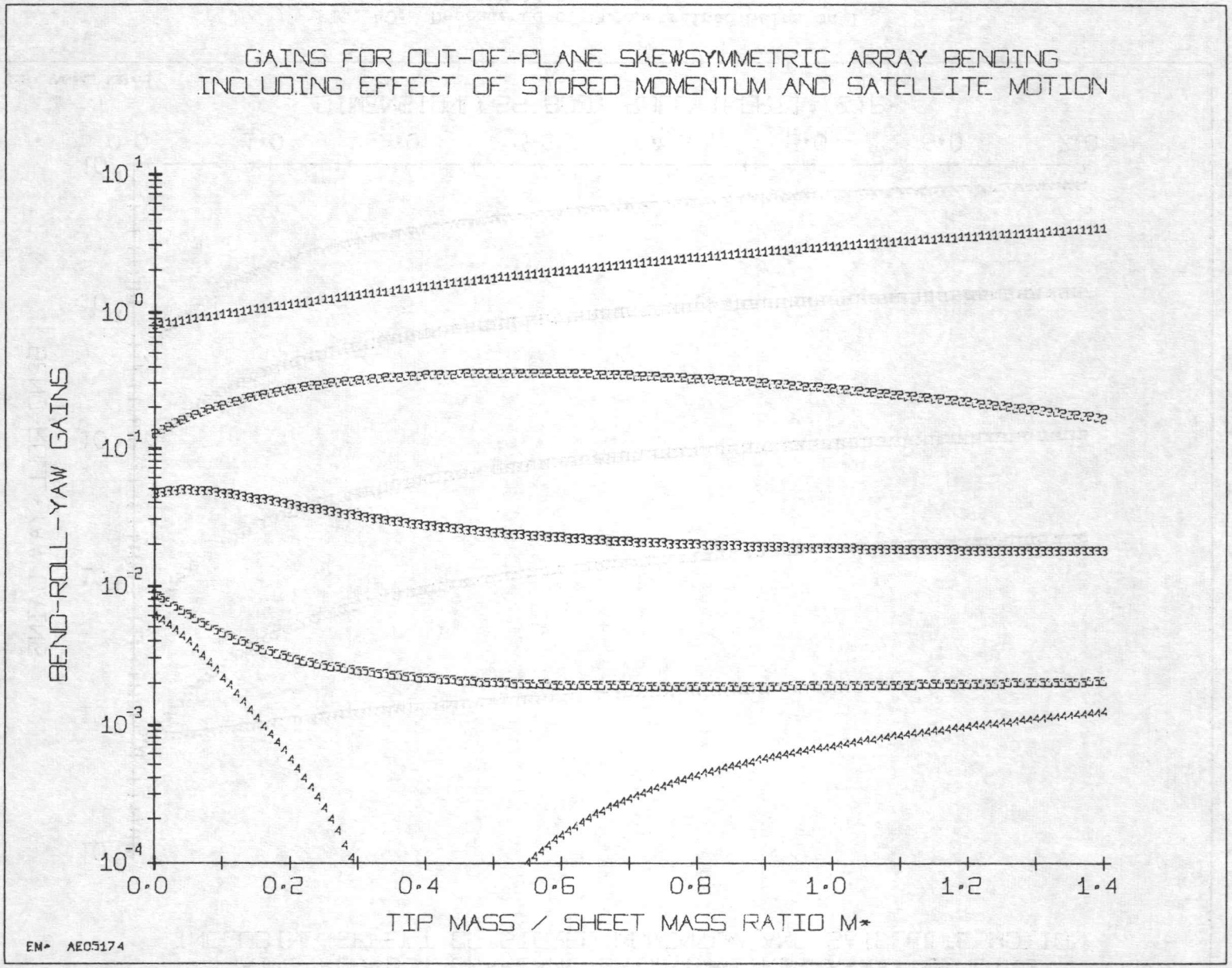

FIG. 39: Dependence of Unconstrained Gains on m*

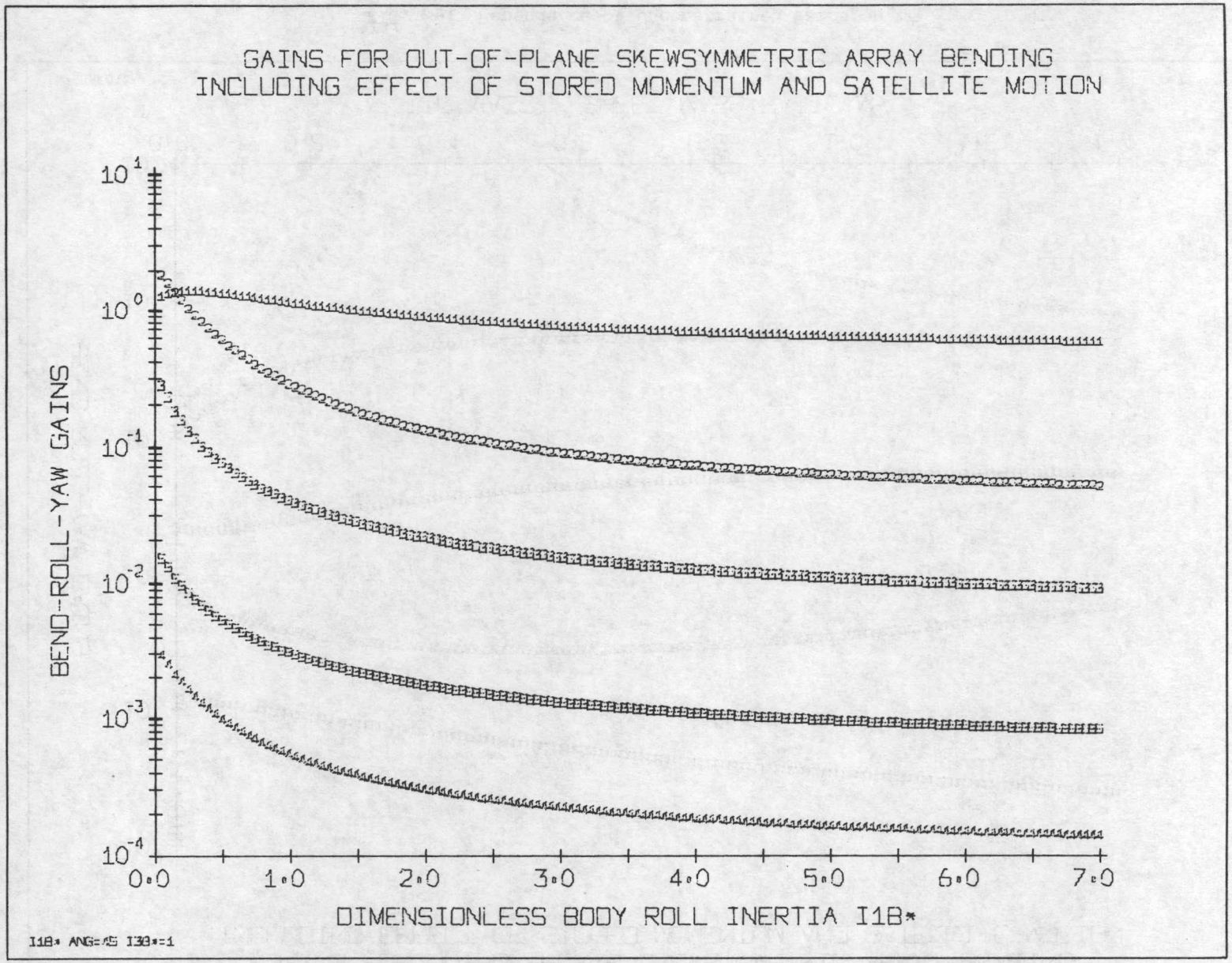

FIG. 40: Dependence of Unconstrained Gains on I_{1b}* (I_{3b}* Held Constant)

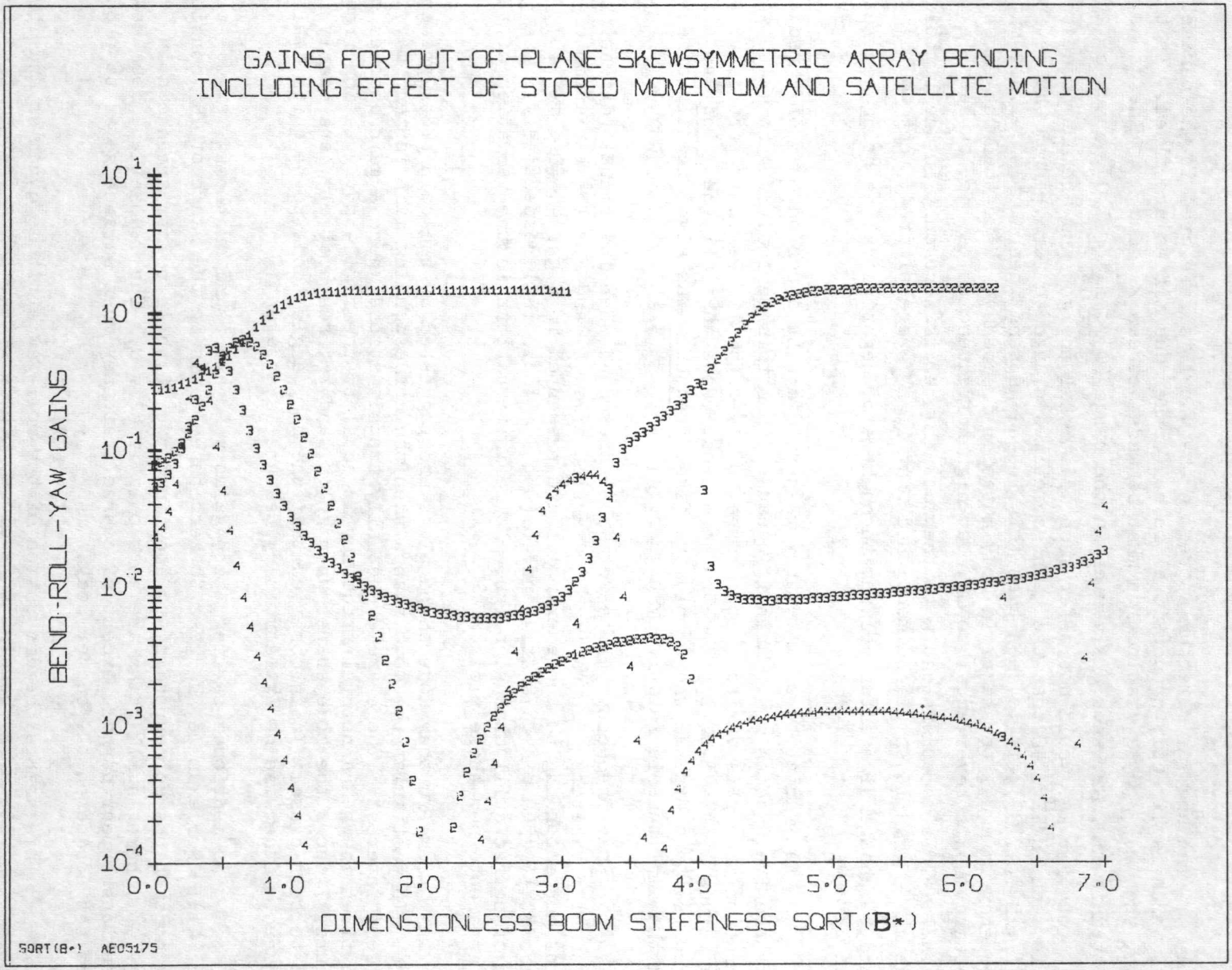

FIG. 41: Dependence of Unconstrained Gains on $\sqrt{B^*}$

effectively the corresponding mode ceases to exist. This accounts for the abrupt end of two curves. It is also found that at some values of $\sqrt{B}^*$ the gains steeply plunge towards zero, and are in fact zero at isolated points. This occurs when there is no net torque acting on the body due to the flexible appendages, so that $\delta_n = 0$.

The angular momentum stored in the wheel is refelcted in the parameter ω_N^*, which is directly proportional to h if other quantities are fixed. In this case, when $\omega_N \neq 0$, a distinction must be made between k_n' and k_n. The gains plotted in Fig. 42, when ω_N^* varies in the range $(0 \leq \omega_N^* \leq 7.0)$, are the latter. The plots for k_n' would not offer much additional insight and are not presented. It is seen in Fig. 42 that the gains sometimes plunge to zero. From the definition of k_n, Eq.(4.109), it is seen that this indeed happens when $\omega_N = \omega_n$, i.e., natural frequency is equal to the rigid-body nutation frequency. Note that the first frequency ω_1 is never equal to ω_N, but higher frequencies may be, as seen in Fig. 21. This is consistent with the fact that k_1 is zero only in the limiting case $\omega_N^* \to 0$. It should be mentioned that if k_n' were plotted, they would be found to change sign after passing through zero, negative values being generated when $\omega_N > \omega_n$.

The variation of k_n with γ is periodic with a period in γ of π radians, like the frequencies ω_n^*. This is because I has this period. Figure 43 shows the variation when γ is varied in the range $(0 \leq \gamma \leq 350^\circ)$. For this particular example the values $I_{1b}^* = 1.0$, $I_{3b}^* = 10.0$ were used. Note that all the gains are affected, in contrast to Fig. 22 where only the first frequency was significantly affected, and the amplitude is relatively higher.

Some frequency plots were also presented when individual (dimensional) physical parameters were varied, in particular σ, ℓ and P. The variation of gains corresponding to these examples are presented in Figs. 44 $(0 < \sigma \leq .07$ slugs/ft$^2)$, 45$(0 < \ell \leq 70$ ft.) and 46 $(0 < P \leq 168.0$ lb$_f)$ respectively. The gains are of course still dimensionless. No definite pattern in the variation of the k_n is apparent from these plots.

Some further mode shape plots are suggested by the gain plots presented here. In particular the mode shapes when the corresponding gain is zero may be of some interest. There are essentially two situations where a gain becomes zero. The first is when a natural frequency is equal to the rigid-body nutation frequency. Figure 47 shows the mode shapes when k_2, k_3 and k_4, respectively, are nearly zero due to this cause. It is observed that the body angle tends to be quite small but nonzero. Otherwise no extraordinary feature is apparent.

As mentioned earlier, zero gains also are found on the k_n vs. $\sqrt{B}^*$ plot (Fig. 41). For example, k_4 goes to zero three times in the range of $\sqrt{B}^*$ considered. The mode shapes corresponding to the first two of these points are shown in Fig. 48. Here, small gains are zero only if $\delta_n = 0$. The blanket and boom deflections appear normal, except of course that they must balance so as to produce zero net torque on the center body.

This brings the discussion of the roll-yaw attitude dynamics and its interaction with array bending to a close. The distinguishing feature from the pitch case is the coupling between two axes introduced by the momentum wheel. However, the flexibility is such as to affect one axis only. The general methods

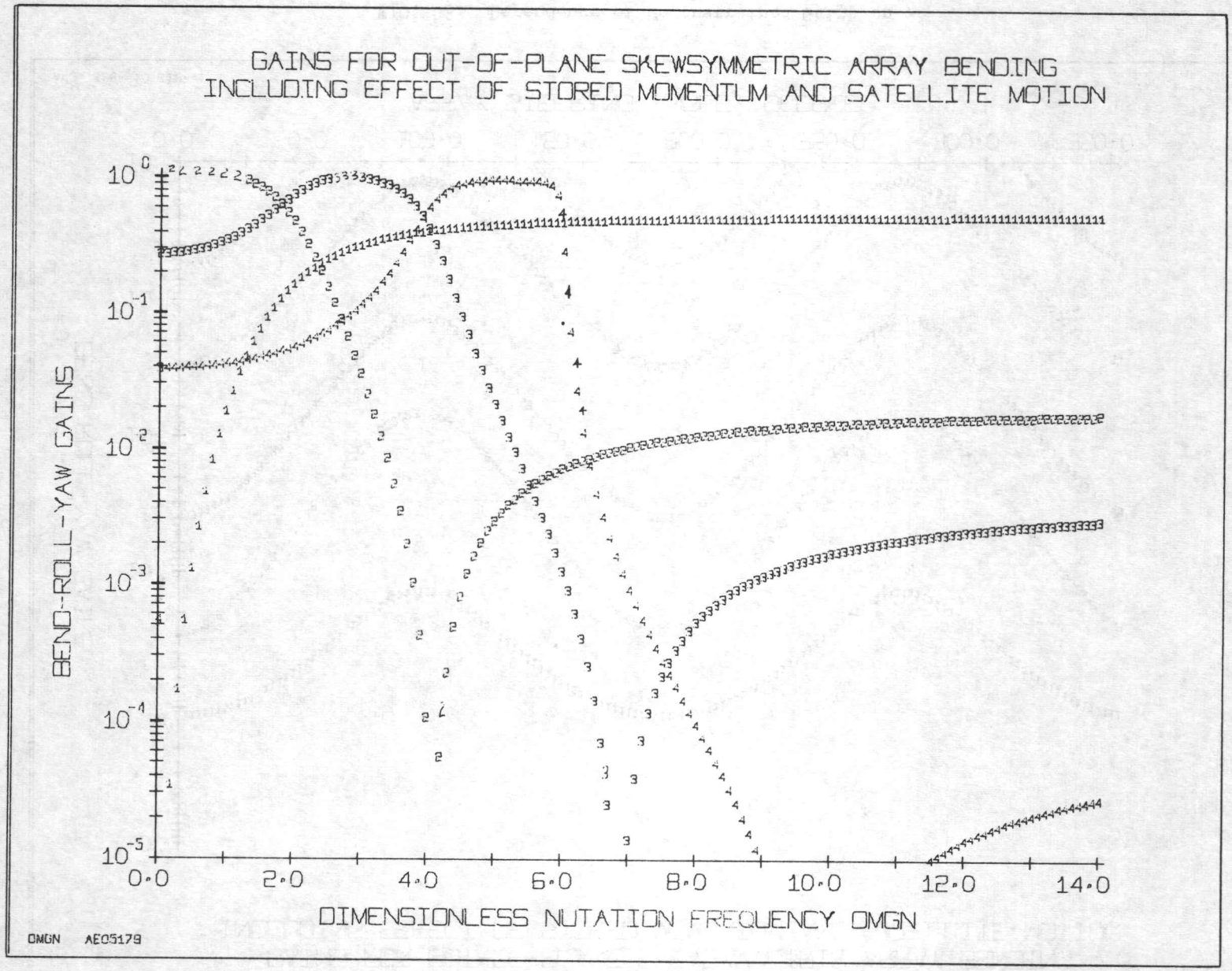

FIG. 42: Dependence of Unconstrained Gains on ω_N^*

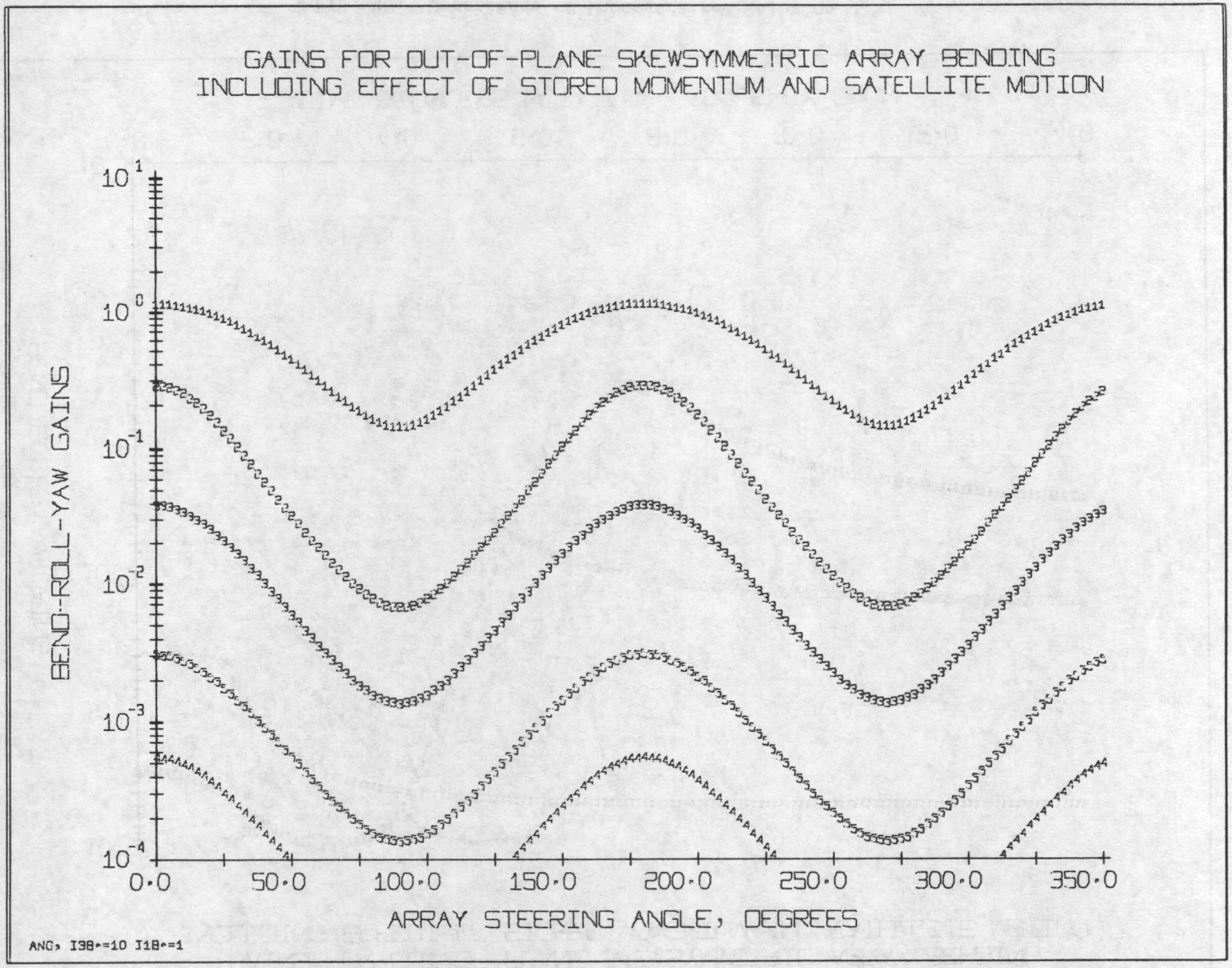

FIG. 43: Dependence of Unconstrained Gains on γ
(Unsymmetrical Configuration)

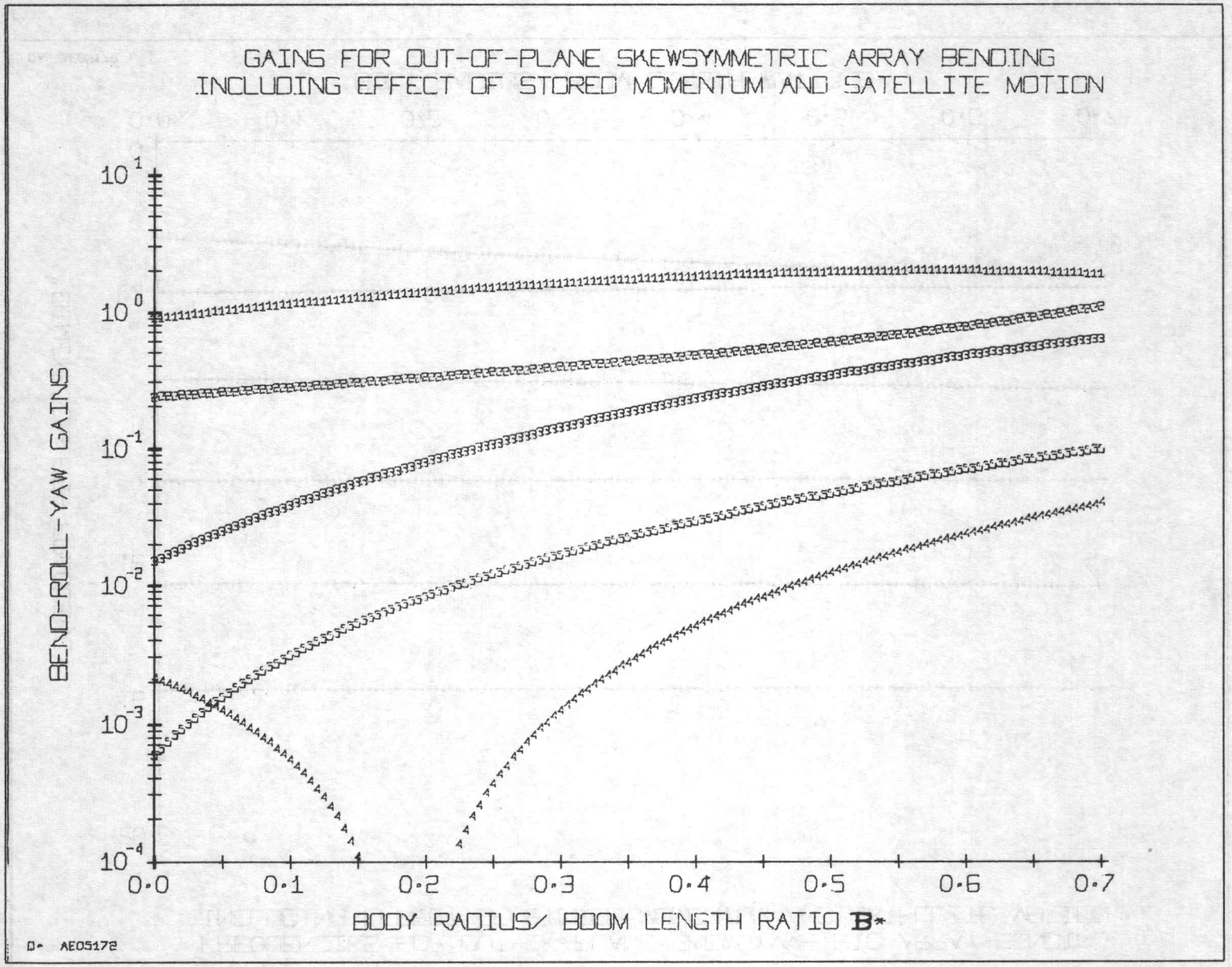

FIG. 44: Dependence of Unconstrained Gains on b*

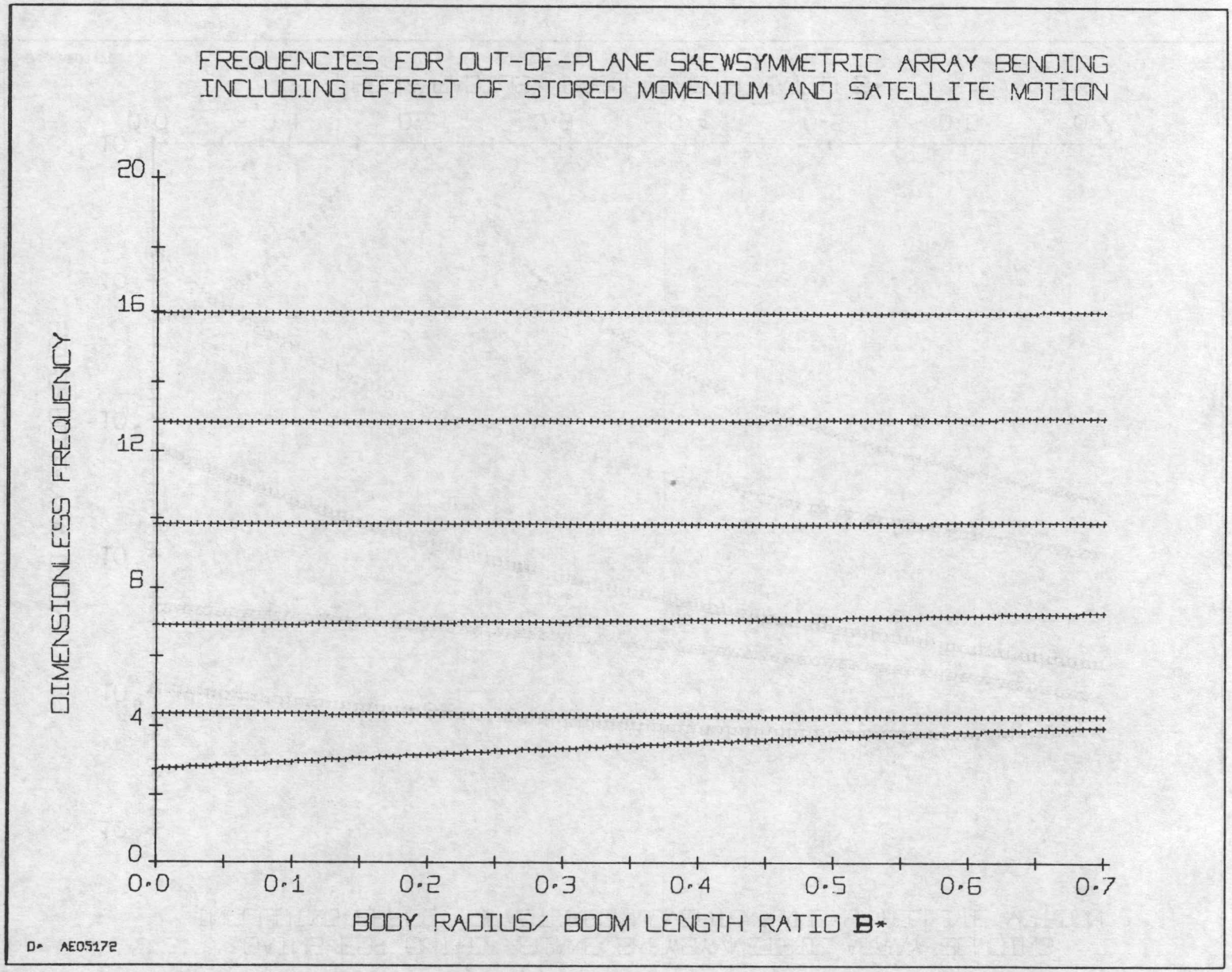

FIG. 45: Dependence of Unconstrained Frequencies on b*

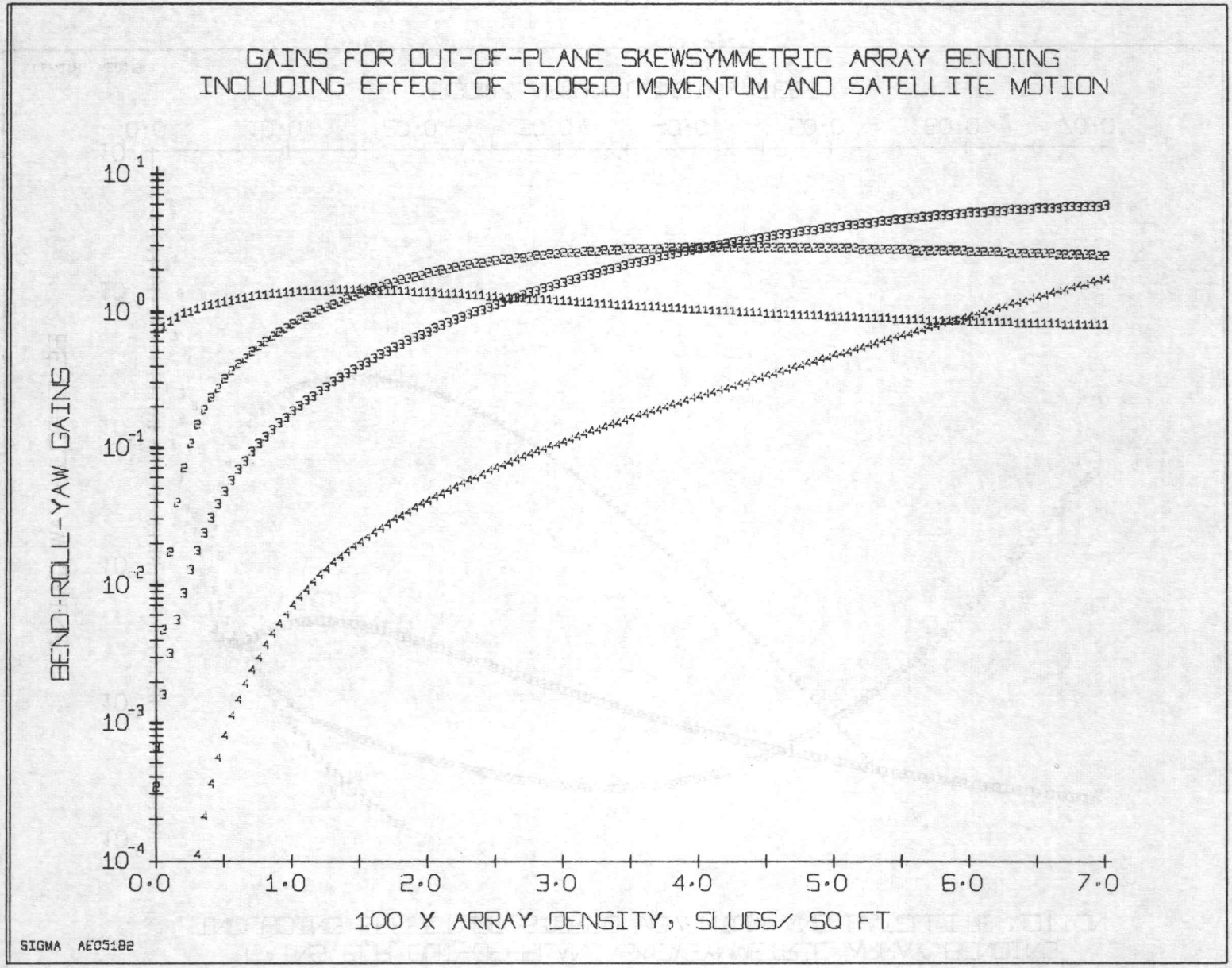

FIG. 46: Dependence of Unconstrained Gains on σ

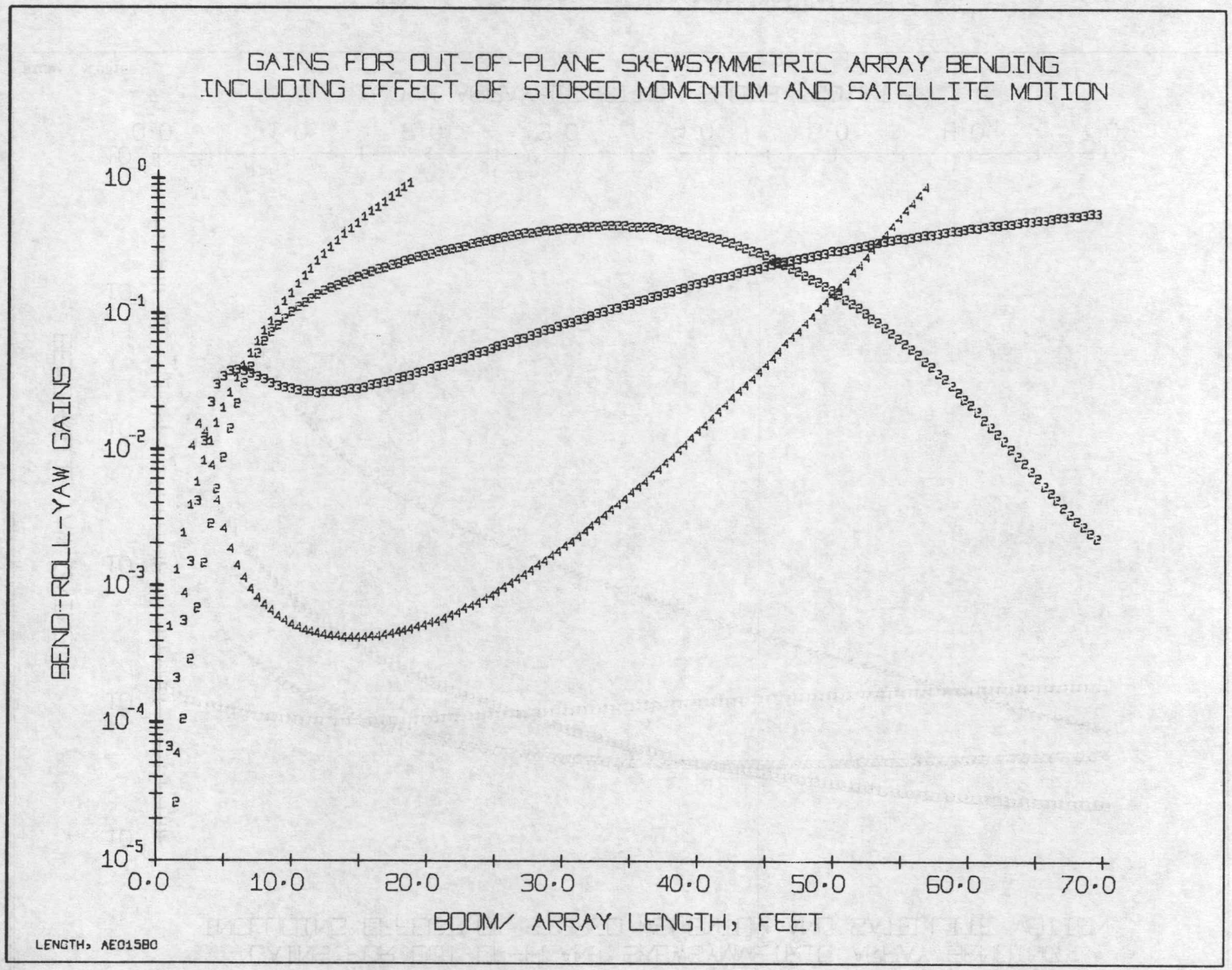

FIG. 47: Dependence of Unconstrained Gains on ℓ

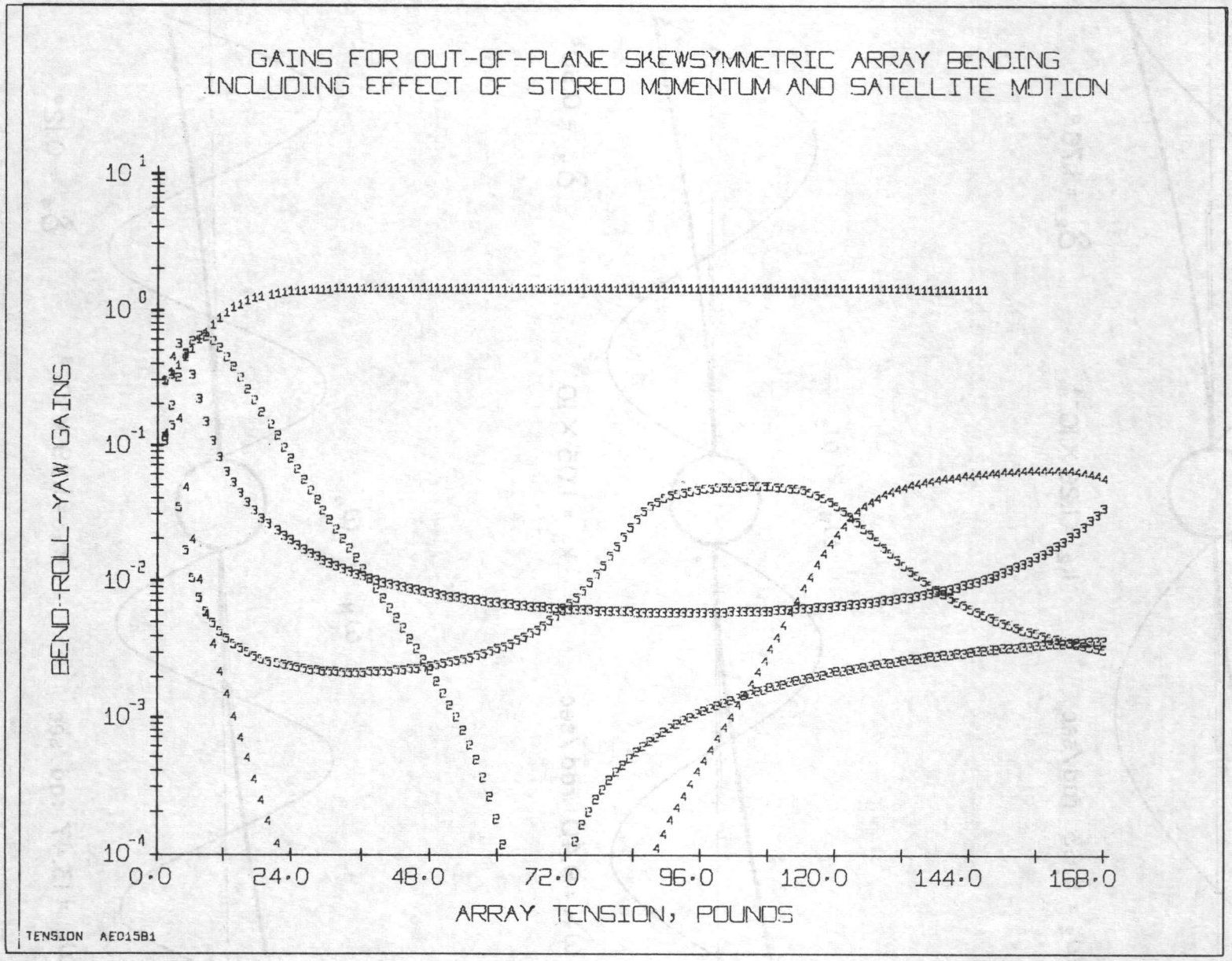

FIG. 48: Dependence of Unconstrained Gains on P

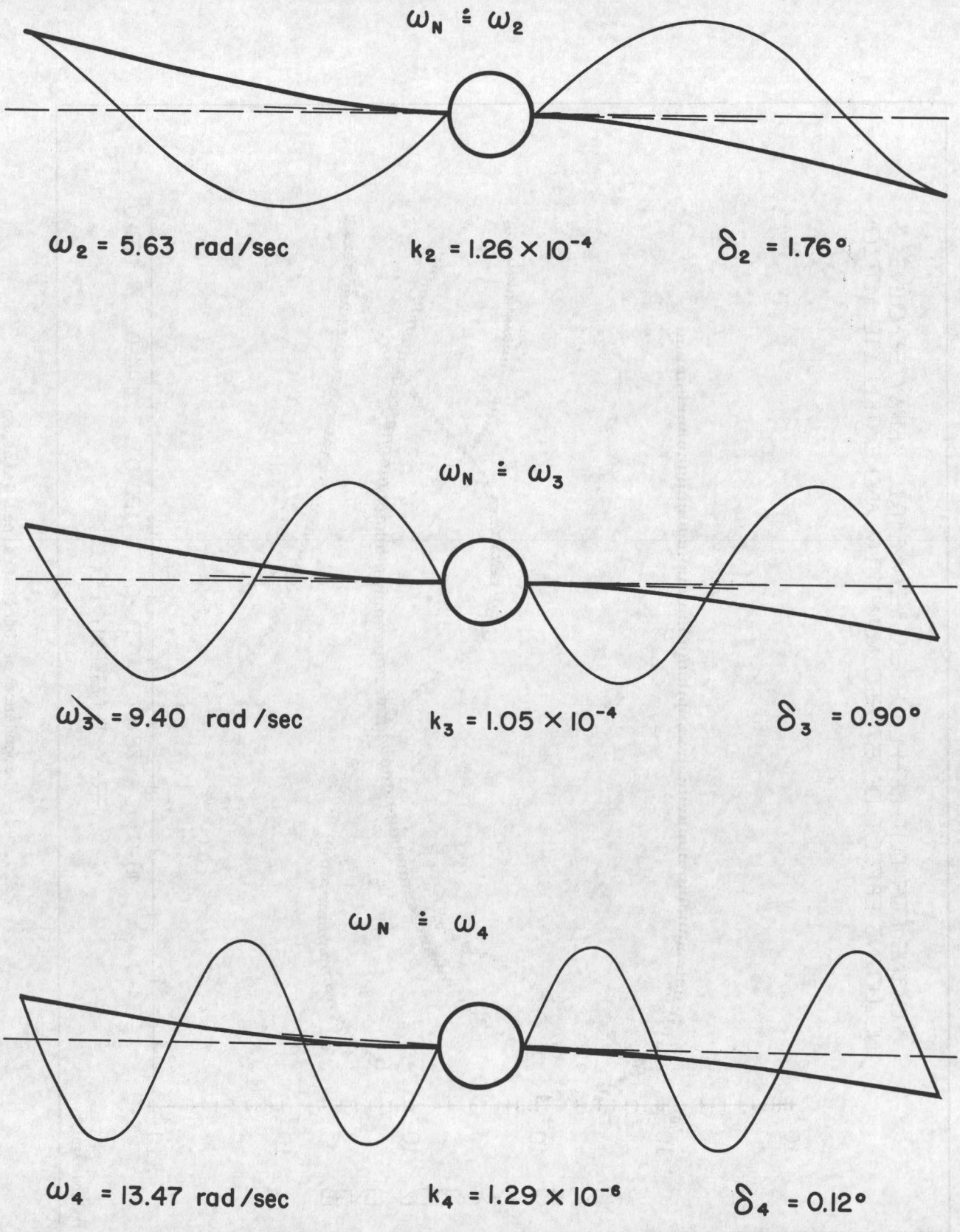

FIG. 49: Unconstrained Mode Shapes for Frequencies ω_n = Rigid Nutation Frequency ω_N, n = 2,3,4. Causing Zero Gains

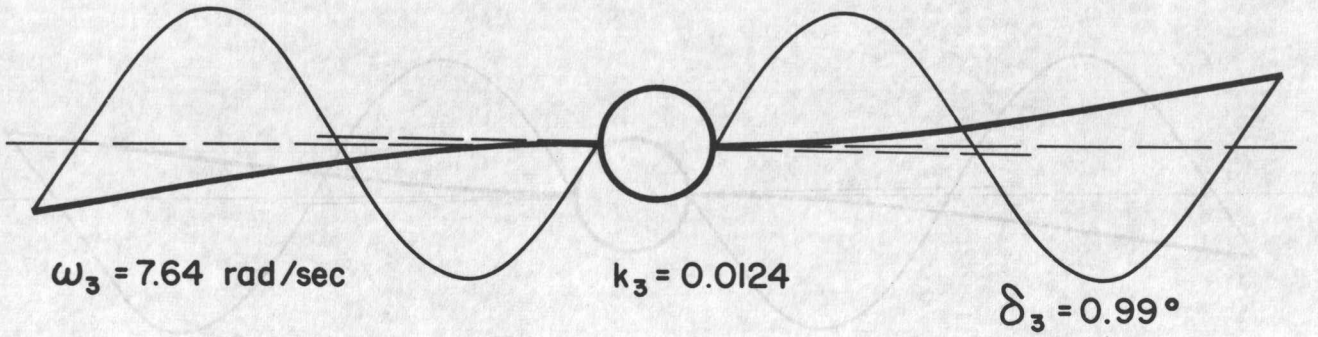

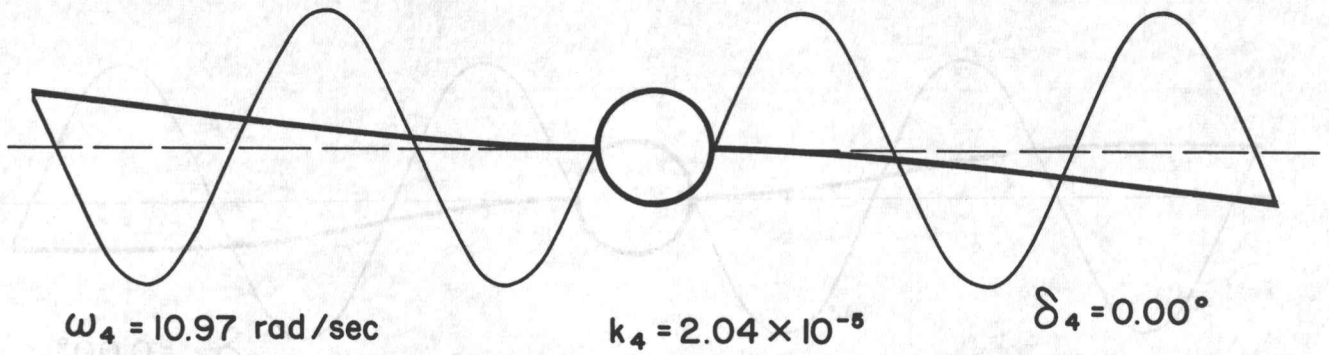

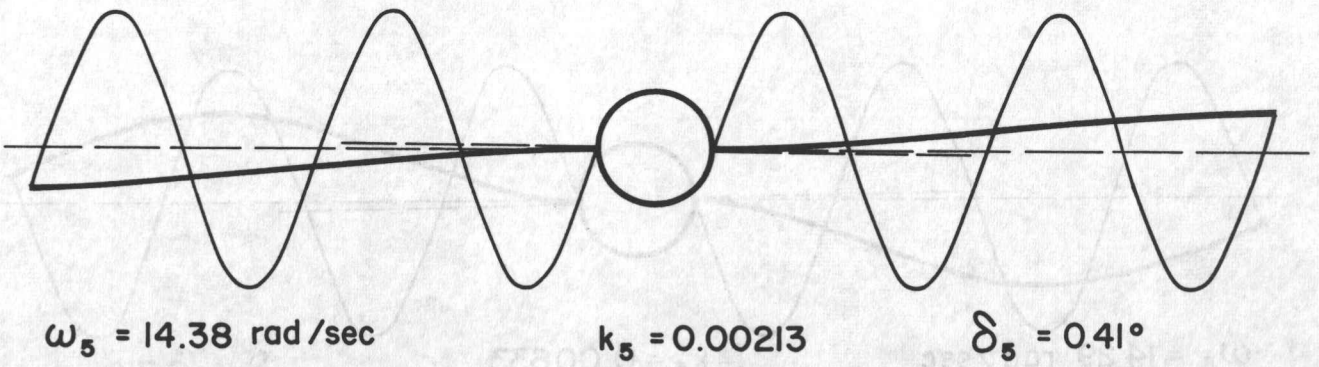

FIG. 50a: Unconstrained Mode Shapes for $\sqrt{B}^*$ = 1.45 where the Gain k_4 is Nearly Zero

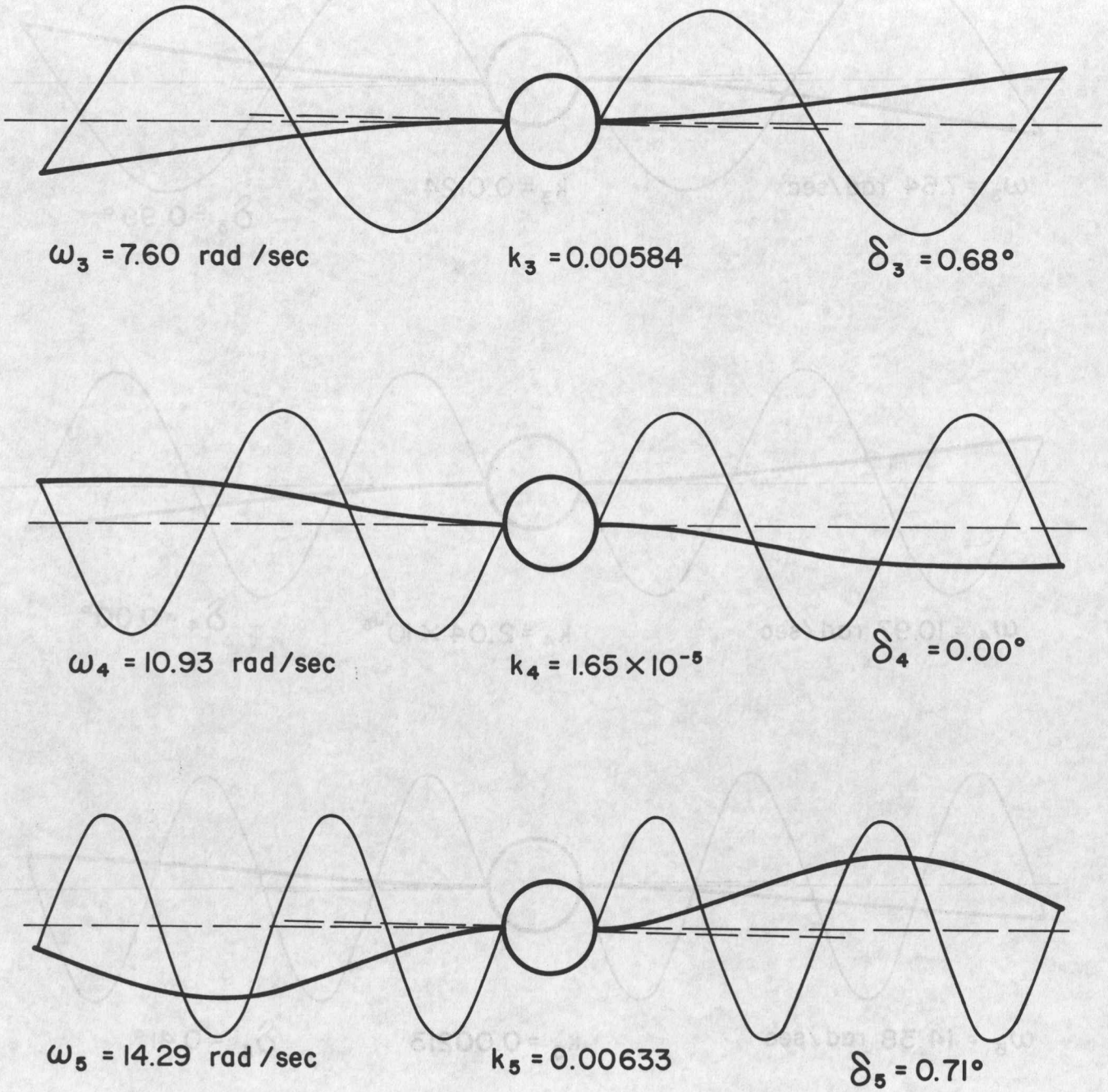

FIG. 50b: Unconstrained Mode Shapes for $\sqrt{B}^*$ = 2.20 where the Gain k_4 is Nearly Zero

used here are applicable equally but the details will differ from application to application.

5. SOME EXTENSIONS

The methods of analysis for a flexible satellite discussed above have been applied to a simple geometrical configuration. However, these methods are applicable to a much wider class of configurations. In particular, the continuum mechanics approach can be extended in several respects, to take account of changes in geometry, different boundary conditions, articulation of components etc. Some of these will be illustrated in the present section.

5.1 Unequal Boom and Array Length

The assumption of equal boom and array lengths is not quite true, as may be seen from Fig. 4. While both the elements end at, and are attached to, the tip piece, the blanket does not start until some distance along the boom; in fact for CTS the "boom" actually extends slightly inwards into the center body. We take the origin ($y = 0$) at the body surface, then if d be the distance from $y = 0$ to the array root, we have

$$v(x,y,t) \equiv 0, \quad 0 \leq y \leq d \qquad (5.1)$$

Let the length of the boom be denoted ℓ; the blanket length is then $(\ell - d)$. Since the boom does not contribute to the twisting stiffness, the only effect in twist/pitch is to change the numerical value for 'ℓ' to be used while calculating the dimensional frequencies. The dimensionless plots presented are unchanged. Of course, while calculating gains the condition (5.1) must be accounted for.

The roll-yaw/bending case is affected more substantially, for a new dimensionless parameter ($d^* \equiv d/\ell$) is introduced. Considering the constrained case first, the motion equations (4.28) are unchanged, except that (5.1) must be used while calculating f. The boundary conditions (4.29) are also unchanged except that we now have

$$v(d) = 0 \qquad (5.2)$$

This in turn means that the mode shapes $U_n(y)$ in (4.33) are affected; these must now satisfy (5.2) instead of $v(0) = 0$. By analogy with the previous solution (4.34), we can write the solution as

$$V_n(y) = a_3 \sin \kappa_n (y-d), \quad y \geq d \qquad (5.3)$$

It is readily verified that this satisfies the array root condition. For $y < d$, V_n is zero by definition. With (4.34) replaced by (5.3), the analysis proceeds as before, leading to the following changes in the matrix elements (4.36):

$$m_{13} = -P\kappa \cos\kappa(\ell - d)$$

$$m_{23} = -\sin\kappa(\ell - d) \qquad (5.4)$$

The frequencies are found as usual. The orthogonality condition and the normalization adopted earlier are still applicable, because the array contributes zero to the integrals for $y < d$. Hence the gains can be found as before and have the same

properties, with the array inertia I_A being appropriately re-defined as

$$I_A = 2\rho \int_o^{\ell} (b+y)^2 dy + 2\sigma w \int_d^{\ell} (b+y)^2 dy + 2m(b+\ell)^2 \qquad (5.5)$$

The simulation block diagrams are of course unchanged. We do not present any numerical results here because for most applications d is quite small.

The unconstrained case is treated similarly. The governing differential equation (4.49) is unchanged as are the boundary conditions at $y = \ell$. It is readily verified that the following solution satisfies (4.49) and the array root condition:

$$v_n(y) = a_3 \sin\kappa_n(y-d) + [(b+d)\cos\kappa_n(y-d) - (b+y)]\,\delta_n \qquad (5.6)$$

This form becomes identical to the earlier expression (4.54) when d = 0. Inserting the above expression, the analysis proceeds as before, leading to some changes in the matrix elements (4.56). In making these changes, it must be remembered that (5.6) is only applicable for $y \geq d$, v_n being zero by definition, for $y < d$. The modified elements are given below.

$$m_{11} = I(1-\omega_N^2/\omega^2) - 2m(b+\ell)^2 + 2mb(b+\ell)\,ch\alpha\ell + 2m(b+\ell)\,\frac{sh\alpha\ell}{\alpha}$$

$$+ 2\sigma w\left[\frac{b(b+d)}{\kappa}\,s\kappa(\ell-d) + \frac{b+d}{\kappa^2}\,(c\kappa(\ell-d) + \kappa\ell\, s\kappa(\ell-d) - 1)\right.$$

$$\left. - \frac{1}{3}(\ell^3-d^3) - b(\ell^2-d^2) - b^2(\ell-d)\right]$$

$$+ 2\rho\left[b^2\,\frac{sh\alpha\ell}{\alpha} + b\ell\,\frac{sh\alpha\ell}{\alpha} + \frac{\alpha\ell\, ch\alpha\ell - sh\alpha\ell}{\alpha^3} - (b^2\ell + b\ell^2 + \frac{1}{3}\ell^3)\right]$$

$$m_{14} = 2\sigma w\left[\frac{b+d-(b+\ell)c\kappa\,(\ell-d)}{\kappa} + \frac{1}{\kappa^2}\,s\kappa\,(\ell-d)\right]$$

$$m_{24} = -P\kappa c\kappa\,(\ell-d) \qquad (5.7)$$

$$m_{34} = -s\kappa(\ell-d)$$

The frequencies are found as usual. Again, the orthogonality and normalization conditions and the gains are still applicable, and the simulation block diagrams and the gain identities derived earlier are unchanged.

5.2 Boom Root Flexibility

The support boom was assumed to be rigidly cantilevered at the root. In reality it has some flexibility in bending which can be modelled at a coil spring at the root, obeying the condition

$$B\,u''(0) = k\,u'(0) \qquad (5.8)$$

Here k is a spring constant, not to be confused with the constrained gains k_n. Thus (5.8) replaces the condition $u'(0) = 0$, and the remaining boundary conditions and motion equations are unchanged. This changes the boom mode shapes, whereas the unequal length case affected chiefly the array modes. Again, pitch is not affected by root flexibility because the boom does not contribute to the twisting stiffness.

In this subsection, we shall assume equal boom and array lengths for simplicity, as before. Consider the constrained case first. The general solution is

$$U_n(y) = a_1 ch\,\alpha_n y + a_2 sh\alpha_n y + b_1 c\beta_n y + b_2 s\beta_n y$$

Applying $U_n(0) = 0$ and (5.8) respectively to this gives

$$a_1 + b_1 = 0$$

$$B\,(\alpha_n^2 a_1 - \beta_n^2 b_1) = k(\alpha_n a_2 + \beta_n b_2)$$

$$\therefore \quad b_1 = -a_1, \qquad b_2 = \frac{B(\alpha_n^2 + \beta_n^2)}{k\,\beta_n}\, a_1 - \frac{\alpha_n}{\beta_n}\, a_2 \tag{5.9}$$

Hence the solution in (4.34) is replaced by

$$U_n = a_1(ch\alpha_n y - c\beta_n y) + a_2\left(sh\alpha_n y - \frac{\alpha_n}{\beta_n} s\beta_n y\right) + p\, a_1 s\beta_n y$$

where

$$p = \frac{B(\alpha_n^2 + \beta_n^2)}{k\,\beta_n} \tag{5.10}$$

Thus an additional term appears due to root flexibility, which goes to zero as the stiffness $k \to \infty$, as expected. This additional term leads to the following <u>additions</u> to the matrix elements given in (4.36):

$$\begin{aligned} \Delta m_{11} &= p(-B\beta^2 c\beta\ell + P\beta c\beta\ell + m\Omega^2 s\beta\ell) \\ \Delta m_{21} &= p\, s\beta\ell \\ \Delta m_{31} &= p\,\beta^2 s\beta\ell \end{aligned} \tag{5.11}$$

The remaining analysis proceeds as before. The orthogonality condition (4.38-4.39) still holds; although this is not obvious since one of the boundary conditions is different, it may be shown following the lines suggested in Section 4. The gains and their properties, as well as the simulation block diagrams remain unchanged. A new parameter, k, is now introduced - numerical examples showing its effect on frequencies and gains will be given for the unconstrained case only.

For the unconstrained modes, the general solution is

$$u_n(y) = a_1 ch\alpha_n y + a_2 sh\alpha_n y + b_1 c\beta_n y + b_2 s\beta_n y - (b+y)\delta_n$$

Applying the conditions at the root gives

$$a_1 + b_1 - b\delta_n = 0$$

$$B(\alpha_n^2 a_1 - \beta_n^2 b_1) = k\,(\alpha_n a_2 + \beta_n b_2 - \delta_n) \qquad (5.12)$$

$$\therefore \quad b_1 = -(a_1 - b\delta_n), \quad b_2 = -\frac{\alpha_n}{\beta_n}\left(a_2 - \frac{\delta_n}{\alpha_n}\right) + pa_1 - \frac{B\beta_n}{k}\, b\, \delta_n$$

where p is defined as in (5.10). Incorporating these conditions into the solution and redefining the arbitrary constants as done in Section 4 enables the solution to be written as

$$u_n(y) = a_1(ch\alpha_n y - c\beta_n y) + a_2\left(sh\alpha_n y - \frac{\alpha_n}{\beta_n}\, s\beta_n y\right)$$

$$+ \delta_n(bch\alpha_n y - \alpha_n^{-1} sh\alpha_n y - b - y) \qquad (5.13)$$

$$+ pa_2 s\beta_n y + \frac{B\alpha_n}{k}\, b\, \delta_n sh\alpha_n y$$

The terms at the end are extra terms arising from the root flexibility, and vanish as the stiffness $k \to \infty$, as expected, carrying these extra terms into the analysis as before leads to the following additions to the matrix elements given in (4.56):

$$\Delta m_{11} = \frac{Bb}{k}\alpha\left[2m(b+\ell)sh\alpha\ell + \frac{2\rho}{\alpha}\left\{-b - \frac{sh\alpha\ell}{\alpha} + (b+\ell)ch\alpha\ell\right\}\right]$$

$$\Delta m_{12} = p\left[2m(b+\ell)sh\alpha\ell + \frac{2\rho}{\beta}\left\{b + \frac{s\beta\ell}{\beta} - (b+\ell)\, c\beta\ell\right\}\right]$$

$$\Delta m_{21} = \frac{Bb}{k}\,\alpha\,(B\alpha^2 ch\alpha\ell + P\alpha\, ch\alpha\ell + m\omega^2\, sh\alpha\ell)$$

$$\Delta m_{22} = p\,(-B\beta^2 c\beta\ell + P\beta c\beta\ell + m\omega^2 s\beta\ell)$$

$$\Delta m_{31} = -\frac{Bb}{k}\,\alpha\, sh\alpha\ell$$

$$\Delta m_{32} = p\, s\beta\ell \qquad (5.14)$$

$$\Delta m_{41} = \frac{Bb}{k}\,\alpha^2\, sh\alpha\ell$$

$$\Delta m_{42} = -p\,\beta^2 s\beta\ell$$

The remaining analysis proceeds as before. Again, the same orthogonality condition (4.60, 4.61) is valid despite the changed boundary conditions, as may be proved along the lines shown in section 4. The gains and simulation block diagrams are unchanged.

Numerical Example

Due to k, a new dimensionless parameter is introduced into the frequency and gain variation:

$$\omega_n^* = \omega_n^* \ (\rho^*, m^*, b^*, B^*, I_{1b}^*, I_{3b}^*, \omega_N^*, \gamma, k^*) \qquad (5.15)$$

Here the definitions (4.72) are valid, and

$$k^* \equiv B/k\ell \qquad (5.16)$$

We consider the same numerical example as before, with the nominal parameters as in (4.73).

Figure 51 shows the variation of ω_n^* with k^* in the range $(0 \leq k^* \leq 14.0)$, with other parameters held fixed at their nominal value. The values for $k^* = 0$ of course correspond to $k \to \infty$, i.e., the rigidly cantilevered boom. As the boom root becomes more flexible (increasing k^*) the frequencies drop gradually as expected. For $k^* \to \infty$ the situation resembles a hinged-boom condition.

The effect of k^* on the unconstrained gains k_n is seen in Fig.52. The gains are seen to change only gradually, except that the behaviour of gains going to zero is observed here also. The lower modes, especially the first gain, is not affected much by k^* in contrast to the first frequency, which shows the largest sensitivity near $k^* = 0$.

5.3 Sun-Tracking of the Solar Array

The spacecraft main body is earth-pointing and the array is sun-pointing. Therefore a requirement exists for rotation of the array relative to the spacecraft. A uniform relative rotation at the rate of once per day is conceptually simple but difficult to implement. In any case, a further source of array excitation arises in this manner. It will now be shown how the analysis of Section 3 can be extended in a straightforward manner to include this relative motion.

The angle of the array with respect to the main body has been denoted γ, and heretofore γ was treated as a constant. We now have

$$\gamma = \gamma(t) \qquad (5.17)$$

It is possible to take the torque on the array as given, write a new equation of motion for the array root, and thence provide a new differential equation corresponding to the new unknown function $\gamma(t)$. However, since the emphasis here is on the influence of flexibility, we shall take $\gamma(t)$ as known (rather than the torque which governs it).

5.3.1 Equations of Motion

First, the motion equation for the overall spacecraft must be reexamined.

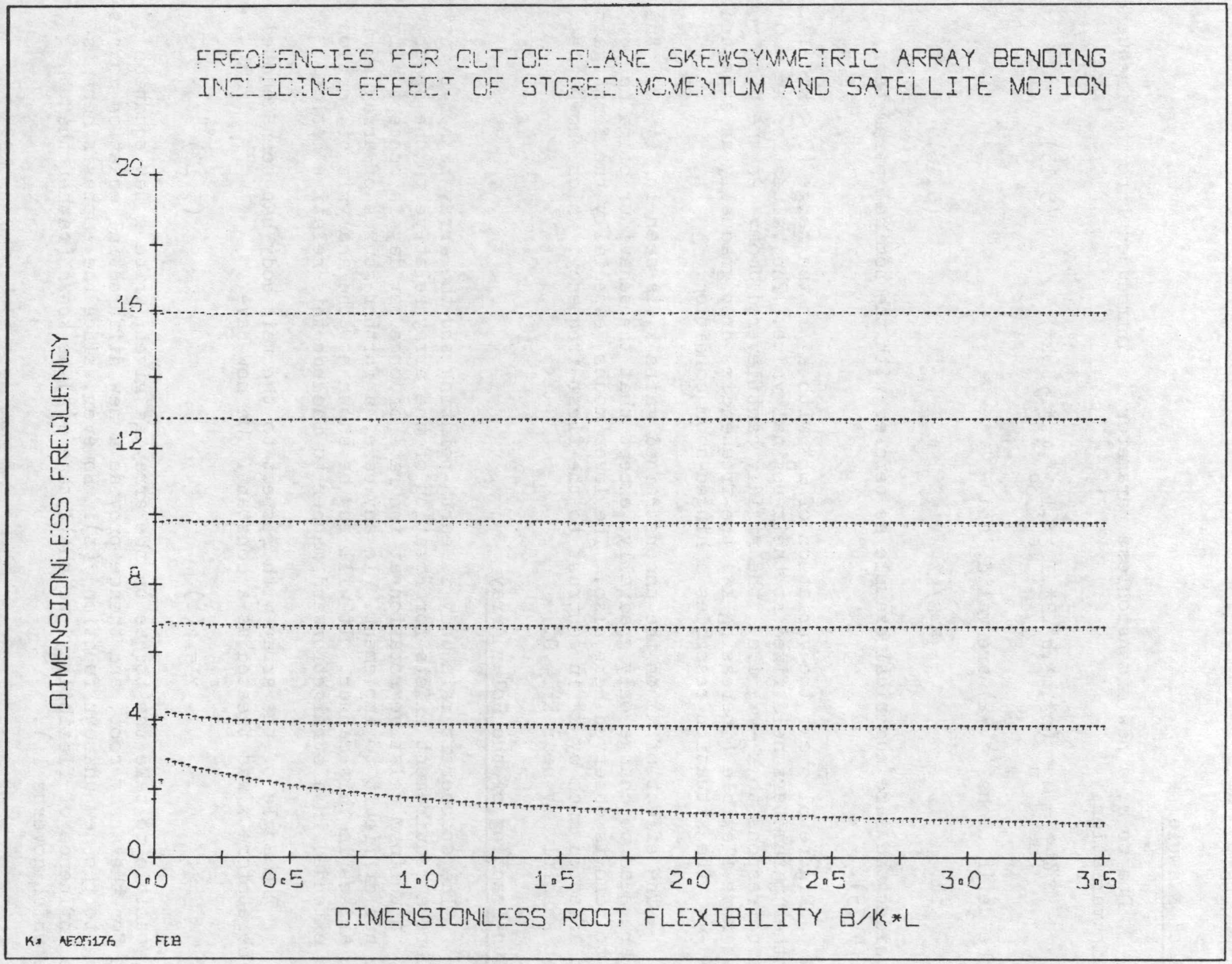

FIG. 51: Dependence of Unconstrained Frequencies on k*

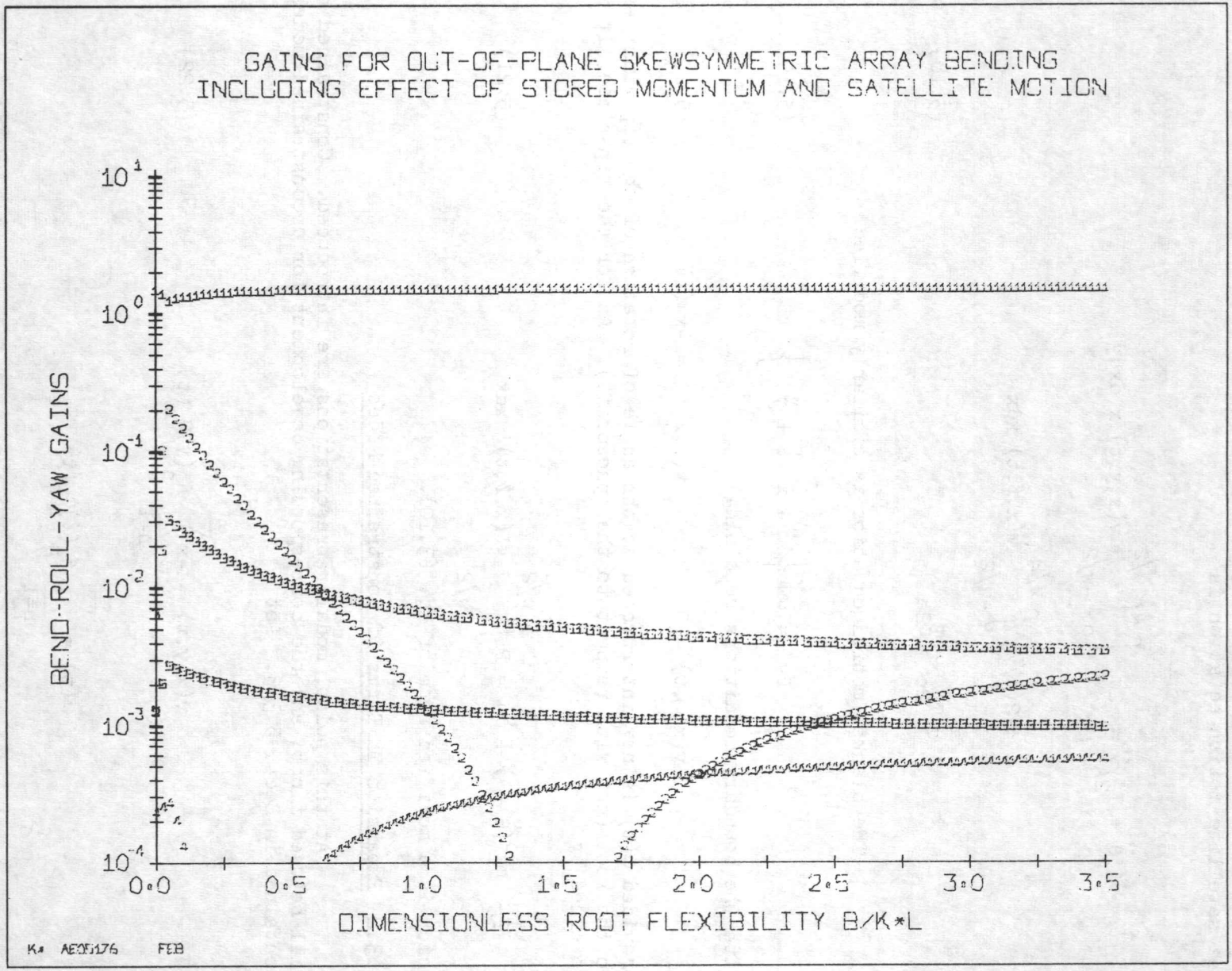

FIG. 52: Dependence of Unconstrained Gains on k*

In Eq. (3.2) we must replace $\dot{\theta}$ by $\dot{\theta} + \dot{\gamma}$ within the two integrands; the term $I_{2b}\dot{\theta}$ is unchanged. Then, to Eq. (3.3) the term $I_{2A}\dot{\gamma}$ must be added, where I_{2A}, the pitch inertia of the whole array, is given by Eq. (3.59). Therefore, using Eq. (3.5), the satellite motion equation is

$$I_2\ddot{\theta} + I_{2A}\ddot{\gamma} = 2\sigma \int_0^{\ell}\int_{-w/2}^{w/2} \ddot{v}(x,y,t)\, x\, dxdy$$

$$+ 2(m/w) \int_{-w/2}^{w/2} \ddot{v}(x,\ell,t)\, xdx$$

$$+ T_{2c} + T_{2e} \qquad (5.18)$$

The blanket motion equation is similarly modified

$$Pv'' = \sigma w \left\{ \ddot{v} - x\,(\ddot{\theta} + \ddot{\gamma}) \right\} \qquad (5.19)$$

With the boundary conditions remaining

$$v(x,0,t) = 0 \quad ; \quad v(x,\ell,t) = -x\alpha(t) \qquad (5.20)$$

provided $\alpha(t)$ is now interpreted as the angle of rotation of the tip with respect to the root (not with respect to the spacecraft). As for the tip-piece, it is governed by

$$\frac{1}{12}\, mw^3(\ddot{\theta} + \ddot{\gamma} + \ddot{\alpha}) = P\int_{-w/2}^{w/2} v'(x,\ell,t)\ \ xdx \qquad (5.21)$$

which is a modified form of Eq. (3.10).

5.3.2 Expansion In Terms Of Constrained Modes

At this point, modal representations are introduced. Constrained modes will be used first, and the corresponding development for unconstrained modes is contained in Sect. 5.3.3. Let

$$v(x,y,t) = -x\sum_{n=1}^{\infty} A_n(y)Q_n(t) \qquad (5.22)$$

$$\alpha(t) = \sum_{n=1}^{\infty} A_n(\ell)Q_n(t)$$

When substituted into the equations of motion, these expansions yield:

$$\left.\begin{aligned}\sum_{n=1}^{\infty}(\ddot{Q}_n + \Omega_n{}^2 Q_n)A_n(y) + \ddot{\theta} + \ddot{\gamma} = 0 \\ \sum_{n=1}^{\infty}(\ddot{Q}_n + \Omega_n{}^2 Q_n)A_n(\ell) + \ddot{\theta} + \ddot{\gamma} = 0\end{aligned}\right\} \qquad (5.23)$$

which should be compared with Eqs. (3.65,66). The spacecraft motion equation becomes

$$I_2\ddot{\theta} + I_{2A}\ddot{\gamma} = \sum_{n=1}^{\infty} F_n\ddot{Q}_n + T_{2c} + T_{2e} \qquad (5.24)$$

[F_n was defined by Eq.(3.68)].

Next, to uncouple the equation for the degrees of freedom associated with structural flexibility, perform an operation on Eqs. (5.23) as indicated in Eq.(3.70). The orthogonality and normality conditions are employed to render the dependence of $Q_m(t)$ thus:

$$\ddot{Q}_m + \Omega_m{}^2 Q_m = \frac{F_m}{\sigma w^3 \ell}(\ddot{\theta} + \ddot{\gamma}) \quad (m = 1,2,\ldots) \qquad (5.25)$$

these operations, when inserted into Eq.(5.24), can be written in terms of Laplace transformed variables (denoted by overbars) as follows

$$s^2(\bar{\theta} + \bar{\gamma}) = \sum_{n=1}^{\infty} \frac{s^2 K_n}{s^2 + \Omega_n^2}\, s^2(\bar{\theta} + \bar{\gamma}) + \frac{\bar{T}_{2c} + \bar{T}_{2e}}{I_2} + \frac{I_{2b}}{I_2}\, s^2\bar{\gamma} \qquad (5.26)$$

and this in turn, may be represented by the block diagram shown in Fig. 53. The sum $I_2 = I_{2A} + I_{2b}$. This figure, when compared with Fig. 8, shows that the addition of an arbitrary rotation of the array with respect to the main body can be incorporated without great difficulty.

5.3.3 Expansion In Terms of Unconstrained Modes

As an alternative to Eq. (5.22) an expansion in terms of unconstrained modes is now considered, namely

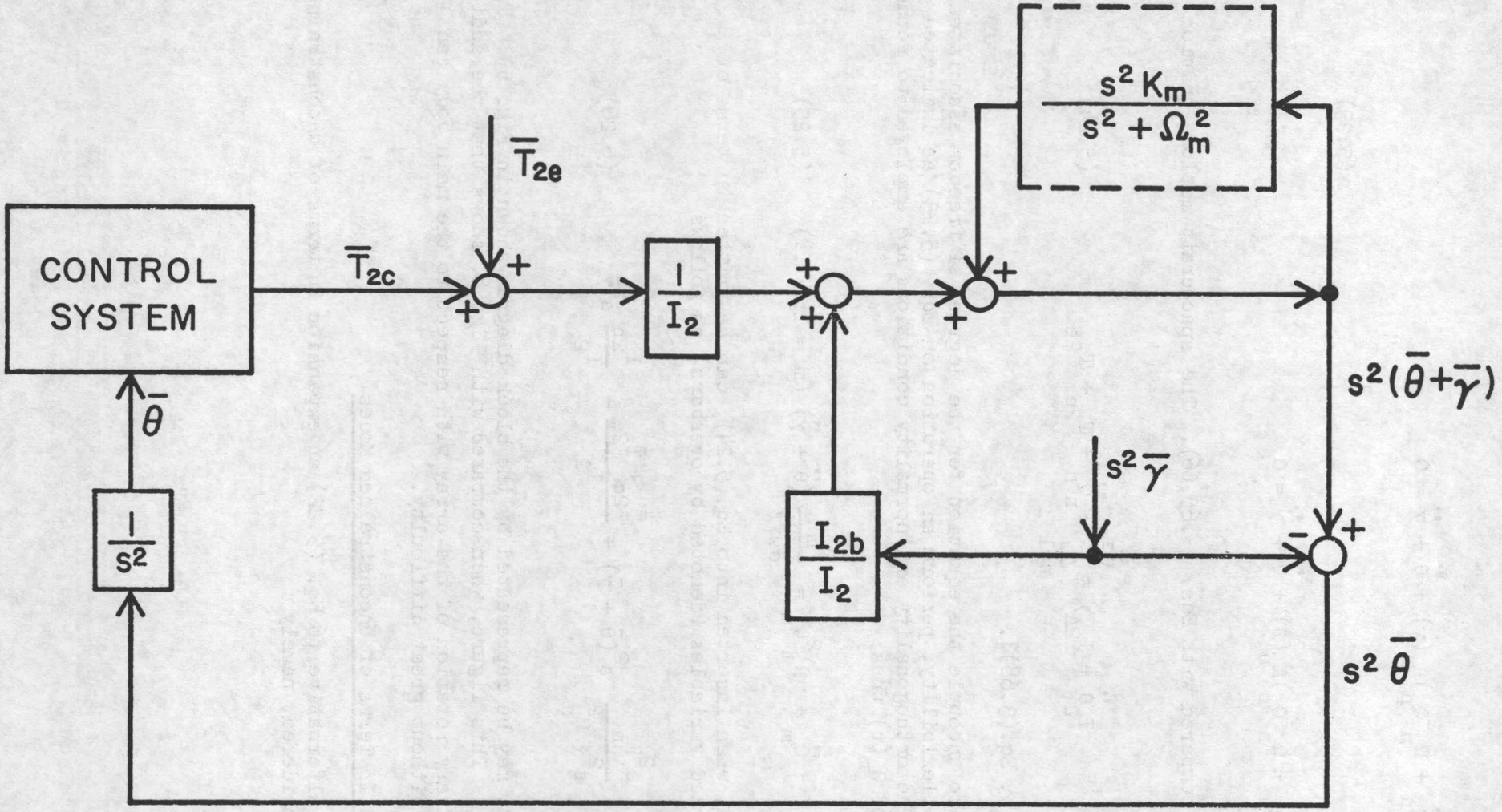

FIG. 53: Pitch Attitude Control Block Diagram Incorporating Both Constrained Twisting Modes and Array Tracking

$$\theta(t) = \sum_{n=1}^{\infty} \theta_n q_n(t) + \Theta(t)$$

$$v(x,y,t) = -x \sum_{n=1}^{\infty} \alpha_n(y)\, q_n(t) \qquad \Bigg\} \qquad (5.27)$$

$$\alpha(t) = \sum_{n=1}^{\infty} \alpha_n(\ell)\, q_n(t)$$

When substituted into the equations of motion, these expansions yields

$$\sum_{n=1}^{\infty} (\ddot{q}_n + \omega_n^2 q_n)\Big[\, \alpha_n(y) + \theta_n \Big] + \ddot{\Theta} + \ddot{\gamma} = 0$$

$$\Bigg\} \qquad (5.28)$$

$$\sum_{n=1}^{\infty} (\ddot{q}_n + \omega_n^2 q_n)\Big[\, \alpha_n(\ell) + \theta_n \Big] + \ddot{\Theta} + \ddot{\gamma} = 0$$

which should be compared with Eqs. (3.86,87). The spacecraft motion equation becomes

$$I_2 \ddot{\Theta} + I_{2A} \ddot{\gamma} = T_{2c} + T_{2e} \qquad (5.29)$$

which should be compared with Eq. (3.85). The last equation may be rewritten, using Laplace transform notation, as

$$s^2(\bar{\Theta} + \bar{\gamma}) = (\bar{T}_{2c} + \bar{T}_{2e})/I_2$$

$$+ (I_{2b}/I_2)\, s^2 \bar{\gamma} \qquad (5.30)$$

This form is of more direct utility.

The modal equations (5.28) are uncoupled by the procedure indicated in Eq. (3.88). When orthogonality and normality conditions are employed, the uncoupled equations become

$$\ddot{q}_m + \omega_m^2 q_m = \left(\frac{f_m}{\sigma w^3 \ell - f_m \theta_m} \right) (\ddot{\Theta} + \ddot{\gamma}) \qquad (5.31)$$

In Laplace transform notation then, Eqs. (5.27a), (5.21), and (5.30) are combined

as follows

$$s^2\bar{\theta} = s^2\bar{\Theta} + \sum \frac{s^2 k_n}{s^2 + \omega_n^2} s^2(\bar{\Theta} + \bar{\gamma})$$

$$s^2(\bar{\Theta} + \bar{\gamma}) = (\bar{T}_{2c} + \bar{T}_{2e})/I_2 + (I_{2b}/I_2)\, s^2\bar{\gamma} \qquad (5.32)$$

which may be represented by the block diagram shown in Fig. 54. This figure should be compared with Fig. 10 showing the relatively simple incorporation of an arbitrary array motion with respect to the main body. It is also of interest to compare the duality of Figs.53 and 54 with that of Figs. 8 and 10.

6. CONCLUDING REMARKS

The analysis associated with attitude control of flexible spacecraft entails a combination of attitude dynamics, structural dynamics, and control system dynamics. Unfortunately, the present discussion draws to a close before the latter discipline is given the attention it would deserve in the applications. Nevertheless, certain definite conclusions are possible in connection with the presentation of the former two. Some of these bear on the form, and others on the content, of the preceeding analysis.

With regard to the form of the analysis the prominent alternatives were examined in Sect. 1.4. Of these, the methods of continuum mechanics have been emphasized because the particular class of spacecraft under consideration could be modelled in a relatively simple manner to a high degree of accuracy. In view of the extensive analytical framework which has been constructed on this basis, it can be concluded that the traditional methods of analysis are quite viable provided the geometry of the flexible elements is uncluttered. Such calculations, made on the basis of 'closed form' results are of great help to the attitude control designer for (at the least) preliminary design. Moreover, unless simulation shows that there is a substantial interaction between the attitude control system and the modal coordinates, it is not likely that more detailed calculations are warranted using, for example, the method of finite elements. On the other hand, if preliminary simulations made with the aid of a somewhat idealized closed form analysis give warning that in the course of controlling the spacecraft attitude, significant modal amplitudes are excited, then further investigation using finite elements or, indeed, any other promising technique is recommended.

Even more important perhaps are the conclusions on the content of the analysis. Whatever approach is used, the object is most likely to be a modal representation of structural flexibility, and each mode is characterized by its natural frequency and its modal gain. The concept of natural frequency is familiar; the concept of modal gain is less so. The natural frequency depends on the relative magnitude of stiffness and inertia as weighted by a particular mode shape. A qualitative appreciation of the modal gains can be gained from Eqs. (A-9) and (A-13) for pitch/twist, or the corresponding equations for roll-yaw/bending, Eqs. (4.85) and (4.116). In the case of constrained modes, the modal gain is an indicator of the fraction of the total spacecraft inertia which may be associated with a given (constrained) mode. These fractions have their sum equal to $I_f/(I_f + I_r)$, the proportion of the total satellite that is flexible. This proportion may, of course,

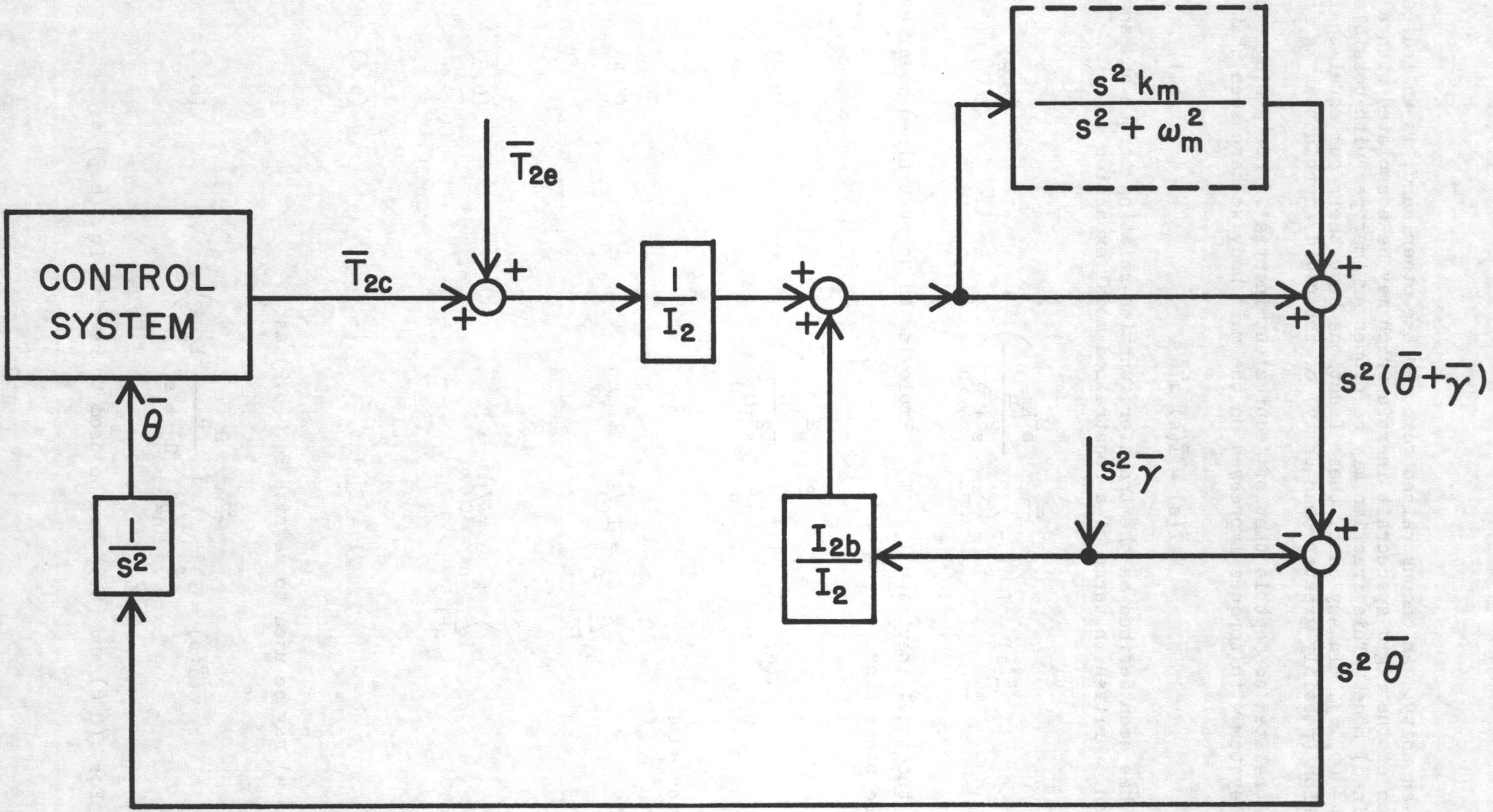

FIG. 54: Pitch Attitude Control Block Diagram Incorporating Both Unconstrained Twisting Modes and Array Tracking

be as high as unity. An unconstrained gain, on the other hand, is an indicator of the fraction of the rigid spacecraft inertia which may be associated with a given (unconstrained) mode. This fraction may be proper or improper with possible values in the range $(0, \infty)$. In any case, these fractions have their sum equal to I_f/I_r, the proportion (possibly greater than unity) of the rigid inertia that is flexible.

A related concept is that of 'equivalent inertia'. For a single degree of freedom system with torques impressed on the main body we have seen that

$$\bar{T}(s) = \bar{I}(s)\, s^2 \bar{\theta} \tag{6.1}$$

where $\bar{I}(s)$ has been defined as the transfer function relating torque and angular acceleration. Written in terms of a constrained modal expansion

$$\bar{I}(s) = I \left(1 - \sum_{n=1}^{\infty} \frac{s^2 K_n}{s^2 + \Omega_n^2} \right) \tag{6.2}$$

where I is the total inertia = $I_r + I_f$. Employing an unconstrained modal expansion, on the other hand,

$$\bar{I}(s) = I \left(1 + \sum_{n=1}^{\infty} \frac{s^2 k_n}{s^2 + \omega_n^2} \right)^{-1} \tag{6.3}$$

We recall the sums

$$\sum_{n=1}^{\infty} K_n = I_f/I \tag{6.4}$$

$$\sum_{n=1}^{\infty} k_n = I_f/I_r \tag{6.5}$$

Since

$$I = I_r + I_f \tag{6.6}$$

Equation (6.4) may be used to rewrite Eq. (6.2) as

$$\bar{I}(s) = I_r + \sum_{n=1}^{\infty} \left(\frac{\Omega_n^2}{\Omega_n^2 + s^2} K_n I \right) \tag{6.7}$$

Similarly, Eqs. (6.6) and (6.5) may be used to rewrite Eq. (6.3) as

$$\bar{I}(s)^{-1} = I_r^{-1} - \sum_{n=1}^{\infty} \left(\frac{\omega_n^2}{\omega_n^2 + s^2} \; k_n \; I^{-1} \right) \qquad (6.8)$$

These forms for the 'equivalent inertia' shed considerable light on the role played by the modal gains. Beginning with Eq. (6.7), the limit for zero stiffness ($\Omega_n^2 \to 0$; n = 1,2,---) is $\bar{I}(s) = I_r$ as expected, while the limit for zero flexibility ($\Omega_n^2 \to \infty$; n = 1,2,...) is $\bar{I}(s) = I_r + \Sigma K_n I = I_r + I_f = I$ as expected. When $s = i\Omega_n$, $\bar{I}(i\Omega_n) \to \infty$ showing that no attitude motion results from sinusoidal excitation at an appendage natural frequency; the appendage acts as a vibration absorber. Turning to Eq. (6.8), the limit for zero stiffness ($\omega_n^2 \to 0$; n = 1,2,...) is $\bar{I}(s) = I_r$ as expected, while the limit for zero flexibility ($\omega_n^2 \to \infty$; n = 1,2,...) is $\bar{I}(s)^{-1} = I_r^{-1} - (\Sigma k_n) I^{-1} = I_r^{-1} - (I_f/I_r) = I^{-1}$ as expected. When $s = i\omega_n$, $\bar{I}(i\omega_n) = 0$ showing that the steady state tends to resonance.

A third modal parameter is the damping ratio ζ_n, corresponding to the desire to represent dissipative mechanisms by an equivalent linear viscous damping. The expression $s^2 + \Omega_n^2$ is replaced by $s^2 + 2\zeta_n \Omega_n s + \Omega_n^2$. However this procedure is not rigorous and the term $2\zeta_n \Omega_n s$ is usually added after the structural analysis is completed. For that reason this term has not been added to the block diagrams of this report; the reader may add such a term if he wishes. In practice, a measure of damping is provided by the attitude control system itself. That is, even if $\zeta = 0$, attitude oscillations will be attenuated, at least till their amplitude is within the deadband of the sensor or controller. If satisfactory performance depends on a $\zeta > 0$, then it is essential to examine carefully the implications of the fact that this dissipative model is only an approximate one and that reliable values of ζ are often not readily available.

Some conclusions may be reached also on the relative desirability of the unconstrained vs. constrained modal expansions. These two alternatives have been developed in parallel throughout the report and it is clear that they both have an equally firm foundation. Spacecraft designers seem to use constrained modes whereas aircraft designers tend to use unconstrained (ie., system) modes; this latter state of affairs (for aircraft) probably stems from the fact that there is no part of the aircraft noticably more rigid than any other. In any case, the unconstrained modes have appealing characteristics. As discussed in Appendix A, they simulate the attitude motion most accurately in the frequency bands of greatest importance, namely, the system resonances. By contrast, the constrained modes simulate the attitude most accurately in the frequency bands of least importance, namely, the system zeros (vibration absorber behaviour). The analysis of flight data would also be expected to reveal the system (ie., unconstrained) natural frequencies.

On the other hand, ground tests of appendages would tend to give the constrained modal information most directly, hopefully including the equivalent linear viscous damping ratio, ζ. In fact, the constrained modes are inherently characterizations of the appendages alone; both the natural frequencies, Ω_n, and the dimensional gains, K_n', depend only on array parameters. Therefore these modes may be more natural to use in situations where the array excitation is more

general in nature (for example, during acquisition when 'small deflections' may be assumed even though 'small angles' may not be assumed). Moreover, it was shown in Appendix A that any given number, N, of system frequencies can be accurately modelled with the aid of N + 2 constained modes, especially if the appendages are not large. So unless there is a severe limit on the number of modes which can be simulated (for example, the number of amplifiers on an analog computer, or the computing time on a digital computer) the primary advantage of the unconstrained expansion is less important. Furthermore, the task of analysis is reduced if constrained modes are used. It is our experience that the development is more difficult to handle if the case of unconstrained modes; the orthogonality condition, and the proper fashion in which to impose this condition, are not straightforward. Thus, speaking somewhat loosely, if there is more computer power available than analytical power, the constrained mode approach is probably the wisest course. Not that the latter is without pitfalls; a curious instance occurs when the gains K_n are miscalculated in such a way that $\Sigma K_n > 1$. This is physically impossible without a negative body inertia, and unstable behaviour is the penalty for this oversight.

The additional complexity of the unconstrained modal expansion just discussed is particularly evident if there is stored angular momentum. This is clear from Section 4 where the parallel developments for both modal expansions were presented. Indeed, it could have been even complex in the mathematical sense of the word had not the assumption been tenable if no in-plane array deflections.

Some specific conclusions pertaining to the class of configurations analyzed here also follow from the results presented. A dominant behaviour observed is that the dimensionless frequencies are relatively insensitive to parameters variations. This applies to both the constrained ('flexible-part-only') and unconstrained ('system') frequencies. The most obvious exceptions to this are the parameters $\sqrt{B}^*$ and $\omega_N{}^*$, which affect the bending frequencies substantially, albeit in a restricted range of parameter values. In general then,

$$\omega_n{}^* \equiv \omega_n \frac{\sigma w \ell^2}{P} \simeq \text{const.} \qquad (6.9)$$

Let us now look at some practical implications of (6.9). An important consideration is the interaction between the control-system bandwidth and the structural frequencies. As an indicator of this let us consider the ratio of the lowest "flexible" unconstrained frequency ω_f and a characteristic control frequency ω_c and attempt to relate it to spacecraft design criteria, namely power requirement W and the pointing accuracy (deadband of the control system) D.

Among the parameters in (6.1), σ is usually fixed by the solar cell mass density, and w by the diameter of the spacecraft which, in turn, is constrained by the launch vehicle diameter. For given w, the power generated is directly proportional to the length ℓ. A further constraint relating P and ℓ arises from preventing the possibility of buckling of the support boom. If we take P to be a given fraction of the buckling load, that is a definite value of $B^* = P\ell^2/B$, then it follows from these constraints and (6.9) that

$$\omega_f \sim \sqrt{B}/\ell^4 \sim \sqrt{B}/W^2 \qquad (6.10)$$

Assuming that the stiffness B is provided by a thin-walled STEM boom as for CTS and other applications, we have $B \sim td^3$ where t and d are the boom thickness and diameter respectively. On the other hand the density $\rho \sim td$, so that for a given weight, $B \sim d^2$. Inserting this gives

$$\omega_f \sim d/W^2 \tag{6.11}$$

Considering now the control-system frequencies, the kind of controller used is obviously of fundamental importance. Besides this, ω_c may be expected to depend on the torque level T, the spacecraft moment of inertia I, and the pointing accuracy D. For example, if we consider a mass-expulsion reaction control system operating in a soft limit-cycle mode (pulsing only on one side of the controller deadband), then it may be shown that the limit cycle frequency behaves as

$$\omega_c \sim \sqrt{\frac{T}{ID}} \tag{6.12}$$

Note that this does not depend on the thrust level and the minimum impulse bit, because the controller is assumed to be such that these characteristics are designed for efficient soft limit cycle operation. In any case, dimensional analysis also yields a relation of the form (6.12). We can expand on this further. For the configuration studied, and given σ, w, we know that $I \sim \ell^3$. Furthermore, the major source of torque T is the solar radiation pressure torque, and this may be assumed to be proportional to the solar panel area, i.e., $T \sim \ell$ for fixed w. Substituting these relations in (6.12) and remembering the proportionality between ℓ and W, we have

$$\omega_c \sim \frac{1}{W\sqrt{D}} \tag{6.13}$$

Our indicator of control system - flexibility interaction is then

$$\frac{\omega_c}{\omega_f} \sim \frac{W}{d\sqrt{D}} \tag{6.14}$$

The boom diameter turns up here for a good reason: it has direct control over flexural stiffness for a given weight. However the important thing observed from (6.14) is that as power requirements for synchronous satellites with large flexible solar arrays go up, and pointing accuracy requirements become more stringent, the interaction problem looms larger. The concern is somewhat tempered by the fact that for a given mission, W and D are inversely related, i.e., less power is needed for an antenna which can be pointed to greater accuracy. The boom diameter d appears to be the only "free" parameter for spacecraft structural design to avoid controller-flexibility interaction, under these circumstances.

Another parameter whose effect on frequencies is directly affected by flexibility is ω_N*. For low values of ω_N, the rigid-body nutation frequency is approximately a system frequency. As ω_N is increased however, the system nutation frequency does not increase linearly, but levels off to a constant value (Fig. 21), since the flexible part of the spacecraft plays an increasing role in the motion. Since in the rigid concept of the spacecraft ω_N appears as the basic dynamics frequency, another indicator of the influence of flexibility is the

proximity of the lowest (nutation) system frequency to ω_N.

As a matter of interest, the preceding discussion raises the question of how important flexibility is for the CTS mission, which in a very real sense prompted the research reported here. It turns out that, at least in the nominal on-orbit control situation, flexibility does not affect the dynamics or control-system performance significantly. It can definitely be said that the stored angular momentum for CTS is negligible insofar as its interaction with flexibility is concerned, judging from the second criterion discussed above. However, CTS is perhaps also an excellent example of how unexpected sources of excitation can turn up. The Attitude Control analysis and design team found that the control system for maintaining the array sun-pointing attitude had a frequency spectrum which directly excited the solar panels in the pitch/twist mode, leading to a resonance phenomenon. In this case a simple re-design of the controller solved the problem, but there are numerous other sources of concern relating to flexibility effects on modern spacecraft. See, for example, Ref. 7 . And, as just demonstrated above, this trend can be expected to continue in future spacecraft designs for which the analysis of flexibility effects will be of great importance. It is hoped that the present report has been a significant step in that direction.

REFERENCES

1. Hughes, P. C. — "Flexibility Considerations for the Pitch Attitude Control of the Communications Technology Satellite", CASI Transactions, Vol.5, No.1, March 1972, pp.1-4.

2. Hughes, P. C. — "Attitude Dynamics of a Three-Axis Stabilized Satellite with a Large Flexible Solar Array". Journal of the Astronautical Sciences, Vol. XX, No.3, Nov-December, 1972, pp.166-189.

3. Hughes, P. C. — "Attitude Control of Satellites with Large Flexible Solar Arrays", AIAA Paper No. 72-733, Presented at the CASI/AIAA Meeting, Ottawa, Canada, July 1972.

4. Franklin, C. A. Davison, E. H. — "A High Power Communications Technology Satellite for the 12 and 14 GHz Bands", AIAA Paper No. 72-540, Presented at the 4th AIAA Communications Satellite Systems Conference, Washington, D.C. USA, April 1972.

5. Frisch, H. P. — "Thermal Bending Plus Twist of a Thin-Walled Cylinder of Open Section with Application to Gravity-Gradient Booms", NASA TN D-4069, August 1967, and "Coupled Thermally-Induced Transverse Plus Torsional Vibrations of a Thin-Walled Cylinder of Open Section", NASA TR R-333, March 1970.

6. Cherchas, D. B. — "Coupled Bending-Twisting Vibrations of a Single Boom Flexible Solar Array and Spacecraft", CASI Transactions, Vol.6, No.1, March 1973.

7. Likins, P. W. Bouvier, H. K. — "Attitude Control of Nonrigid Spacecraft", Astronautics and Aeronautics, May 1971.

APPENDIX A: RELATIONSHIPS BETWEEN CONSTRAINED AND UNCONSTRAINED MODAL REPRESENTATIONS

One of the themes of this report is the duality between the constrained and unconstrained modal representations of structural flexibility. This Appendix will explore certain relationships between them and, it is hoped, shed further light on the question of which representation to choose in a specific instance.

From Eq. (3.74), the pitch motion of the satellite (Laplace transformed) was given:

$$\left(1 - \sum_{n=1}^{\infty} \frac{s^2 K_n}{s^2 + \Omega_n^2}\right) \bar{\theta} = \bar{\Theta} \tag{A.1}$$

This motion is in response to external and controlling influences as represented by $\bar{\Theta}(s)$, and the constrained modal representation has been used in Eq. (A.1). Compare this now with the unconstrained modal representation, as given by Eq. (3.92):

$$\left(1 + \sum_{n=1}^{\infty} \frac{s^2 k_n}{s^2 + \omega_n^2}\right) \bar{\Theta} = \bar{\theta} \tag{A.2}$$

This was pointed out in Ref. 3 where the identity

$$\left(1 + \sum_{n=1}^{\infty} \frac{s^2 k_n}{s^2 + \omega_n^2}\right)\left(1 - \sum_{n=1}^{\infty} \frac{s^2 K_n}{s^2 + \Omega_n^2}\right) = 1 \tag{A.3}$$

was deduced. In particular, setting $s = j\omega_m$ we have

$$\sum_{n=1}^{\infty} \frac{K_n}{\omega_m^2 - \Omega_n^2} = \frac{1}{\omega_m^2} \qquad (m = 1,2,\ldots) \tag{A.4}$$

and setting $s = j\Omega_m$ we have

$$\sum_{n=1}^{\infty} \frac{k_n}{\omega_n^2 - \Omega_m^2} = \frac{1}{\Omega_m^2} \qquad (m = 1,2,\ldots) \tag{A.5}$$

These equations are of theoretical importance since they establish the relationships between the set $(K_n, \Omega_n;\ n = 1,2,\ldots)$ and the set $(k_n, \omega_n;\ n = 1,2,\ldots)$. Thus knowing one set, Eqs. (A.4) and (A.5) may be used to find the other set.

Before proceeding with such calculations a result for an infinite sum of gains is noted. Form the following expression:

$$\frac{1}{6}\ \sigma w^3 \int_o^{\ell} (3.65)dy + \frac{1}{6}\ mw^2\ (3.66) = 0 \qquad (A.6)$$

In view of Eq. (3.68), this becomes

$$-\sum_{n=1}^{\infty} F_n(\ddot{Q}_n + \Omega_n^2 Q_n) + I_{2A}\ddot{\theta} = 0 \qquad (A.7)$$

where the inertia is introduced with the aid of Eq. (3.59). As the final step, Eq. (3.72) is used for $\ddot{Q}_n + \Omega_n^2 Q_n$; recalling the definition of the constrained gains, Eq. (3.75), we arrive at

$$\left(-I_2 \sum_{n=1}^{\infty} K_n + I_{2A} \right) \ddot{\theta} = 0 \qquad (A.8)$$

For non-trivial motion therefore

$$\sum_{n=1}^{\infty} K_n = \frac{I_{2A}}{I_2} \qquad (A.9)$$

which is the result sought. Since all the gains are positive [see Eq. (3.75)] Eq. (A.9) has the effect of placing a bound on K_{N+1} once $(K_n;\ n = 1,\ldots,N)$ are known.

A similar result can be demonstrated for the unconstrained modal gains. Form the following expression:

$$\frac{1}{6}\ \sigma w^3 \int_o^{\ell} (3.86)dy + \frac{1}{6}\ mw^2\ (3.87) = 0 \qquad (A.10)$$

In view of Eq. (3.39), this becomes

$$\sum_{n=1}^{\infty} (I_{2A}\ \theta_n - f_n)(\ddot{q}_n + \omega_n^2 q_n) + I_{2A}\ \ddot{\theta} = 0 \qquad (A.11)$$

where again the inertia is introduced with the aid of Eq. (3.59). As the final step, Eq. (3.90) is used for $\ddot{q}_n + \omega_n^2 q_n$; recalling that $f_n = I_2\theta_n$, and the definition of the unconstrained gains, Eq. (3.93), we arrive at

$$\left[-I_{2b} \sum_{n=1}^{\infty} k_n + I_{2A} \right] \ddot{\theta} = 0 \qquad (A.12)$$

For non-trivial motion therefore

$$\sum_{n=1}^{\infty} k_n = \frac{2I_{2A}}{I_{2b}} = \frac{2I_{2A}}{I_2 - 2I_{2A}} \qquad (A.13)$$

These results, Eqs. (A.9, 13) are analogous to those for roll-yaw as given by Eqs. (4.85,116) respectively.

Return now to the subject of determining unconstrained modal parameters given the unconstrained ones, or vice versa. In practice, only a few modes are actually used. If only N modes are considered, then Eqs. (A.4,5) become 2N equations to be solved for the unknown parameters. For example, suppose then the constrained parameters (K_n, Ω_n; n = 1,...N) are known and it is desired to calculate the unconstrained parameters (k_n, ω_n; n = 1,...,N). Then, first, take the N equations given by Eq. (A.4); this may be rewritten as an N^{th} order polynomial in ω^2 whose N roots are $\omega_1^2, ---, \omega_N^2$. Second, use the N equations given by Eq. (A.5). Now that the ω_n^2 are known, these become a set of N linear algebraic equations in the N unknowns (k_n; n = 1,...N). The symmetry of Eqs.(A.4,5) makes it clear that they are applied in the reverse order if it is desired to go in the other direction, that is, knowing (k_n, ω_n; n = 1,...,N) to find (K_n, Ω_n; n = 1,...,N).

This procedure will now be illustrated for two typical situations. The first is 'membrane'-like (or 'string'-like, or 'sheet'-like behaviour); the second is 'rod'-like behaviour. In the former instance, it is natural to assume that $\Omega_n \sim n$, and there is no loss of generality in taking

$$\Omega_n = n \quad (n = 1,2,...) \quad \text{(membrane)} \qquad (A.14)$$

Experience has shown that $K_n \sim \Omega_n^{-2}$; this may be seen by using, for example, Eq. (3.75) for a string. Equation (3.76) is also of this form except for slight deviations for the first few modes). Denoting the proportionality by p, we have

$$K_n = p/\Omega_n^2 \quad (n = 1,2,...) \qquad (A.15)$$

The physical significance of p is learned from Eq. (A.9).

$$\sum_{n=1}^{\infty} K_n = \frac{I_f}{I_f + I_r} \qquad (A.16)$$

where I_f is the inertia associated with the flexible portion of the structure, and I_r is the inertia associated with the relatively rigid part of the structure (the part that is constrained not to move for the 'constrained' modes). $I_f + I_r$ is therefore the total inertia. Using Eqs. (A.15) and (A.14), the interpretation of p is found as

$$p = \frac{p_{OM}}{1 + (I_r/I_f)} \qquad \text{(membrane)} \qquad (A.17)$$

where

$$p_{OM} = \left\{ \sum_{n=1}^{\infty} \left(\frac{1}{n^2} \right) \right\}^{-1} \qquad (A.18)$$

The value of p_{OM} happens to be 2.60014...; but the important point is that p is an indicator of the relative magnitudes of the inertias of the flexible and rigid portions of the vehicle. Specifically, smaller values of p (and hence of the gains) correspond to more predominently rigid satellites.

To study 'rod'-like behaviour, it may be assumed that, in place of Eq.(A.14),

$$\sqrt{\Omega}_n = n \qquad (n = 1,2,\ldots) \qquad \text{(rod)} \qquad (A.19)$$

Since Eq. (A.15) and (A.16) are still appropriate, this leads to, instead of Eq. (A.17),

$$p = \frac{p_{OR}}{1 + (I_r/I_f)} \qquad \text{(rod)} \qquad (A.20)$$

where

$$p_{OR} = \left\{ \sum_{n=1}^{\infty} \left(\frac{1}{n^4} \right) \right\}^{-1} \qquad (A.21)$$

The value of P_{OR} happens to be 2.08363...; but again the importance of p stems from its direct relationship to the proportion of the vehicle that is flexible.

For both these simple models ('membrane' and 'rod') the calculation of unconstrained gains and frequencies will now be made. While so doing, a significant trend will be evident that bears on the choice of modal representation. The presumption will be that the most important parameter regions in which to model satellite flexibility accurately are those leading to large attitude response, that is, in the neighbourhood of the unconstrained natural frequencies. So the position may be taken that a flexibility model is worthy insofar as it gets the system frequencies correct. Clearly an expansion in terms of unconstrained modes satisfies this requirement automatically. It can be decided what upper limit on frequency is of interest and then simply include all unconstrained modes whose frequencies are less than it is. The situation for a constrained modal expansion is less clear. If N constrained modes are used then there will indeed be N system frequencies but the approximation $\infty \doteq N$ leads to errors in these frequencies - they will not be equal to ω_1^2, ω_2^2, -- except as $N \to \infty$. To study the size of such errors, the approximate values of $\omega_1^2, --, \omega_N^2$ may be found by solving Eqs. (A.4,5), where Σ_1^{∞} is replaced by Σ_1^N, as described two paragraphs ago. The size of the error will depend on, in addition to N, the I_r/I_f ratio. The frequency results are shown in Fig. (A.1) for 'membrane'-like behaviour and in Fig. (A.2) for 'rod'-like behaviour. When I_r/I_f is large (vehicle predominantly

rigid), it is clear that the first N system frequencies are adequately predicted by using an expansion in terms of N constrained modes. For small I_r/I_f (vehicle predominantly flexible) it is necessary to use N + 1 or N + 2 constrained modes to represent the first N system (unconstrained) frequencies accurately. Similar remarks can be made for the gains which are plotted in Fig. (A.3) for 'membranes' and for Fig.(A.4) for 'rods'.

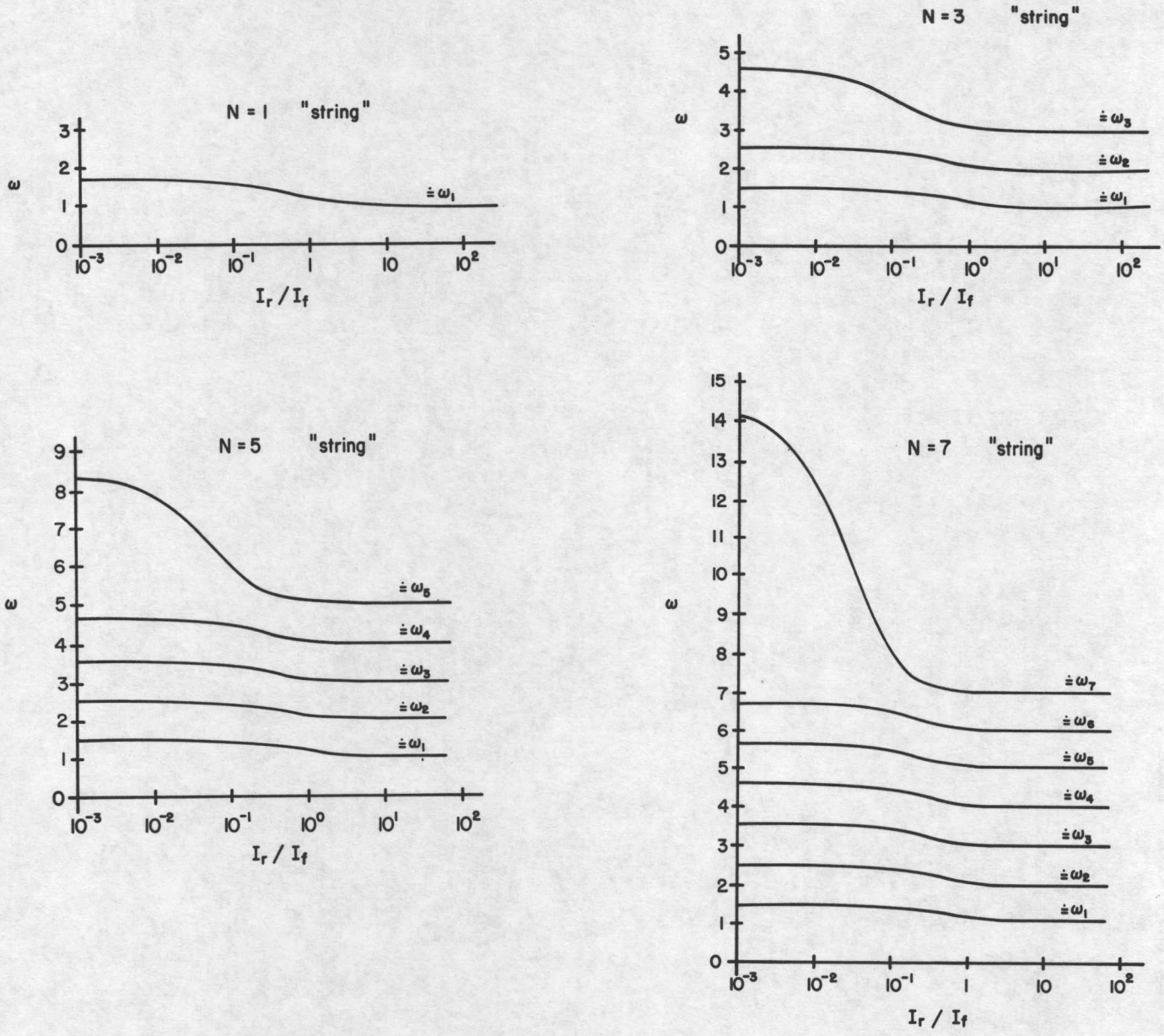

FIG. A.1 Approximate Unconstrained (i.e., System) Frequencies Implied by N Constrained Modes (Membrane-like Behaviour)

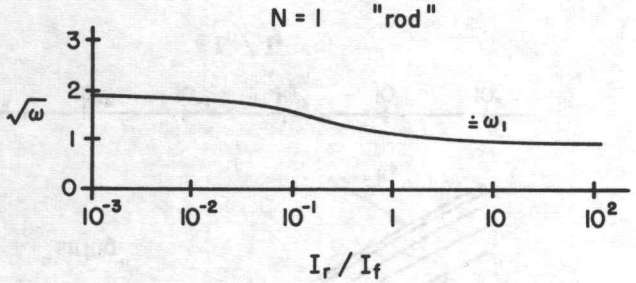

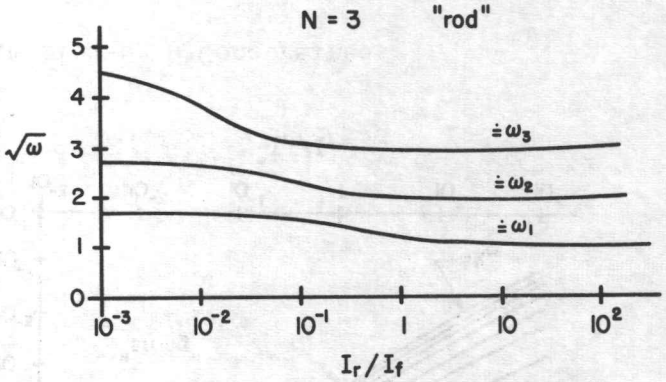

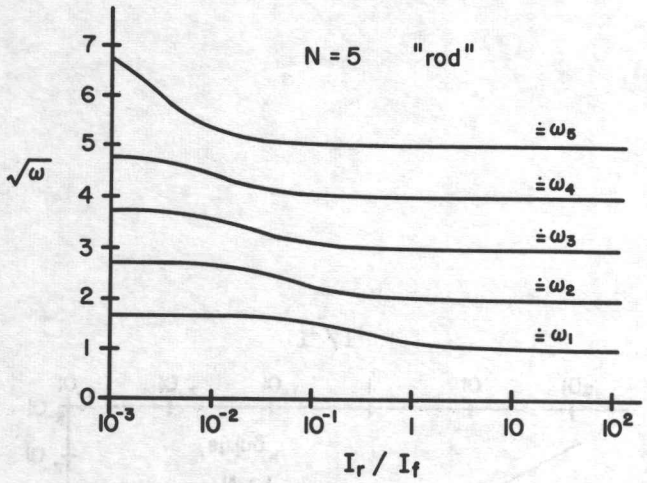

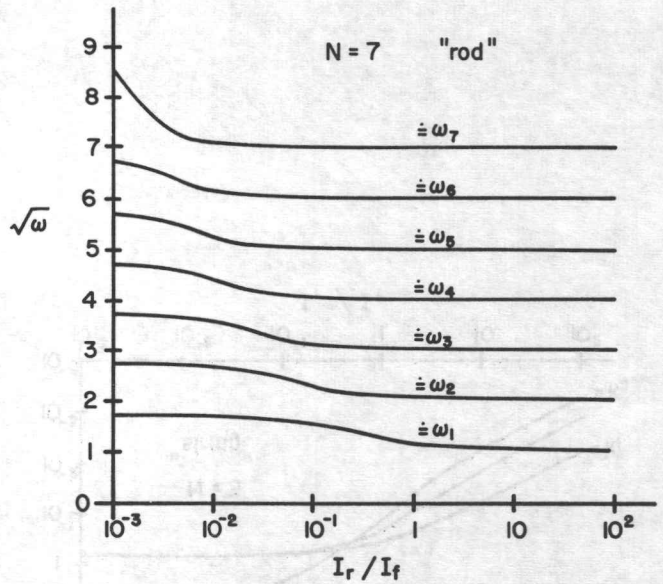

FIG. A.2 Approximate Unconstrained (i.e., System) Frequencies Implied by N Constrained Modes (Rod-like Behaviour)

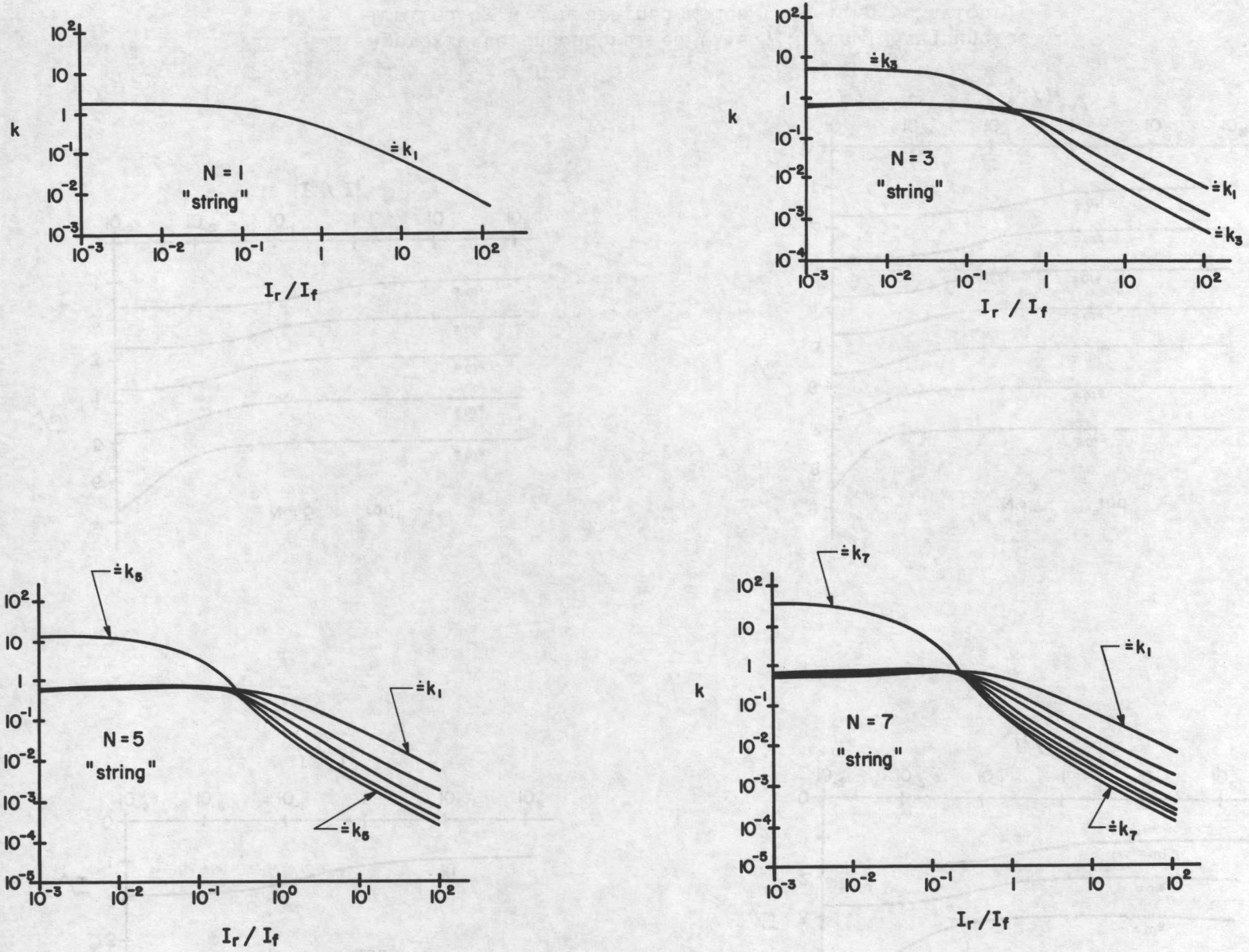

FIG. A.3 Approximate Unconstrained Gains Implied by N Constrained Modes (Membrane-like Behaviour)

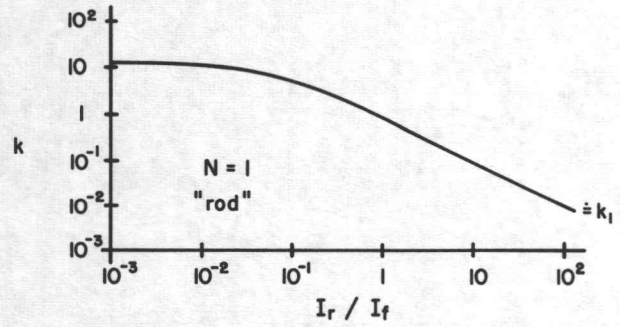

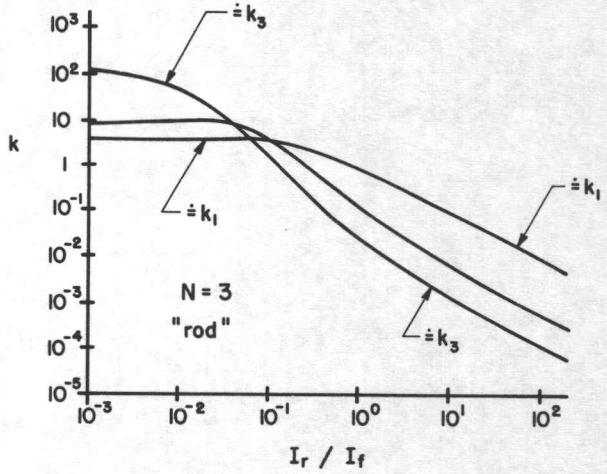

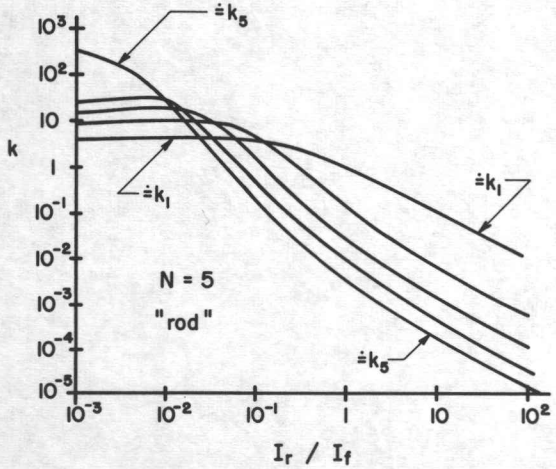

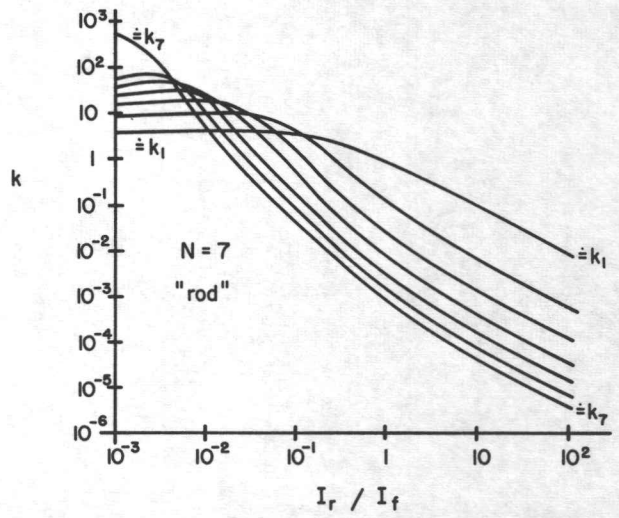

FIG. A.4 Approximate Unconstrained Gains Implied by N Constrained Modes (Rod-like Behaviour)

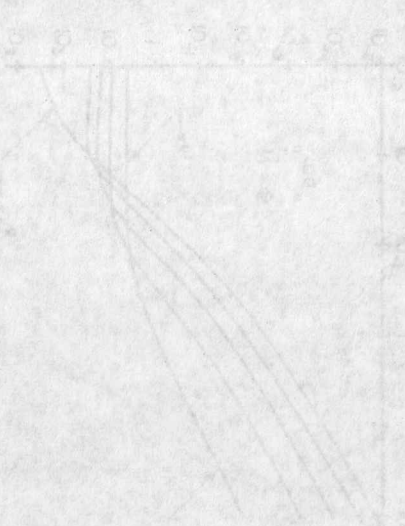

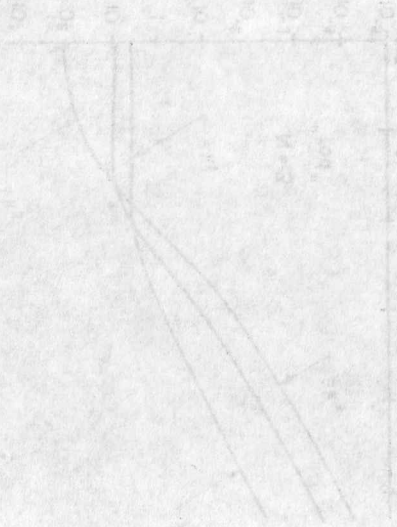

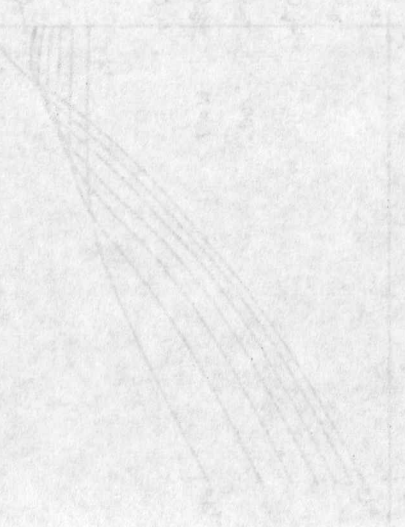

APPENDIX B: VARIATION OF MOMENTS OF INERTIA

Herein we derive the expressions for moments of inertia of the spacecraft, in particular the variation due to rotation of the solar arrays relative to the center body. We make two simplifying assumptions -

(i) The axis of rotation passes through the spacecraft center of mass, which is assumed to coincide with the mass centers of the body and array separately. This is not quite true for the CTS, but the error introduced is small and can be readily accounted for if desired.

(ii) The offset between the boom and the array is neglected, compared with the width and length of the blanket. Thus the boom and blanket are coplanar, and the boom centerline in the undeflected state coincides with the axis of rotation and the pitch axis.

The geometry of rotation under the above assumptions is shown in Fig. B.1. Let the body inertia matrix in the roll-yaw (unprimed) frame be given as

$$\mathcal{I}_B = \begin{bmatrix} I_{1b} & 0 & 0 \\ 0 & I_{2b} & 0 \\ 0 & 0 & I_{3b} \end{bmatrix} \qquad (B.1)$$

Similarly, the array inertia matrix in the rotating (primed) frame is constant and is given by

$$\mathcal{I}_{A'} = \begin{bmatrix} I_{1A} & 0 & 0 \\ 0 & I_{2A} & 0 \\ 0 & 0 & I_{3A} \end{bmatrix} \qquad (B.2)$$

Expressions for I_{1A} etc can be readily written down owing to the planar mass distribution. We have

$$I_{1A} = 2(\rho + \sigma w)\int_0^{\ell} (b+y)^2 dy + 2m(b+\ell)^2$$

$$= \frac{2}{3}(\rho + \sigma w)\ell(b^2 + b\ell + \ell^2) + 2m(b+\ell)^2$$

$$I_{2A} = 2(\sigma\ell + \frac{m}{w})\int_{-w/2}^{w/2} x^2\, dx$$

$$= \frac{1}{6}(\sigma\ell w^3 + mw^2) \qquad (B.3)$$

and $I_{3A} = I_{1A} + I_{2A}$.

Note that the tip mass is assumed to be uniformly distributed along its length, and that the expression for I_{3A} follows from the planar mass distribution.

We need now to transform $\mathcal{I}_{A'}$ to the unprimed frame; the appropriate

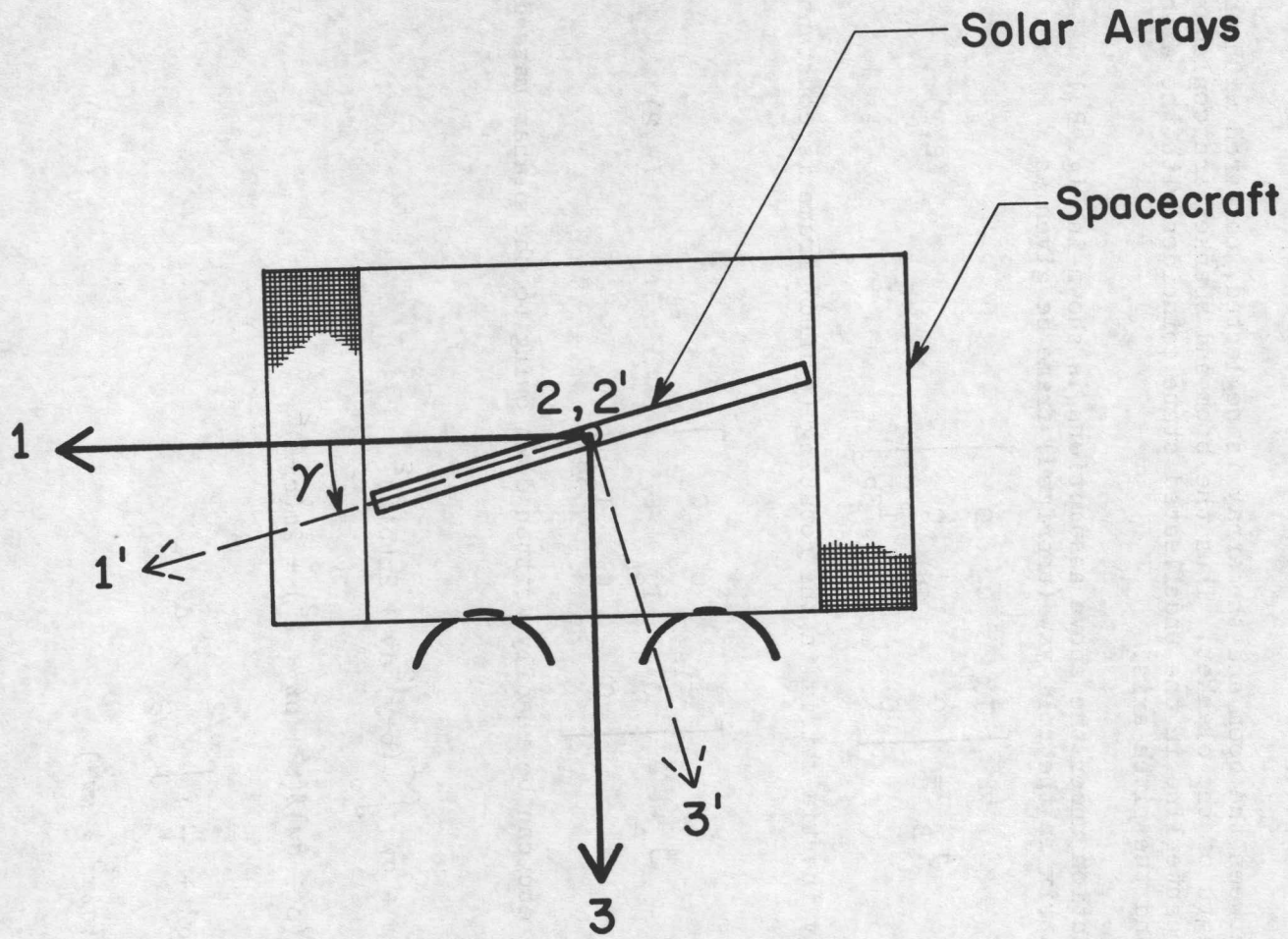

FIG. B.1 Array Rotation Geometry

transformation matrix is

$$\mathcal{L} = \begin{bmatrix} \cos\gamma & 0 & -\sin\gamma \\ 0 & 1 & 0 \\ \sin\gamma & 0 & \cos\gamma \end{bmatrix} \qquad (B.4)$$

The total inertia matrix in the 1-2-3 frame is then, from the rule for transforming matrices,

$$\mathcal{I} = \mathcal{I}_B + \mathcal{L}^T \mathcal{I}_A \cdot \mathcal{L}$$

or,

$$\mathcal{I} = \begin{bmatrix} I_{11} & 0 & I_{13} \\ 0 & I_{22} & 0 \\ I_{13} & 0 & I_{33} \end{bmatrix}$$

where

$$\begin{aligned} I_{11} &= I_{1b} + I_{1A}\cos^2\gamma + I_{3A}\sin^2\gamma \\ I_{22} &= I_{2b} + I_{2A} \\ I_{33} &= I_{3b} + I_{3A}\cos^2\gamma + I_{1A}\sin^2\gamma \\ I_{13} &= (I_{3A}-I_{1A})\sin\gamma\cos\gamma \end{aligned} \qquad (B.5)$$

Using the last of (B.3), these can be further re-arranged as follows:

$$\begin{aligned} I_{11} &= I_{11}^{\,o} + I_{2A}\sin^2\gamma\,, \quad I_{22} = I_{22}^{\,o} \\ I_{33} &= I_{33}^{\,o} - I_{2A}\sin^2\gamma\,, \quad I_{13} = \tfrac{1}{2} I_{2A}\sin^2\gamma \end{aligned} \qquad (B.6)$$

The zero superscript refers to the "nominal" moments of inertia, i.e., with $\gamma = 0$. We see that

(i) The nominal body-fixed axes are no longer principal axes; a product of inertia occurs due to array rotation.

(ii) The changes in the moments of inertia from the nominal principal-axes values ($\gamma = 0$) are periodic with γ, having a period of 180^o which corresponds to 12 hours in orbit. Secondly, the amplitude of these changes is of the order of I_{2A} which is usually quite small compared to any of the other inertias (e.g. for CTS, $I_{2A} \simeq 3$ slug-ft^2 whereas $I_{11}^{\,o}, I_{33}^{\,o} \simeq 650$ slug-ft^2). The net result is that the effects of rates of change of the inertia moments are negligible, and we are quite justified in treating the variable inertia on a quasi-static basis.

The effect of γ on the unconstrained gains and frequencies in bending was shown numerically in Section 4, Figs. 22 and 43. The pitch gains and frequencies are not directly affected by γ, since I_2 remains unchanged.

APPENDIX C: BOOM AND ARRAY DYNAMICS

In this section we analyze the motion of the boom and sheet separately, considering their natural frequencies and relating these to the frequencies of the combined system. This helps to explain some of the features noted on the plots given in Section 4. The buckling condition is also derived.

C.1 Twisting

In the twisting mode, the boom is assumed to contribute negligible stiffness. Hence the dynamics are the same as those analyzed in Section 3 under constrained motions; only the array frequencies are involved, subject to boundary conditions given in Section 3. Hence twist will not be considered further.

C.2 Bending: Boom Only

The governing differential equation for the boom is

$$Bu'''' + Pu'' + \rho\ddot{u} = 0 \tag{C.1}$$

The appropriate boundary conditions are

$$u(o) = u'(o) = 0, \quad u''(\ell) = 0 \tag{C.2}$$

$$\left(Bu''' + P\left(u' - \frac{u}{\ell}\right) - m\ddot{u}\right)\Big|_{y=\ell} = 0$$

In the last of (2) it is assumed effectively that a massless sheet exists which transmits tension, and does not deflect itself. Thus the tension P does not remain fixed in direction, but always points towards the origin. As usual, we seek a solution of the form $u(y,t) = U(y)\cos\omega t$, which when substituted into (C.1) and (C.2) leads to the following equations for the mode shape function $U(y)$:

$$BU'''' + PU'' - \rho\omega^2 U = 0$$

$$U(o) = U'(o) = 0, \; U''(\ell) = 0 \tag{C.3}$$

$$BU''' + P(U' - U/\ell) + m\omega^2 U\Big|_{y=\ell} = 0$$

The following solution to (3) may be verified, which satisfies the boundary conditions at $y = 0$:

$$U = c_1(\cosh \alpha y - \cos\beta y) + c_2\left(\sinh \alpha y - \frac{\alpha}{\beta}\sin\beta y\right)$$

where

$$\alpha = \left(\left(\sqrt{P^2 + 4\rho\omega^2 B} - P\right) / 2B\right)^{1/2}$$

$$\beta = \left(\left(\sqrt{P^2 + 4\rho\omega^2 B} + P\right) / 2B\right)^{1/2} \tag{C.4}$$

The two remaining boundary conditions at $y = \ell$ can be arranged in matrix form to give a system of linear homogeneous equations for c_1 and c_2:

$$A\,\underline{c} = 0 \tag{C.5}$$

where

$$\underline{c} = (c_1, c_2)^T$$

and

$$\begin{aligned}
a_{11} &= \alpha^2 \cosh\alpha\ell + \beta^2 \cos\beta\ell \\
a_{12} &= \alpha^2 \sinh\alpha\ell + \alpha\beta\sin\beta\ell \\
a_{21} &= \alpha(P + B\alpha^2)\sinh\alpha\ell + \beta(P-B\beta^2)\sin\beta\ell \\
&\quad + (m\omega^2 - P/\ell)(\cosh\alpha\ell - \cos\beta\ell) \\
a_{22} &= \alpha(P + B\alpha^2)\sinh\alpha\ell - \alpha(P-B\beta^2)\cos\beta\ell \\
&\quad + (m\omega^2 - P/\ell)(\sinh\alpha\ell - \frac{\alpha}{\beta}\sin\beta\ell\ )
\end{aligned} \tag{C.6}$$

The characteristic equation for ω is found by setting the determinent of (C.5) to zero, which is the only condition under which a non-trivial solution exists:

$$a_{11}a_{22} - a_{21}a_{12} = 0 \tag{C.7}$$

For plotting purposes the frequencies found from this are nondimensionalized by "array" parameters

$$\omega^* = \omega\sqrt{\sigma w \ell^2/P} \tag{C.8}$$

Here σ and w are of course not related to the boom dynamics.

C.3 Buckling

The condition for buckling of the boom can be derived by a static analysis ($\omega = 0$) similar to the one above. Since the boundary conditions and "equation of motion" do not change except for the elimination of time derivatives, we can derive this condition more simply by taking the limit of (C.7) as $\omega \to 0$. We have

$$\lim_{\omega \to 0} \alpha = 0, \quad \lim_{\omega \to 0} \beta = \sqrt{P/B} \tag{C.9}$$

In taking the limit of (C.6), it is necessary to retain terms of first order in α to arrive at non-trivial terms in the expansion (C.7). Thus to first order in α,

$$\begin{aligned}
a_{11} &\simeq \beta^2\cos\beta\ell, \quad a_{12} \simeq \alpha\beta\sin\beta\ell \\
a_{21} &\simeq -(P/\ell)(1-\cos\beta\ell) \\
a_{22} &\simeq +(P/\ell)(\alpha\sin\beta\ \ell/\beta)
\end{aligned} \tag{C.10}$$

Substituting into (C.7) and dividing by $\alpha P/\ell$ ($\alpha \neq 0$ following the standard procedure for limits) gives

$$\beta \sin\beta\ell \cos\beta\ell + \beta \sin\beta\ell(1-\cos\beta\ell) = 0$$

Hence, buckling occurs when

$$\beta\ell = n\pi, \quad n = 1,2,...$$

In terms of P, substituting for β from (C.9), we have

$$B^* \equiv \frac{P\ell^2}{B} = n^2\pi^2, \quad n = 1,2,... \tag{C.11}$$

where the notation corresponds to that in the text, Eq. 4.43. The lowest buckling load occurs when $\sqrt{B^*} = \pi$. Note that this agrees with the frequency plots presented in the text. This result is not affected by boom density or tip mass.

C.4 Bending: Array Only

In the absence of the boom, the array obeys the simple string equation:

$$Pv'' = \sigma w \ddot{v} \tag{C.12}$$

The boundary conditions appropriate to a free end are

$$v(o) = 0, \quad v'(\ell) = 0 \tag{C.13}$$

The natural mode shape V(y) corresponding to (C.12) and satisfying the boundary condition at y = 0 is

$$V(y) = c_1 \sin\kappa y \ , \ \kappa \equiv \sqrt{\frac{\sigma w\, \omega^2}{P}} \tag{C.14}$$

Applying the condition at $y = \ell$, non-trivial solutions exist only for

$$\kappa\ell = n\pi/2 \ , \qquad n = 1,3,....$$

Hence the dimensionless natural frequencies defined by (8) are simply

$$\omega^* = \tfrac{1}{2} n\pi, \quad n = 1,3,5,... \tag{C.15}$$

C.5 Array-Boom Interaction: Numerical Example

When the array and boom are allowed to vibrate as one system, the configuration is identical to that considered under constrained (bending) modes previously. It can in fact be shown, by considerations of equilibrium at the tip where these two vibrating elements are attached, that the combined characteristic equation of Section 4 follows from knowing the individual characteristic equations derived above. We shall not prove this here, but by a numerical example we demonstrate the relationship of the constrained natural frequencies to the boom and array frequencies obtained from (C.7) and (C.15) respectively.

The numerical values of the relevant dimensionless parameters ρ^*, m^* and B^* will be taken identical to those in the text, Eq. 4.73. The frequencies ω_n^* were shown as a function of $\sqrt{B^*}$ in Fig. 16. The straight horizontal lines correspond to the array frequencies (C.15), and the curved lines to the boom frequencies. Note that in Eq. C.8, while ω is independent of P, ω^* goes to infinity as $P \rightarrow 0$, forced by $\sqrt{B^*} \equiv \sqrt{P}\ell^2/B$.

The similarity of Fig. 16 to Fig. 15 for the constrained natural frequencies has already been discussed. Indeed the curves differ mainly in the region when the array and boom frequencies are close together. A notable exception is that the expected curve corresponding to (C.15) with $n = 1$ does not appear in the constrained frequencies. This may be attributed to the fact that, when the boom is also vibrating, the boundary condition at $y = \ell$ in (C.13) is not quite appropriate. The equivalence of buckling loads should also be noted. Heuristically, one may say that the boom and array are weakly coupled, since they are attached only at one point along their length, i.e., at the tip. This fact can be interpreted as the reason for the closeness of the frequencies of the contained system to those of its components. However, no attempt is made here to pursue this argument quantitatively.

UTIAS REPORT NO. 179

Institute for Aerospace Studies, University of Toronto

DYNAMICS OF LARGE FLEXIBLE SOLAR ARRAYS AND APPLICATION TO SPACECRAFT ATTITUDE CONTROL SYSTEM DESIGN

Hughes, P.C., Garg, S. C.   75 pages (approx)   59 figures

1. Spacecraft Attitude Dynamics 2. Spacecraft Attitude Control 3. Solar Arrays
4. Spacecraft Structural Flexibility
I. Hughes, P.C., Garg, S. C.   II. UTIAS Report No. 179

Many current three-axis controlled spacecraft have appendages of considerable size and possessing significant structural flexibility. This report examines the resulting interaction between the attitude dynamics and the elastic degrees of freedom. The representation of these additional degrees of freedom in terms of natural modes is discussed and two distinct classes of modes are defined. For both classes, 'constrained' and 'unconstrained', the object of the analysis is to find the natural frequencies of oscillation and the modal gains. The latter indicate the relative influence of each mode on the angular acceleration of the spacecraft. The relationships between these classes of modes, and certain important properties of the modal gains are discussed in general terms. These general considerations are illustrated for a specific satellite configuration which is suggested by the Communications Technology Satellite where the flexibility is provided by a large solar array. The geometrical simplicity of this configuration allows continuum mechanics to be chosen as an appropriate formulation. Numerical results are provided for frequencies and gains (and for both classes of modes) and their dependence on all satellite parameters is exhibited graphically. Both dimensional and dimensionless plots are provided where appropriate. The main contributions of this report include a general discussion of how spacecraft structural flexibility can be represented from an attitude control viewpoint, of how solar arrays in particular can be successfully treated by traditional techniques, and, even more particularly, of the detailed numerical results when such an analysis is applied to a contemporary spacecraft.

Available copies ot this report are limited. Return this card to UTIAS, if you require a copy.

UTIAS REPORT NO. 179

Institute for Aerospace Studies, University of Toronto

DYNAMICS OF LARGE FLEXIBLE SOLAR ARRAYS AND APPLICATION TO SPACECRAFT ATTITUDE CONTROL SYSTEM DESIGN

Hughes, P.C., Garg, S. C.   75 pages (approx)   59 figures

1. Spacecraft Attitude Dynamics 2. Spacecraft Attitude Control 3. Solar Arrays
4. Spacecraft Structural Flexibility
I. Hughes, P.C., Garg, S. C.   II. UTIAS Report No. 179

Many current three-axis controlled spacecraft have appendages of considerable size and possessing significant structural flexibility. This report examines the resulting interaction between the attitude dynamics and the elastic degrees of freedom. The representation of these additional degrees of freedom in terms of natural modes is discussed and two distinct classes of modes are defined. For both classes, 'constrained' and 'unconstrained', the object of the analysis is to find the natural frequencies of oscillation and the modal gains. The latter indicate the relative influence of each mode on the angular acceleration of the spacecraft. The relationships between these classes of modes, and certain important properties of the modal gains are discussed in general terms. These general considerations are illustrated for a specific satellite configuration which is suggested by the Communications Technology Satellite where the flexibility is provided by a large solar array. The geometrical simplicity of this configuration allows continuum mechanics to be chosen as an appropriate formulation. Numerical results are provided for frequencies and gains (and for both classes of modes) and their dependence on all satellite parameters is exhibited graphically. Both dimensional and dimensionless plots are provided where appropriate. The main contributions of this report include a general discussion of how spacecraft structural flexibility can be represented from an attitude control viewpoint, of how solar arrays in particular can be successfully treated by traditional techniques, and, even more particularly, of the detailed numerical results when such an analysis is applied to a contemporary spacecraft.

Available copies of this report are limited. Return this card to UTIAS, if you require a copy.

UTIAS REPORT NO. 179

Institute for Aerospace Studies, University of Toronto

DYNAMICS OF LARGE FLEXIBLE SOLAR ARRAYS AND APPLICATION TO SPACECRAFT ATTITUDE CONTROL SYSTEM DESIGN

Hughes, P.C., Garg, S. C.   75 pages (approx)   59 figures

1. Spacecraft Attitude Dynamics 2. Spacecraft Attitude Control 3. Solar Arrays
4. Spacecraft Structural Flexibility
I. Hughes, P.C., Garg, S. C.   II. UTIAS Report No. 179

Many current three-axis controlled spacecraft have appendages of considerable size and possessing significant structural flexibility. This report examines the resulting interaction between the attitude dynamics and the elastic degrees of freedom. The representation of these additional degrees of freedom in terms of natural modes is discussed and two distinct classes of modes are defined. For both classes, 'constrained' and 'unconstrained', the object of the analysis is to find the natural frequencies of oscillation and the modal gains. The latter indicate the relative influence of each mode on the angular acceleration of the spacecraft. The relationships between these classes of modes, and certain important properties of the modal gains are discussed in general terms. These general considerations are illustrated for a specific satellite configuration which is suggested by the Communications Technology Satellite where the flexibility is provided by a large solar array. The geometrical simplicity of this configuration allows continuum mechanics to be chosen as an appropriate formulation. Numerical results are provided for frequencies and gains (and for both classes of modes) and their dependence on all satellite parameters is exhibited graphically. Both dimensional and dimensionless plots are provided where appropriate. The main contributions of this report include a general discussion of how spacecraft structural flexibility can be represented from an attitude control viewpoint, of how solar arrays in particular can be successfully treated by traditional techniques, and, even more particularly, of the detailed numerical results when such an analysis is applied to a contemporary spacecraft.

Available copies of this report are limited. Return this card to UTIAS, if you require a copy.

UTIAS REPORT NO. 179

Institute for Aerospace Studies, University of Toronto

DYNAMICS OF LARGE FLEXIBLE SOLAR ARRAYS AND APPLICATION TO SPACECRAFT ATTITUDE CONTROL SYSTEM DESIGN

Hughes, P.C., Garg, S. C.   75 pages (approx)   59 figures

1. Spacecraft Attitude Dynamics 2. Spacecraft Attitude Control 3. Solar Arrays
4. Spacecraft Structural Flexibility
I. Hughes, P.C., Garg, S. C.   II. UTIAS Report No. 179

Many current three-axis controlled spacecraft have appendages of considerable size and possessing significant structural flexibility. This report examines the resulting interaction between the attitude dynamics and the elastic degrees of freedom. The representation of these additional degrees of freedom in terms of natural modes is discussed and two distinct classes of modes are defined. For both classes, 'constrained' and 'unconstrained', the object of the analysis is to find the natural frequencies of oscillation and the modal gains. The latter indicate the relative influence of each mode on the angular acceleration of the spacecraft. The relationships between these classes of modes, and certain important properties of the modal gains are discussed in general terms. These general considerations are illustrated for a specific satellite configuration which is suggested by the Communications Technology Satellite where the flexibility is provided by a large solar array. The geometrical simplicity of this configuration allows continuum mechanics to be chosen as an appropriate formulation. Numerical results are provided for frequencies and gains (and for both classes of modes) and their dependence on all satellite parameters is exhibited graphically. Both dimensional and dimensionless plots are provided where appropriate. The main contributions of this report include a general discussion of how spacecraft structural flexibility can be represented from an attitude control viewpoint, of how solar arrays in particular can be successfully treated by traditional techniques, and, even more particularly, of the detailed numerical results when such an analysis is applied to a contemporary spacecraft.

Available copies of this report are limited. Return this card to UTIAS, if you require a copy.